Activated Carbon Manufacture:
An opportunity for sustainable management of problematic waste biomass

A thesis submitted to Imperial College London for the degree of Doctor of Philosophy

by

Quentin Hoon Nam Cheok

January 2013

Environmental and Water Resource Engineering Section

Department of Civil and Environmental Engineering

Imperial College London

I hereby declare that this thesis and the work reported herein was composed by and originated entirely from me. Information derived from the published and unpublished work of others has been acknowledged in the text and references are given in the list of sources.

Signed: Quentin Hoon Nam Cheok

Date: 4th January 2013

Abstract

The management of waste biomass is an increasing problem. The high water content and mixed composition make its wider utilisation difficult. In addition, there are certain invasive species of flora in the UK which cause significant damage to the natural and built environment. One of the most publicised and problematic species is Japanese Knotweed (*Fallopia japonica*) or JKW. There is a growing recognition that global resources are being consumed at an increasing rate that is not sustainable for the long-term stability of our society. One such commodity material is activated carbon, which is mostly made from coal and imported to the UK in significant quantities (16,000 tonnes per annum). Thus, this research has focussed on investigating the feasibility of utilising waste biomass as a potentially novel and renewable source of activated carbon.

This research required the characterising and assessment of the suitability of green (biomass) waste and JKW as potential feedstock for the production of activated carbon. The JKW biomass was separated into rhizomes (JKWR) and stems (JKWS) and experiments were conducted independently. Some of the characterisation tests conducted included CHNS analysis, thermal degradation behaviour and lignocellulosic content analyses. Using high temperature carbonisation and steam activation, waste biomass was converted into activated carbon. For the purpose of this work, the parameters that were investigated were activation temperature, time and water flow rate. The resulting adsorbents were characterised using established international as well as peer-reviewed methods in order to determine their capabilities as activated carbons. These included BET surface area measurement, butane working capacity, phenol adsorption tests as well as iodine number determination.

Green waste was not suitable to undergo steam activation as it had high ash content and low carbon content. As a result, the research focussed on the carbonisation and subsequent steam activation of JKW. JKW biomass was carbonised at 600°C for 1h and the JKW chars were activated under optimised conditions at 925°C for 1h under 0.5ml/min water flow rate. BET surface areas in excess of 900m^2/g were achieved and this compared very favourably with a benchmark international commercial carbon, Filtrasorb 400. It was observed that increased steam activation temperatures resulted in activated carbons with high degrees of microporosity and the relative microporosity decreased with activation temperature. The carbons were also superior to Filtrasorb 400 in phenol and iodine adsorption tests. Further, Langmuir phenol adsorption capacities of 256 mg/g and 222

mg/g and iodine numbers of 1307 mg/g and 1190 mg/g, respectively were measured for JKWS and JKWR carbons.

There are growing concerns over new water pollutants which arise from plastic use. These molecules are known to exhibit oestrogenic activity and hence, their removal is becoming a priority. The application of these carbons for this purpose was tested, using bisphenol-A (BPA) as a surrogate chemical of interest. JKWS activated carbon was able to perform as well as Filtrasorb 400 in BPA adsorption tests achieving at least 300 mg/g capacity, which is extremely promising for a novel, biomass derived activated carbon.

Overall, this research work has clearly demonstrated that rather than regarding waste biomass, and particularly Japanese knotweed, as a problem, it may be an opportunity to provide the UK with a home-sourced and renewable feedstock for commercial activated carbon. Adopting this feedstock would be a major step towards resolving two UK government goals; reducing waste arisings and creating a more sustainable economy by reducing demand for imported products.

Acknowledgements

I would like to thank the Government of Brunei Darussalam for funding my PhD.

I also want to thank Dr. Geoff Fowler and Prof. Stephen Smith for their guidance and supervision.

Many thanks to the original inhabitants of the EWRE Animal House (Room 409): Steven Goodman, Carsten Künzel and Karl Smith for all their support, chats, jokes, discussions, arguments and companionship throughout the four years. Thank you for all your advice, whether they were solicited or unsolicited. We spent a good four years together and I will certainly miss your presences.

To Fei Zhang, Eliana Athanassiades and Suzan Sharifan; the lovely ladies of EWRE: Thank you for putting up with me for all this time.

To all the newbies: Elizabeth Liu, Robert Wright, Athanasios Bourtsalas, Charikleia Spathi, Nicolas Schaeffer, Claire Villette and Srdjan Stankovic: Good luck! I will miss your friendship and companionship during the last few months of the PhD. I look forward to hearing good things in future!

I cannot forget to thank Carol Edwards for all her advice and help in the laboratory.

My gratitude goes to James MacFarlane of the Cornwall County Council for his help in procuring samples for this research.

The most important acknowledgements go to my beloved parents and sister. I would not have been able to complete this without you.

Contents

i. List of Figures 11

ii. List of Tables 15

iii. List of Abbreviations 17

Chapter 1. Introduction 19

1.1 Waste 19

1.2 Waste Management 20

1.3 Waste Biomass 22

1.3.1 Cellulose 22

1.3.2 Hemicellulose 23

1.3.3 Lignin 23

1.4 Composting 25

1.4.1 Open windrow composting 25

1.4.2 In-vessel Composting 27

1.4.3 Advantages and disadvantages of composting 28

1.5 Landfill 29

1.5.1 Processes occurring in landfills 30

1.5.2 Advantages and disadvantages of landfills 31

Chapter 2. Potential waste biomass candidates 33

2.1 Green Waste 33

2.2 Japanese Knotweed (*Fallopia japonica*) 34

2.2.1 Habitat 35

2.2.2 Reproductive methods 35

2.2.3 Problems associated with JKW 37

2.2.4 Current control methods 38

2.2.5 Disposal options 39

2.3 JKW as waste biomass 40

2.4 Summary 41
Chapter 3. Adsorbents 43
3.1 Porosity 43
3.2 Adsorption 44
3.2.1 Adsorption from the gas phase 44
3.2.2 Type IV isotherms, capillary condensation and the Kelvin equation 47
3.2.3 The Horvath–Kawazoe method 48
3.3 Adsorption isotherms of solutes from aqueous solutions 49
3.4 Mathematical models of adsorption 52
3.4.1 The Freundlich Model 52
3.4.2 The Langmuir Model 54
3.4.3 The BET Model 55
3.4.4 The t-plot 56
3.5 Activated Carbons 59
3.5.1 The manufacture of activated carbons 59
3.5.2 Carbonisation 60
3.5.3 Degradation of lignocellulosic components during carbonisation 62
3.5.4 Activation methods 65
3.5.5 Physical Structure of activated carbon surface 67
3.5.6 Chemical structure of the activated carbon surface 68
3.6 Steam activation of waste biomass 69
3.7 Applications of activated carbons 70
3.8 Summary 71
Chapter 4. Aim and Objectives 73
4.1 Overall aim of the research 73
4.2 Objectives 73
Chapter 5. Characterisation of waste biomass (GW, JKWS and JKWR) 74
5.1 Introduction 74

5.2 Materials 75
5.3 Methods 77
5.3.1 Size reduction 77
5.3.2 Moisture content 78
5.3.3 Lignocellulosic content 78
5.3.4 Ash content 79
5.3.5 Thermal Analysis using TGA 80
5.3.6 CHNS analysis 81
5.4 Results 82
5.4.1 Moisture content 82
5.4.2 CHNS and ash content 83
5.4.3 Lignocellulosic content 84
5.4.4 Thermal analysis using TGA 86
5.5 Summary 92
Chapter 6. Carbonisation 94
6.1 Introduction 94
6.2 Results 96
6.2.1 GW Carbonisation 96
6.2.2 JKW Carbonisation 99
6.3 Carbonisation Summary 105
Chapter 7. Steam activation optimisation 107
7.1 Experimental protocols 108
7.1.1 Bulk char production 109
7.1.2 Elemental analysis of Japanese knotweed and its chars 109
7.1.3 Scanning electron microscopy 111
7.1.4 Characterisation and testing of activated carbons 112
7.1.5 Burn-off 113
7.1.6 Ash content 114

7.1.7 Contact pH 114
7.1.8 Apparent Density 114
7.1.9 N_2 adsorption at -196°C 115
7.1.10 Butane working capacity 116
7.1.11 Iodine number determination 118
7.1.12 Phenol adsorption 119
7.2 Results and Discussion I: Effect of Activation Temperature 122
7.2.1 Elemental analysis using ICP 122
7.2.2 Sample Yields/Burn-off reactions of JKWR and JKWS char with water 124
7.2.3 N_2 adsorption at -196°C 131
7.2.4 Butane working capacity 142
7.2.5 Iodine number determination 146
7.2.6 Phenol adsorption 151
7.2.7 Summary of effect of activation temperature 165
7.3 Results and Discussion II: Effect of activation time and water flow rate 166
7.3.1 Sample Yields/Burn-off reactions of JKWR and JKWS char with water 166
7.3.2 N_2 adsorption at -196°C 169
7.3.3 Pore size distribution 173
7.3.4 Butane working capacity 174
7.3.5 Iodine number 175
7.3.6 Phenol adsorption 177
7.4 Summary 178
Chapter 8. Application testing (Bisphenol-A adsorption) 181
8.1 Introduction 181
8.1.1 BPA removal 184
8.2 Experimental protocols 185
8.2.1 pH and point of zero charge determination 186
8.2.2 Surface chemistry using Boehm titration 186

8.2.3 Ball-pan hardness 188
8.2.4 BPA adsorption 189
8.3 Results and Discussion 190
8.3.1 pH, pH_{PZC} and surface chemistry 190
8.3.2 BPA adsorption kinetics 191
8.3.3 BPA adsorption isotherms 193
8.3.4 Ball-pan hardness 197
8.4 Summary 200
Chapter 9. Overall discussions and suggestions for future work 202
9.1 Chemical characterisation, thermal analysis and carbonisation of waste biomass 205
9.2 Steam activation optimisation 206
9.2.1 Influence of activation temperature 207
9.2.2 Influence of activation time and water flow rate 208
9.3 Application of optimised JKWS and JKWR carbons for BPA adsorption 209
9.4 Conclusions 210
9.5 Suggestions for future work 212
Chapter 10. References 214
Appendix I 227

i. List of Figures

Figure 1-1: The waste hierarchy pyramid. 21
Figure 1-2: A cellulose polymer chain with the cellobiose unit within parenthesis. n is typically 400-1000 (Swatloski et al., 2002). 23
Figure 1-3: Possible molecular structure of lignin (Gregory, 2007). 24
Figure 1-4: Compost windrow being turned by machinery to improve aeration and regulate temperature (Groundgrocer.com, 2012). 26
Figure 1-5: Major stages of degradation in landfills (Waste Management Paper 26B, 1995). 30
Figure 2-1: Clumps of Japanese knotweed growing in the wild (a) and heart-shaped leaves with creamy-white flower panicles (b). 35
Figure 2-2: Exponential spread of Japanese Knotweed on the British Isles., plotted with data from BSBI (2011). 36
Figure 2-3: Distribution of Japanese knotweed in the British Isles at a resolution of 10km^2 (Bailey, 2012). 40
Figure 3-1: The five adsorption isotherm types (I-V) suggested by Brunauer et al. (1940) and Type VI, as suggested by Gregg and Sing (1982). Point B is the point at which the monolayer is completely formed and is taken as the monolayer capacity of the adsorbent. 45
Figure 3-2: IUPAC classification of Type IV hysteresis loop. 46
Figure 3-3: Classification of isotherm shapes for the adsorption of solutes from aqueous solutions (Giles et al., 1974b). 50
Figure 3-4: Typical form of adsorption corresponding to Freundlich equation for aqueous adsorption (Moreno-Castilla, 2004). 53
Figure 3-5: Idealised illustrations of t-plots obtained for (a) non-porous, (b) microporous, (c) mesoporous and (d) micro- & mesoporous materials (Coulter, 1991). 57
Figure 3-6: A typical t-plot (Coulter, 1991). X is the point of origin of extrapolation from second linear region. 58
Figure 3-7: Thermal analysis plot show the different stages of thermal decomposition of biomass in nitrogen atmosphere. Starting temperature was 25°C. 61
Figure 3-8: Thermal degradation of hemicellulose, cellulose and lignin in nitrogen atmosphere (Yang et al., 2007). 63
Figure 3-9: Comparison of three-dimensional crystal lattice of graphite (a) and (b) the turbostratic. 68
Figure 3-10: Functional groups of basic character: (a) chromene (Garten et al., 1957) (b) pyrone-like (Boehm, 1966). 69

Figure 5-1: As-received green waste sample. 75
Figure 5-2: (a) Japanese knotweed rhizome crown with soil, caked in between roots and (b) Japanese knotweed stems. 76
Figure 5-3: (a) JKWR air-dried without soil and (b) oven-dried JKWS. 76
Figure 5-4: (a) JKWR pieces cut by band saw (b) JKWS pieces broken by hand. 77
Figure 5-5: (a) JKWR and (b) JKWS after going through the cross-beater mill with 10mm pre-breaker plates. 77
Figure 5-6: Changes in pH, C:N ratio and temperature during composting (Lester et al., 1999). 84
Figure 5-7: TGA plot of GW, JKWS and JKWR at 1°C/min to 1000°C in nitrogen. 87
Figure 5-8: DTG plots of GW, JKWS and JKWR at 1°C/min to 1000°C in nitrogen. 88
Figure 5-9: Proximate analysis plot for JKWS. (a)moisture content, (b) volatile matter content, (c) fixed carbon content and (d) ash content. 89
Figure 5-10: Proximate analysis plots of GW, JKWS and JKWR. 90
Figure 6-1: Frontal schematic view of Carbolite HTR 11/XX rotary furnace. 95
Figure 6-2: Carbonisation yields of GW at different temperatures. 97
Figure 6-3: Char yield trends for JKWS and JKWR carbonisation using Carbolite HTR 11/75. 100
Figure 6-4: Bio-oil yield trends for JKWS and JKWR carbonisation using Carbolite HTR 11/75. 101
Figure 6-5: Gas yield trends for JKWS and JKWR carbonisation using Carbolite HTR 11/75. 102
Figure 6-6: Amount of volatile matter content remaining in JKWS and JKWR chars carbonised at different temperatures. 104
Figure 7-1: Assembly of apparatus used for apparent density. 115
Figure 7-2: Experimental set-up for BWC determination (Allen et al., 1999) 117
Figure 7-3: Comparison of the alkaline earth metals in JKW biomass, char and acid washed char 123
Figure 7-4: Effect of activation temperature on the burn-off of JKWS and JKWR char at 0.5h activation time and 0.1ml/min water flow rate. 124
Figure 7-5: The decrease of carbon content of produced JKWS and JKWR activated carbons (0.5h activation time and 0.1ml/min water flow rate) as a function of activation temperature. 126
Figure 7-6: SEM photos of JKWR biomass at (a) 140x (b) 1000x (c) 4300x magnification with JKWS biomass at (d) 140x (e) 1000x and (f) 4300x magnification. 128
Figure 7-7: SEM photos of JKWR char at (a) 140x (b) 300x magnification with JKWS char at (c) 140x and (d) 300x magnification. 129
Figure 7-8: SEM photos of JKWR AC 825-0.5-0.1ml at (a) 140x (b) 4300x magnification with JKWS AC 825-0.5-0.1ml at (c) 140x and (d) 4300x magnification. 130

Figure 7-9: Development of BET surface area with burn-off for acid washed and unwashed JKWS AC. 132
Figure 7-10: N_2 adsorption isotherms of JKWS AC at increasing activation temperatures. The desorption branches are shown in dotted lines. 133
Figure 7-11: N_2 adsorption isotherms of JKWR AC at increasing activation temperatures. The desorption branches are shown in dotted lines. 134
Figure 7-12: N_2 adsorption isotherms of F400, the commercial AC used for comparison purposes. . 135
Figure 7-13: Mesopore size distribution for JKWS AC 925-0.5-0.1ml, activated at 925°C for 0.5 hour with 0.1ml/min water flow rate. 139
Figure 7-14: Mesopore size distribution for JKWR AC 925-0.5-0.1ml activated at 925°C for 0.5h with 0.1ml/min water flow rate. 141
Figure 7-15: The effect of increasing activation temperature on butane activity and BWC of JKWS and JKWR carbons activated at 0.5h and 0.1ml/min water flow rate. 142
Figure 7-16: Correlation between the increase in butane activity of produced JKWS and JKWR carbons and the micropore surface area. 144
Figure 7-17: The effect of activation temperature on butane retentivity of JKWS and JKWR carbons activated at 0.5h and 0.1ml/min water flow rate. 145
Figure 7-18: Effect of activation temperature on iodine number. Activation time: 0.5h and water flow rate: 0.1ml/min. 147
Figure 7-19: Effect of activation temperature of X_{BET} of iodine in produced JKWR and JKWS carbons. 150
Figure 7-20: Variation of phenol solution pH after adsorption by JKWS and JKWR carbons. 153
Figure 7-21: Phenol adsorption kinetics of F400. Initial phenol concentration: 200ppm. 154
Figure 7-22: Adsorption isotherms for JKWS activated carbons produced at increasing activation temperatures. Activation time: 0.5h and water flow rate: 0.1ml/min. 155
Figure 7-23: Adsorption isotherms for JKWR activated carbons produced at increasing activation temperatures. Activation time: 0.5h and water flow rate: 0.1ml/min. 156
Figure 7-24: Phenol adsorption isotherm of F400 at different C_e values. 158
Figure 7-25: Langmuir plot of JKWS AC 925-0.5-0.1ml, produced at 925°C for 0.5h at 0.1ml/min water flow rate. 159
Figure 7-26: Freundlich isotherm plot of JKWS AC 925-0.5-0.1ml, produced at 925°C for 0.5h at 0.1ml/min water flow rate. 160
Figure 7-27: Effect of activation temperature on Q_0 of produced JKWS and JKWR carbons. 161
Figure 7-28: Change in Q_0 against BET surface area of produced JKWS and JKWR carbons. 162

Figure 7-29: Values of X_{BET} as a function of activation temperature for produced JKWS and JKWR carbons.....163
Figure 7-30: The effect of water flow rate and activation time on JKWS and JKWR carbons activated at 925°C.....167
Figure 7-31: Carbon contents of (a) JKWS and (b) JKWR carbons produced at 925°C activation temperature.....168
Figure 7-32: N_2 adsorption isotherms for JKWS carbon. 169
Figure 7-33: N_2 adsorption isotherm for JKWR carbon.....170
Figure 7-34: The effect of water flow rate and activation time on the BWC of produced JKWS and JKWR carbons at 925°C. 174
Figure 8-1: Typical flow sheet for drinking water treatment for lowland river. 181
Figure 8-2: Molecular formula of BPA. 182
Figure 8-3: Calibration plot of BPA at 275.5nm wavelength. 191
Figure 8-4: BPA adsorption kinetics isotherms of F400 and optimised JKWS and JKWR carbons. Initial BPA concentration: 200ppm. 192
Figure 8-5: Percentage BPA adsorption by produced carbons and F400. 193
Figure 8-6: Langmuir adsorption isotherms of BPA adsorption using optimised JKW carbons and F400.....194
Figure 8-7: Influence of solution pH on BPA adsorption by optimised JKWS and JKWR carbons and F400.....196
Figure 8-8: SEM photographs of optimised JKWS carbon at (a) 300X, (b) 1100X and optimised JKWR carbon at (c) 300X and (d) 1100x. 199

ii. List of Tables

Table 3.1: Classification of pores. 43
Table 3.2: Adsorption isotherms with associated porosity characteristics (Gregg and Sing, 1982). 46
Table 3.3: Summary of adsorption isotherms associated with aqueous adsorption (Giles et al., 1974a, Giles et al., 1974b). 51
Table 3.4: Comparison of product yields between low temperature pyrolysis (carbonisation) and fast pyrolysis (Mohan et al., 2006). 60
Table 5.1: Moisture content of GW, JKWS and JKWR compared to other different types of waste biomass. Data obtained from Ioannidou and Zabaniotou (2007). SD values determined from 3 measurements. 82
Table 5.2: CHNS values of GW, JKWS and JKWR compared to those of other waste biomass found in literature (Ioannidou and Zabaniotou, 2007). 83
Table 5.3: Lignocellulosic contents of GW, JKWS and JKWR compared to other waste biomass. Data obtained from Basso et al. (2002) and Butterman and Castaldi (2010). 85
Table 5.4: Proximate analysis data of GW, JKWS and JKWR in comparison to other waste biomass. . 91
Table 6.1: Char, bio-oil and gas yields of GW carbonisation at 5°C/min and 1h dwell time. 97
Table 6.2: Char yields from the carbonisation of GW on ash-free basis. 98
Table 6.3: Average char yields of JKWS and JKWR at carbonisation temperature of 600°C for 1h in the Carbolite HTR 11/75. SD values obtained from 3 different measurements. 99
Table 7.1: Measured technical details for Calgon Filtrasorb 400. 108
Table 7.2: Alkaline earth metals content of OTL standard. 122
Table 7.3: Carbon content of JKWS and JKWR biomass, char and activated carbons produced at different activation temperatures (0.5h activation time and 0.1ml/min water flow rate). 127
Table 7.4: Textural properties of JKWS AC produced from acid washed and unwashed chars. 131
Table 7.5: Parameters obtained from N_2 adsorption data of produced JKWS and JKWR AC at increasing activation temperatures. 136
Table 7.6: Pore volume parameters for produced JKWS and JKWR AC at increasing temperatures at 0.5h activation time and 0.1ml/min water flow rate. 140
Table 7.7: Data obtained from determination of BWC of produced JKWS and JKWR carbons. 146
Table 7.8: Surface area characteristics of produced JKWR and JKWS carbons with F400. 149
Table 7.9: Textural characteristics with Langmuir and Freundlich constants for phenol adsorption for JKWR and JKWS ACs. 157

Table 7.10: Surface area analysis and Langmuir model data for JKWS and JKWR carbons produced at different activation temperatures. 164
Table 7.11: Steam activation parameters for JKWR and JKWS char. 166
Table 7.12: Parameters of JKWS and JKWR determined from gas adsorption data. 172
Table 7.13: Effective Horvath-Kawazoe micropore size diameter and mesopore size diameter of produced JKWS and JKWR carbons. 173
Table 7.14: Butane adsorption and desorption characteristics of produced JKWS and JKWR carbon at 925°C activation temperature. 175
Table 7.15: Iodine numbers of produced JKWS and JKWR carbons at 925°C with different activation times and water flow rates. 176
Table 7.16: Langmuir and Freundlich parameters for phenol adsorption by JKWS and JKWR carbons produced at 925°C with different activation times and water flow rates. 178
Table 8.1: Efficiencies of BPA removal techniques found in literature. 185
Table 8.2: Repeatability of the AC yields of JKWS and JKWR activated at optimised conditions (925°C for 1h with 0.5ml/min water flow rate). SD values obtained from 3 different measurements. 190
Table 8.3: Surface chemistry of optimised JKWS and JKWR carbons and F400. 190
Table 8.4: Langmuir parameters for optimised JKWS and JKWR carbons and F400. 195
Table 8.5: Ball-pan hardness numbers of optimised carbons and F400. 197
Table 8.6: Particles size distributions and bulk densities of optimised JKWS and JKWR carbons with precursor char bulk densities. 198

iii. List of Abbreviations

AC	Activated carbon
ASTM	American Society for Testing and Materials
BET	Brunauer, Emmet and Teller
BMW	Biodegradable municipal solid waste
BPA	Bisphenol A
BSBI	Botanical Society of the British Isles
BWC	Butane working capacity
C/L	Cellulose to lignin ratio
C:N	Carbon to nitrogen ratio
CA	Civic amenity
CCS	Carbon capture and sequestration/storage
CHN	Carbon, hydrogen and nitrogen
CHNS	Carbon, hydrogen, nitrogen and sulphur
DSC	Differential scanning calorimetry
DTG	Differential thermogravimetric analysis
EDC	Endocrine-disrupting chemical
EU ETS	European Union Emissions Trading System
EU	European Union
GAC	Granular activated carbon
GHG	Greenhouse gas
GW	Green waste
GWP	Global warming potential
HK	Hovarth and Kawazoe
ICP-OES	Inductively-coupled plasma – optical emission spectrometry
IUPAC	International Union of Pure and Applied Chemistry
JKW	Japanese knotweed
JKWR	Japanese knotweed rhizome
JKWS	Japanese knotweed stem

K_F	Freundlich constant
MC	Moisture content
MSW	Municipal solid waste
NIMBY	Not in my back yard
OTL	Oriental tobacco leaves
PAC	Powdered activated carbon
pH_{PZC}	Point zero charge pH
pK_a	Acid dissociation constant
PTFE	Polytetrafluoroethylene
Q_0	Langmuir adsorption capacity
R^2	Correlation coefficient
R_L	Langmuir constant
RO	Renewables Obligation
RSD	Relative standard deviation
SA	Surface area
SD	Standard deviation
SEM	Scanning electron microscopy
TG	Thermogravimetric analysis
TGA	Thermogravimetric analyser
VOC	Volatile organic compounds
X_{BET}	Proportion of BET surface area
X_M	Proportion of micropore surface area

Chapter 1. Introduction

1.1 Waste

Waste is defined in the EU Waste Legislation Directive 75/442/EEC as "any substance or object which the holder disposes of or is required to dispose of pursuant to the provisions of national law in force". It is also defined as "(of a material, substance, or by-product) eliminated or discarded as no longer useful or required after the completion of a process" (Simpson and Weiner, 2002). In both definitions, it is implied that waste does not have a monetary value and as such, it is simply disposed of, possibly creating environmental and health problems (Williams, 2006).

Although the nature of waste can be heterogeneous, it can be generally categorised into three classifications: hazardous, non-hazardous and inert wastes. Hazardous wastes are wastes that are harmful to human health and/or to the environment, either immediately or over an extended period of time (Environment Agency, 2012c). Examples of hazardous waste include lead acid batteries and fluorescent tubes. Non-hazardous wastes, as its name implies, do not cause any harm to humans and the environment and these could be edible oils, for example. Inert wastes are substances do not undergo any significant physical, chemical or biological transformations and some examples of these are bricks and concrete from demolition sites.

The EU has created a Waste Catalogue, which is a hierarchical list of waste descriptions established by European Commission Decision 2000/532/EC in order to define wastes generated by industrial processes (Environment Agency, 2012a). These are divided into three groups:

- Absolute Entries,
- Mirror Entries and
- Unclassified Entries.

Absolute Entries are wastes which remain hazardous even after treatment, whereas Mirror Entries are only considered hazardous depending on the threshold level (concentration) of any dangerous substance that might be present. Unclassified entries are wastes that do not have any hazardous properties. The classification and definition of waste then gives rise to the possibility of its management so as to have the minimal impact on human and environmental health.

1.2 Waste Management

The EU promotes the sustainable management of waste over disposal because in this way, raw resources are protected and end-of-life materials are prevented from entering the waste stream. One of the main objectives of the 6th EU Environmental Action Programmes (2001-2010) focuses on the sustainable management of natural resources and waste, with the reduction of waste as a specific objective. The actions needed to reach these targets include:

- The development of a strategy for the sustainable management of natural resources by laying down priorities and reducing consumption;
- The taxation of natural waste use;
- Establishing a strategy for waste recycling;
- The improvement of existing waste management schemes;
- Investment into waste prevention and its integration into other EU policies and strategies.

One of the policies arising from the Environmental Action programmes is the EU Waste Framework Directive (75/442/EEC 1975), which was first introduced in 1975 and its most recent iteration is Directive 2008/98/EC.

The general objectives of the EU Waste Framework Directive are (Vehlow *et al.*, 2007):

- The reduction of waste generation,
- The prohibition of uncontrolled discarding discharge and disposal of waste,
- The promotion of integrated waste management systems following the philosophy of avoidance recycling and conversion of wastes with preference to material and energy recovery.

The Directive 2008/98/EC introduces the "polluter pays principle" and the "extended producer responsibility". It incorporates provisions on hazardous waste and waste oils (old Directives on hazardous waste and waste oils being repealed with the effect from 12 December 2010), and includes two new recycling and recovery targets to be achieved by 2020: 50% preparing for re-use and recycling of certain waste materials from households and other origins similar to households, and 70% preparing for re-use, recycling and other recovery of construction and demolition waste (European Commission, 2012a).

The EU waste hierarchy pyramid is seen in Figure 1-1 (Strategy Unit, 2002).

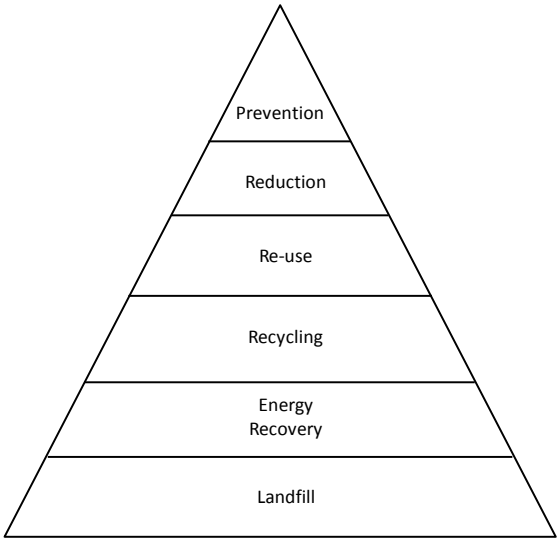


Figure 1-1: The waste hierarchy pyramid.

The prevention of waste is the most desirable option (Tier 1) as this strategy advocates the avoidance of producing wastes during manufacture. If the production of waste is unavoidable then its generation should be minimal (Tier 2). The 're-use' stage (Tier 3) involves collecting and re-using the same discarded product, e.g. glass bottles or retreaded tyres. Re-use also includes new uses for the items that have served their original purpose such as using shredded tyre rubber as mulch in playgrounds. Recycling (Tier 4) is when end-of-life products are processed and re-manufactured into new products and this result in a net saving of energy costs of the recycled material compared to virgin production. Energy recovery (on Tier 5) focuses on capturing the energy released during the incineration of waste or using the landfill gas generated during the degradation processes in landfills. The least desirable option is disposal to landfills (Tier 6). This is due to the production of methane and carbon dioxide, which are greenhouse gases (GHGs), as the wastes degrade in landfills. A further point of concern is the leachate, a potentially toxic liquid residue which may enter the water course (Williams, 2006).

As a direct result of the EU Waste Framework Directive, the EU Landfill Directive was introduced in 1999. This Directive requires EU Member States to commit to a reduction in the landfilling of biodegradable municipal solid waste (BMW) to 75% of 1995 arisings by 2010, 50% by 2013 and 35% by 2020 (Williams and Kelly, 2003). The 2002 Landfill (England and Wales) Regulations implements the EU Landfill Directive, which seeks to prevent or reduce the negative effects of the landfilling of

waste to the environment and human health (Vrijheid, 2000), into UK law. These effects include groundwater pollution, the emission of GHGs and losses of local amenity (Martin and Scott, 2003).

In order to de-incentivise the disposal of waste to landfill, a tax per tonne of waste was introduced with the Landfill Tax Regulations in 1996 (Martin and Scott, 2003). This landfill tax currently stands at £64 per tonne for hazardous and non-hazardous wastes and £2.50 per tonne for inert wastes in the 2012/2013 tax year. It is intended to encourage sustainable waste management via alternative methods such as recycling and re-use (Martin and Scott, 2003).

As of 2010, the UK has met its 2010 Landfill Directive target (DEFRA, 2010b). However, it was noted in a report by the Audit Commission that the UK still sends more waste to landfill than many other western European countries and that at its current rate of use, the landfill sites in the UK will only be viable for 7 more years. Furthermore, methane from landfill sites account for 3% of total UK GHG emissions (Audit Commission, 2008). In order to meet future targets in 2013 and 2020, measures such as recycling, composting, biogas production and material & energy recovery have to be implemented. Landfill has to be the last resort for waste disposal.

One such waste stream that would benefit from diversion away from landfill is biomass, due to the fact that it is biodegradable and as such, its degradation products will contribute to climate change.

1.3 Waste Biomass

Biomass is a term for all organic material that is derived from plants (including algae, trees and crops) and includes all land- and water-based vegetation, as well as all organic wastes (McKendry, 2002). A plant's architecture is made up of lignocellulose, a fibrous material that forms the cell walls of the plant. It consists of three major components: lignin, cellulose and hemicellulose plus inorganic materials. Biomass typically consists of approximately (by weight) 40% cellulose, 25% hemicellulose and 20% lignin (Lange, 2007).

1.3.1 Cellulose

Cellulose is a polymer of glucose, comprising linear (1,4)-D-glucopyranose units, linked in a β-configuration, with an average molecular weight (MW) of about 100,000 (McKendry, 2002). The

long, unbranched structure of cellulose with its intra- and intermolecular bonds contributes to its high thermal stability and mechanical strength, shown in Figure 1-2 (Yang *et al.*, 2007, Theander, 1985). The repeating unit of the cellulose chain is called a cellobiose unit, shown within the square parenthesis.

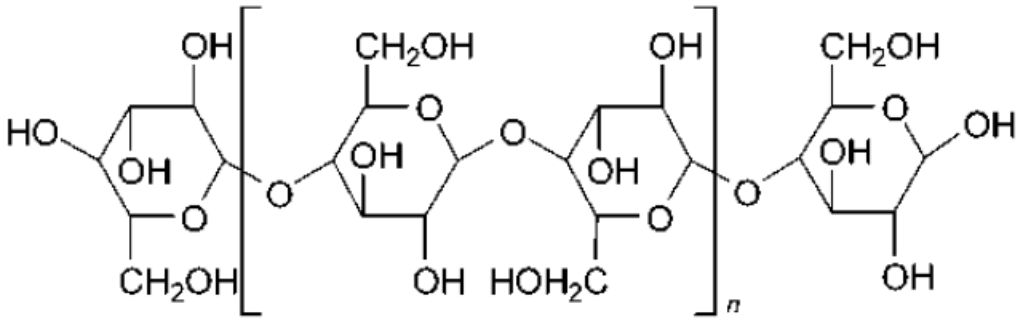


Figure 1-2: A cellulose polymer chain with the cellobiose unit within parenthesis. n is typically 400-1000 (Swatloski et al., 2002).

1.3.2 Hemicellulose

Hemicellulose is a polysaccharide mixture, made up almost wholly out of sugars such as glucose, mannose, xylose and arabinose and methlyglucuronic and galaturonic acids (Yang *et al.*, 2007, McKendry, 2002) with an average MW of less than 30,000 (McKendry, 2002). It is heterogeneously branched with a lower boiling point than the other components, with the branches volatilising easily to form CO, CO_2 and low MW hydrocarbons (Yang *et al.*, 2007). Hemicelluloses differs from cellulose because it consists primarily of xylose and other five-carbon monosaccharides (McKendry, 2002).

1.3.3 Lignin

Lignin can be regarded as a group of amorphous compounds with high MW. They are made up of a three carbon chain attached to six carbon atom ring structures called phenyl-propanes and can have up to two methoxyl side groups attached to the ringed structures (McKendry, 2002). The monomer units form lignin through radical dimersation, oligomerisation, polymerisation and cross-linkage (Mohan *et al.*, 2006). Lignin is responsible for the rigidity of the biomass structure (Suhas *et al.*, 2007).

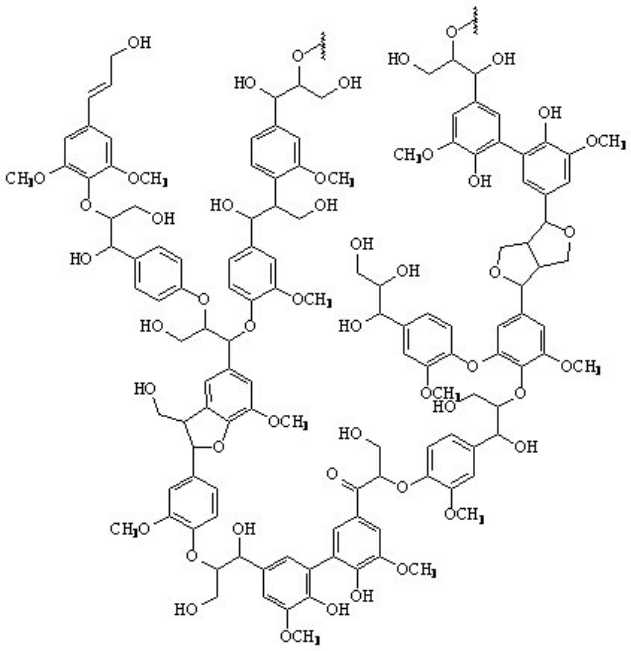


Figure 1-3: Possible molecular structure of lignin (Gregory, 2007).

The varying combination of lignocellulosic content is what determines the physical properties in biomass. For example, woody plant species are typically characterised by slow growth and are composed of tightly bound fibres whereas herbaceous plants are usually perennial with loosely bound fibres, indicating a lower lignin content (McKendry, 2002). Additionally, biomass also contains a variety of minor components such as proteins, terpenic oils, fatty acids/esters and inorganic materials which are mainly based on N, P and K (Lange, 2007).

Biomass is considered to be a sustainable source of renewable energy and it can provide (Lange, 2007):

- Secured access to energy
- Mitigation of climate change
- Development/maintenance of agricultural activities.

However, as the cultivation of biomass increases for energy production, the amount of agricultural residue generated also causes disposal issues. This is especially the case when producing first generation fuels from biomass, called bio-fuels. The reason for this is that only the energy-dense part of the plant such as oil seeds and grain (Moore, 2008) are used to produce energy and the rest of the plant (stalks, branches, hulls, etc.) is discarded, creating waste biomass.

Depending on the nature of the waste biomass, the disposal routes are either composting or disposal to landfill, with the latter the most popular option of waste disposal in the UK (DEFRA, 2011).

1.4 Composting

Composting is a thermophilic, aerobic microbial decomposition process in which the organic substances are degraded by microbes over a period of several weeks to form a dark brown, loamy substance. The biodegradable material is piled onto large, pyramid-like heaps, about 3m high and 9m wide called windrows. In order to ensure that enough oxygen permeates throughout the windrow, it is turned periodically using machinery, as seen in Figure 1-4. Turning also improves heat distribution which regulates the temperature and moisture within the windrow. Composting can be carried out in open windrows, which is the most common or using enclosed reactors called in-vessels.

1.4.1 Open windrow composting

Open windrow is the simplest form of composting but pre-treatment of the waste is needed. The waste is normally ground into 4-7mm particle size to aid aeration (Lester *et al.*, 1999).



Figure 1-4: Compost windrow being turned by machinery to improve aeration and regulate temperature (Groundgrocer.com, 2012).

Composting can be divided into four phases: mesophilic, thermophilic, cooling and maturation or curing. At the start of the process, the green waste is at ambient temperature and is usually slightly acidic. This is due to the simple organic acids produced by acidogenic bacteria, which cause a drop in pH. However, as the indigenous mesophilic organisms multiply, the temperature rises rapidly.

1.4.1.1 Mesophilic stage

When temperatures rise above 40°C, the activity of the mesophiles (microorganisms that grow best at moderate temperatures; 30-35°C) is reduced and degradation is taken over by the thermophilic fungi. The pH turns alkaline and ammonia may be liberated if excess readily-available nitrogen is present. At 60°C, the thermophilic fungi die off and the reaction is sustained by the spore-forming bacteria and the actinomycetes, a group of bacteria responsible for degradation of organic matter at elevated temperatures. At temperatures of over 60°C, waxes, proteins and hemicelluloses are readily degraded, although cellulose and lignin fractions are scarcely degraded. As the rapidly

degradable material is depleted, the reaction rate slows down, until eventually the rate of heat generation becomes less than the rate of heat loss from the surface of the heap and the mass starts to cool down. The bacterial and fungal biomass generated in the initial phases of composting can become food for a succession of higher organisms which may be associated with the process, including protozoa, rotifers and nematodes (Lester *et al.*, 1999).

1.4.1.2 Thermophilic stage

Once the temperature drops below 60°C, the thermophilic fungi from the cooler outside of the mass can re-invade the heap centre and commence their major degradation of cellulose. The hydrolysis and subsequent assimilation of the polymeric material is a relatively slow process; hence the rate of heat generation decreases still further and the temperature falls towards ambient. At about 40°C, the mesophilic organisms recommence activity, either from the germination of heat-resistant spores or by re-invasion from outside. The pH drops again slightly but usually remains slightly alkaline.

1.4.1.3 Cooling and curing stage

The nutrient levels available to the microorganisms in the compost are an important factor affecting the time course of composting. If the C:N (carbon:nitrogen) ratio is greater than 80, composting will generally not occur at all. At just under 80 composting will occur, but slowly. The rate of composting will increase as the C:N ratio falls. This is because at low nitrogen levels, the composting process can only be maintained if the nitrogen is recycled through successive generations of degradative organisms while carbonaceous degradation takes place. This is a slower process than would occur if the nitrogen were in a plentiful, more readily available form. As the nitrogen is conserved within the process, the C:N ratio changes as the composting process proceeds (Lester *et al.*, 1999).

The compost end-product can then be used as a soil conditioner, mulch, topsoil constituent, Turf Dressing, and growing medium (WRAP, 2010).

1.4.2 In-vessel Composting

An alternative to open windrow composting involves mechanical aeration and mixing inside closed reactors and is known as in-vessel composting. This solves the odour problems associated with open

windrow composting as well as shortening the time taken for stabilisation to occur (Lester *et al.*, 1999). In-vessel composting is advantageous because:

- Less land area is required
- The composting process can be more closely controlled
- The effects of weather are minimised
- Less bulking agent is required
- The quality of the product is more consistent
- Less manpower is needed to operate the system and staff exposure to material is minimised
- Process air can be collected and treated to minimise odorous emissions (Environmental Protection Agency, 2000).

Conversely, the disadvantages associated with in-vessel composting are as follows:

- The initial capital investment is high when compared to traditional composting methods.
- Since it is heavily mechanised, there are maintenance costs to consider.
- Due to the large amount of carbonaceous material in storage, the potential for fires must be assessed during facility design. However, this can be avoided by sufficient aeration and moisture (Environmental Protection Agency, 2000).

1.4.3 Advantages and disadvantages of composting

Composting offers several advantages and these are (Environmental Protection Agency, 2000):

- Use of compost as a soil conditioner which will return nutrients to the soil as long as the feedstock is suitable,
- Compost can be handled much easier than some other digested bio-solids,
- It is very friable with a consistency of peat soil and there are no restrictions placed upon it for end-use, provided they meet strict pathogen reduction regulations.

Some disadvantages are listed below:

- Compost from mixed refuse may contain high concentrations of heavy metals, which could potentially require the contaminated compost to be landfilled instead;

- The discharge of bio-aerosols is also a problem. These are biological agents that are released into the atmosphere during turning of windrows and can affect the health of workers at the facilities and the wider public (Marchand *et al.*, 1995, Bünger *et al.*, 2000, Taha *et al.*, 2006). Bio-aerosols can be anything small enough to be emitted into the air, from fungal spores such as *Aspergillus fumigatus* to pollen and dust;

- Composting produces GHGs such as methane, carbon dioxide and nitrous oxide during the decomposition of the organic matter (Jäckel *et al.*, 2005, Fukumoto *et al.*, 2003, Chang *et al.*, 2009, Andersen *et al.*, 2010). Methane has 23 times the Global Warming Potential (GWP) of carbon dioxide and nitrous oxide has 296 times the GWP of carbon dioxide (IPCC, 2001). All of these gases exacerbate the effects of climate change;

- Volatile organic compounds (VOCs) are a large group of anthropogenic or biogenic organic compounds with relative high vapour pressures and these compounds can be potential air pollutants, due to their malodorous and hazardous properties, as well as contributing to global warming, stratospheric ozone depletion and tropospheric ozone formation (Komilis *et al.*, 2004);

- The gaseous emissions are responsible for the odours associated with composts and as a result, large composting facilities face a 'Not in My Back Yard' (NIMBY) attitude from the local inhabitants. Improperly managed open composting facilities could potentially affect sub-surface water tables if they leach (Kjeldsen *et al.*, 2002).

1.5 Landfill

A landfill is an 'engineered method of disposing solid waste on land in a manner that protects the environment by spreading the waste in thin layers, compacting it to the smallest practical volume and covering it with compacted soil by the end of each working day or at more frequent intervals if necessary' (Corbitt, 1999).

In 2009-10, 49% (w/w) of the UK's MSW is landfilled (DEFRA, 2011) and 67% of the MSW collected is biodegradable (Parfitt, 2010) and as such, can and should be diverted away from landfill. There is a

likely trend towards smaller numbers of larger landfills due to the economies of scale, which is attributed to the higher costs of landfilling as a result of the EU Landfill Directive.

1.5.1 Processes occurring in landfills

There are five main stages of degradation in landfills. These are hydrolysis, fermentation, acetogenesis, methanogenesis and oxidation. These are not distinct stages but can occur simultaneously in different sections of the landfill until it stabilises. A summary of the processes is shown in Figure 1-5.

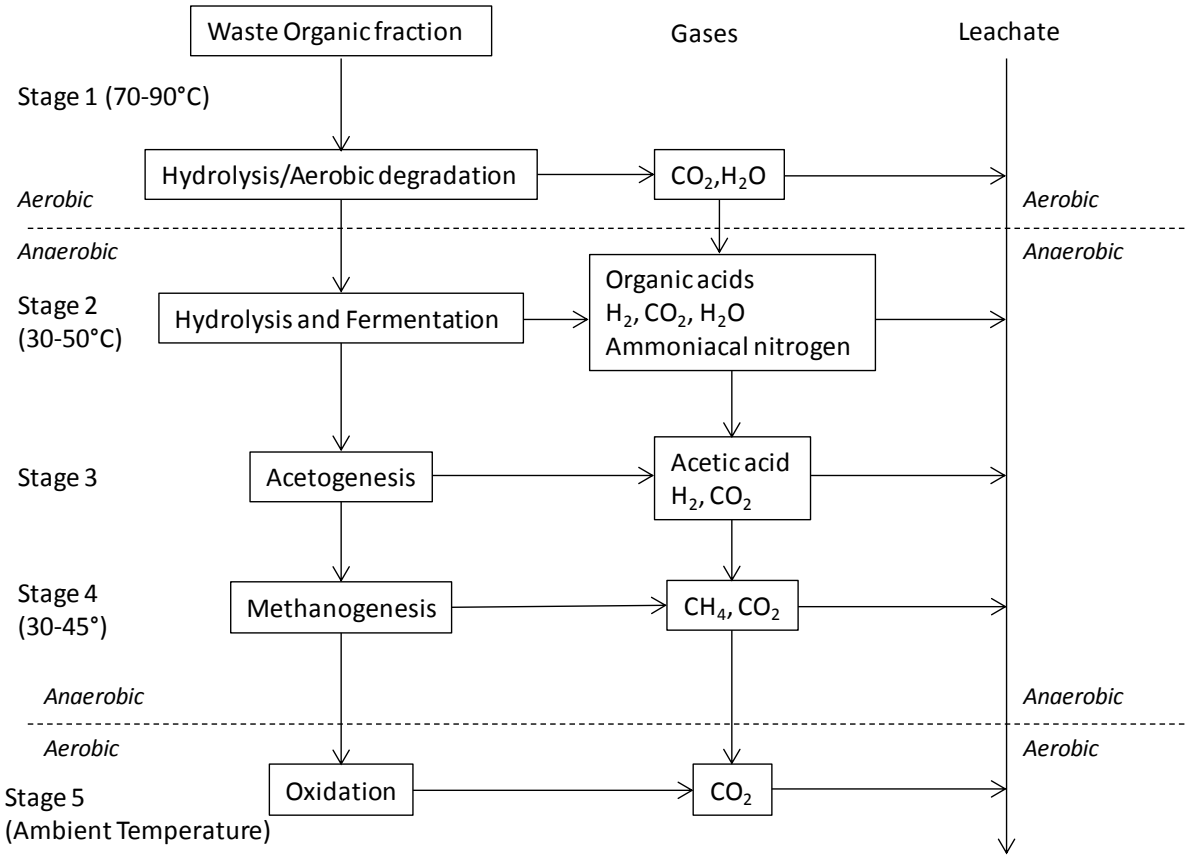


Figure 1-5: Major stages of degradation in landfills (Waste Management Paper 26B, 1995).

At Stage 1 of the degradation process, the hydrolysis stage takes place under aerobic conditions and can last days or weeks, depending upon the amount of air (oxygen) trapped in the void spaces of the compacted waste. During Stage 2, fermentation occurs due to the depletion of oxygen reserves by the activity of aerobic bacteria. Anaerobes begin colonising the landfill and produce sugars from carbohydrates, proteins and lipids.

Acetogenesis is the third stage of the process and the conditions are still anaerobic. This causes the landfill and the leachate to develop acidic conditions which promotes the dissolution of metal ions. The leachate has increased amounts of metal ions and a pH of 4 or less. Hydrogen sulphide may also be produced at this stage.

The fourth stage is methanogenesis and is responsible for the generation of the main component of landfill gas, methane. The methane gas is generated by the methanogens utilising the organic acids and hydrogen as feedstock. As a result, hydrogen levels deplete and leachate pH increases during methanogenesis. The processes that occur are relatively slow and may take several years to complete and does not commence until about 6 months to several years after deposition of the waste in the landfill.

The final stage is oxidation where the degradation reactions end due to a depletion of organic acids used in producing methane and carbon dioxide. At this stage, aerobic conditions set in and aerobes convert residual methane to carbon dioxide and water.

1.5.2 Advantages and disadvantages of landfills

The major benefit of landfilling waste is the relative low cost compared with other disposal options and that a wide variety of wastes are suitable for landfill (Williams, 2006). In fact, landfill is still the final destination of a lot of wastes that have been 'treated' by disposal methods such as incineration. For example, incinerator bottom ash has to be disposed of into landfills.

The collection and utilisation of landfill gas from a well-managed and engineered landfill site is another advantage but landfill achieves a lower conversion efficiency than incineration of about one-third less due to conversion of organic materials into non-combustible gas and leachate (Williams, 2006).

The same landfill gas; which mainly consists of methane, can also accumulate and reach explosive concentrations if not properly managed, causing it to be a cause of concern with older landfill sites. Older landfill sites are also often associated with uncontrolled leakages.

The emission of GHGs from landfills is aggravated by the disposal of biodegradable municipal waste (BMW) into landfills. In order to lessen the gaseous emissions, BMW such as waste biomass can be diverted away and alternative, sustainable methods of waste biomass management could be implemented.

Chapter 2. Potential waste biomass candidates

2.1 Green Waste

Green waste forms part of the waste biomass stream. However, the exact definition of green waste is difficult to establish (DEFRA, 2010a) due to the varied and heterogeneous nature of the waste, as well as the differences in international definitions.

For example, in Australia, green waste consists of garden and food waste (Lundie and Peters, 2005) whereas green waste is defined as consisting of garden and park waste; made up of organic materials such as grass clippings, hedge cuttings, pruning, leaves and wood as well as inorganic materials (soil and stones) in Denmark (Boldrin and Christensen, 2010). However, the National Association of Waste Disposal Officers (NAWDO, 1998) in the UK defines green waste as waste consisting of:

- grass cuttings,
- flower cuttings,
- hedge clippings,
- prunings,
- weeds,
- leaves,
- dead plant material,
- soil-bound roots.

Hence, the definition of green waste used in this project will be the list as defined by the National Association of Waste Disposal Officers. It is generally agreed by researchers that the composition and amount of green waste produced varies seasonally (Boldrin and Christensen, 2010, Andersen *et al.*, 2010). However, there is insufficient data and statistics regarding green waste generation due to the fact that many European countries mixed green waste with food waste (Eurostat, 2005)

Green waste makes up 17-30% of the municipal solid waste (MSW) in the UK (Parfitt, 2002, Parfitt *et al.*, 2001) depending on seasonal variations and local authority policies on collections (Burnley, 2007).

In 2005/06, 2.4 million tonnes of green waste from households was generated in the UK (DEFRA, 2007), with 3.7 million tonnes reported in 2009/10. Green waste is usually composted as a means of disposal. There are three main ways of composting (Jones *et al.*, 2008):

- Home composting,
- Disposal at civic amenity (CA) site and composted by local authority in windrows or in-vessels,
- Collection by local authority for centralised composting.

In 2008, 45% of green waste was home composted, 10% was sent to CA sites and 40% was collected and centrally composted (Jones *et al.*, 2008).

2.2 Japanese Knotweed (*Fallopia japonica*)

A widely-publicised and problematic plant species is Japanese knotweed (*Fallopia japonica*) or JKW (BBC, 2011c). It is a large, herbaceous perennial plant, native to China; Japan; parts of Korea and Taiwan, introduced to the UK during the Victorian era as an ornamental plant and cattle fodder. It is a member of the *Polygonaceae* family and is commonly referred to the following genera: *Polygum, Reynoutria* and *Fallopia* (Beerling *et al.*, 1994). In 1855, a specimen was sent to Kew Gardens and by 1905, the Journal of the Royal Horticultural Society no longer advised the planting of JKW unless it was 'most carefully kept in check' (Child and Wade, 2000).

JKW has smooth tubular stems, which grow up to 3m high, and extend from a large underground rhizome crown which acts as a carbohydrate store during winter months (Shaw *et al.*, 2009). They are usually seen in clumps as shown in Figure 2-1 (a). The stems are light green in colour, often with red flecks ending in creamy-white flower panicles (Beerling *et al.*, 1994), as seen in Figure 2-1 (b). Fully-grown leaves are heart-shaped and are up to 120mm in length as seen in Figure 2-1 (b). It has an extensive underground rhizome system which can extend up to 7m away from the parent plant. The rhizome itself is of a dark brown exterior with a bright orange interior (Child and Wade, 2000).

(a)  (b) 

Figure 2-1: Clumps of Japanese knotweed growing in the wild (a) and heart-shaped leaves with creamy-white flower panicles (b).

2.2.1 Habitat

In the UK, JKW normally occurs in a variety of relatively productive, usually man-made environments such as spoil heaps; along canal, stream and river banks; road verges; railway embankments; vacant lots; neglected gardens; etc. suggesting that human disturbance assists its distribution (Child and Wade, 2000).

The species is able to tolerate acidic soil and soil contaminated with heavy metals, or soils having a high salt content. It also has a high resistance to sulphur dioxide pollution and is often found growing alongside volcanic fumaroles with high atmospheric concentrations of sulphur dioxide (Child and Wade, 2000).

2.2.2 Reproductive methods

The plant spreads itself by asexual reproduction, using the rhizomes to develop several aerial stems. At the end of the growing season, the aerial stems produce underground winter buds at the base of the plants and then wither. The following spring, the winter buds produces new aerial stems, in similar positions and this forms a cluster of stems around the main rhizome. As a result, the patch develops outwards, the shoot density of Fallopia japonica decreases in the centre, exhibiting a phenomenon known as 'central die-back' (Adachi *et al.*, 1996, Bashtanova *et al.*, 2009).

The stems are also capable of reproduction; they have been shown to produce adventitious roots in suitable conditions in as little as a few days, followed by axilliary shoot production if the conditions were maintained (Beerling *et al.*, 1994).

A hypothesis is that the entire population of JKW found in the UK are the consequence of a male-sterile clone (Bailey and Conolly, 2000). Molecular evidence generated by Hollingsworth and Bailey (2000) provide strong evidence to support this hypothesis. The exponential spread of JKW in the UK as seen in Figure 2-2 has been achieved without the advantage of sexual reproduction; which normally contributes to long-distance dispersal (Levin, 2000). The data for the plot in Figure 2-2 was obtained from the Botanical Society of the British Isles (BSBI, 2011).

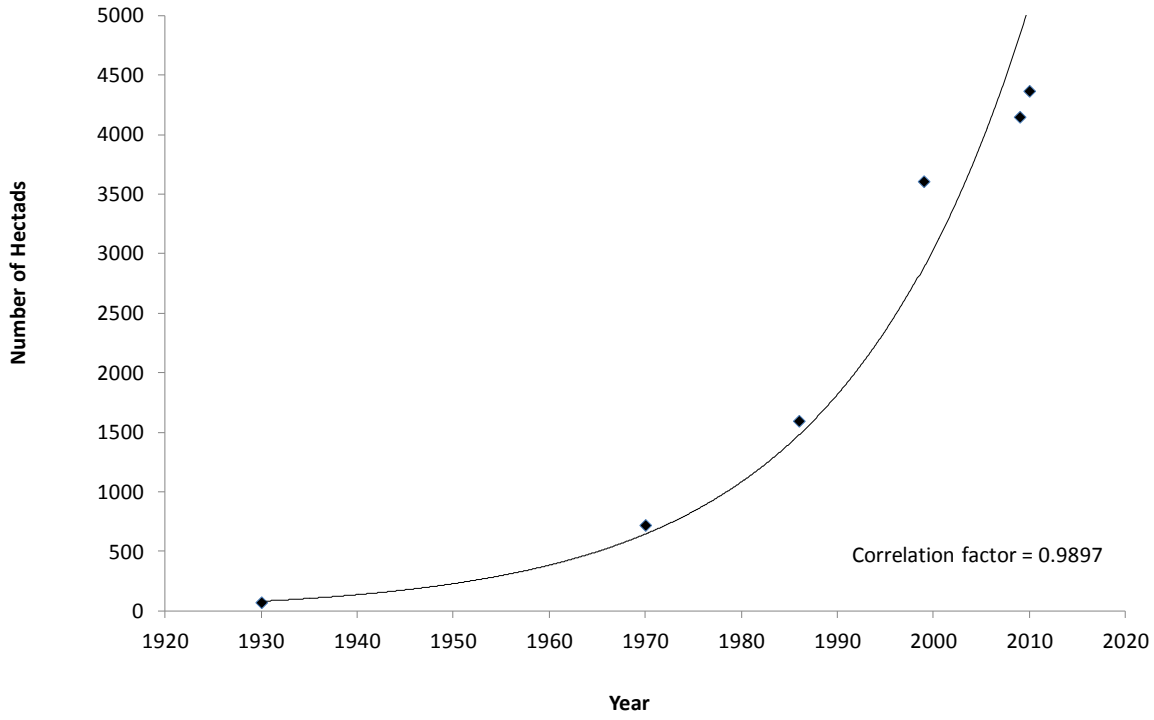


Figure 2-2: Exponential spread of Japanese Knotweed on the British Isles., plotted with data from BSBI (2011).

The initial introduction of JKW into the wild was a result of garden throw-outs and subsequently, from earth-moving projects involving established plants; it has been reported that rhizome fragments as small as 4 grams could produce shoots 70% of the time (Brock and Wade, 1992). Illegal fly-tipping of waste and top soil containing rhizome fragments are also to blame, as well as natural occurrences such as flooding events; which spread the rhizomes downstream (Shaw *et al.*, 2009, Beerling *et al.*, 1994).

Unlike in its native Japan, JKW does not suffer from biological predation in the UK (Bailey, 2003), allowing it to thrive unchecked.

2.2.3 Problems associated with JKW

The presence of JKW is usually correlated with a decrease in biodiversity of the local environment (Maerz *et al.*, 2005, Gerber *et al.*, 2008, Shaw *et al.*, 2009, BBC, 2011a). Studies have also shown that JKW releases allelochemicals from its rhizomes to inhibit the growth of competing species (Weston *et al.*, 2005, Vrchotova and Sera, 2008).

The destruction caused by the propagation of JKW also affects the man-made environment. Cases have been documented of growing shoots breaking through pavements and asphalt; of rhizomes perforating foundations, walls, land drainage works and flood defence structures (Beerling *et al.*, 1994, Child and Wade, 2000). There have also been documented cases where JKW has invaded properties and homes and caused the house price to drop by more than 80% (BBC, 2011b). As a result, some mortgage lenders refuse loans on JKW-infested properties (Driscoll-Woodford, 2010). A recent case where the presence of JKW has affected homes was reported in Guernsey where a site earmarked for social housing was overgrown and development had to be delayed (BBC, 2012). Recently, the Olympic Park site in Stratford has been reported to be affected by the growth of JKW (Bailey, 2012) and it has been estimated to cost up to £70 million to treat (Booth, 2007).

Devon County Council (2010) has compiled a list of the problems caused due to the spread of JKW:

- Damage to paving and tarmac areas
- Damage to flood defence structures
- Damage to archaeological sites
- Reduction of biodiversity by out-shading native vegetation
- Restriction of access to riverbanks for anglers, bank inspection and amenity use
- Increases erosion when the bare ground is exposed in the winter
- Obstructs visibility and access on roads and paths
- Reduction in land values
- Increased risk of flooding through dead stems washed into river and stream channels

- Increased risk of soil erosion and bank instability following removal of established stands in riparian areas
- Accumulation of litter in well established stands
- Aesthetically unsightly
- Expensive to treat (£1/m^2 for a spraying regime over 3 years not including re-landscaping).

JKW is listed as an invasive species in the US, UK and Canada; and where it grows, it is a successful competitor. JKW forms a dense canopy which overshadows and inhibits the growth of other plants (Beerling *et al.*, 1994, Child and Wade, 2000). The plant eventually replaces existing vegetation, including other rhizomatous species such as bracken (*Pteridium aquilinum*).

2.2.4 Current control methods

JKW is listed under Schedule 9, Section 14 of the Wildlife and Countryside Act 1981 and it is an offence to plant or otherwise cause the species to grow in the wild. It is also classed as a 'controlled' waste by the Environmental Protection Act (EPA) 1990, where its disposal must be at a licensed landfill site according to EPA (Duty of Care) Regulations 1991.

JKW growth and spread can be managed using traditional methods such as cutting, grazing, pulling and digging. The goal is to repeatedly deplete the rhizome of its reserves, hindering the plant's ability to regenerate over time (Weston *et al.*, 2005).

Pulling and digging may remove both the rhizomes and the stems but this is dependent upon soil conditions and perseverance and all removed plant material must be burnt to avoid re-growth (Bond and Turner, 2006, Soll, 2004) or buried to a minimum depth of 3m (Bailey and Conolly, 2000). However, this may not be the best practise as it is labour-intensive and it took 3 years to eliminate just a small patch (Bond and Turner, 2006) as well as creating opportunities for spreading plant fragments (Seiger, 1991) and as such, is not recommended for larger patches of JKW (Weston *et al.*, 2005, Bond and Turner, 2006).

Herbicidal treatment is only recommended for use by qualified personnel and preferably, away from water courses and riparian habitats; depending upon the type of herbicides used. The most common herbicides used are glyphosate; 2,4-D amine; triclopyr and picloram. The first two are approved to

be used near water and the latter two are prohibited for use near water. Herbicide treatment must be carried for at least 3 years before JKW stops growing back.

2.2.5 Disposal options

The options available for JKW waste are as follows:

- On-site burning,
- On-site or off-site burial,
- Off-site disposal into landfill.

The Environment Agency recommends burning or burying any cut stem or rhizome material on-site (Environment Agency, 2012b). Burning of any in-situ plants is ineffective and not recommended (Child and Wade, 2000). However, if burning is required, this must take into account any local by-laws and the potential to cause a nuisance or pollution. Permission must be sought from the Environment Agency unless exempt under Paragraph 30 of Schedule 3 of the Waste Management Licensing Regulations 1994; which only permits burning of plant tissue on the land where it was produced and the total quantity burnt does not exceed 10 tonnes in 24 hours. On-site burial must be in trenches with a minimum depth of 5m and lined with root barrier membranes. Once filled, the membrane is also used to cover the waste biomass before being filled with inert fill or top soil. Only JKW that has not been treated with herbicides or with non-persistent herbicides are allowed to be buried. This is to prevent any adverse effects the herbicide might have on the environment (Environment Agency, 2012b).

Cut plant material should be collected and allowed to dry out in small piles on-site. They should be regularly inspected to ensure that they are not spread around by wind or moving construction vehicles. Cut stems are not recommended to be placed in compost heaps (Child and Wade, 2000). As a last resort, if JKW cannot be treated on site by burying or burning, it is sent off for disposal in a landfill.

2.3 JKW as waste biomass

Figure 2-3 shows the spread of JKW around the British Isles (BSBI, 2011). Each dot represents at least one record in a 10km square.

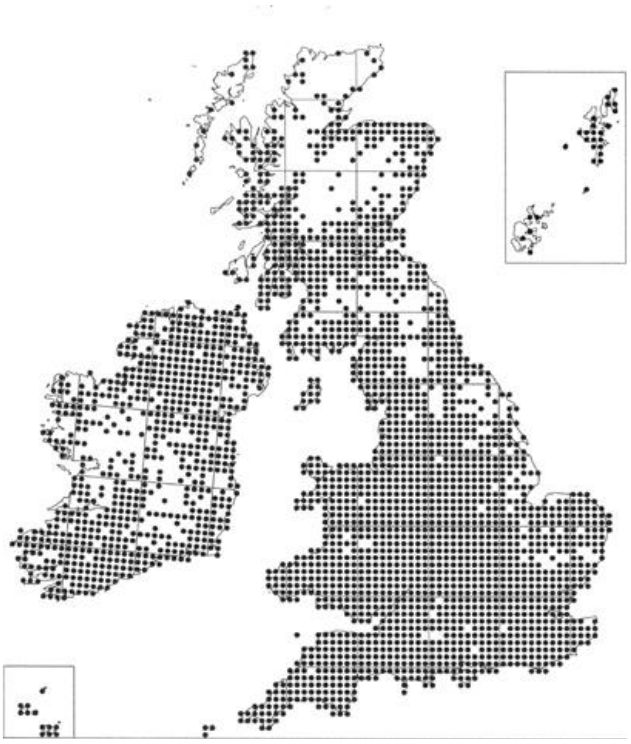


Figure 2-3: Distribution of Japanese knotweed in the British Isles at a resolution of 10km^2 (Bailey, 2012).

JKW is found on nearly every surface on the British Isles, as evidenced in Figure 2-3. In 2 locations in the UK, Brock (1994) has estimated an average occurrence of about 9 tonnes/ha of JKW above-ground stem (JKWS) and about 15 tonnes/ha of JKW underground rhizome (JKWR). From the data collected by Brock (1994) and BSBI (2011), it can be calculated that there are approximately 2.6 x 10^8 tonnes of JKWS and 4.3x10^8 tonnes of JKWR in the UK and Republic of Ireland (see Appendix I for calculations).

The fact that JKW is a successful invasive species is helped by the fact that it is a male-sterile clone of a species (Hollingsworth and Bailey, 2000) and as such, has a very effective vegetative reproduction by woody rhizomes. This enables it to spread widely and quickly to the point that a single stand can occupy a large area (Bailey, 2012)

According to the Non-Native Species Secretariat (2011) , JKW costs the UK economy £166 million annually and it would cost up to £1.56 billion to eradicate JKW in the UK using current methods (DEFRA, 2003). Researchers have listed JKW as the second most economically damaging invasive species in the UK (BBC, 2010).

2.4 Summary

Waste biomass has potential for the recovery of energy and valuable materials. Thus, processing waste biomass for usage has the benefit of eliminating any required pre-treatment processes and disposal with added costs (as in the case of disposal to landfill). Therefore, if alternative treatment/disposal routes can be identified, which produce high-value products from that waste, the proceeds from the end products could partially off-set the costs of treatment and disposal.

Conversion of waste biomass into low-cost, high surface area adsorbents is being proposed in this project to demonstrate the valorisation of JKW, as a sustainable, alternative means to disposal and so diverting it from landfill.

Examination of literature indicated that the potential for converting GW and/or JKW into high surface area adsorbents has previously not been investigated.

Green waste was chosen as a potential precursor due to its status as 'waste' and its wide-spread availability. Even though some of it is composted and sold as a soil conditioner, conversion to adsorbents would yield a much higher market price in a much shorter time span than composting whilst controlling gaseous emissions.

Japanese knotweed was chosen because it is a waste biomass with an unsustainable disposal route (burning, burial or landfill) which leads to atmospheric emissions. Possible valorisation of the end-product would offset the costs of removal and manufacture. Japanese knotweed can be separated into two main parts: the above ground stems (JKWS) and the underground rhizomes (JKWR). Both parts of the plant were characterised for their suitability as precursors to adsorbents.

Both JKWS and JKWR were studied holistically to ensure that the complete plant gets utilised in the alternative "disposal" method and to determine the potential of the entire plant to be converted

into adsorbents. Additionally, both parts of the plant are capable of reproducing and it is vital that the entire plant be rendered inactive by the carbonisation and activation processes to minimise the risk of reproduction.

Chapter 3. Adsorbents

The conversion of waste biomass into activated carbons could prove to be a viable, alternative and sustainable way to manage waste biomass. Activated carbons are a type of adsorbent used in water purification, solvent recovery and odour removal amongst other uses.

Adsorbents are materials that possess surfaces which exhibit affinities for other substances. The term, adsorption as defined by the International Union of Pure and Applied Chemistry (IUPAC) is "the enrichment of one or more components in an interfacial layer", where the component (*adsorbate*) is adsorbed onto the surface (*adsorbent*) (Gregg and Sing, 1982).

3.1 Porosity

Pores act as a passage between the external and internal surfaces of a solid, allowing gases and liquids to pass into, through or out of the solid. Porosity is a collective term for these pores and their distribution in the solid structure (Fletcher, 2008).

Dubinin (1960) first suggested the classification of pores according to their average width and this has since been formally adopted by IUPAC; the classification is shown in Table 3.1 (Gregg and Sing, 1982):

Table 3.1: Classification of pores.

Type of pore	Width
Micropore	Less than 2nm
Mesopore	Between 2nm and 50nm
Macropore	More than 50nm

In micropores, the probability that adsorbate molecules come into contact with each other is very high, owing to the close proximity of the adsorbent walls; thus the amount adsorbed is enhanced (at a certain pressure). Furthermore, micropores make up >95% of the total surface area of common activated carbons (El-Geundi, 1997), depending on the degree of activation. In mesopores, capillary condensation takes place and in macropores, the pores are too wide to sufficiently map an isotherm in detail due to the uniformity of the relative pressures (Gregg and Sing, 1982).

3.2 Adsorption

There are two types of forces responsible for adsorption: physical (physisorption) and chemical (chemisorption) adsorption. Physisorption relies upon electrostatic Van der Waal's forces between the adsorbate and adsorbent molecules and is only apparent over a small range whereas chemisorption is a result of the formation of a chemical bond between the adsorbate and adsorbent. Thus, chemisorption is much stronger. However, only physisorption is considered in this project.

3.2.1 Adsorption from the gas phase

The relationship between the quantity of adsorbate adsorbed and the relative pressure at constant temperature is called the adsorption isotherm and is given by Equation 3-1.

Equation 3-1: $$n = f\left(\frac{P}{P^0}\right)_T$$

Where n=amount adsorbed, P=vapour pressure of adsorbate, P^0=saturation vapour pressure of adsorbate and T= temperature (Gregg and Sing, 1982).

For adsorption from a solution, the adsorption isotherm is the relationship between the quantity of adsorbate adsorbed as a function of the equilibrium concentration in the bulk solution at constant temperature (Faust and Aly, 1998).

Adsorption isotherms assist in the selection of adsorbents for specific applications, in estimating the surface area and adsorption capacities, the volume of the pores and their distribution (Pollard, 1990, Smíšek and Černý, 1970). Five different types of adsorption isotherms (Type I – Type V) have been suggested by Brunauer *et al.* (1940) and these are shown in Figure 3-1. Additionally, a rare adsorption isotherm (Type VI) can also be seen in Figure 3-1 (Gregg and Sing, 1982).

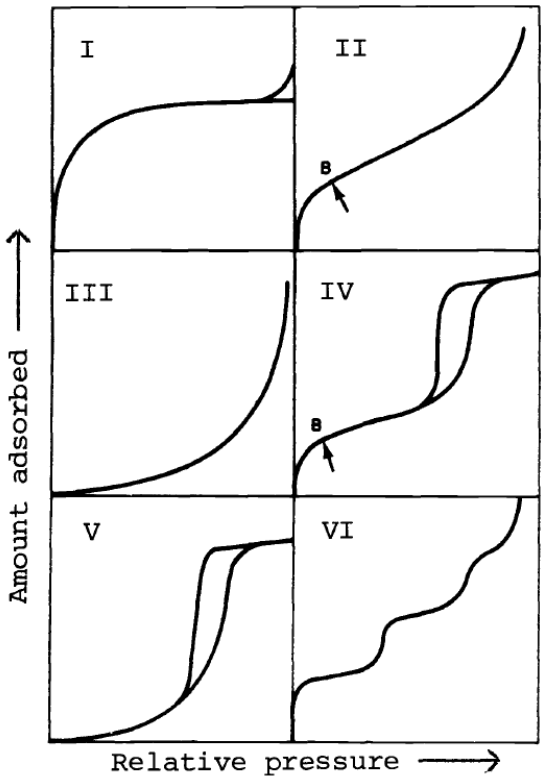


Figure 3-1: The five adsorption isotherm types (I-V) suggested by Brunauer et al. (1940) and Type VI, as suggested by Gregg and Sing (1982). Point B is the point at which the monolayer is completely formed and is taken as the monolayer capacity of the adsorbent.

The isotherm type gives an indication of the adsorption mechanism occurring in the sample (see Table 3.2). A Type I isotherm indicates the filling of micropores, which occurs due to enhanced adsorbent-adsorbate interactions in micropores (Williams and Reed, 2006).

Type II indicates multiple monolayer adsorption; with the thickness of the adsorbed layers increasing with relative pressure and is usually obtained with non-porous or macroporous adsorbents with complete reversal of adsorption possible.

Type III isotherms show that the bonds between adsorbent and adsorbates are weak whereas a Type IV isotherm is an indication of vapour condensation in the pores of a solid, which occurs when the vapour pressure is less than unity. This is an effect known as capillary condensation, which is represented as a hysteresis loop (Gregg and Sing, 1982, Sing, 1985). The hysteresis loop shows that there is a mechanism of pore filling and emptying occurring. Pore filling is represented by the bottom plot line whereas pore emptying is represented by the upper plot line.

A Type V isotherm is similar to the Type III and Type IV isotherms in that it demonstrates weak interactions between the adsorbent and adsorbate with the inclusion of a hysteresis loop that exhibits pore filling and emptying.

Type VI isotherms are associated with layer-by-layer adsorption on a highly uniform surface, the shape being system and temperature dependent (Williams and Reed, 2006).

Point B in Type II and IV adsorption isotherms indicate the end of monolayer filling and the amount of adsorbates adsorbed at Point B is the monolayer capacity of the adsorbent.

Table 3.2: Adsorption isotherms with associated porosity characteristics (Gregg and Sing, 1982).

Isotherm	Type of porosity in solid
Type I	Microporous
Type II	Non-porous/Macroporous
Type III	Weak adsorbent-adsorbate interactions in a non-porous or macroporous solid
Type IV	Mesoporous
Type V	Weak adsorbent-adsorbate interactions in a microporous or mesoporous solid
Type VI	Stepwise multilayer adsorption on a uniform non-porous surface

For Type IV isotherms, the hysteresis loop can be further classified into H1, H2, H3 and H4 types. These are shown in Figure 3-2.

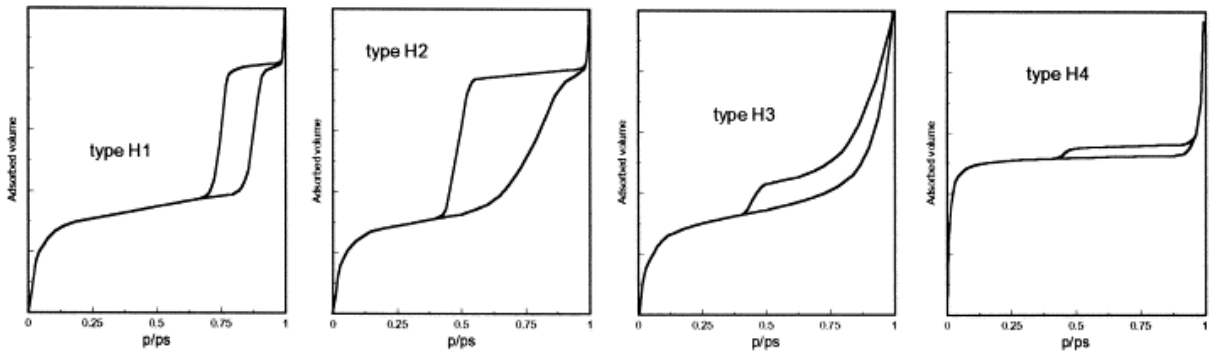


Figure 3-2: IUPAC classification of Type IV hysteresis loop.

H1 type is usually associated with agglomerates or uniform powders, H2 is associated with certain silica gels with poorly defined sizes and H3 and H4 are indicative of adsorbents with slit-shaped pores or plate-like particles (Gregg and Sing, 1982).

3.2.2 Type IV isotherms, capillary condensation and the Kelvin equation

Adsorbate molecules adsorb onto the surface of an adsorbent by layers and once the initial monolayer is completely formed, it is assumed that the next layer is formed or adsorbed on top of the existing monolayer. This causes the isotherm to extend upwards, indicating a higher uptake of adsorbate molecules. Once desorption occurs, a hysteresis loop is formed and does not follow the initial adsorption isotherm path.

It has been proposed by Zsigmondy that capillary condensation occurred within the pores as the pressure of adsorbing gas was increased (Gregg and Sing, 1982). This was based upon the work of Lord Kelvin and the equation in which he proposed that vapour pressure of the gas above a curved surface was different to that above a flat surface.

The Kelvin equation is in turn, based on the Young-Laplace equation which showed that the pressures on opposite sides of the liquid-vapour boundary was related to the curvature r1 and r2 as well as to the surface tension of the liquid (Gregg and Sing, 1982).

$$\Delta P = P^{\alpha} - P^{\beta} = \gamma\left(\frac{1}{r_1} - \frac{1}{r_2}\right)$$

Where: P^{α} = Pressure of liquid

P^{β} = Pressure of vapour

γ = surface tension of liquid

During capillary condensation within a pore, the liquid is in equilibrium with its vapour and thus, mechanical equilibrium (Young-Laplace equation) and chemical equilibrium (Gibb's chemical potential theory) can be expressed as the Kelvin equation:

$$\ln\frac{P}{P_0} = \frac{2\gamma V_L}{RT}\frac{1}{r_m}$$

Where: V_L = molar volume of liquid

R= Gas constant

T= Temperature in Kelvin

r_m = mean radius of curvature

From the Kelvin equation, it is derived that capillary condensation occurs at pressure P, which is determined by r_m. The Kelvin equation is usually used to determine the pore size distribution of adsorbents, in which the desorption branch of the isotherm was used by Barrett *et al.* (1951).

Assumptions used by Barrett *et al.* (1951) include:

i. Pores of adsorbent are open cylinders
ii. The amount of adsorbate in equilibrium with its gaseous phase is retained by the adsorbent as a result of physical adsorption onto the adsorbent walls and capillary condensation in the inner capillary volume.

As the method for pore size distribution determination assumes that the pores are cylindrical and it is known that the shapes of pores are of different forms, pore-size distribution data must be taken with caution and only used for comparative purposes.

3.2.3 The Horvath–Kawazoe method

The Horvath-Kawazoe (HK) method (Horvath and Kawazoe, 1983) was developed to determine the effective pore diameters of pores in microporous solids. The authors assumed that the micropores of the porous solids were slit-like and were confined between two graphitized layers. Horvath and Kawazoe derived their equation using Lennard-Jones functions and the Gibbs free energy of adsorption. The HK equation correlates the effective pore diameter of a micropore to the adsorption isotherm (Coulter, 1991).

Equation 3-2: $$RT\ ln\left(\frac{P}{P^0}\right) = K\frac{N_a A_a + N_A A_A}{\sigma^4(l-d)} \times \left[\frac{\sigma^4}{3\left(\frac{l-d}{2}\right)^2} - \frac{\sigma^{10}}{9\left(\frac{l-d}{2}\right)^9} - \frac{\sigma^4}{3\left(\frac{d}{2}\right)^3} + \frac{\sigma^{10}}{9\left(\frac{d}{2}\right)^9}\right]$$

Where:

R=Ideal gas constant (J/mol)

T=Adsorption temperature (K)

P=Adsorption pressure (Torr)

P^0=Saturation pressure of adsorbate at temperature, T in (Torr)

K=Avogardo's number

N_a=Number of atoms per unit area of adsorbent

N_A=Number of molecules per unit area of adsorbate

A_a=Lennard-Jones constant for adsorbent

A_A=Lennard-Jones constant for adsorbate atom at zero interaction energy

l=Distance between nuclei of two layers (nm)

d_A=Diameter of adsorbent molecule (nm)

d_a=Diameter of adsorbate molecule (nm)

$d=d_A + d_a$ (nm)

σ=Distance between surface and gas atom at zero interaction energy (nm)

The above Equation 3-2 correlates the adsorption pressure to the distance between two layers of the adsorbent and hence, an expression that correlates the volume adsorbed to the effective pore diameter (1-d_a) may be obtained. This is expressed as:

Equation 3-3: $$\frac{W}{W_0} = f(l - d_a)$$

Where:

W=volume of gas adsorbed

W_0=maximum volume of gas adsorbed.

The constants σ, N_a and N_A were obtained from other sources of literature as reported by Horvath and Kawazoe. They proposed that their equation is applicable for pore sizes between 0.35nm and 1.4nm. The plotting of $\frac{W}{W_0}$ against $(l - d_a)$ provides the pore size distribution.

3.3 Adsorption isotherms of solutes from aqueous solutions

Giles *et al.* (1974b) introduced a classification of adsorption isotherms for the adsorption of solutes from aqueous solutions. The classification divides the isotherms, based upon their initial slopes into four main classes named: S, L, H and C classes. These classes relate to behaviour at higher concentrations and are further sub-divided into subgroups of 1, 2, 3, etc. This is shown in Figure 3-3 and explained in Table 3.3.

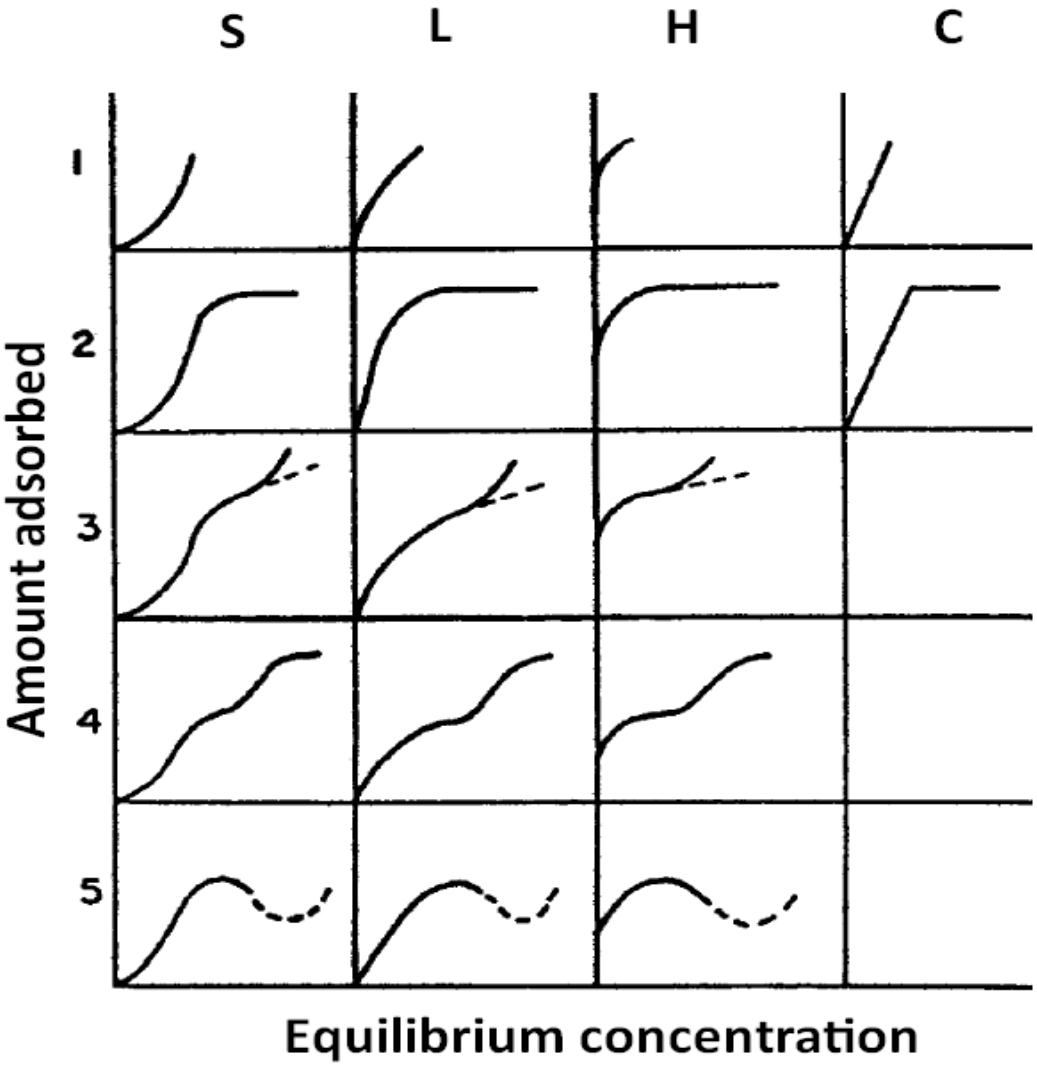


Figure 3-3: Classification of isotherm shapes for the adsorption of solutes from aqueous solutions (Giles et al., 1974b).

Table 3.3: Summary of adsorption isotherms associated with aqueous adsorption (Giles et al., 1974a, Giles et al., 1974b).

Type of Curve	Explanation
S	Activation energy for desorption of the solute molecules is concentration-dependent and/or is diminished by negative effects of the solvent or the presence of a second solute in the solution.
L	Valid for either mono-disperse or aggregated solutes; most common isotherm.
H	Extremely strong adsorption of charged solute molecules onto oppositely-charged surfaces, resulting in a long plateau.
C	Non-ionic molecules interact with hydrophobic molecules such as when dyes are adsorbed onto hydrophobic fibres.
Sub-group 1	Insufficiently concentrated solution to complete the monolayer.
Sub-group 2	Monolayer has been formed and the effective surface covered by each solute molecule and hence, the capacity can be determined from the height of the plateau.
Sub-group 3	Absence of a plateau is caused by the formation of subsequent hydrophobic layers on top of the first hydrophobic monolayer.
Sub-group 4	Presence of a second plateau which is due to the completion of a second monolayer.
Sub-group 5	Adsorption by high solute concentrations where solute-solute forces can caused some desorption

Therefore, the aqueous adsorption isotherms are able to aid in the identification of the adsorption mechanism, differentiation between adsorption of mono-disperse and associated species and specific surface measurement of finely divided or porous solids (Giles *et al.*, 1974a).

3.4 Mathematical models of adsorption

The adsorption theories used in this study were the Freundlich, Langmuir and BET theories. Additional models used to assist in the interpretation of gas adsorption data are the t-plot and the Horvath and Kawazoe equation.

3.4.1 The Freundlich Model

The Freundlich (1906) isotherm is often described as a limiting form of the Langmuir isotherm and is perhaps one of the most widely-used mathematical description of adsorption in aqueous systems (Faust and Aly, 1998).

The Freundlich equation is an empirical expression that encompasses the heterogeneity of the surface and the exponential distribution of sites and their energies (Faust and Aly, 1998).

For adsorption from solution, the Freundlich equation is expressed as seen in Equation 3-4:

Equation 3-4: $$\frac{x}{m} = K_F C_e^{\frac{1}{n}}$$

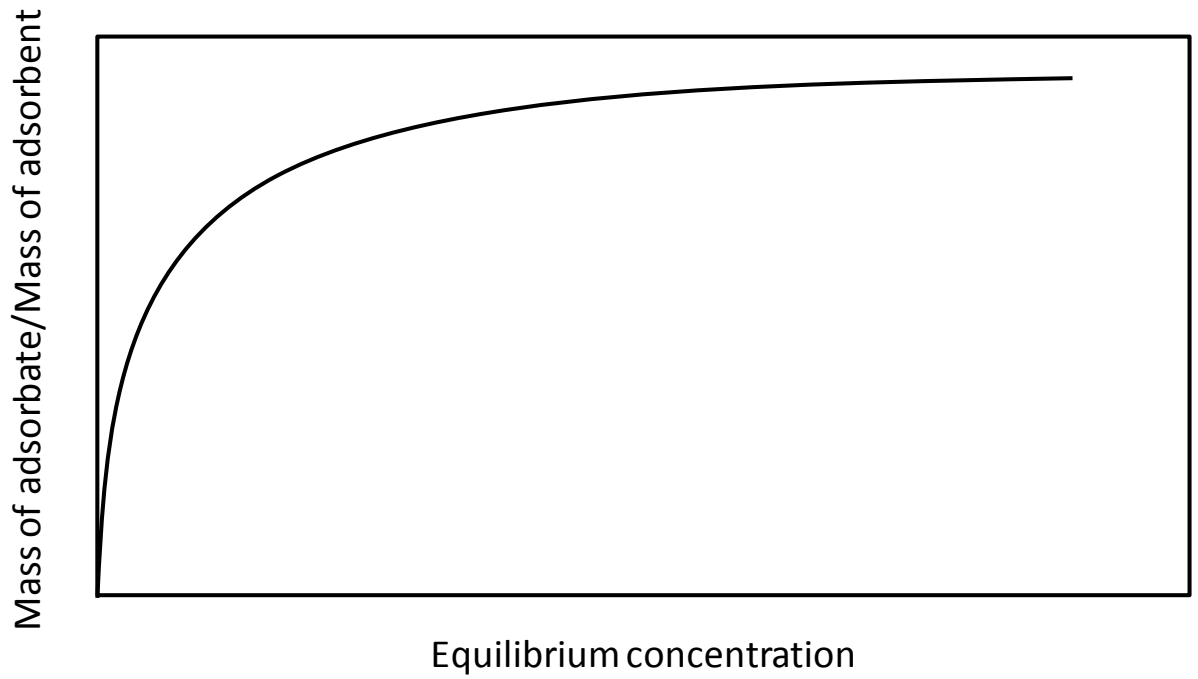


Figure 3-4: Typical form of adsorption corresponding to Freundlich equation for aqueous adsorption (Moreno-Castilla, 2004).

The plot in Figure 3-4 shows a typical aqueous adsorption isotherm according to the Freundlich equation (Equation 3-4).

The linearised form is expressed as:

Equation 3-5: $$\ln \frac{x}{m} = \ln K_F + \frac{1}{n} \ln \mathrm{C_e}$$

Where: x/m=amount of adsorbate (x) adsorbed by amount of adsorbent (m) and C_e = equilibrium concentration of adsorbate. K_F is a rough indicator of the adsorption capacity (Hameed and Rahman, 2008).

The values of n and k can be obtained from the slope (1/n) and intercept (ln k) of the linear plot ($\ln(\mathrm{x/m})$ vs $\ln \mathrm{C_e}$) given by Equation 3-5 and n is always greater than unity, indicating favourable adsorption conditions (Hameed and Rahman, 2008, Fierro *et al.*, 2008).

Steep slopes ($1/\mathrm{n}$ close to 1) indicate high adsorptive capacity at high equilibrium concentrations covered by the isotherm. Relatively flat slopes ($1/\mathrm{n} \ll 1$) indicate that the adsorptive capacity is only slightly reduced at the lower equilibrium concentrations (Faust and Aly, 1998).

3.4.2 The Langmuir Model

Langmuir (1918) derived his kinetic equation to account for gaseous adsorption, with the assumption that adsorption was only limited to a single molecular level and that the adsorbent gas was an ideal gas adsorbed onto an idealised surface. It was the first theoretically developed adsorption isotherm and as such, many subsequent theories are either based on the Langmuir equation or developed using the theory (Bansal, 2005).

Equation 3-6: $$\frac{V}{V_m} = \frac{bp}{1+bp}$$

Where: V=volume of gaseous adsorbate adsorbed; V_m = volume needed for single molecular coverage of adsorbent; p=gaseous pressure and b=empirical constant.]

Equation 3-6 assumes that (Smíšek and Černý, 1970):

- The surface of the adsorbent is homogenous, with equal adsorbing sites equal; i.e., any adsorbate particle striking the surface has the same probability of being adsorbed at any site;
- There are no interactions between adsorbed molecules on adjacent sites;
- Each site accommodates only one adsorbate molecule and only a monolayer of molecules form on the adsorbent surface.

For adsorption from solution:

Equation 3-7: $$\frac{x}{m} = \frac{Q_0 b C_e}{1+bC_e}$$

Where: $\frac{x}{m}$=Amount of adsorbate adsorbed per unit of mass adsorbent; C_e =Equilibrium concentration of adsorbate; Q_0 = monolayer capacity of adsorbent.

The linear form (Hameed and Rahman, 2008) of the Langmuir model can be represented by:

Equation 3-8: $$\frac{C_e}{\left(\frac{x}{m}\right)} = \frac{1}{Q_0 b} + \frac{C_e}{Q_0}$$

When $\frac{C_e}{\left(\frac{x}{m}\right)}$ is plotted against C_e, a straight line should result, possessing slope $\frac{1}{Q_0}$ and y-intercept, $\frac{1}{Q_0 b}$.

Reliable Q_0 values can only be obtained for Type I isotherms (Section 3.1) as mentioned by Faust and Aly (1998) and these values represent the Langmuir monolayer capacity of the adsorbent.

The essential characteristics of the Langmuir isotherm can be given by a dimensionless separation factor, R_L (Hall *et al.*, 1966) and is defined by:

Equation 3-9: $$R_L = \frac{1}{1+bC_0}$$

Where b=Langmuir constant and C_0 = highest phenol concentration (mg/l).

The value of R_L determines whether the type of isotherm is favourable ($0<R_L<1$), linear ($R_L=1$), unfavourable ($R_L>1$) or irreversible ($R_L=0$) (Hameed and Rahman, 2008).

3.4.3 The BET Model

The BET equation (Brunauer *et al.*, 1940) was developed from Langmuir's model and is used to describe multilayer adsorption. It assumes that:

- Only the first layer of adsorbate molecules is bound by Van der Waal's forces to the adsorbent surface;
- Subsequent layers are not bound by Van der Waal's forces and thus, have the same properties as in a liquid state;

- Heat of adsorption (of the adsorbate) is equal to the heat of condensation (of adsorbate) for all layers above the first monolayer;
- and under saturation pressure, an unlimited (infinite) number of layers can be adsorbed onto the adsorbent surface (Smíšek and Černý, 1970).

The BET equation is shown below:

Equation 3-10: $$\frac{V}{V_m} = \frac{C\frac{P}{P^0}}{\left(1-\frac{P}{P^0}\right)\left(1-\frac{P}{P^0}+\frac{P}{P^0}C\right)}$$

Equation 3-10 can then be re-arranged to form the linear equation:

Equation 3-11: $$\frac{\frac{P}{P^0}}{V\left(1-\frac{P}{P^0}\right)} = \frac{1}{V_m C} + \frac{C-1}{V_m C}\frac{P}{P^0}$$

Where: P/P^0 = relative gas pressure; C= BET constant, related to the enthalpy of adsorption; V= volume of gas adsorbed and V_m= volume of gas needed to form monolayer. A plot of $\frac{\frac{P}{P^0}}{V\left(1-\frac{P}{P^0}\right)}$ against $\frac{P}{P^0}$ should give a straight line with gradient equal to $\frac{C-1}{V_m C}$ and a y-axis intercept of $\frac{1}{V_m C}$.

3.4.4 The t-plot

The t-plot analysis method was developed by Lippens and de Boer (1965) as a method of distinguishing between mesoporous surface areas and microporous volumes.

The method consists of plotting the adsorption isotherm in terms of the volume of gas adsorbed against the statistical film thickness, t. The statistical film thickness is the thickness of the layer of gas; based on the assumption that gas molecules are adsorbed layer-by-layer until all available pores are filled (Coulter, 1991). Figure 3-5 shows the four idealised scenarios that can occur when plotting volume of gas adsorbed against film thickness, t.

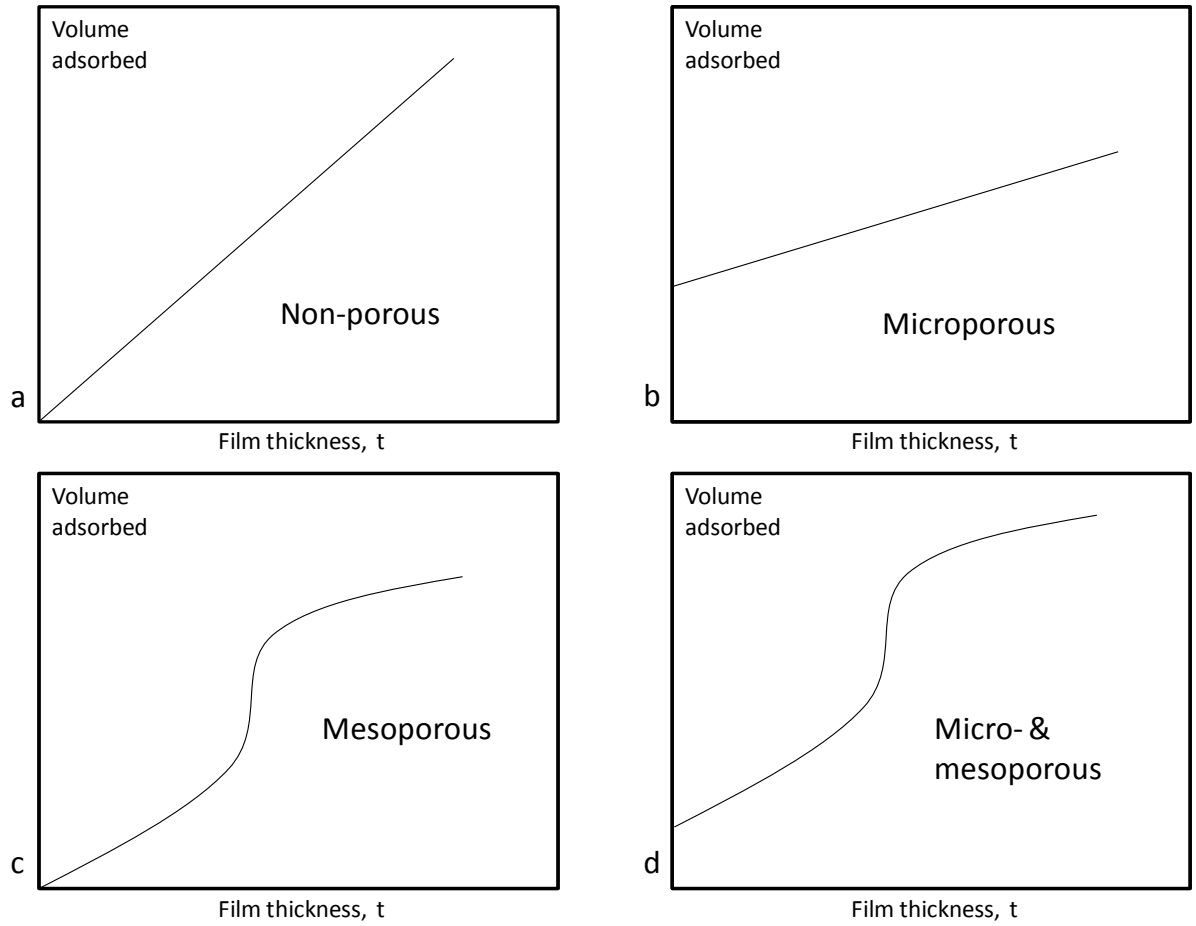


Figure 3-5: Idealised illustrations of t-plots obtained for (a) non-porous, (b) microporous, (c) mesoporous and (d) micro- & mesoporous materials (Coulter, 1991).

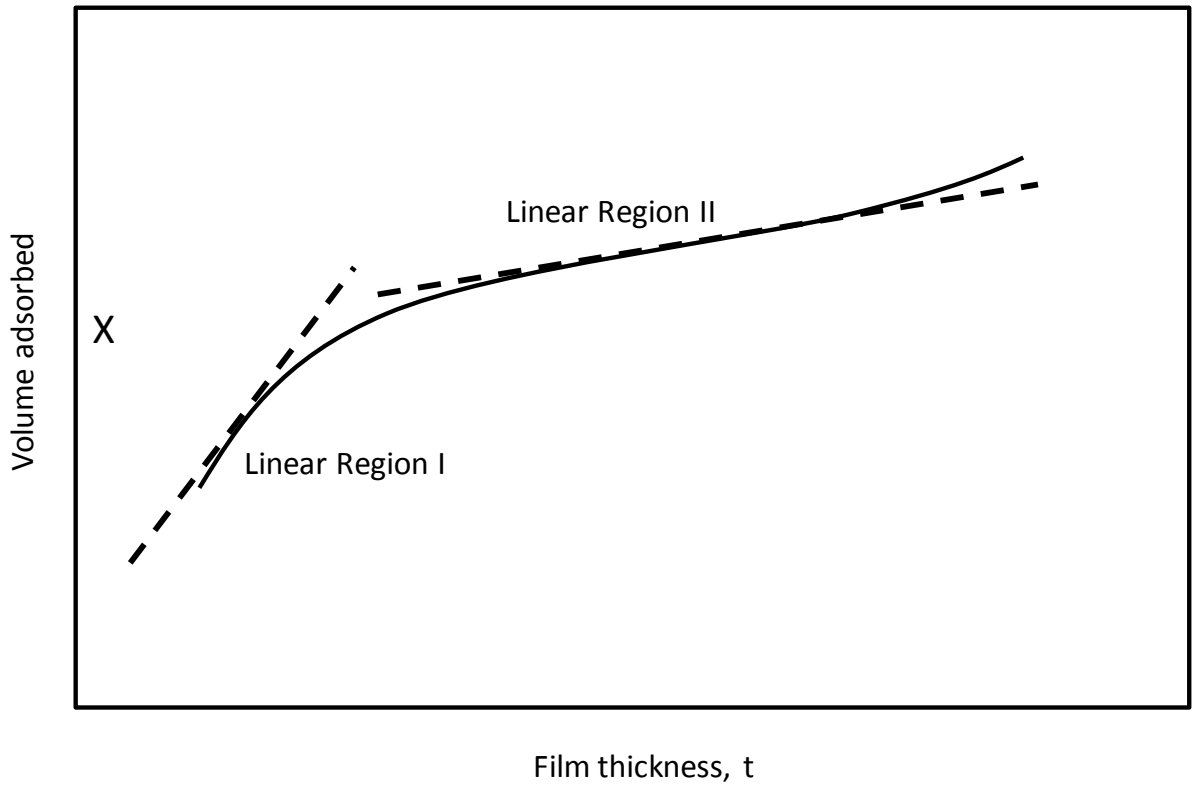


Figure 3-6: A typical t-plot (Coulter, 1991). X is the point of origin of extrapolation from second linear region.

Sing (1967) explained that the first linear region is due to the filling up of micropores and surface coverage of larger pores; the second linear region is due to layer-by-layer filling taking place in the meso- and macropores, but not in micropores.

To establish the micropore volume, a straight line is extrapolated from the second linear region to the y-axis at point X (Merchant and Petrich, 1993). The value is then multiplied by the ratio of the gas and liquid densities of the adsorbate (0.00156 for nitrogen) to obtain a value in cm^3 per gram of solid (Coulter, 1991).

Meso- and macropore surface area is obtained by multiplying the slope of the second linear region extended through the origin (Merchant and Petrich, 1993) by 15.47 to obtain a value in m^2 per gram of solid (Coulter, 1991).

Total surface area, according to the t-plot is obtained by extrapolating the first linear region to origin and multiplying the slope of this line by 15.47 to convert to m^2 per gram.

It has been stated that the t-plot method is limited due to its reliance on the BET theory for monolayer volume and is limited to adsorbents with a well defined Point B (Fowler, 1995). As such, it will be used for comparison purposes only in this study.

3.5 Activated Carbons

Activated carbons (AC) is a term that includes a wide range of amorphous carbonaceous adsorbents that exhibit a high degree of porosity and an extended inter-particulate surface area (Bansal, 2005). Historically, activated carbons have been used by the ancient Egyptians for water purification and medicinal purposes. In recent times, they were used for purifying drinking water through to purifying sugar; from adsorbing phosgene gas during World War I to controlling odours in refrigerators. Activated carbons are also administered to counteract certain kinds of ingested food poisoning by adsorbing toxins (Marsh and Rodríguez-Reinoso, 2006).

Activated carbons are one of the most versatile materials in controlling pollution of water and gas effluents. In 1995, it cost between US$0.70 and US$1.75 per kilogram (Marsh and Rodríguez-Reinoso, 2006) with estimates of the worldwide sales of US$1 billion in 1997 (Humphrey and Keller, 1997) and worldwide usage is predicted to increase to 1.9 million tonnes in 2016 (Freedonia, 2012). The per capita consumption of activated carbons per year is 0.5kg in Japan, 0.4kg in the US, 0.2kg in Europe and 0.03kg in the rest of the world (Bansal, 2005) and as the rest of the world moves towards better emission controls and cleaner water, usage of activated carbons will undoubtedly increase.

3.5.1 The manufacture of activated carbons

Activated carbons are made by 'carbonising' a suitable feedstock such as coal or biomass and then by 'activating' the char made during carbonisation. It may be produced as powdered activated carbon (PAC) or granular activated carbon (GAC). PAC usually has particle size distributions such that at least 80% is less than 44µm (Faust and Aly, 1998), whilst GAC's are between 0.5mm and 5mm (Suhas *et al.*, 2007). Suitable feedstocks usually have the following criteria (Marsh and Rodríguez-Reinoso, 2006, Ioannidou and Zabaniotou, 2007, Bouchelta *et al.*, 2008):

- Low inorganic matter content

- Good availability and low cost
- Consistency
- High carbon content
- Low degradation during storage
- Ease of activation.

3.5.2 Carbonisation

Carbonisation is the process of thermal degradation of a material in an inert atmosphere. It is also known as pyrolysis and during the pyrolysis of biomass; the lignocellulosic components decompose into the products formed (González *et al.*, 2003). These are a black solid known as char; a tarry liquid known as bio-oil and synthesis gas or 'syngas'.

The carbonisation process can be controlled by varying the temperature, heating rate or dwell (char residence) time; resulting in varying the yields of the products formed. Generally, a low carbonisation temperature (<500°C) and low heating rate favours the formation of char whereas a high carbonisation temperature with a faster heating rate increases the yield of the volatile substances, as seen in Table 3.4. Table 3.4 also shows the yields of other products obtained from the carbonisation of biomass. However, the definition of a "slow" heating rate versus a "fast" heating rate is arbitrary.

Table 3.4: Comparison of product yields between low temperature pyrolysis (carbonisation) and fast pyrolysis (Mohan et al., 2006).

Component	Low temperature pyrolysis (carbonisation)	High temperature pyrolysis
Char yield (%)	35	12
Bio-oil yield (%)	30	75
Gas Yield (%)	35	13

In Figure 3-7, it can be seen that three steps occur: The initial phase of carbonisation starts from temperatures up to approximately 200°C as (a) the feedstock is being dried. Above this temperature, the biomass material begins to degrade, with the evolution of carbon monoxide, carbon dioxide and acetic acid. Exothermic decomposition starts in the region of 200-300°C, during which a considerable amount of tar, methanol and other substances are formed (b). This is usually seen as an efflux of

volatiles; in the form of cloudy gas being produced in the reactor. Consolidation of the char structure occurs between 500-1000˚C with a very small weight loss (c) and the biomass carbon content is usually about 80% (Smíšek and Černý, 1970, Rodriguez-Reinoso and Molina-Sabio, 1992).

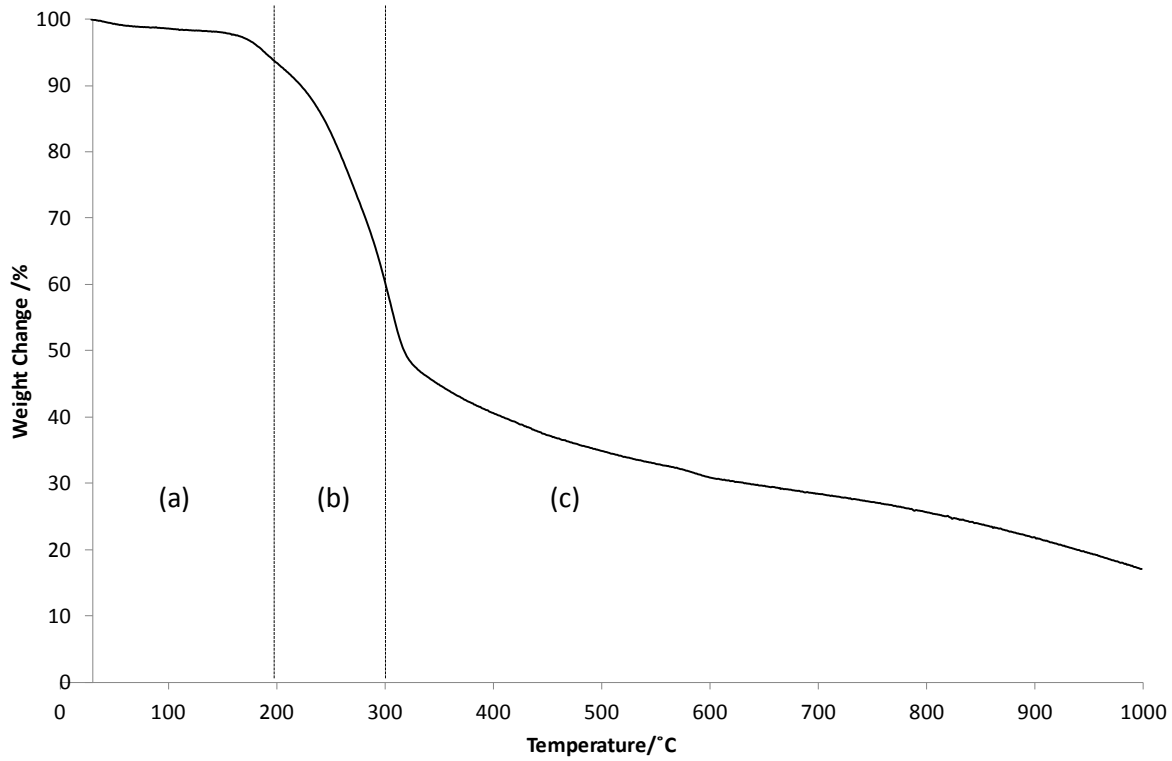


Figure 3-7: Thermal analysis plot show the different stages of thermal decomposition of biomass in nitrogen atmosphere. Starting temperature was 25°C.

3.5.2.1 Char

Carbonisation yields comparatively higher amounts of char than volatiles and is favoured by processes requiring high char yields. It is formed by carbonisation and devolatilisation processes, as previously mentioned in Section 3.5.2. The char can be used as a fuel source (Abdullah and Wu, 2009), soil amendment (Lehmann *et al.*, 2006), liming agent (Fowles, 2007, Laird *et al.*, 2009), carbon sequestration agent (Laird, 2008, Fowles, 2007, Lal, 2004) and activated carbon precursor (Azargohar *et al.*, 2006, Ioannidou and Zabaniotou, 2007, Marsh and Rodríguez-Reinoso, 2006, Mohan *et al.*, 2006).

3.5.2.2 Bio-oil

Bio-oil obtained from carbonisation reactions are a dark brown, mobile liquid with approximately half the calorific value of transport fuels (Bridgwater *et al.*, 1999, Czernik and Bridgwater, 2004). They are a miscible, multi-component mixture of polar organics and water due to its formation during depolymerisation and fragmentation reactions of lignin, cellulose and hemicellulose (Bridgwater *et al.*, 1999). Rapid quenching then solidifies the intermediate products of the pyrolysis reaction, ensuring that no further reactions occur that might decrease yield (Mohan *et al.*, 2006). Bio-oils can be used as precursors for chemicals production, a substitute for fuel oil or diesel in boilers, furnaces, engines and turbines for electricity generation (Mohan *et al.*, 2006). Some key differences between bio-oils and transport fuels are the high oxygen and water content of bio-oils; both of which reduces the calorific content, making direct usage without modification difficult.

3.5.2.3 Syngas

Syngas is the non-condensable fraction of the carbonisation process and contains varying amounts of hydrogen, carbon monoxide, carbon dioxide, methane and other low molecular weight hydrocarbons. Most syngas produced is used for the synthesis of ammonia for fertiliser production. It is also used as a source of hydrogen in oil refining processes and methanol production (Soetaert and Vandamme, 2009). Another use of syngas is in the Fischer-Tropsch process, which uses syngas as a feedstock to produce liquid hydrocarbons (Andre and Mark, 2004).

3.5.3 Degradation of lignocellulosic components during carbonisation

In the context of the lignocellulosic content of biomass, Kucuk and Demirbas (1993) observed that hemicelluloses are the first component to break down during carbonisation at temperatures between 197-257°C, celluloses at 237-347°C and lignin at 277-497°C. However, Yang *et al.* (2007) noted that in their experiments using a thermogravimetric analyser (TGA) that hemicellulose decomposes between 220-315°C, cellulose decomposes between 315-400°C and lignin decomposes over a wide range of temperatures; from 100-900°C as observed in Figure 3-8. This was explained by different inherent structures and chemical nature of the 3 components (McKendry, 2002): Hemicellulose was found to contain more C=O bonds; cellulose had higher contents of OH and C-O bonds and lignin had more methoxyl-O-CH_3 groups (Yang *et al.*, 2007).

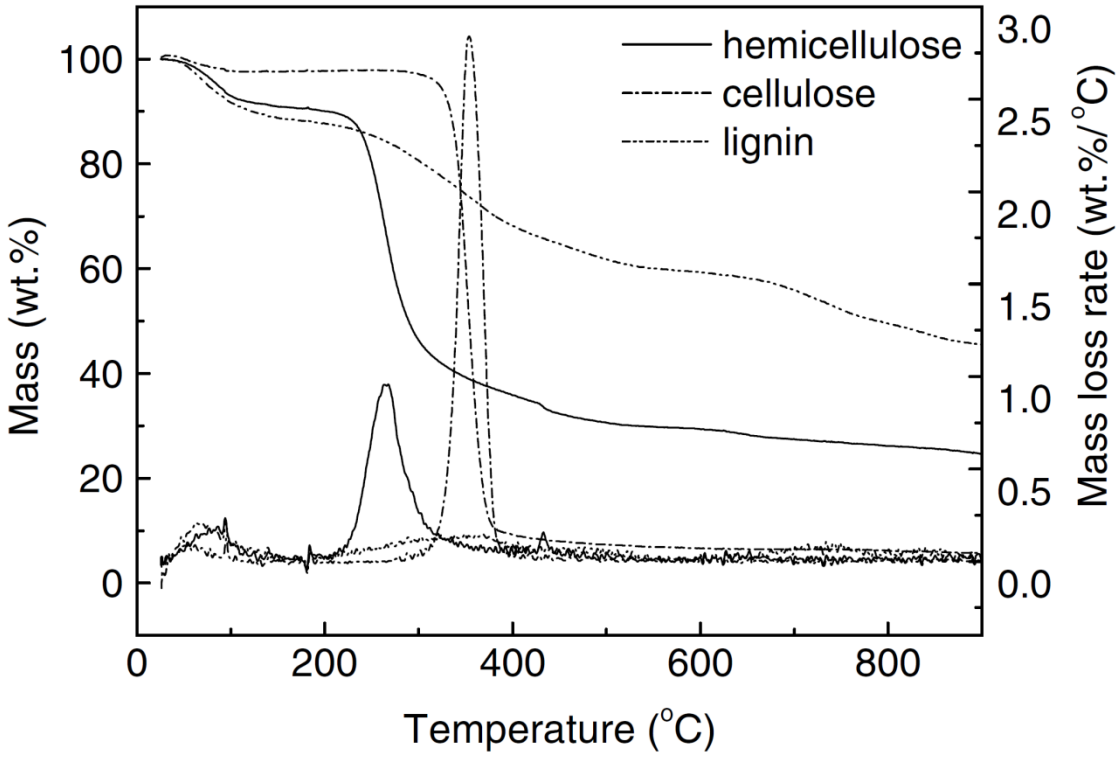


Figure 3-8: Thermal degradation of hemicellulose, cellulose and lignin in nitrogen atmosphere (Yang et al., 2007).

Cellulose degrades via two main different pathways. The first pathway, which occurs at the lower temperature range (<300°C) includes:

- Bond scission
- Production of free radicals
- Elimination of water forming anhydrocellulose
- Formation of carbonyl, carboxyl and hydroperoxide group
- Evolution of carbon monoxide and carbon dioxide
- Production of charred residue.

The formation of anhydrocellulose at <300°C gives a higher bio-char yield. This is also influenced by the heating rate; if the heating rate is very high, the residence time of the biomass at temperatures <300°C is insignificant. This gives less time for dehydration reactions and for the formation of anhydrocellulose, decreasing char yield (Demirbas, 2004).

The second pathway occurs at temperatures above 300°C, where the remaining cellulose is decomposed into a tarry pyrolysate containing levoglucosan, other anhydroglucose compounds, randomly linked oligosaccharide and glucose decomposition products (Shafizadeh, 1982).

Hemicellulose is believed to thermally decompose into water-soluble fragments and very short molecular units, which then decompose into volatiles, resulting in more volatile products and less char than cellulose (Soltes and Elder, 1981).

At lower carbonisation temperatures (120-300°C), the weak bonds between the lignin molecules are cleaved. Examples are cleaving of OH functional group linked to β or γ carbons, releasing water; cleaving of β-γ carbon bonds to form formaldehydes and breaking of aryl ether linkages to yield monomeric phenols. At temperatures higher than 500°C, aromatic ring cracking and condensation occurs, releasing hydrogen (Pandey and Kim, 2011).

Lignin has been suggested as the main component responsible for most of the char produced during carbonisation (Zanzi *et al.*, 2002, González *et al.*, 2003) whereas cellulose and hemicellulose produce mainly volatile matter (Reed and Williams, 2004).

The thermal degradation rates of the lignocellulosic components in biomass are as follows (Demirbas and Arin, 2002, Demirbas, 2004, Babu, 2008):

Hemicellulose > Cellulose > Lignin

The quality and form of the char will determine the final properties of the activated carbon (Fowler, 1995). The chemical reactions proceed in a manner that produces the most energetically stable molecule. For aliphatic molecules, as the chain length increase; the molecule tends to be less stable whereas for aromatic molecules, stability is increased with increasing aromatic rings (Fitzer *et al.*, 1971). This implies that carbonisation will increase the aromatic bulk of the molecule (Fowler, 1995).

During carbonisation, most of the hydrogen, nitrogen, oxygen and sulphur atoms are removed in gaseous form due to the pyrolytic decomposition of the feedstock (in a process known as devolatilisation) and the 'freed' carbon atoms are re-arranged into crystalline structures known as elementary graphitic crystallites, resulting in a relatively "purer" carbon form (Lima *et al.*, 2009). The arrangement of the crystalline structure is irregular and as such, tarry substances produced during

pyrolysis fill and block the interstitial spaces in between the carbon atoms. This results in char with poor adsorption capabilities (Smíšek and Černý, 1970). In order to obtain a char of improved surface area and porosity, it must be 'activated'.

3.5.4 Activation methods

There are two methods of activating a char: chemical activation and physical activation. Both methods involve the use of an activating agent to increase the porosity of the char, resulting in a large surface area.

3.5.4.1 Chemical Activation

Chemical activation involves the use of an agent which influences the course of pyrolysis; dehydrating the carbon precursor, keeping tar formation to a minimum, increasing the aromatisation processes of carbonisation (Smíšek and Černý, 1970, Bansal *et al.*, 1988, Williams and Reed, 2006) and in doing so, prevents the blockage of interstitial pore space in the carbon. Commonly-used activating agents are zinc chloride, potassium hydroxide/carbonate and phosphoric acid (Marsh and Rodríguez-Reinoso, 2006).

The activating agent is mixed with the precursor and the mixture is reacted at an elevated temperature in an inert atmosphere. Once activation has been completed, the activating agent must be removed from the activated carbon before usage. This usually involves washing with acids to remove the un-reacted chemicals (Molina-Sabio and Rodŕıguez-Reinoso, 2004).

Chemical activation allows the use of lower reaction temperatures (when compared to physical activation) and both carbonisation and activation is able to occur simultaneously. As with carbonisation, reaction temperature plays a role in the extent of activation. Moreover, an important factor to consider during chemical activation is the degree of impregnation; the weight ratio of activating agent to precursor.

Due to the fact that chemical activation is able to occur at lower temperatures; at times and often at temperatures below which complete carbonisation occurs, the chemical composition of chemically activated carbons fall between those of the precursor and the char (without activation) (Marsh and Rodríguez-Reinoso, 2006).

3.5.4.2 Physical activation

Physical activation is a two-stage process, first involving the carbonisation of the feedstock and after, activation of the produced char. The physical activating agent is introduced at high reaction temperatures (usually between 800°C and 1000°C) (Mui *et al.*, 2004), reacting with the tar and disorganised carbon; exposing the elementary crystallites to further action by the activating agent.

Common activating agents are steam, carbon dioxide and oxygen (Molina-Sabio *et al.*, 1996, Rodríguez-Reinoso *et al.*, 1995, Rodríguez-Reinoso *et al.*, 2000). The reaction between the char and the mentioned agents is often referred to as gasification and it is often carried out at 800-1000°C, depending on the activating agent used.

Oxygen reacts exothermically with the carbon, hence reaction rates are difficult to control and this just consumes the carbon material without increasing porosity (Marsh and Rodríguez-Reinoso, 2006). Reactions with steam and carbon dioxide are endothermic and easier to control. However, this requires the application of direct heating to the reaction to drive the CO_2 (Equation 3-12) or steam (Equation 3-13) activation process.

Equation 3-12: $C + CO_2 \rightarrow 2CO \qquad \Delta H = +159 \frac{kJ}{mol}$

Equation 3-13: $C + H_2O \rightarrow CO + H_2 \qquad \Delta H = +117 \frac{kJ}{mol}$

Due to the high temperatures used during gasification, the water gas shift reaction (Equation 3-14), which is catalysed by the carbon surface, is at equilibrium (Marsh and Rodríguez-Reinoso, 2006).

Equation 3-14: $CO + H_2O \leftrightarrow CO_2 + H_2 \qquad \Delta H = -41 \frac{kJ}{mol}$

During physical activation, the char carbon structure reacts with the activating agent, resulting in mass losses as the reaction progresses. The difference in mass between the char and the resulting activated carbon; expressed as a percentage is termed “burn-off” (Chang *et al.*, 2000, Williams and Besler, 1996).

In the steam activation of char, activation proceeds by micropore formation and is followed by pore enlargement as the steam reacts with the carbon (Williams and Reed, 2006). These include the opening of inaccessible pores through removal of tars and disorganised carbon, which is suggested to be complete after about 10% burn-off (Marsh and Rodríguez-Reinoso, 2006). At 50% burn-off, selective activation creates new pores in the carbon structure (Williams and Reed, 2006). The extent of microporosity development also depends on the precursor (Stoeckli and Ballerini, 1991, Gergova *et al.*, 1994).

Gergova *et al.* (1994) made a study in comparing the porosity produced during steam activation of pure lignin and cellulose and observed that lignin carbons had higher total pore volume compared to cellulose carbons and that cellulose carbons contained almost equal volumes of micro- and macropores. This behaviour is only indicative of pure lignin and cellulose chars and in biomass, the activation behaviour is most likely to change. The workers did suggest that from these results, it is apparent that differences in lignin and cellulose content of the precursors to activated carbons may influence the porous structure of the produced activated carbons.

Reed and Williams (2004) have also concluded that characteristics of produced activated carbons are influenced by their feedstock, with materials having high lignin contents producing the most char and subsequent activated carbon yield. Biomass with high lignin contents also makes activated carbons with the highest micropore surface area in their study.

In general, a higher degree of burn-off leads to higher surface areas and less AC yield. Steam activation is known to widen the microporosity of char precursors more than CO_2, yielding activated carbons with a micro- and mesoporous structure (Tennant and Mazyck, 2003, González *et al.*, 1994, Molina-Sabio *et al.*, 1996). The porous structure of the activated carbon also dependant on the biomass precursor used (Dias *et al.*, 2007).

3.5.5 Physical Structure of activated carbon surface

Activated carbons have a microcrystalline structure that builds up during carbonisation. It has parallel layers of hexagonal carbon atom rings, as in graphite but is less ordered, termed ‘turbostratic’ by Bisco and Warrens (1942) and seen in Figure 3-9. The disorder is caused by the presences of heteroatoms such as oxygen and hydrogen and by defects such as vacant lattice sites in the activated carbon structure (Marsh and Rodríguez-Reinoso, 2006, Bansal, 2005).

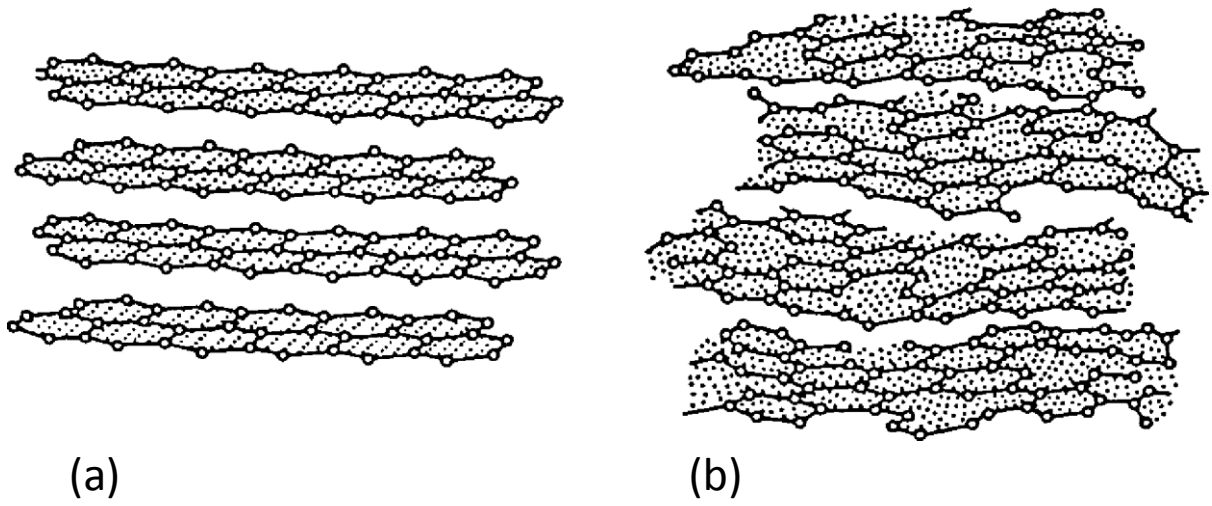


Figure 3-9: Comparison of three-dimensional crystal lattice of graphite (a) and (b) the turbostratic structure (Bokros, 1969).

3.5.6 Chemical structure of the activated carbon surface

The adsorption capacity of activated carbons is not only determined by its physical (porous) structure, but is also strongly influenced by its chemical structure. The chemical structure is usually associated with the considerable amounts of oxygen and hydrogen present in the carbon lattice. Additionally, there are also bonded sulphur, nitrogen and halogen atoms. These heteroatoms originate from the feedstock and become part of the chemical structure during impartial carbonisation or during activation (Bansal, 2005).

X-ray diffraction studies have shown that the heteroatoms give rise to C-O, C-H, C-N, C-S and C-halogen surface compounds, called surface groups or surface complexes and these compounds modify the surface characteristics and properties of the activated carbons (Marsh and Rodríguez-Reinoso, 2006). From these surface groups, C-O groups are the most important as they influence characteristics such as wettability, polarity and acidity; physico-chemical properties such as catalytic, electrical and chemical reactivity are also affected (Bansal *et al.*, 1988, Marsh and Rodríguez-Reinoso, 2006).

Steenberg (1944) proposed the term 'H'-activated carbons for carbons that contain basic surface groups and 'L'-activated carbons for those that contain acidic groups. The acidic surface groups are formed when carbon is treated with oxygen at temperatures up to 400°C or by using oxidising agents

at room temperature. These acidic surface groups are thermally less stable and can decompose on heat treating in a vacuum or in an inert atmosphere between 350 and 750°C to evolve CO_2. The acidic surface groups are responsible for the hydrophilic and polar nature of the carbon; and are postulated to be carboxylic, lactone and phenolic groups (Bansal, 2005).

The basic surface group are less well-characterised and are obtained when a carbon surface, freed of all oxygen groups by heat treatment in vacuum or in an inert atmosphere at 1000°C, is contacted with oxygen after cooling. A pyrone-type structure has been proposed by Garten *et al.* (1957), which has been referred to as a chromene structure. This is seen in Figure 3-10.

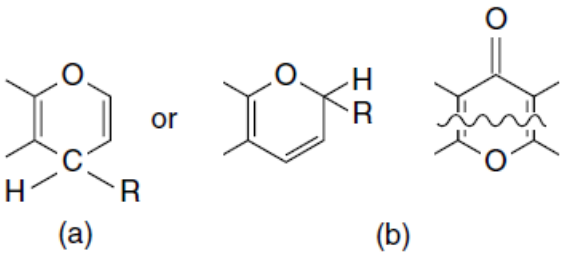


Figure 3-10: Functional groups of basic character: (a) chromene (Garten et al., 1957) (b) pyrone-like (Boehm, 1966).

More research is needed before an agreed structure for the basic surface groups of activated carbons can be accepted (Bansal, 2005).

3.6 Steam activation of waste biomass

Waste biomass has been documented as precursors for AC production with high adsorption capacities, considerable mechanical strength and low ash content (Ioannidou and Zabaniotou, 2007). Rice husks, corn cobs, olive residues, sunflower shells, pine cones, rape seeds and cotton residues were some of the waste biomass activated using steam (Haykiri-Acma *et al.*, 2006, El-Hendawy *et al.*, 2001, Malik, 2003). Carbonisation temperatures used ranged from 400°C to 850°C whereas activation ranged between 600°C to 900°C. Corn cob AC was observed to reach surface areas of 1315 m^2/g and were microporous (Chang *et al.*, 2000) whereas steam was observed to more effective than CO_2 activation by Lussier *et al.* (1994). Work done by Bacaoui *et al.* (2001) determined that olive cakes made the best AC when activated at 822°C for 68mins.

These waste biomass AC have been used to remove different dyes, herbicides, heavy metals and volatile organic compounds (Dias *et al.*, 2007). It was shown that AC prepared from waste biomass removed significant amounts of dyes, Hg (II) and Ni (II) quicker than conventional methods of removal such as precipitation and coagulation (Kadirvelu *et al.*, 2003). As a result, it is apparent that the steam activation of waste biomass has been proven to be effective in producing high surface area AC.

3.7 Applications of activated carbons

Activated carbon is a popular, worldwide commodity and estimated consumption stood at 750,000 tonnes per annum and is expected to increase due to increasing concern over environmental pollutants (Roskill Information Services Ltd., 2003).

Activated carbons are selected, depending on their characteristics to remove unwanted odours, colours and components from foodstuffs. In liquid-phase usage, they are used to remove colour, taste or odours from a solution or to concentrate or remove a solute from solution. In gas-phase applications, they are used to purify gas or air streams through the adsorption of contaminants (Roskill Information Services Ltd., 2003).

Some examples of activated carbon applications are (Bansal, 2005):

- preparation of alcoholic beverages
- decolourisation of oils and fats (used in conjunction with bleaching clays)
- decolourisation of sugar
- decolourisation of organic components in chemicals and pharmaceuticals
- recovery of gold
- refining of liquid fuels
- removal of contaminants from exhaust gases
- removal of toxins from human body.

3.8 Summary

Current waste biomass management strategies relate to disposal into landfill (and to a lesser extent, composting) with little scope for re-use, although energy recovery is being slowly adopted (DEFRA, 2008). However, with the introduction of the Landfill Regulations, waste biomass disposal to landfill is actively discouraged, particularly because of its biodegradability and contributing GHGs. The Landfill Tax acts as a deterrent to landfill disposal and also as an incentive for the development of alternative routes of disposal, particularly recovery and re-use.

Green waste, also known as garden waste, generally consists of biodegradable plant material as well as the occasional food and kitchen waste. It is converted into compost, a low-cost dark brown soil conditioner. Composting is being actively encouraged as a means of reducing biodegradable waste sent to landfill. However, composting is also a source of methane, a potent GHG (Jäckel *et al.*, 2005, Hellebrand, 1998, Beck-Friis *et al.*, 2000). Composting also takes a relatively long time (4-6 weeks) to stabilise GW and depending on the type of composting, requires either a lot of space or high capital expenditure or both.

Japanese knotweed is an invasive plant species in the UK introduced during Victorian times and has invaded much of the UK country side. It reduces biodiversity wherever it is found, by outcompeting native flora and disrupting native fauna. It also causes damage to the built environment by breaking thorough asphalt, destroying flood defences, etc. Current control methods require labour, time and chemicals; and ultimately, the waste biomass will still be disposed into a landfill if it cannot be burnt or buried on site.

One of the main disadvantages of the current disposal options for waste biomass is that the final product (if any) has little or no value and its treatment may have an impact upon the environment and thus, there exists an opportunity to exploit that outcome. Valorisation of waste biomass can be achieved by using activated carbon conversion technology. This can also be seen as an alternative disposal route, a decrease in reliance on landfill disposal and as a result, move the waste up the waste hierarchy.

The conversion of waste biomass into activated biomass is being investigated in this research to determine its capabilities in adsorption. This prevents the waste biomass from being disposed in an unsustainable way e.g., into landfill. Additionally, during the manufacture of activated carbon from

waste biomass feedstock, the conversion of this carbonaceous feedstock sequesters the anthropogenic carbon incorporated in the biomass during its growth as char and ultimately, activated carbon, which is a relatively stable form of carbon. This prevents the release of CO_2 during natural decomposition of the waste biomass and further reducing the long-term impact of its disposal.

Activated carbons are highly porous, carbonaceous materials (Smíšek and Černý, 1970) used in both liquid and gas purification processes (Marsh and Rodríguez-Reinoso, 2006). They can be made from carbonaceous material such as coal, peat or lignite but these feedstocks are non-renewable. Current research is investigating utilising waste biomass as a precursor for activated carbons (Karagöz *et al.*, 2008, Tay, 2009, Rengaraj *et al.*, 2002) as it is renewable, widely-available, cheap (Karagöz *et al.*, 2008, Ioannidou and Zabaniotou, 2007) ,sustainable and as a means of reusing the waste biomass (Amaya *et al.*, 2007).

In order to explain the adsorption process, this research will rely on the theories previously discussed in Section 3.4.

The conversion of waste biomass to activated carbons was chosen because:

- The conversion technology is simple to apply,
- The infrastructure is already available without needing further investment or modification,
- Demand for activated carbons is increasing,
- Conversion to activated carbon is a form of carbon storage, where carbon from the biomass is concentrated (stored) in the activated carbon,
- It can be a viable, alternative disposal route for waste biomass; i.e., diversion from landfill,
- The high cost of manufacturing activated carbons could be offset with a cheap and widely-available precursor,
- The product can be of high value and of beneficial use as a pollution control agent.

Chapter 4. Aim and Objectives

4.1 Overall aim of the research

This project aims to investigate the feasibility of converting waste biomass (green waste and Japanese knotweed) into a high surface area adsorbent while simultaneously moving the management of waste biomass up the waste hierarchy, from disposal to reuse and recovery. This involves conducting research to investigate the potential of making activated carbons from the mentioned waste biomass as well as examine the effectiveness of the produced activated carbons in line with industry standards to ensure compatibility and demonstrating its application and effectiveness compared to a commercial benchmark activated carbon.

4.2 Objectives

Two waste biomass feedstocks, green waste and Japanese knotweed will be subjected to screening tests to assess their suitability for conversion into activated carbons using steam activation.

Preliminary characterisation tests will be carried out on the two different samples and these will include ash content analysis, elemental analysis and moisture content analysis. The goal is to select the best feedstock out of the two for steam activation and to determine the optimum conditions to produce activated carbons with the highest surface area.

The following objectives are set out:

- Characterisation and preparation of sample feedstock,
- Determination of optimal conditions for batch carbonisation of both types of feedstock,
- Steam activation of produced feedstock char using lab-scale rotary furnace at different activating conditions,
- Conducting standard tests according to international and/or peer-reviewed methods,
- The comparison of results between different activated carbons,
- Application testing of optimised activated carbons with the highest surface areas,
- Comparison of adsorptive properties of produced activated carbons with a commercial-grade carbon.

Chapter 5. Characterisation of waste biomass (GW, JKWS and JKWR)

5.1 Introduction

A comprehensive characterisation of the waste biomass (GW, JKWS and JKWR) was carried out and the physical and chemical properties determined included:

- Lignocellulosic content
- Moisture content
- Ash content
- Proximate analysis
- Ultimate analysis
- Calorific value

The tests would give an indication of the suitability of the waste biomass as precursors. The ash and carbon content were of particular significance as they affect the characteristics of the activated carbons produced (Gergova *et al.*, 1994).

5.2 Materials

Green waste (GW) and Japanese knotweed samples were obtained from Cornwall. The GW samples were partly composted which can be seen in Figure 5-1, with high moisture content. The samples also had a smell reminiscent of rotting vegetation. The as-received samples of JKW stem and rhizome are shown in Figure 5-2. The rhizomes were caked in fresh, moist soil and the stems had high water content.



Figure 5-1: As-received green waste sample.

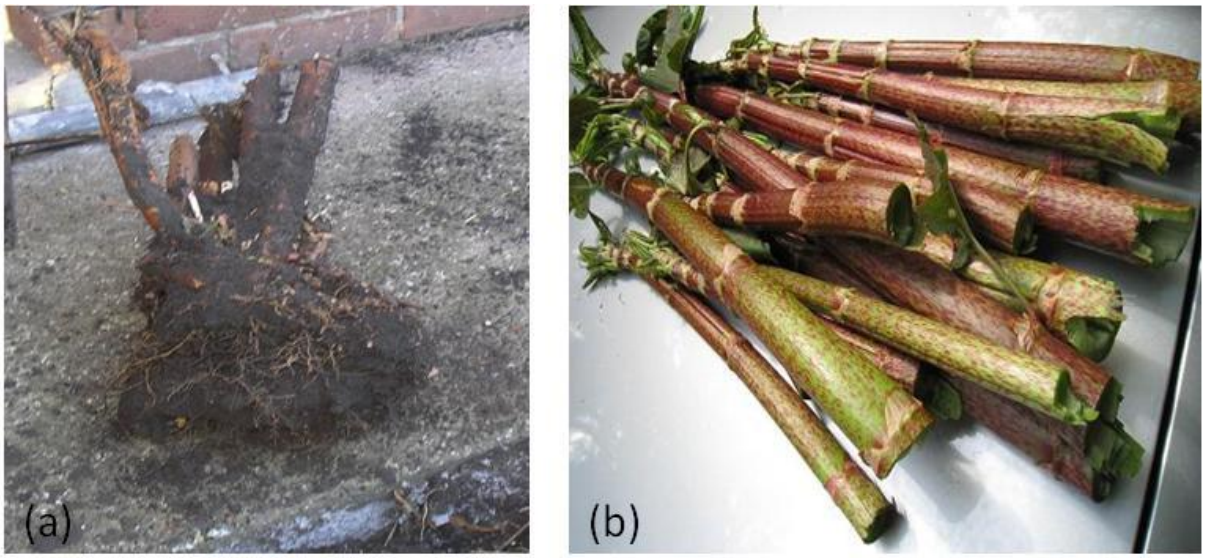


Figure 5-2: (a) Japanese knotweed rhizome crown with soil, caked in between roots and (b) Japanese knotweed stems.

The oven-dried JKWR and JKWS are shown in Figure 5-3.



Figure 5-3: (a) JKWR air-dried without soil and (b) oven-dried JKWS.

JKWR crowns were cut into smaller pieces using a band saw whereas JKWS pieces wore broken manually by hand. These samples are shown in Figure 5-4 . The particle sizes were reduced so that it would fit into the cross-beater mill.

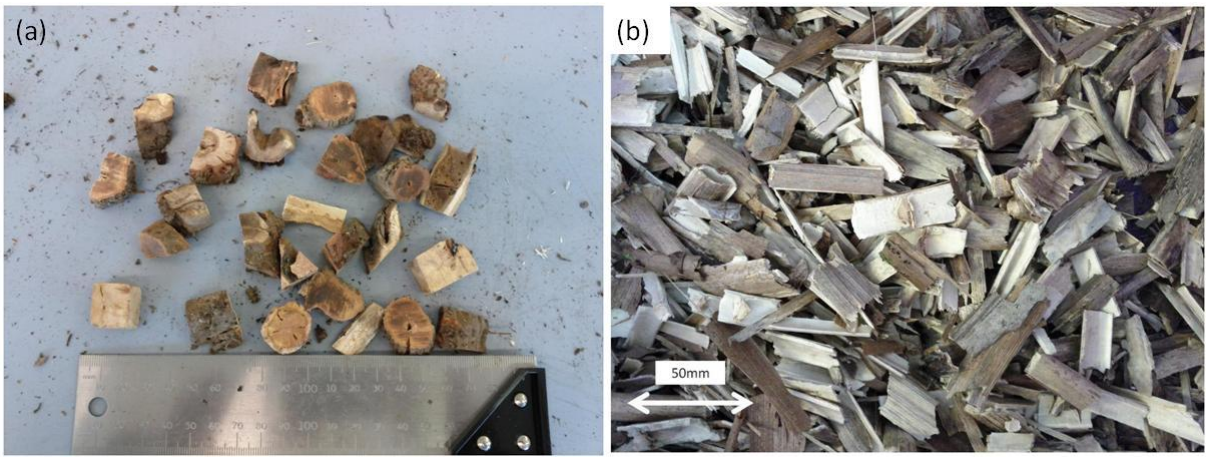


Figure 5-4: (a) JKWR pieces cut by band saw (b) JKWS pieces broken by hand.

The photographs shown in Figure 5-5 shows the milled samples which are <10mm and sieved to <2mm.

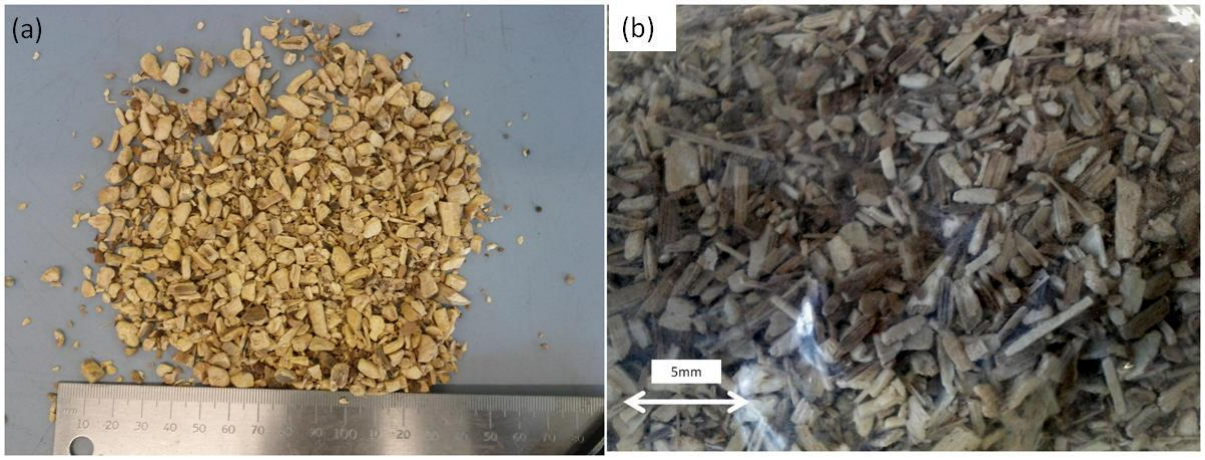


Figure 5-5: (a) JKWR and (b) JKWS after going through the cross-beater mill with 10mm pre-breaker plates.

5.3 Methods

5.3.1 Size reduction

Size reduction of the as-received waste biomass samples were needed prior to characterisation and carbonisation in order to ensure that they fit in the quartz reactor used for carbonisation and steam activation.

The GW and JKWS samples were oven-dried whereas JKWR samples were first air-dried to enable the soil to dry out and removed by wire brushing the rhizome pieces.

Once dried, JKWS samples were broken by hand into 30-50mm sizes whereas GW samples did not require this step. JKWR samples were more difficult to reduce in size. The large rhizome crowns had to be cut using a band saw into 30-50mm sizes.

All size-reduced samples were crushed in a Glen Creston cross beater mill (Glen Creston Ltd., London, UK) with a 10mm pre-breaker plate.

5.3.2 Moisture content

Moisture content (MC) was determined in triplicate using ASTM Method D4442-07 (ASTM, 2007b). Samples were oven-dried at 105°C for at least 24 hours or until there was no further weight change. The oven used was a Gallenkamp Size 2 Hotbox oven (Weiss-Gallenkamp, Loughborough, UK). Samples were allowed to cool in a desiccator before weighing to avoid re-adsorption of moisture from the atmosphere.

The moisture content was calculated using Equation 5-1:

$$\text{Equation 5-1:} \quad MC, \% = \frac{(A-B)}{B} \times 100$$

Where: A= original mass in g and B= oven-dried mass in g.

5.3.3 Lignocellulosic content

The lignocellulosic content of the waste biomass samples were carried out in triplicate according to ASTM Method D1106-96 (2007) for lignin (ASTM, 1996a) and ASTM Method D1109-84 (2007) (ASTM, 1984) for hemicellulose.

In determining lignin content, the waste biomass is hydrolysed with strong acids, leaving the insoluble lignin as a residue. The sample is first extracted by ethanol-toluene using Soxhlet extraction apparatus to remove waxes, fats, resins and some gums. The residue is then hydrolysed

using 72% sulphuric acid (Analar grade), washed with distilled water, filtered, dried and weighed to determine lignin content.

Hot alkali extracts low molecular weight carbohydrates consisting mainly of hemicelluloses and degraded cellulose in biomass (ASTM, 1984). The sample is boiled in a beaker of 1% sodium hydroxide (Analar grade), using a water bath to maintain the temperature. The sample is then filtered, washed, dried and weighed. The hemicellulose content is determined according to Equation 5-2:

$$\text{Equation 5-2:} \quad \frac{W_1 - W_2}{W_1} \times 100$$

Where: W_1= weight of moisture-free sample and W_2= weight of dried sample after treatment with NaOH.

The cellulose content is determined by subtracting the lignin, hemicellulose and ash contents from the total sample weight.

5.3.4 Ash content

The ash content of the waste biomass was determined according to ASTM Method D1102-84(2007) (ASTM, 2007a). The ash content of a precursor is important in determining its suitability as a feedstock for activated carbon (Marsh and Rodríguez-Reinoso, 2006).

Pre-dried samples were weighed and placed in pre-ignited porcelain crucibles with lids. These were then placed into a muffle furnace and heated slowly to 600°C to avoid flaming and lids were used to protect the sample inside the crucible from strong drafts. The muffle furnace used was a Gallenkamp Size 2 muffle furnace.

Samples were left in the furnace until all carbonaceous material was burnt off and only inorganic ash was left. The crucibles were allowed to cool to room temperature in desiccators before being weighed.

The ash content of the sample was calculated using Equation 5-3.

Equation 5-3: $$Ash, \% = \frac{W_1}{W_2} \times 100$$

Where: W_1= weight of ash and W_2= weight of oven-dried sample.

5.3.5 Thermal Analysis using TGA

Thermal analysis of the biomass samples and subsequent char samples was conducted using a Rheometric Scientific STA 1500. Thermal analysis involves measuring the weight changes as a sample is heated in an inert/non-inert atmosphere. This is termed thermo-gravimetric analysis (TGA). TGA also refers to the instrument, the thermo-gravimetric analyser.

The plot of weight change versus temperature is known as a thermogravimetric (TG) plot and its derivative is known as a DTG (derivative thermogravimetric) plot. The common procedure involves placing the sample in a crucible and placing the crucible on a high precision microbalance, which records the weight changes during heating of the furnace. This gives a TG plot for the sample and the DTG is determined by the software.

The STA 1500 thermal analyser also makes use of a technique called Differential Scanning Calorimetry (DSC). DSC makes use of a crucible containing an inert reference material in addition to the sample crucible. The difference in temperature between the two crucibles and the amount of energy needed to heat either crucible is measured. This allows the determination of an endothermic or exothermic reaction. A negative heat flow value indicates that the sample temperature has decreased due to an endothermic reaction and that heat was supplied to the sample crucible whereas a positive heat flow indicates that the sample temperature increased due to an exothermic reaction and that heat flow was supplied to the reference crucible (Beshara, 2010).

Alumina crucibles of ca. 4.5mm diameter were used. Nitrogen was used as the inert atmosphere and air was used for a reactive atmosphere. All samples to be tested were ground and sieved to ≤ 500µm to homogenise the samples. For the purposes of this project, the TG analysis was of more importance than the DSC analysis.

The TGA was used to perform initial tests on the thermal degradation behaviour of the samples in an inert atmosphere. Flow rate was set to 50 ml/min. The TGA was used to determine the temperature

of the onset of biomass degradation and the temperature at which maximum weight loss occurred. It was also used to determine the proximate analyses of the samples.

Proximate analysis gives the moisture content, volatile matter, fixed carbon and ash contents of the sample (Robinson *et al.*, 2010). The TGA allows for small samples to be used and the results can be used to design experiments based on the thermal characteristics of the feedstock samples.

The parameters for proximate analysis using the thermal analyser are as follows:

- Heating the sample to 105^{o}C in an inert atmosphere initially to drive off the moisture,

- The temperature of the furnace is then increased to 950^{o}C to determine the volatile matter content of the sample,

- The furnace is allowed to cool down to 600^{o}C where the inert atmosphere is substituted for an oxidising atmosphere (air/oxygen); allowing for combustion and therefore, the determination of the fixed carbon and ash contents.

The method for proximate analysis as described was taken from Robinson *et al.* (2010), who modified ASTM Method E870-82.

The fixed carbon content, as given by the proximate analysis of biomass, indicates the amount of non-volatiles carbon available that is not converted into bio-oils and syngas, which should end up in the char and finally, the activated carbon. The volatiles content gives us the expected total yield of bio-oil and syngas.

5.3.6 CHNS analysis

CHNS (carbon-hydrogen-nitrogen-sulphur) was performed by an external laboratory, MEDAC Ltd. in Surrey UK. This test was done by combustion analysis where the samples are flash combusted with the help of oxidation catalysts at 900°C and the combustion products are analysed using a chromatographic column where the individual components are separated and eluted as nitrogen, carbon dioxide, water and sulphur dioxide to determine the concentrations of C, H, N & S in the

sample (MEDAC Ltd., 2007). The oxygen content is determined by difference, based on the assumption that the sample only contained CHNS and O including incombustible inorganic minerals.

5.4 Results

5.4.1 Moisture content

The intrinsic moisture content (MC) of the waste biomass is shown in Table 5.1 along with standard deviation (SD) values. Both JKWS and GW showed higher MC values than JKWR but similar to other types of waste biomass, as depicted in Table 5.1.

Table 5.1: Moisture content of GW, JKWS and JKWR compared to other different types of waste biomass. Data obtained from Ioannidou and Zabaniotou (2007). SD values determined from 3 measurements.

Types of waste biomass	Moisture content (%)	SD (%)
GW	56.5	2.3
JKWS	60.4	2.9
JKWR	8.1	0.3
Olive tree prunings	7.1	-
Cherry tree prunings	40	-
Sugar beet leaves	75	-
Barley straw	15	-
Peach tree prunings	40	-

It is apparent that most waste biomass which consists of leaves and stalks has higher moisture content. This could be an effect of the prevailing weather conditions during harvesting on the overall biomass moisture content (McKendry, 2002) as well as the observed mesic stems and leaves of JKW.

The issue with feedstock that contain high moisture is that more energy is required for the sample to reach a suitable temperature for carbonisation, due to the additional energy needed to vaporise the water before carbonisation reactions will occur.

5.4.2 CHNS and ash content

It can be observed in Table 5.2, it can be seen that the CHNS contents of JKWS and JKWR are similar to other types of waste biomass found in literature. However, GW exhibits very low C and H values whilst having a very high amount of ash (58.73%). Similar ash content results in green waste have also be observed and have been attributed to soil content of the green waste (Andersen *et al.*, 2010).

Table 5.2: CHNS values of GW, JKWS and JKWR compared to those of other waste biomass found in literature (Ioannidou and Zabaniotou, 2007).

Waste biomass	C (%)	H (%)	N (%)	S (%)	O (%)*	C:N ratio	Ash (%)
GW	19.52	2.54	1.40	0.00	17.81	13.9	58.73
JKWS	45.70	5.68	0.63	0.37	45.83	73.5	1.56
JKWR	46.30	5.36	1.62	1.12	44.62	28.2	4.43
Olive tree prunings	49.90	6.00	0.70	n/a	43.40	71.3	4.75
Barley straw	46.80	5.53	0.41	0.06	41.90	114.1	4.90
Peach tree prunings	53.00	5.90	0.32	0.05	39.10	165.6	1.00

* Oxygen content determined by difference.

The sulphur content of both JKWS and JKWR are unusually high for biomass, especially the values for JKWR. It is known that in its native habitat of Japan, JKW can be found growing on volcanic slopes as mentioned in Section 2.2. The high sulphur content of the obtained JKW samples is most likely due to the fact that the samples were harvested from the vicinity of old tin mines and smelters near Redruth in Cornwall, where it can tolerate the high sulphur content of the surrounding soils. The sulphur was released into the surrounding areas as a result of the smelting of the tin ores (Sturgess, 2001).

Also presented in Table 5.2, are the ash contents of GW, JKWS and JKWR compared to other waste biomass examples. Ash is considered a diluent in activated carbon as it has little potential as an adsorbent and has been shown to inhibit surface area development (Valix *et al.*, 2004). It has also been suggested that inorganics may fill or block some portions of existing micropore volume which may help explain the low surface area observed in carbons with high ash content (Pendyal *et al.*, 1999, Rodríguez-Mirasol *et al.*, 1993). As a result, any waste biomass with high ash contents are not recommended for activation.

The C:N ratio is a factor which affects the time course and rate of composting. As composting progresses, the C:N ratio falls as seen in Figure 5-6.

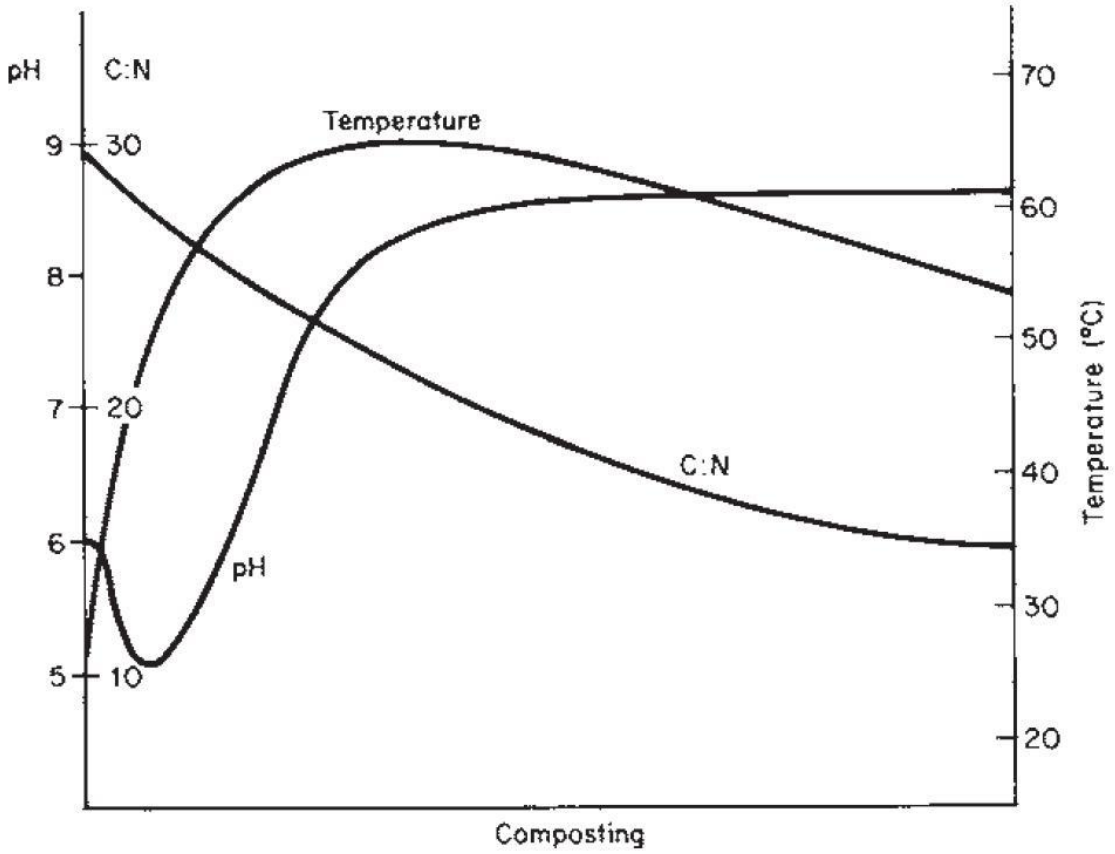


Figure 5-6: Changes in pH, C:N ratio and temperature during composting (Lester et al., 1999).

It can be inferred from Figure 5-6 that the GW received for this project was in the later stages of degradation i.e., it stable and mature as evident by the C:N ratio of 13.9 as observed by Andersen *et al.* (2010) and Confesor *et al.* (2008). The low C:N ratio will have negative implications for the activated carbons produced from this precursor; essentially due to the lack of carbon for pore-forming processes that occur during steam activation.

5.4.3 Lignocellulosic content

The combination of lignin, cellulose and hemicellulose gives the biomass its characteristics and affects its behaviour during carbonisation and activation. The lignocellulosic contents of the waste biomass used in this project are shown in Table 5.3.

Table 5.3: Lignocellulosic contents of GW, JKWS and JKWR compared to other waste biomass. Data obtained from Basso et al. (2002) and Butterman and Castaldi (2010).

Waste biomass	Lignin (%)	Hemicellulose (%)	Cellulose (%)*	Holocellulose+ (%)	Ash (%)
GW	2.6 ± 1.3	30.4 ± 1.2	8.3 ± 2.3	32.9	58.7 ± 0.9
JKWS	19.9 ± 0.9	46.7 ± 2.1	31.8 ± 1.2	78.5	1.6 ± 0.03
JKWR	21.2 ± 0.8	24.9 ± 0.9	52.4 ± 1.6	77.3	4.4 ± 0.1
Olive husk	50.6	24.2	25.2	49.4	-
Corncob	15.5	32.5	52.0	84.5	-
Tea waste	43.5	23.3	33.2	56.5	-
Peanut shell	30.0	19.0	36.0	55.0	-

*Cellulose content determined by difference. +calculated from addition of hemicellulose and cellulose contents.

JKWR and JKWS show very similar lignin contents, which is not surprising as they are just two different parts of a same plant. They both also have similar holocellulose content, responsible for volatiles production during carbonisation. The holocellulose content is the total amount of hemicellulose and cellulose.

GW has very low lignin content and low holocellulose content. This suggests that during carbonisation, there will be less char produced as a result of the relatively low lignin content and high holocellulose content. Additionally, the SD values of the lignocellulosic content of GW are very high, indicating a high degree on heterogeneity in the sample stock. For example, the SD value of the GW lignin content is 1.3%, which equates to a RSD value of 50%. GW cellulose content has SD value of 2.3% and a RSD value of 27.7%.

The cellulose to lignin ratio (C/L) has been used to distinguish between fresh and mature wastes in landfills and can be used to determine the maturity of compost. These can vary from 0.16-0.8 for mature wastes and up to 4.04 for fresh wastes (Komilis and Ham, 2003). Most wastes that have reached their extent of degradation show a C/L ratio of less than 0.5 at the end of the composting process. The profile of the ratio is explained by the fact that cellulose loss is greater than that of lignin during composting.

The GW sampled in this project has a C/L ratio of 3.2, indicating that it is relatively fresh. However, this does not correlate to visual examination of the sample (Figure 5-1) as well as the C:N ratio in Section 5.4.2. Further examination of literature shows that high C/L values were recorded for food wastes and wastes mixed with office paper. Furthermore, green waste streams mixed with branches

can inflate C/L ratios due to the low cellulose content and high lignin content of this material (Komilis and Ham, 2003). This is evident in Figure 5-1. Grass, which has a relatively high C/L starting ratio, could also influence the overall C/L ratio of GW as it makes up the majority of the waste. Both scenarios were the cause of high C/L ratio of the GW samples received for this project.

As previously mentioned in Section 3.5.3, biomass with high lignin and cellulose contents produce more char during carbonisation and judging from the data presented in Table 5.3, the hypothesis is that JKWR will produce marginally more char than JKWS.

5.4.4 Thermal analysis using TGA

The different components of biomass display different thermal properties and the thermal properties of the aggregate represents the sum of its major organic components (Shafizadeh, 1982).

5.4.4.1 Thermal degradation behaviour

The thermal degradation of the 3 waste biomass samples in nitrogen is shown in Figure 5-7. As the sample crucible is very small, samples were ground and sieved to ≤500μm to improve homogeneity as previously mentioned in Section 5.3.5. A low heating rate of 1°C/min was selected to have a high resolution of the weight loss points that occurred during the thermal degradation in nitrogen.

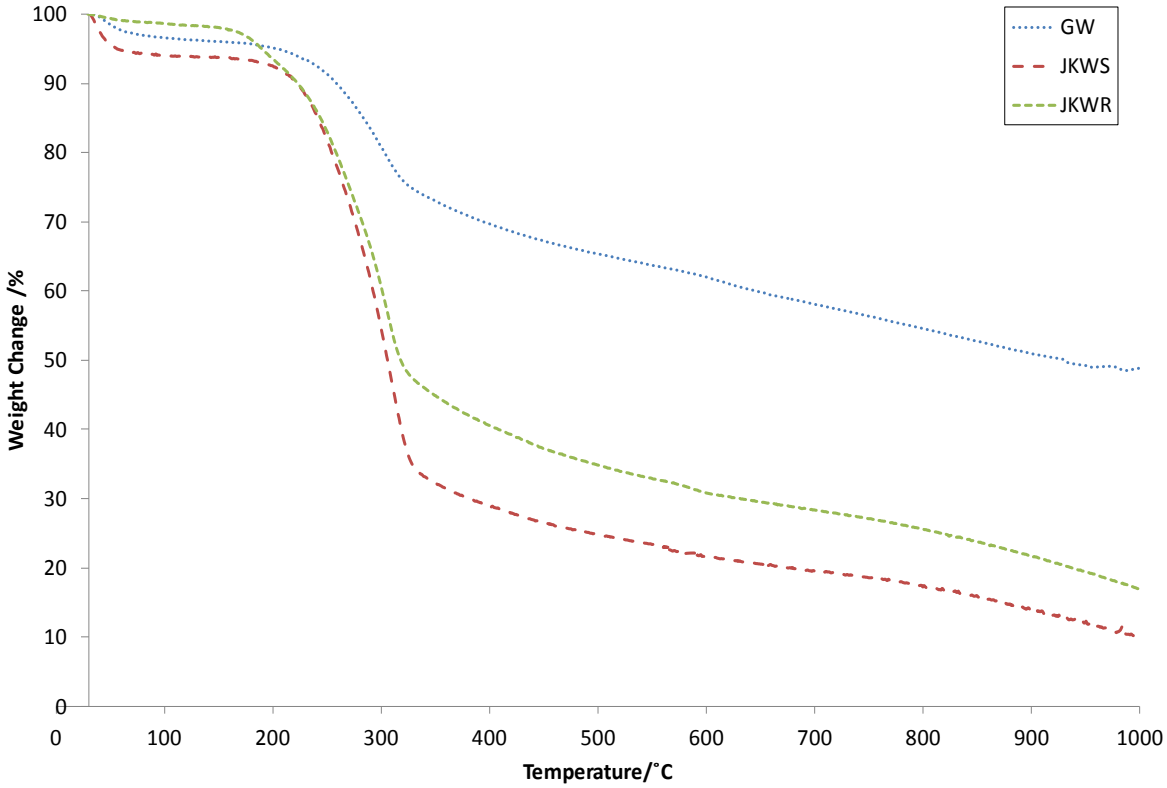


Figure 5-7: TGA plot of GW, JKWS and JKWR at 1°C/min to 1000°C in nitrogen.

The initial weight loss is due to the evaporation of moisture contained in the samples. It can be seen that the moisture losses are complete by 150°C for GW, 180°C for JKWS and 190°C for JKWR. The difference in temperatures of moisture loss is due to the different moisture contents of the samples.

The onset of thermal decomposition starts at between 150°C and 200°C with the main thermal degradation step observed at 300°C, where major devolatilisation occurs. This main weight loss is completed by 380°C and further temperature increase only results in minor weight loss.

The char yield can be obtained from Figure 5-7 as it is the amount of sample remaining at the end of the analysis. The char yield of GW at 1000°C is much higher than that of JKWS and JKWR, suggesting that when activated, GW could produce higher yields. However, it is also known that the high char yield is inflated, mainly due to the high ash content of GW as discussed in Section 5.4.2. JKWS had marginally less yield than JKWR and this has to do with the lower lignocellulosic content and marginally lower ash content of JKWS when compared to JKWR.

Figure 5-8 shows the DTG plots with respect to time (min) which give the rate of weight loss for GW, JKWS and JKWR. It can be seen that JKWS showed greater devolatilisation rates when compared to JKWR and GW.

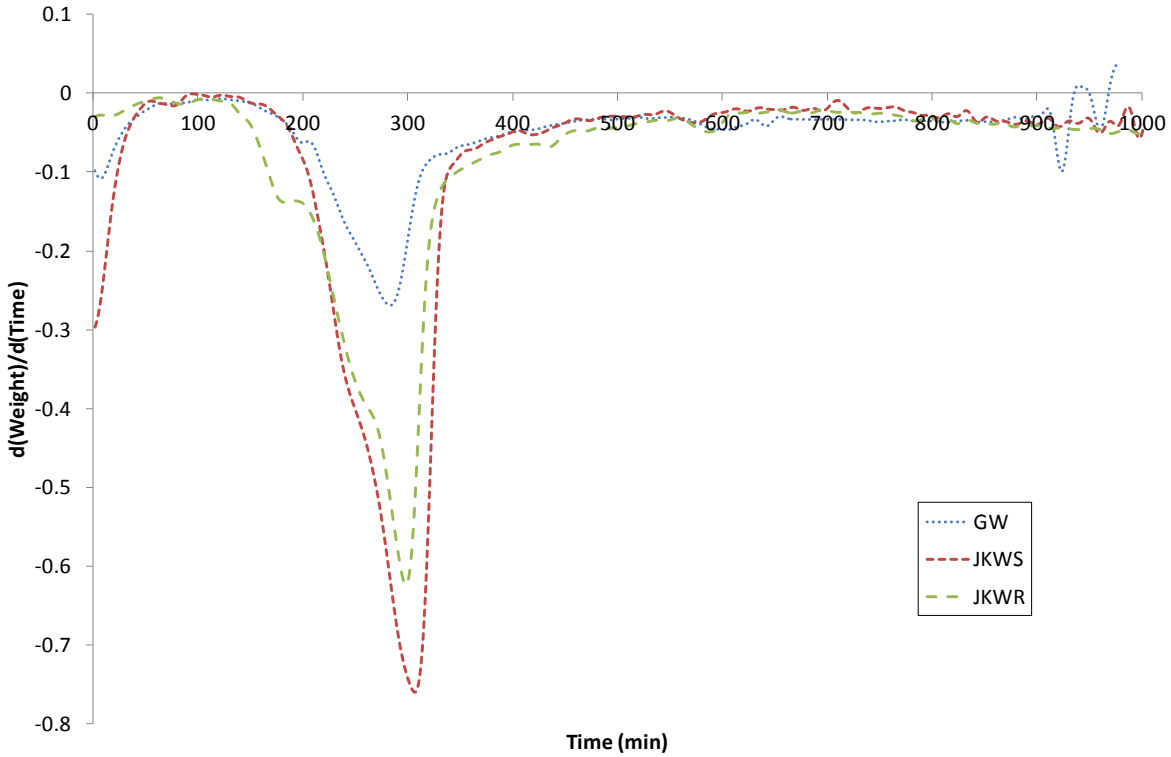


Figure 5-8: DTG plots of GW, JKWS and JKWR at 1°C/min to 1000°C in nitrogen.

From Figure 5-8, it is observed that devolatilisation reactions starts at 150°C, peaks at 300°C and starts to level off at 350°C. The trend observed is typical of thermal degradation reactions of biomass in a non-oxidising atmosphere. In this case, the degradation was carried out in nitrogen. At higher temperatures (above 500°C), it can be seen that the devolatilisation rate plateaus, indicating the completion of significant reactions and the commencement of carbon rearrangement reactions which form char.

The devolatilisation rate of GW at 300°C is less than JKWS and JKWR, which can be attributed to the lower holocelullosic (cellulose and hemicellulose) content as seen in Table 5.3 in Section 5.4.3. The lower temperature DTG peak of JKWS and JKWR which starts at 200°C and ends at 250°C (seen as a shoulder) is a result of the onset of decomposition of hemicellulose in nitrogen and the main higher temperature peak at 300°C was mainly due to the decomposition of cellulose, which is thermally more stable than hemicellulose (Williams and Besler, 1996). Lignin decomposes over a wide range of temperatures and is indiscernible as a peak in the DTG plots.

There is an agreement but not an exact correlation to observations in literature as pure cellulose and hemicellulose decomposes at lower temperatures and there could be other inhibiting factors in the complex biomass matrix (Williams and Besler, 1996).

5.4.4.2 Proximate analysis

The proximate analysis of JKWS using the STA 1500 thermal analyser is shown in Figure 5-9; Where:

a) Moisture content,
b) Volatile matter content,
c) Fixed carbon content
d) Ash content.

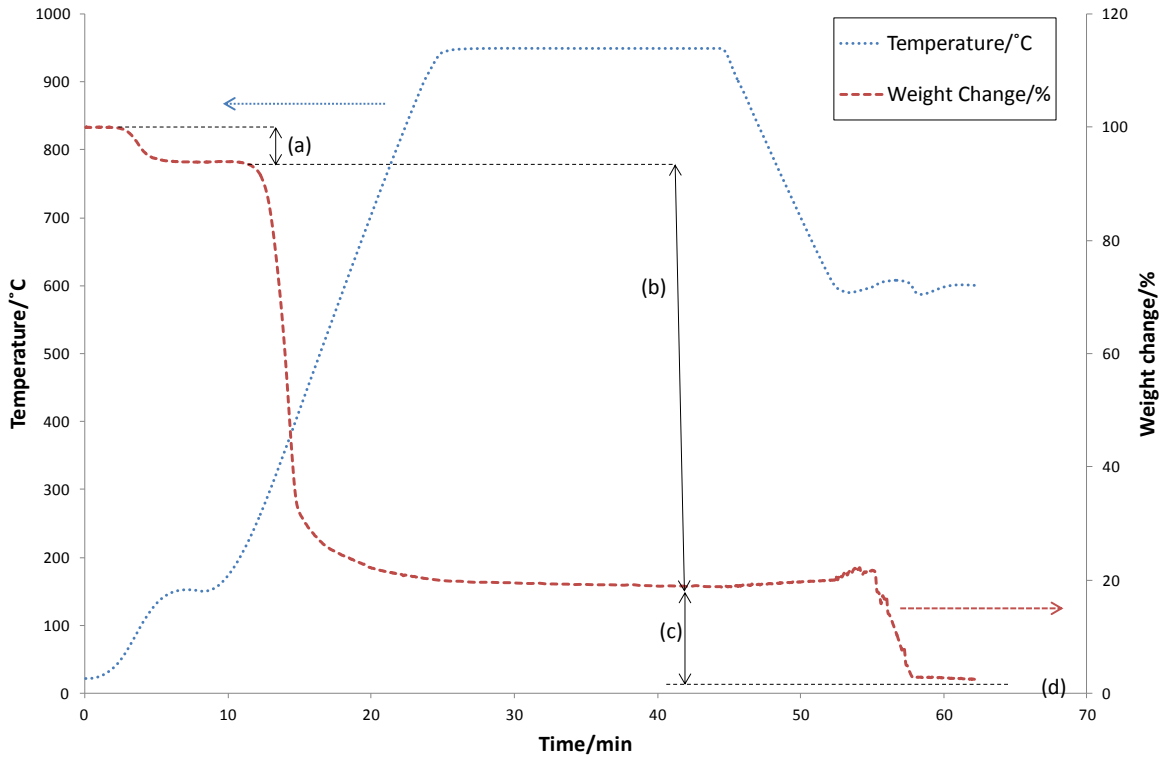


Figure 5-9: Proximate analysis plot for JKWS. (a)moisture content, (b) volatile matter content, (c) fixed carbon content and (d) ash content.

The artefact between t=50min and t=60min on the weight change plot is due to the manual selection of gases; from nitrogen to air. The pressure of the nitrogen line is dissimilar to that of the air line and when switching over, causes the hangdown balance to oscillate slightly.

The artefact at the same time on the temperature plot is due to the controller of the thermal analyser, where it overcompensates as it heats the furnace to 600°C after cooling from 950°C.

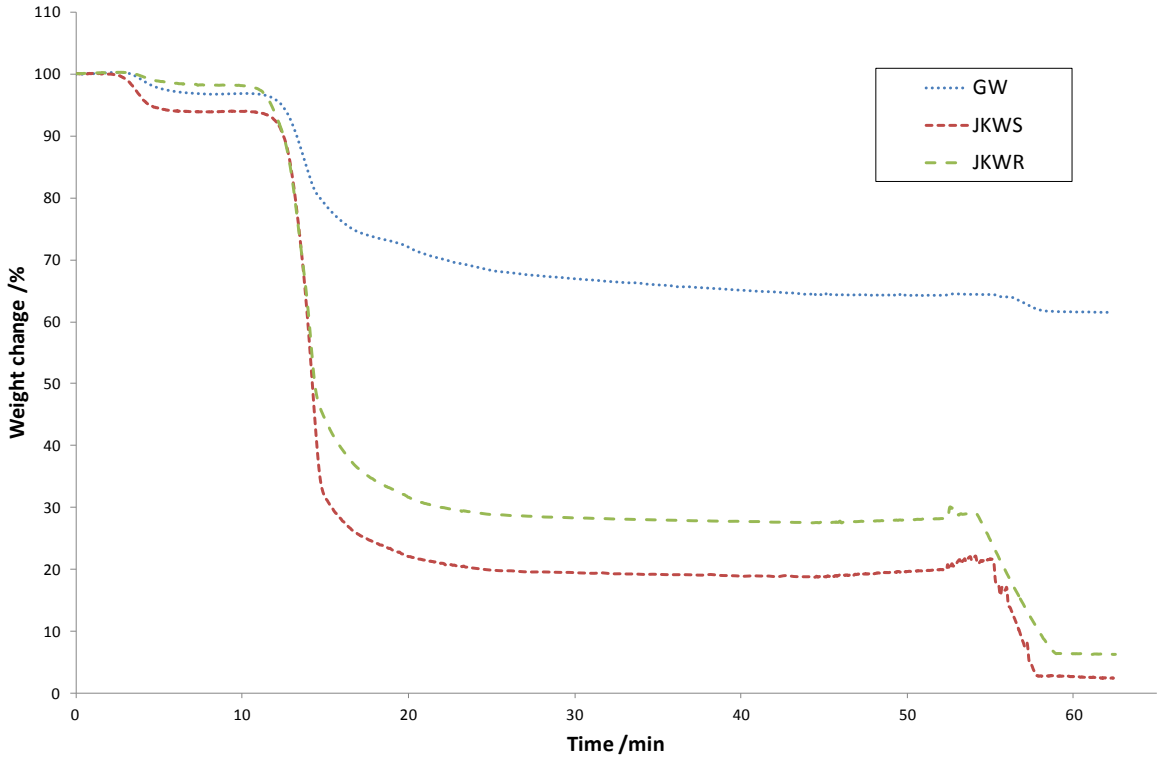


Figure 5-10: Proximate analysis plots of GW, JKWS and JKWR.

The proximate analysis plots of JKWS and JKWR show similar thermal degradation behaviour in nitrogen and air. The GW plot indicates low fixed carbon content and high ash content, the latter as previously mentioned in Section 5.4.2.

The fixed carbon content differs from the carbon content analysed by MEDAC Ltd. in Section 5.4.2 due to the manner in which they are determined. The sample undergoes complete combustion at high temperatures during CHNS analysis and products are in gaseous form. This also takes the carbon contained in the volatile matter into account.

During proximate analysis, the fixed carbon content does not include the carbon found in the volatile matter, which is given off during pyrolysis up to 950°C under nitrogen. Therefore, the fixed carbon content obtained during proximate analysis is a good indicator of the carbon amount that is concentrated and sequestered in the final activated carbon product i.e., the carbon matrix.

Table 5.4: Proximate analysis data of GW, JKWS and JKWR in comparison to other waste biomass.

Waste biomass	Moisture content (%)	Volatile matter content (%)	Fixed carbon content (%)	Ash content (%)
GW	3.2±0.3	32.5±3.3	2.8±2.0	61.5±4.1
JKWS	6.1±0.2	74.9±2.9	16.3±0.8	2.7±0.1
JKWR	1.9±0.1	70.5±3.9	21.2±1.0	6.4±0.2
Corncob	n/a	85.0	13.6	1.0
Almond shell	n/a	74.0	22.7	3.3
Hazelnut shell	n/a	70.3	28.3	1.4
Wheat straw	n/a	63	23.5	13.4
Wood bark	n/a	66.6	31.8	1.6

* Other waste biomass data obtained from Demirbaş (2003). SD obtained from 3 different measurements.

The data obtained from proximate analysis (Table 5.4) shows close agreement with the previous characterisation data presented in Sections 5.4.1, 5.4.2 and 5.4.3. The slight discrepancies in the actual numbers can be attributed to the fact that samples used for the thermal analyser are much smaller and hence, prone to higher relative error.

In comparison to some other examples of waste biomass, it is apparent that GW has very low volatile matter and more importantly, low fixed carbon content. Research undertaken by Andersen *et al.* (2010) in Denmark indicates that average volatiles content of stabilised and matured green waste compost had an annual average of 23.2%. In comparison to GW used in the project, it can be inferred that the GW samples obtained are close to maturity. This evidence can also be correlated to the observations in Section 5.4.2.

The obtained data for GW also shows large variations and this can be attributed to its heterogeneity. Furthermore, most of the fixed carbon will be oxidised during steam activation as steam is particularly reactive, resulting in activated carbons with little or no carbon content, high ash content and low surface areas.

JKWS and JKWR had 74.9% and 70.5% volatile matter respectively, which correlate closely to the holocellulosic content (78.5% and 77.3%, respectively) of the two waste biomass samples, as can be seen from data presented in Table 5.3 and Table 5.4. This is because the thermal degradation of

cellulose and hemicellulose releases volatiles in gaseous form (Williams and Besler, 1996), seen as a significant decrease in weight in Figure 5-10, between t=15min and t=55min. It can also be seen that the lignin content of the waste biomass correlates positively with the fixed carbon content (Demirbaş, 2003), as determined by proximate analysis using the TGA when comparing data between Table 5.3 and Table 5.4.

5.5 Summary

The selection of AC precursors is influenced by ash content, carbon content, availability; cost and ease of activation (Chang *et al.*, 2000, Dabrowski *et al.*, 2005, Marsh and Rodríguez-Reinoso, 2006).

GW samples received for this project had high ash content (58%) and low elemental carbon content (19%). The high ash content is believed to be due to the soil particles that have been mixed with the GW samples, as also observed by Boldrin and Christensen (2010). As the GW samples received were in an advanced state of degradation, this has stabilised the ash content since it is not degraded whereas most of the biodegradable component of GW has been decomposed. This explains the consistently high ash content of GW samples.

The semi-degraded nature of GW implies that most of the biogenic carbon has been degraded by microorganisms during composting, resulting in a low fixed carbon content value when determined by proximate analysis using TGA. The fixed carbon content forms the basic structure upon which activated carbon is made. AC precursors, particularly those to be activated by steam should have high initial carbon content as during activation, the steam will oxidise the carbon structure to create and widen pores, thereby affecting yield of produced carbons.

High quantities of inorganic minerals in the form of ash leads to ACs with poor microporosity (Valix *et al.*, 2004). At this point, after the characterisation tests; it can be inferred that GW would not be suitable as a precursor for ACs.

Both JKWS and JKWR showed potential in being precursors for AC. Both had relatively low ash content (1.6% and 4.4%, respectively) and high carbon content (46.3% and 45.7%). All characterisation test results had consistently low RSD values, indicating good homogeneity of all samples. This can be explained by the fact that all JKW found in the UK are clones of a single male-sterile plant (Hollingsworth and Bailey, 2000) and since it does not spread by sexual reproduction,

all plant samples should be exactly the same. This has excellent repercussions for its role as an AC precursor since it can be certain that each batch will be the same, barring environmental influences.

The next step of the project is to trial several carbonisation parameters to determine the optimal set of parameters for maximum char product; which should contain minimal volatile matter and to analyse the products for their potential in making activated carbons.

Chapter 6. Carbonisation

6.1 Introduction

The next stage of the investigation involved the determination of optimum conditions for the batch carbonisation of the JKW precursor. The carbonisation parameters to be tested, and which have been recognised as being influential in this process, were (Katyal *et al.*, 2003, Román *et al.*, 2008):

- Heating rate
- Carbonisation temperature
- Dwell time

The key criteria for char acceptable for use in steam activation are for the char to contain minimal volatile matter and maximum post-carbonisation char yield for steam activation. Carbonisation optimisation tests were performed on JKWS and the same optimised parameters were applied to JKWR carbonisation to enable a direct comparison between the products.

Initial carbonisation tests were carried out using a small rotary furnace; a Carbolite HTR 11/75 (Carbolite Ltd., Derbyshire, UK) to conserve the samples, given that the preparation of samples especially JKWR was a laborious task. Once carbonisation parameters were established, batch carbonisation was carried out in a quartz reactor using the larger version of the Carbolite rotary furnace, the Carbolite HTR 11/150 furnace (Carbolite Ltd., Derbyshire, UK). The quartz reactors were made by Multi-Lab Ltd. in Newcastle-upon-Tyne, UK. The carbonisation temperature, heating rate and dwell times were controlled by a Eurotherm controller (Invensys Eurotherm, Worthing, UK).

Samples were weighed and loaded into the quartz reactor, which was then mounted into the furnace. All the carbonisation parameters were set via the controller. The quartz reactor used in the Carbolite HTR 11/150 holds approximately 150g of JKWS and 250g of JKWR, compared to 25g of JKWS and 30g of JKWR in the Carbolite HTR 11/75. A nitrogen gas purge rate of 100ml/min for the Carbolite HTR 11/150 was selected and a rotation rate of 10 rpm was kept constant for all carbonisation experiments to promote even carbonisation of the samples in the reactor. A schematic diagram of the reactor placed inside the furnace is shown in Figure 6-1.

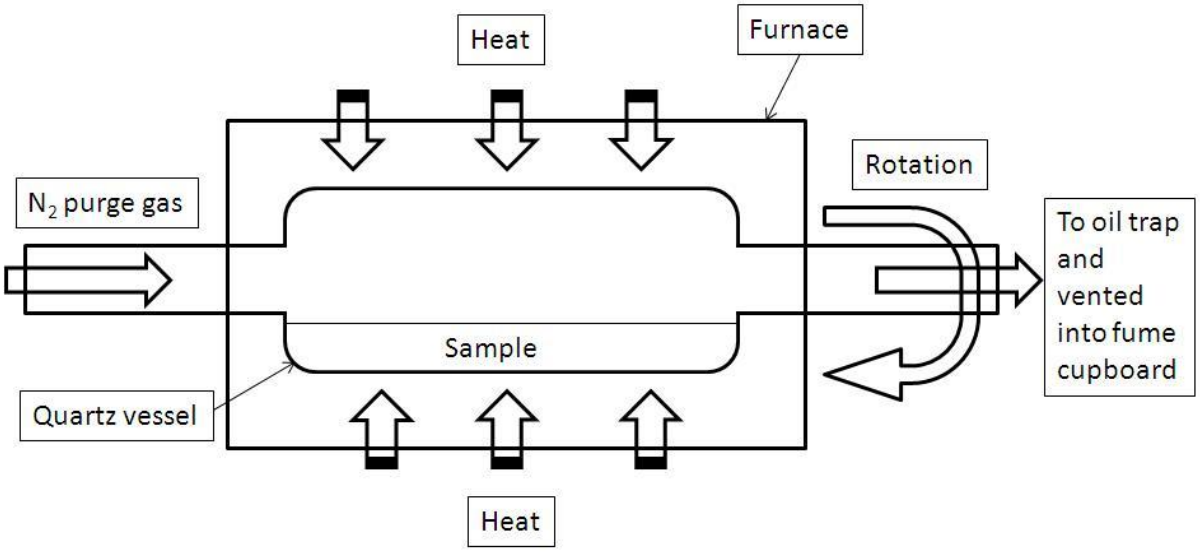


Figure 6-1: Frontal schematic view of Carbolite HTR 11/XX rotary furnace.

The volatiles were condensed into a large, upright, cylindrical oil trap. The pyrolysis bio-oil was collected and weighed along with char from the reactor whereas any gas was allowed to escape into the fume hood. The yield of syngas was determined by difference between the total feedstock weight, char and bio-oil weights.

A 2-step batch process which involved separate carbonisation and activation steps was used in order to enable accurate yield calculations and to separate the bio-oil from the char produced during carbonisation to avoid any possible contamination of the activated carbon made during and after steam activation.

Although characterisation tests indicated that high ash and low carbon contents made GW unsuitable as AC precursors, it was decided to perform some carbonisation tests on a larger scale to determine if the inconsistent results were due to the heterogeneity of the GW samples obtained. Moreover, heterogeneity in the composition of GW has been documented (Boldrin and Christensen, 2010).

The next steps were to optimise char production by establishing preferred heating rate, carbonisation temperature and dwell time. From literature (Mohan *et al.*, 2006, Williams and Besler, 1996, Babu, 2008, Bridgwater *et al.*, 1999), it is known that a low heating rate and carbonisation temperature results in high char yield.

As shown in the TGA results from Section 5.4.4, carbonisation for all waste biomass samples was essentially complete from a temperature of 400°C upwards and there was not much change in the sample weight at higher carbonisation temperatures, as can be seen in Figure 5-8. Therefore, a carbonisation temperature range of 400°C to 800°C with a heating rate of 5°C/min (Julcour Lebigue *et al.*, 2010) was chosen to maximise char production. The 1°C/min heating rate that was used during TG analysis was not selected as it would take too long to perform the carbonisation experiment. Furthermore, the larger Carbolite HTR 11/150 to be used for batch carbonisation does not support high heating rates (>10°C/min) so a compromised heating rate of 5°C/min was reached. Higher heating rates will decrease the char yield and increase the volatiles yield (Mohan *et al.*, 2006, Williams and Besler, 1996).

It has been reported that the evaporation of levoglucosan (formed during the <300°C pyrolytic reactions of cellulose) and volatile pyrolysis products is highly endothermic (Shafizadeh, 1982). In order to ensure completion of pyrolytic/carbonisation reactions and hence, the production of stable char alongside maximum char yield from the samples in the quartz reactor, a 1 hour dwell time was incorporated into all carbonisation experiments (Román *et al.*, 2008).

6.2 Results

6.2.1 GW Carbonisation

Approximately 30g of GW sample was carbonised in the Carbolite HTR 11/75. A nominal nitrogen gas flow rate of 100ml/min was used and the carbonisation temperatures chosen ranged from 300°C to 800°C. The selection of temperatures was based on the TG and DTG data plots in Section 5.4.4; according to which, pyrolysis was essentially complete from 400°C for GW and the minimum char yield should be approximately 58% w/w at 800°C.

Table 6.1: Char, bio-oil and gas yields of GW carbonisation at 5°C/min and 1h dwell time.

Carbonisation Temperature/°C	Char yield/%	Bio-oil yield/%	Gas yield/%	Total volatile* matter/%
300	86.9 ± 1.6	4.3 ± 0.6	8.8 ± 2.0	13.1
400	68.1 ± 4.9	10.2 ± 5.8	21.7 ± 4.5	31.9
500	70.9 ± 0.3	16.1 ± 0.8	13.0 ± 1.1	29.1
600	65.4 ± 8.2	6.1 ± 2.2	28.5 ± 9.9	34.6
700	64.7 ± 0.5	18.8 ± 1.1	17.2 ± 0.6	36.0
800	58.0 ± 1.0	5.8 ± 3.0	36.3 ± 3.1	42.1

* Data obtained by addition of bio-oil and gas yields. SD values obtained from 3 different measurements.

Carbonisation experiments were run three times and yields were averaged with the standard deviations (SD) calculated to show reproducibility of the results, which are shown in Table 6.1.

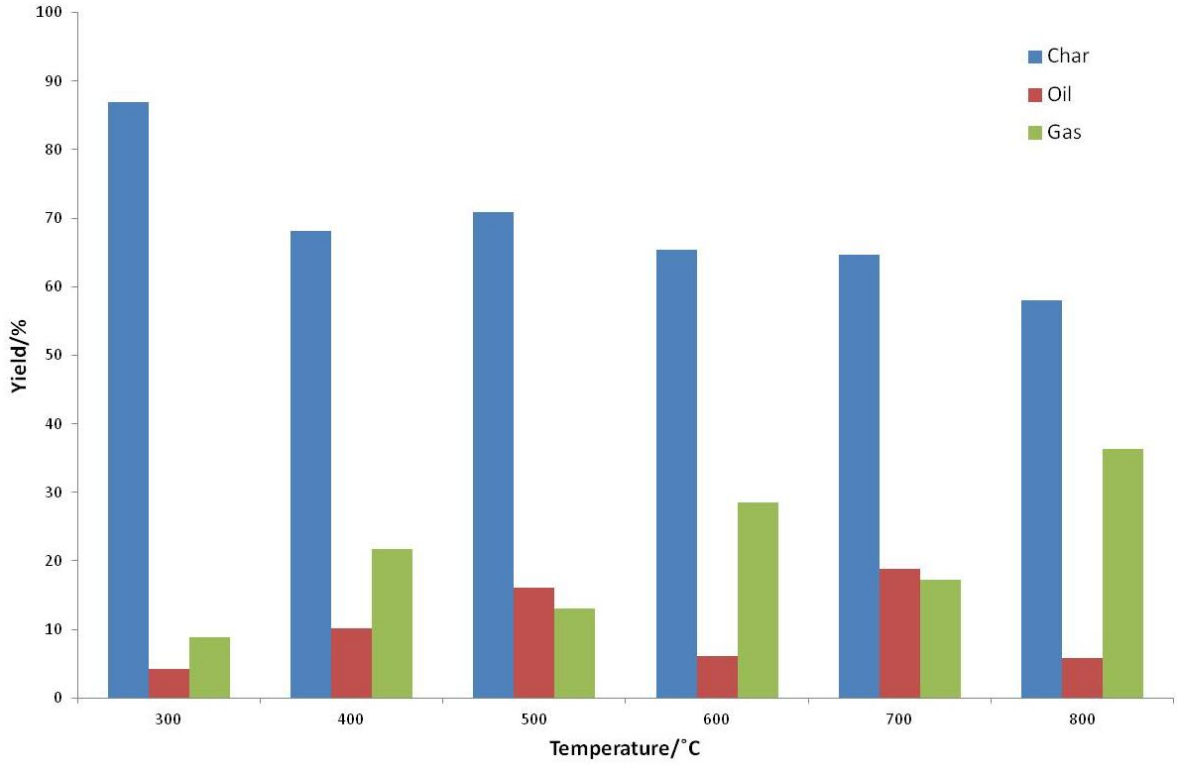


Figure 6-2: Carbonisation yields of GW at different temperatures.

Figure 6-2 shows the yields generated by carbonisation at the aforementioned temperatures. It is apparent that volatiles yields (bio-oil and gas) measured are inconsistent; they do not follow any

known trend. Volatiles yield are expected to increase with increasing carbonisation temperatures as mentioned in Section 3.5.2.

In comparison, char yields do show a decrease with higher carbonisation temperatures as per literature as seen in Figure 6-2. However, the trend is irregular. Char yields for each temperature have relatively low SD values, indicating good repeatability but this is down to the consistently high ash content, which inflates the 'char' content. In fact, once the ash content of GW has been factored into the char yields, it can be seen that there is very little char left and in some cases, no char yield at all as in the 800°C experiment as seen in Table 6.2.

Table 6.2: Char yields from the carbonisation of GW on ash-free basis.

Carbonisation Temperature/°C	Char yield on ash-free basis/%
300	28.9
400	10.1
500	12.9
600	7.4
700	6.7
800	0.0

The irregular patterns of bio-oil and gas yields indicate that the intrinsic heterogeneity of GW plays a major role in its thermal decomposition behaviour. However, the total volatile matter (gas and bio-oil) does increase with temperature, which is in line with literature data (Mohan *et al.*, 2006), which suggests that a better volatile condensation system might be needed. Quenching of gases could be carried out to increase the bio-oil yield. Additionally, bio-oil is formed from the thermal degradation of holocellulose and from Section 5.4.3; the holocellulose content of GW is less than half of the holocellulose content of JKWS and JKWR. Further, the characterisation tests of GW indicated that the samples received are in an advanced state of decay. Moreover, the implemented technology of carbonisation at relatively low temperatures and heating rates does not encourage the formation of bio-oils and syngas (Mohan *et al.*, 2006). Hence, as the objective of this project was to determine the suitability of the waste biomass as precursors for activated carbons, no further investigations were conducted into optimising volatiles yield.

6.2.2 JKW Carbonisation

JKWR and JKWS was carbonised at 5°C/min from 300°C to 800°C in nitrogen and held for 1h at each respective temperature in the Carbolite HTR 11/75.

JKW exhibited high homogeneity, thus it was decided that all experiments in this section would be only run once and a random carbonisation run was selected to be run in triplicate and the RSD values from that experiment was applied to the other samples. The repeatability of the Carbolite HTR 11/75 is shown in Table 6.3 using 600°C carbonisation experiments. This temperature was chosen as it exhibited the highest SD during GW carbonisation and a comparison between GW, JKWS and JWKR carbonisation can be conducted.

As can be seen in Table 6.3, the results of batch carbonisation of both JKWS and JKWR were within 2% of the triplicate runs, indicating a repeatable methodology as well as a consistent and homogeneous feedstock. In comparison to GW carbonisation at 600°C in Table 6.1, JKWS and JKWR demonstrated lower SD values, particularly for char yield.

Table 6.3: Average char yields of JKWS and JKWR at carbonisation temperature of 600°C for 1h in the Carbolite HTR 11/75. SD values obtained from 3 different measurements.

Char yield	**JKWS**	**JKWR**
Average/%	24.09	31.09
Standard deviation/%	0.10	0.33
RSD/%	1.42	1.07
Bio-oil yield		
Average/%	44.30	37.40
Standard deviation/%	1.22	1.62
RSD/%	2.74	4.32
Syngas yield		
Average/%	31.62	31.51
Standard deviation/%	1.04	1.51
RSD/%	3.30	4.81

It can also be observed in Table 6.3 that JKWR had higher char yields than JKWS. Gonzalez *et al.* (2009) and (Zanzi *et al.*, 2002) observed that the char yield is highest for biomass precursors with the

highest lignin content and this is reflected in this study, with JKWR possessing a marginally higher lignin content of 21.2% and JKWS having 19.9% as observed in Table 5.3.

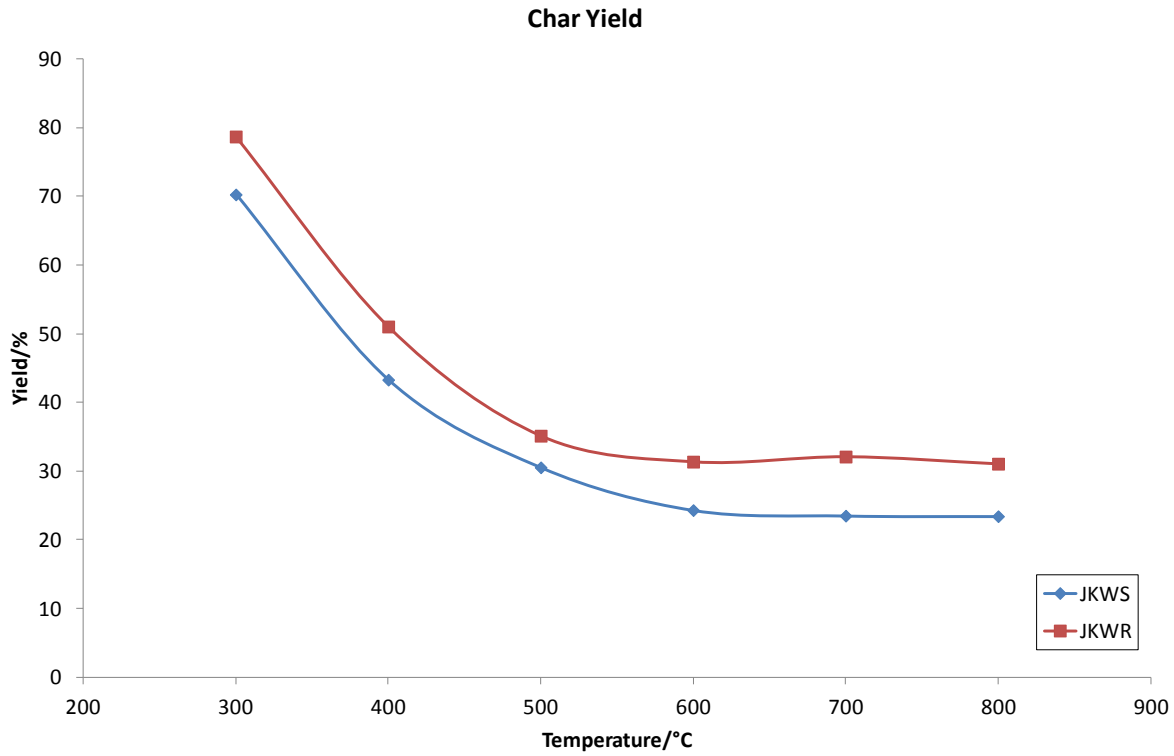


Figure 6-3: Char yield trends for JKWS and JKWR carbonisation using Carbolite HTR 11/75.

As seen in Figure 6-3, a decrease in char yield is observed from 300°C to 500°C but at 600°C, the trend starts to plateau. This agrees with trends observed in literature for the carbonisation of biomass (Lua *et al.*, 2004, Beis *et al.*, 2002, Demirbas, 2004). The char yield is particularly high at 300°C due to the dehydration reactions occurring, resulting in the formation of anhydrocellulose, which increases the char yield (Williams and Besler, 1996, Shafizadeh, 1982). However, there is still a substantial amount of uncarbonised matter remaining at 300°C, which suggests that the depolymerisation and carbonisations have not stabilised (Williams and Besler, 1996).

The char yield of JKWR decreased from 78.8% at 300°C to 31.1% at 800°C whereas JKWS char yield decreased from 70.3% to 23.4% at the same temperature range. As carbonisation proceeds, the biomass carbon structure is being re-organised to form an irregular but energetically stable char structure as carbonisation temperatures increase.

The formation of char can be explained by the decomposition of lignin, which forms the bulk of the char carbon structure (Demirbas and Arin, 2002). At the lower temperatures, weak bonds are

cleaved whereas at the higher temperatures, aromatic cracking and condensation occurs. This is accompanied by the dehydration of cellulose in the formation of char (Yang *et al.*, 2007, Shafizadeh, 1982, Demirbas and Arin, 2002).

JKWR had a slightly higher char yield at all temperatures due to the marginally higher lignin content (21.2%) over JKWS (19.9%). JKWR also had a much higher cellulose content (53.4% to 31.8%), which also contributes to the char yield, particularly at the low heating rates used. The decrease in char at high temperatures is due to the devolatilisation reactions that occur, which remove the non-carbon atoms to form low MW, volatile hydrocarbons. This results in increases in bio-oil and gas yields, as observed in Figure 6-4 and Figure 6-5.

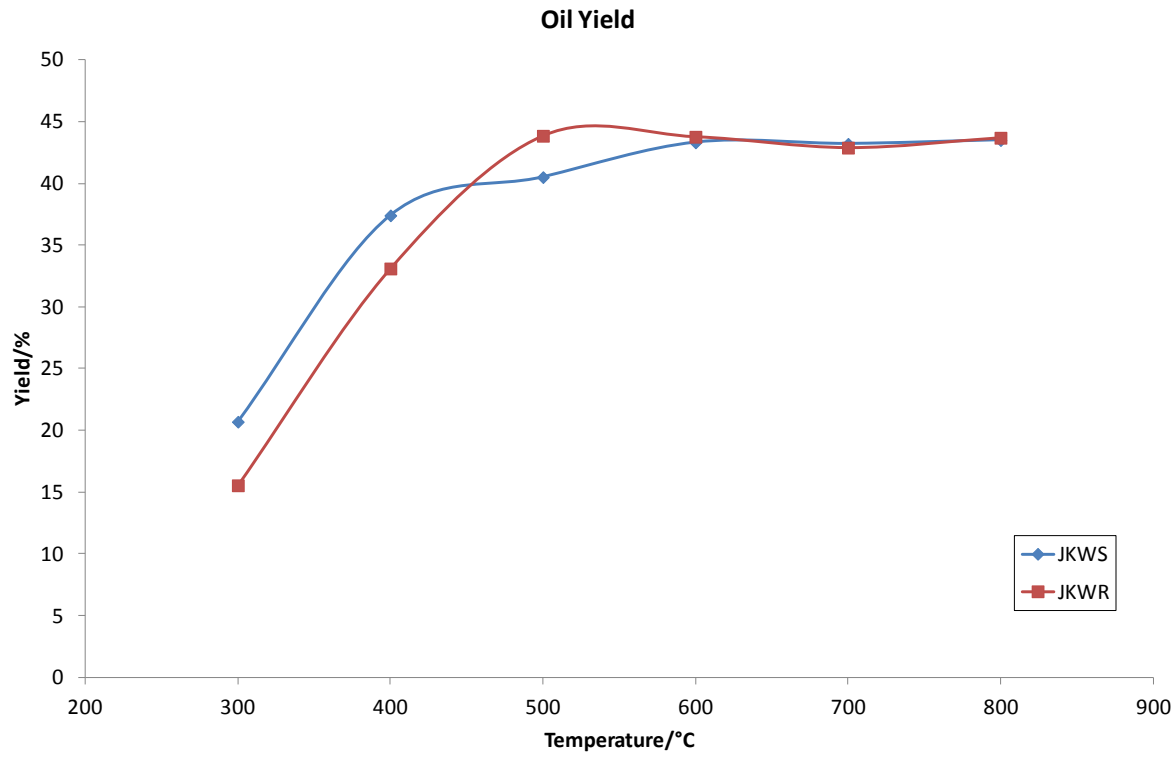


Figure 6-4: Bio-oil yield trends for JKWS and JKWR carbonisation using Carbolite HTR 11/75.

The bio-oil yields of JKWR increased from 15.5% to 43.7% between 300°C and 500°C as seen in Figure 6-4. It can be seen that at the same temperature range, JKWS oil yields increased from 20.7% to 43.5%.

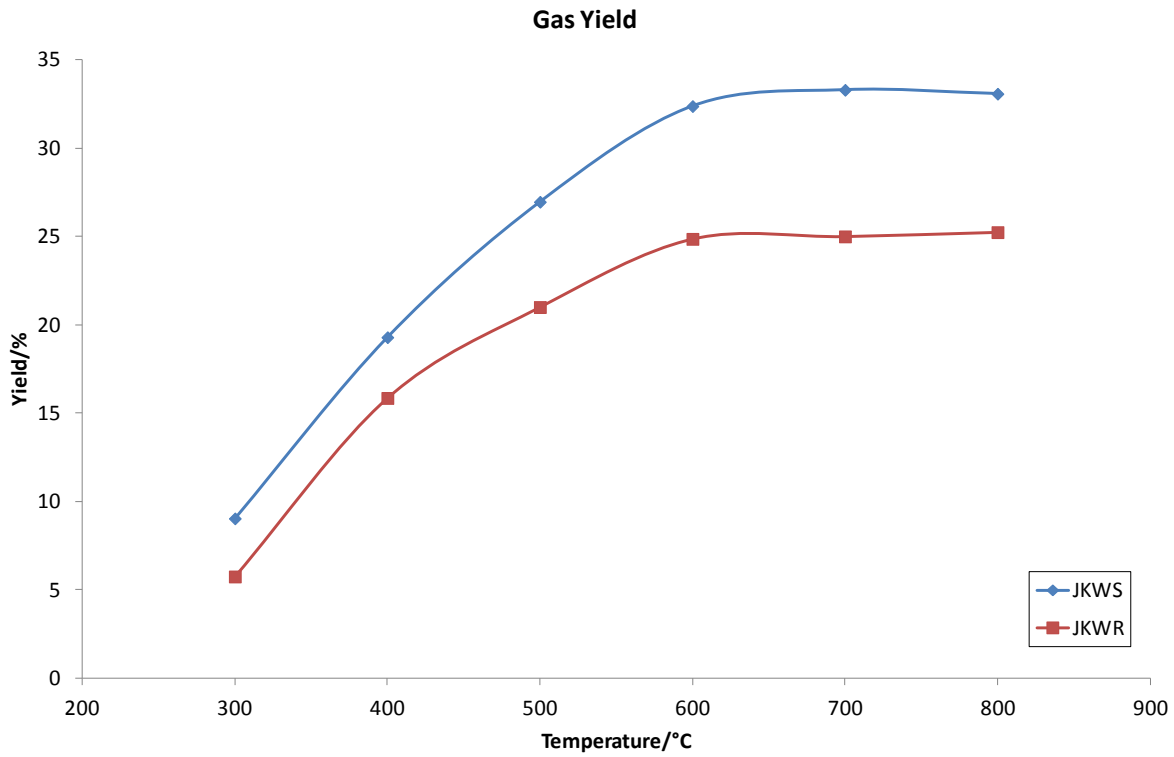


Figure 6-5: Gas yield trends for JKWS and JKWR carbonisation using Carbolite HTR 11/75.

The gas yields of JKWR were observed to have increased from 5.7% to 25.0% between 300°C and 600°C in Figure 6-5 as a result of the carbonisation process. JKWS gas yields increased from 9% to 33.1% at the same temperature range. Hemicellulose makes the largest contribution to the volatiles content (bio-oil and syngas) by forming very short molecular units, which decompose further. Yang *et al.* (2007) reported that hemicellulose decomposition resulted in high CO_2 yields due to its high carboxyl content and this contributes to the gas yield.

At low carbonisation temperatures, the degradation of lignin does not significantly influence the char yield as it is thermally stable (Yang *et al.*, 2007). Charring reactions can be inferred to have been completed once char yields stabilise as the insignificant weight loss at temperatures above 500°C indicate that the basic structure is already formed (Molina-Sabio and Rodŕiguez-Reinoso, 2004).

Bio-oil yields are at minimum levels at 300°C as the main contributing reaction to bio-oil yield has just started. This reaction involves the secondary degradation of cellulose at temperatures >300°C produces more levoglucosan and less anhydrocellulose, which contribute to bio-oil and char yields, respectively (Shafizadeh, 1982). As the carbonisation temperature increases, greater heat transfer results between the reactor and the JKW biomass, encouraging primary pyrolysis reactions and initiating secondary autocatalytic reactions, which in conjunction with condensation of some

volatiles produces tar, a main component of bio-oil (Mohan *et al.*, 2006). Therefore, bio-oil yield should increase as temperatures increase up to a point where the primary pyrolysis reactions and secondary autocatalytic reactions are in competition with each other. At this impasse, the influence of the other components of biomass, heating rate and residence (dwell) times will come into effect. From Figure 6-4 and Figure 6-5, JKWR and JKWS bio-oil yields are very similar in weight as well as following the same trend. This is due to the similar holocellulose contents (77.2% to 78.5%), which is responsible for tar production (Fagbemi *et al.*, 2001).

JKWS gas yields, on the other hand are higher than JKWR gas yields at increasing carbonisation temperatures and this can be correlated with the higher hemicellulose content of JKWS as the decomposition of hemicelluloses results in more volatiles, less chars and tars than cellulose (Mohan *et al.*, 2006). Furthermore, devolatilisation reactions are favoured at higher temperatures, as noted by Fagbemi *et al.* (2001).

In order to determine whether the char produced contained any volatile matter, proximate analysis using the thermal analyser was carried out. The results are shown in Figure 6-6. This aided in the determination of the optimum carbonisation temperature. Results obtained are on a percentage weight basis.

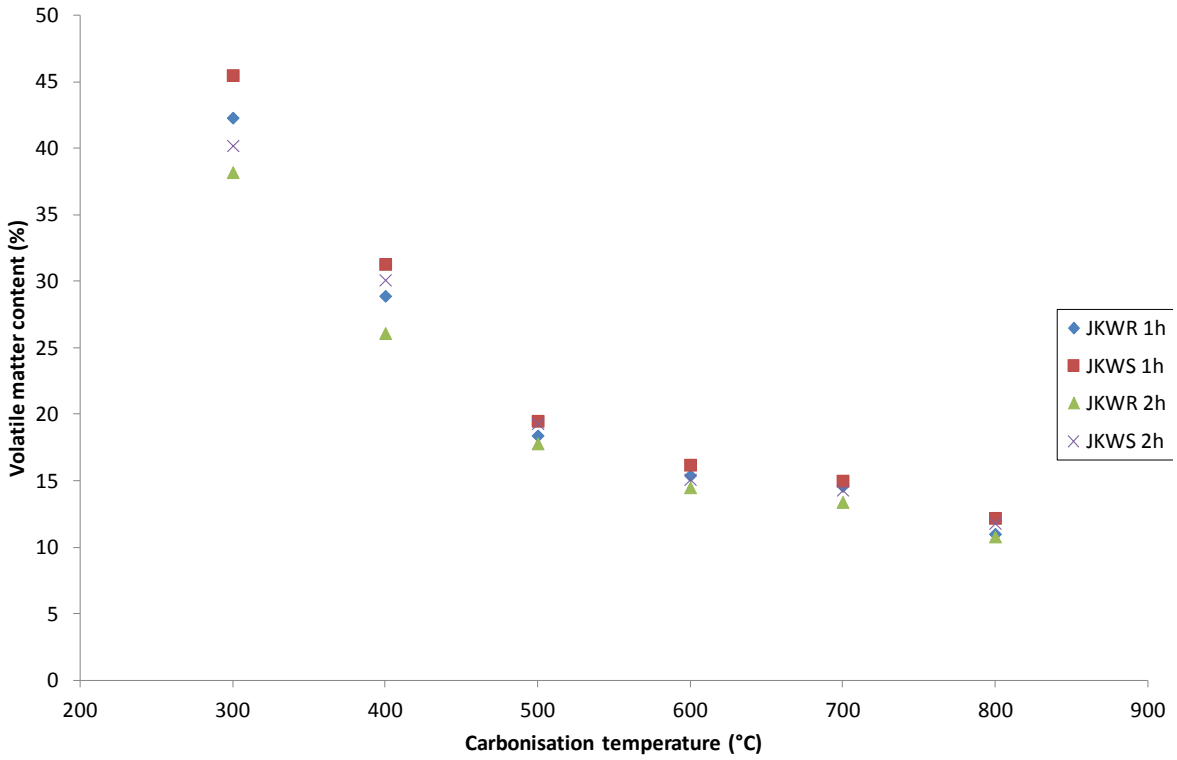


Figure 6-6: Amount of volatile matter content remaining in JKWS and JKWR chars carbonised at different temperatures.

Figure 6-6 shows that as carbonisation temperature increases, the volatile matter content of the char decreases, indicating increasing stabilisation of the char carbon structure, which is an expected result. It can be seen that there is no significant difference in volatile matter content between 1h and 2h dwell times, especially at the higher carbonisation temperatures. Nevertheless, it shows that with extended dwell time, the chars are tending towards a more stable structure as less volatile matter is released.

The presence of volatile matter could be explained by trapped tarry substances in the porous structure of the char carbon structure (Smíšek and Černý, 1970), which is only released at high temperatures, as observed during the proximate analyses of the chars.

In fact, with the temperature of proximate analysis reaching 950°C, the devolatilisation and carbonisation reactions will proceed regardless until all the carbon in the feedstock is stabilised. In order to obtain a stable form of char with little volatile matter, JKWR and JKWS can either be treated at high temperatures or utilise a lower temperature with long dwell times. From the char yield plot in Figure 6-3, a temperature of 600°C for both JKWS and JKWR was chosen as the compromised carbonisation temperature for batch carbonisation as char yields have started to plateau and using

carbonisation temperatures greater than 600°C does not appear to result in further char yield increases. Additionally, the extra carbonisation time and energy utilised cannot be readily justified.

From Figure 6-6, the difference in reduction of volatile matter at 600°C at different dwell times was only 0.9% for JKWR and 1.1% for JKWS. As such, the dwell time was set to 1h instead of 2h to reduce the amount of energy spent on carbonisation. Furthermore, the char will be heated to temperatures beyond 600°C during steam activation and that will remove any residual volatile matter that might remain trapped in the pores of the carbon structure.

In conclusion, the batch carbonisation of JKWR and JKWS will be performed at a temperature of 600°C at a 5°C/min heating rate with a dwell time of 1h. These parameters have also been utilised by Román *et al.* (2008) for their work in the activation of olive stones.

However, it is noticed that the majority of the products formed during carbonisation of JKWR and JKWS are in the form of volatiles, i.e. bio-oil and syngas. This is a result of the high holocellulosic contents of both feedstocks, as presented in Table 5.3 of Section 5.4.3. Similar observations were made by Gonzalez *et al.* (2009) for almond shells, walnut shells, almond tree prunings and olive stones. JKWS bio-oil yields are slightly higher as a result of the higher hemicellulosic content whereas syngas yields of both were similar. However, since gas yields were calculated by subtraction, they can be influenced by the accuracy of the determination of the other 2 fractions (Gonzalez *et al.*, 2009).

6.3 Carbonisation Summary

The Carbolite HTR 11/75 carbonisation runs of GW effectively confirmed that it is an unsuitable precursor for activated carbons. The high RSD values obtained from the carbonisation of GW (Section 6.2) indicate that the GW samples received were not homogenous enough to be a precursor for activated carbons. Additionally, the high amount of ash recorded during GW carbonisation suggests that there would not be enough fixed carbon present in the GW char for steam activation. GW is inherently heterogeneous due to its make-up of different kinds of organic waste (Andersen *et al.*, 2010, Boldrin and Christensen, 2010, Williams and Kelly, 2003, Williams, 2006). Ultimately, the diverse nature of GW, its high ash and low carbon content makes it unsuitable as a precursor for activated carbons.

A decision was made to disregard further GW as a focus of further research and to concentrate on JKWR and JKWS biomasses instead. The carbonisation of both JKWS and JKWR demonstrated consistent results in terms of char yields and both had high fixed carbon content and low ash content.

JKWR had higher lignin content and thus, produced more char than JKWS. However, the char produced during carbonisation at 600°C by JKWR and JKWS was less than their respective volatile matter (bio-oil and syngas) yields due to the fact that both had much greater holocellulosic yields than lignin.

Chapter 7. Steam activation optimisation

The activation procedure that was selected was physical activation using steam. The choice of steam activation was influenced by its preference in the activated carbon industry (González *et al.*, 1994, Molina-Sabio *et al.*, 1996, Gergova and Eser, 1996). Additionally, steam is a more reactive agent than CO_2 and as a result, is able to achieve adequate burn-off with the application of lower temperatures of activation (San Miguel *et al.*, 2003, Wigmans, 1989, Rodŕiguez-Reinoso *et al.*, 2000). It has also been reported that activated carbons obtained with steam have higher BET surface areas (López *et al.*, 2009) with well-developed micropore structure when compared to activation by CO_2 or O_2 (Wigmans, 1989). This is a consequence of the smaller dimension of the H_2O molecule which permits fast diffusion into the porous system of the carbon, giving it enhanced accessibility towards the micropores and thus, results in a significantly faster reaction rate for the gasification reaction (Wigmans, 1989). Physical activation also enables a moderate degree of control on the development of porosity in the activated carbons (Román *et al.*, 2008), although this is beyond the scope of this project.

Chemical activation was not considered as a suitable process due to the usage of chemicals required for activation, their aggressive nature and harmful by-products (e.g HCl from $ZnCl_2$ activation) and the necessity to wash the produced activated carbon to remove/recover and/or dispose of the abovementioned chemicals after activation. Commercially, chemical activation is rarely applied due to the added complications and costs of operating the process in comparison to physical activation (Fowler, 1995). The environmental impact of steam is also likely to be less than the impact of chemical activating agents and creates less waste at the end of the process (Guo and Chong Lua, 1998). Furthermore, the equipment available to use in this study (the quartz reactors) would be attacked by the chemical activating agents. These reagents are normally alkali- or alkaline earth metal-containing substances which devitrify the quartz reactor used at high temperatures.

To enable a realistic evaluation of the adsorptive properties of the produced JKWS and JKWR carbons, comparisons with a commercial carbon were deemed necessary. The commercial carbon chosen was Chemviron Filtrasorb 400 (Chemviron Carbon Ltd., Ashton-in-Makerfield, UK) was used as the commercial comparison given the fact that it is regarded as the standard activated carbon for water treatment. Its measured technical data is given in Table 7.1.

Table 7.1: Measured technical details for Calgon Filtrasorb 400.

Carbon	Feedstock	Iodine number (mg/g)	BET surface area (m^2/g)	Total Pore Volume (ml/g)	Langmuir Phenol capacity (mg/g)	Butane working capacity (%)	Bulk density (g/cm^3)	Ash content (%)
Calgon F400	Coal	1000	977	226	159	15.6	0.54	9.00

Filtrasorb 400 is written as F400 in this study. The aim of this section is to investigate the steam activation conditions that will produce activated carbons from both JKWS and JKWR with the highest closest properties to the F400. This includes surface area and their performance during characterisation tests.

7.1 Experimental protocols

The conditions investigated for steam activation were:

- Activation temperature
- Activation time
- Water (steam) flow rate

It is known that the activation temperature affects the adsorptive properties of the produced activated carbons, together with the length of time the carbons are allowed to react with different amount of water being introduced into the reactor during steam activation. As such, different combinations of the above-mentioned parameters were investigated to determine the properties induced in the produced JKWS and JKWR activated carbons.

Five different activation temperatures were investigated and these were 825°C, 850°C, 875°C, 900°C and 925°C. In order to aid comparison, the activation time and water flow rate were kept constant at 0.5h and 0.1 ml/min, respectively throughout the experiments determining the effect of activation temperature.

The aim of the activation experiments was to increase BET surface area and to increase the extent of activation, i.e. the burn-off values. Literature states that 40-50% burn-off is optimal for the development of microporous activated carbons (Rodriguez-Reinoso and Molina-Sabio, 1992,

Wigmans, 1989, Román *et al.*, 2008) and burn-off values larger than 50% produce meso- and macroporous carbons (Bansal, 2005) and hence, the experiments conducted in this project are kept to the aforementioned burn-off values.

7.1.1 Bulk char production

In order to produce enough chars for steam activation, JKWS and JKWR were carbonised separately in a Carbolite HTR 11/150 at 600°C using a heating rate of 5°C/min with a 1h dwell time, as discussed previously in Section 6.2.2. The temperature and heating rate was chosen to maximise the char yield and a dwell time was incorporated to ensure the biomass were completely carbonised. In Section 6.2.2, it was shown that a long carbonisation dwell time did not warrant the minor decrease in volatile matter evolved from chars produced at 600°C.

7.1.2 Elemental analysis of Japanese knotweed and its chars

During the initial studies for steam activation of JKWS, it was noted that the quartz reactors were unexpectedly losing mass. The reactors have been used for several decades by the research group and this particular problem has not been noted before, for biomass samples. This led to the conclusion that the JKW samples were releasing unknown substances during steam activation that was attacking the quartz vessels. This was of significant concern given that it increased the risk of reactor failure during steam activation, which may result in a fire if hot char is exposed to air. Thus, an investigation of the cause and hence, the development of a remedy for this issue was implemented.

At high temperatures, alkaline earth metals such as Na, K, Mg and Ca present in the JKW biomass will react with the quartz reactor causing devitrification (Momentive, 2012), which will ultimately lead to failure of the reactor. Given that this issue had been previously observed during initial steam activation tests, steps were taken to determine the metals content of JKWS and JKWR char. Furthermore, experiments were undertaken to decrease the alkaline earth metals content in the char through the application of a proprietary acid washing process.

All elemental determinations of JKW samples were conducted using Inductively-Coupled Plasma with Optical Emission Spectroscopy (ICP-OES). The equipment used was a Perkin Elmer 7300DV ICP-OES.

During ICP-OES analysis, the sample is subjected to high temperatures generated by the argon plasma which causes the sample to dissociate into its atoms, which then ionises. Once the ions decay from their excited states, they release thermal or radiative (emission) energy. The intensity of the light emission at specific wavelengths is detected by the spectrophotometer and is used to determine the concentrations of the elements of interest.

7.1.2.1 Sample preparation

Samples for elemental analysis were prepared using microwave digestion. An Anton Paar Multiwave 3000 microwave reaction system (Anton Paar, Graz, Austria) with a MF100 pressure vessel in a 16 position rotor was used to acid digest the waste biomass and char samples to digest the samples using USEPA Method 3051a (USEPA, 1996). Glassware was soaked in 5% nitric acid for 24 hours before use and immediately prior to use, was rinsed with 1M nitric acid; the matrix for the calibration standards used. The soaking and washing were to remove any contamination that might have been present in the glassware used. The calibration standards were a multi-elemental standard (Merck ICP Multi Elemental Standard Solution IV CertiPUR). The nitric acid used was VWR Analar grade.

0.5g of ground sample (<500µm) was added to the PTFE microwave reaction vessel, along with 9ml of HNO_3 and 3ml of HCl. The heating program of the microwave acid digestion raised the temperature to 175°C in 5.5 min and held it at 175°C for 4.5min. Upon cooling of the reactor vessels, the sample is quantitatively transferred to a 100ml volumetric flask and made up to volume using 1M HNO_3.

Before ICP-OES analysis, the diluted sample was filtered using Whatman cellulose nitrate membrane 0.45µm syringe filters (Whatman, Maidstone, UK). To ensure good quality control, a blank spike and a sample spike were added to separate reaction vessels and underwent the same preparation procedures carried out for actual samples.

The biomass standards used were oriental tobacco leaves (OTL), which were obtained from the Institute of Nuclear Chemistry and Technology in Warsaw, Poland to ensure reproducibility of the digestion and analytical method.

7.1.2.2 Acid washing of JKW chars

There are usually 2 types of ash in biomass: leachable and non-leachable ash. Leachable ash can be removed using acid wash whereas non-leachable ash is embedded within the carbon matrix and cannot be washed with acid (Pendyal *et al.*, 1999).

The produced chars were acid washed with 0.2M HCl for 24 hours. This was repeated three times in a process called the ReACT washing process (Fowler, 2011), which is a proprietary process used by Chemviron Carbon Ltd. to remove metals from activated carbons returned from service prior to reactivation. The chars were washed to reduce the concentration of alkaline earth metals (Ca, Mg, K and Na) before steam activation to minimise the devitrification of the quartz reactor, which can lead to reduced service life and unexpected vessel failure.

A 50g sample of char was placed in a 500ml conical flask with a screw top and 500ml of 0.2M HCl was added (1:10 weight ratio) using a measuring cylinder. The conical flask was then placed onto a Janke & Kunkel (IKA, Staufen, Germany) KS 501 D rotational shaker and shaken at 150 rpm for 24h. The acid wash was renewed every 24 hours for 72 hours. After the final acid wash, the char was then washed with boiling distilled water until a constant pH was reached. The washed chars were then dried in an oven at 105°C for 24h.

The washed and dried chars were microwave digested and the digestate was analysed using ICP-OES.

7.1.3 Scanning electron microscopy

A scanning electron microscope (SEM) permits the observation and characterisation of heterogeneous organic and inorganic materials on a nanometer to micrometer scale. The SEM is able to generate 3D-like images of the surfaces of materials (Goldstein, 2003).

In the SEM, the area to be examined is irradiated with a finely focussed electron beam. The types of signal produced by the interaction of the electron beam with the sample can be used to examine the characteristics of the sample. The 3D appearance of the images is due to the large depth of field of the SEM as well as the shadow relief effect of secondary and backscattered electron contrast (Goldstein, 2003).

Due to weak electron interactions, the sample has to be placed in a vacuum. For non-conductive surfaces i.e., JKW samples the surface needs to be coated with a layer of gold to ensure conductivity whereas carbon samples do not need to be gold coated. In this work, a JEOL 5610LV SEM (JEOL Ltd., Tokyo, Japan) was used, which was located in the Department of Materials, Imperial College London.

7.1.4 Characterisation and testing of activated carbons

All samples of activated carbon produced from JKWS and JKWR were characterised using the following tests:

- Ash content
- BET Surface Area
- Apparent Density
- Butane Working Capacity
- Contact pH
- Iodine number
- Phenol Adsorption

Steam activation was performed in the small rotary furnace; the Carbolite HTR 11/75 using the quartz reactor as previously mentioned in Section 6.1. Due to the difference in bulk densities of the produced JKWS and JKWR chars, the utilised quartz reactor holds 15g of JKWS char and about 25g of JKWR char. The bulk density of the chars was determined to be 0.29g/ml for JKWR char and 0.11g/ml for JKWS char.

To enable steam activation within the quartz reactor, a small diameter stainless steel pipe is inserted into the reactor and water is pumped through the pipe by a calibrated Watson Marlow 101 U/R peristaltic water pump (Watson Marlow Pumps Group, Falmouth, UK). The pump is switched on the moment the furnace reaches the activation temperature to deliver the required flow rate of water into the furnace. The water is vaporised into steam at the activation temperatures.

A nitrogen gas purge flow rate of 100ml/min was kept constant for all activation experiments, along with a 10 rpm rotation of the reactor. The produced AC was allowed to cool down under nitrogen to

room temperature. It should be noted that during activation with steam, the nitrogen gas was kept flowing through the reactor.

A cold-finger condenser, immersed in liquid nitrogen was connected to the gas outlet end of the reactor via a custom-made adaptor to collect the amount of water (steam) unused during activation. The effect of activation temperature, activation time and water flow rate on the activated carbons produced from JKWS and JKWR char by steam activation were investigated.

The produced chars are named using the precursor as a prefix, followed by AC to denote its status as an activated carbon and a string of 3 sets of numbers separated by dashes which indicate the activation temperature, activation time and the water flow rate respectively.

As an example, JKWS AC 825-1-0.1 indicates that the activated carbon was made from JKWS at the activation temperature of 825°C, held at that temperature for 1hr and the water flow rate used during the hold time was 0.1ml/min. The heating rate for all activation experiments was fixed at 5°C/min.

To ensure that the results of testing between JKWS AC and JKWR AC were comparable, all experimental activation parameters that were established based on experiments using JKWS AC were emulated for JKWR AC.

The characterisation of the activated carbons produced was carried out according to the international standards, where applicable.

7.1.5 Burn-off

The burn-off is determined by gravimetric methods and the following relationship is used to calculate burn-off:

Equation 7-1: $$Burn-off, \% = 100 - \left(\frac{Mass\ of\ char\ after\ activation}{Mass\ of\ char\ before\ activation} \times 100\right)$$

7.1.6 Ash content

The ash content was determined using ASTM Method D2866-94 (99) (ASTM, 1994a). Samples of activated carbon are dried at 150°C for at least 3 hours and placed in a crucible that was previously fired at 650°C for 1h, cooled and weighed.

The crucibles are filled with the samples and then fired in the muffle furnace at 650°C for 3-16h and ashing is considered to be complete when a constant weight is achieved. The crucible is weighed after cooling in a desiccator.

Ash content is calculated according to Equation 7-2:

Equation 7-2: $$Total\ ash, \% = \frac{D-B}{C-B} \times 100$$

Where: B= weight of empty crucible in g; C= weight of empty crucible and original sample in g and D= weight of empty crucible and ashed sample in g.

7.1.7 Contact pH

The pH was determined according to the method of Bagreev *et al.* (2001). A dried sample of 0.4g was mixed with 20ml distilled water and shaken overnight. The pH was measured after filtration of the sample. The pH meter used was a calibrated Fisher Hydrus 500 with a VWR pH electrode.

7.1.8 Apparent Density

Apparent density of the produced activated carbons was determined according to ASTM Method D2854-96 (ASTM, 1996b). A diagram of the apparatus used is shown in Figure 7-1:

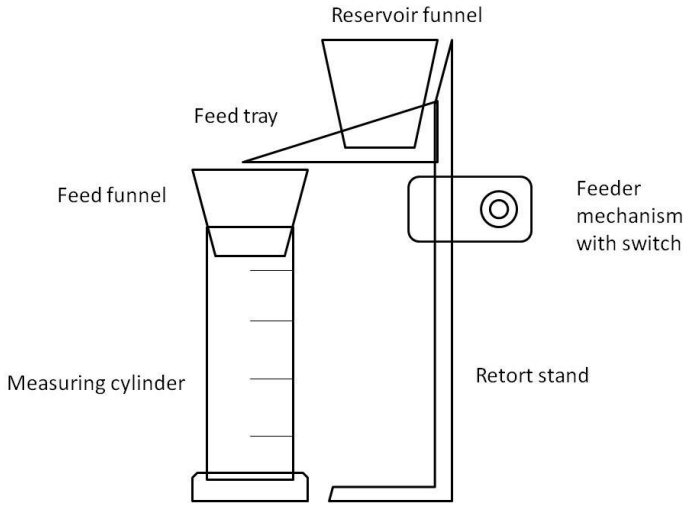


Figure 7-1: Assembly of apparatus used for apparent density.

A representative sample of the carbon is placed in the reservoir funnel without it spilling into the pre-weighed measuring cylinder. The experimental setup is shown in Figure 7-1. The apparatus is then switched on and the sample is fed into the measuring cylinder by the vibrating action of the feeder. This ensures that the sample particles are evenly packed into the cylinder. The measuring cylinder is weighed with the sample and the volume is read off the graduations.

The apparent density is calculated by Equation 7-3:

Equation 7-3: $$Apparent\ density, \frac{g}{ml} = \frac{Mass\ of\ carbon\ in\ g}{Carbon\ volume\ in\ ml}$$

7.1.9 N_2 adsorption at -196°C

The surface area according to the BET theory was measured using a Coulter Omnisorp 100 using nitrogen gas adsorption at -196°C. The instrument operates by using a continuous volumetric technique, meaning that the sample is exposed to a constant flow of nitrogen gas, regulated by a mass flow controller. The rate at which nitrogen is introduced into the sample holder is slow enough that nitrogen adsorbed onto the sample and the nitrogen in the sample tube can be considered to be in equilibrium. This controlled release of nitrogen allows for extremely small changes in pressure to be detected (Fowler, 1995).

7.1.9.1 Sample preparation

Approximately 0.25g of sample is placed into the sample holder and this is connected up to a vacuum in the degassing chamber of the Omnisorp via a sample tube stopcock adaptor. Here, the sample is dried at 150°C and degassed to 10^{-5} Torr. The sample is then removed from the degassing chamber and placed into a Dewar flask filled with liquid nitrogen. The data collected by the instrument allows for the calculation of the BET surface area and the t-plot analysis.

The adsorption of N_2 at -196°C provides an indication of the development of porosity and surface area of the activated carbons produced in this project. The results are interpreted in accordance with the BET theory (Section 3.4.3) for total surface area and total pore volume whereas the t-plot (Section 3.4.4) will be used to interpret the meso- and macropore surface areas along with the micropore volume. Meso- and macropore volume as well as micropore surface area will be determined by difference. The pore size distribution of the carbons is determined by the Horvath-Kawazoe method (Section3.2.3).

The measurement of BET surface area using N_2 will have implications on the analysis of the performance of JKWS as activated carbons as it provides a standard comparison of the surface area available for adsorption for other adsorbates. It also provides an indication of the pore structure of the ACs produced and assists in explanations of adsorption mechanisms.

7.1.10 Butane working capacity

ASTM Method D5228-92 (96) was used to determine the butane working capacity (BWC) of activated carbons (ASTM, 1992). BWC is defined as the difference between the butane adsorbed at saturation and the butane retained per unit volume of carbon after a specific purge. The test also gives a value for the butane activity; the total amount of butane adsorbed onto the carbon sample, expressed as mass of butane per unit weight or volume of carbon.

The BWC of activated carbon is a measure of its ability to adsorb and desorb butane under specific conditions. It also gives a relative measure of the effectiveness of the carbon on other adsorbates. Butane activity is an indication of the micropore volume and butane retentivity is an indication of the pore structure of the AC. The experimental set-up is shown in Figure 7-2.

The adsorption tube is pre-weighed and filled with oven-dried sample using the vibrating feed apparatus for apparent density. The filled adsorption tube is then weighed to determine the weight of the carbon sample and placed in a water bath at 25°C. Butane is passed through the sample for a specific amount of time and the amount of butane adsorbed is weighed. The butane adsorbed gives the butane activity of the AC. To determine BWC, the butane is purged from the sample using air for a specified time and re-weighed and the difference between the saturated sample and purged sample gives the BWC of the AC.

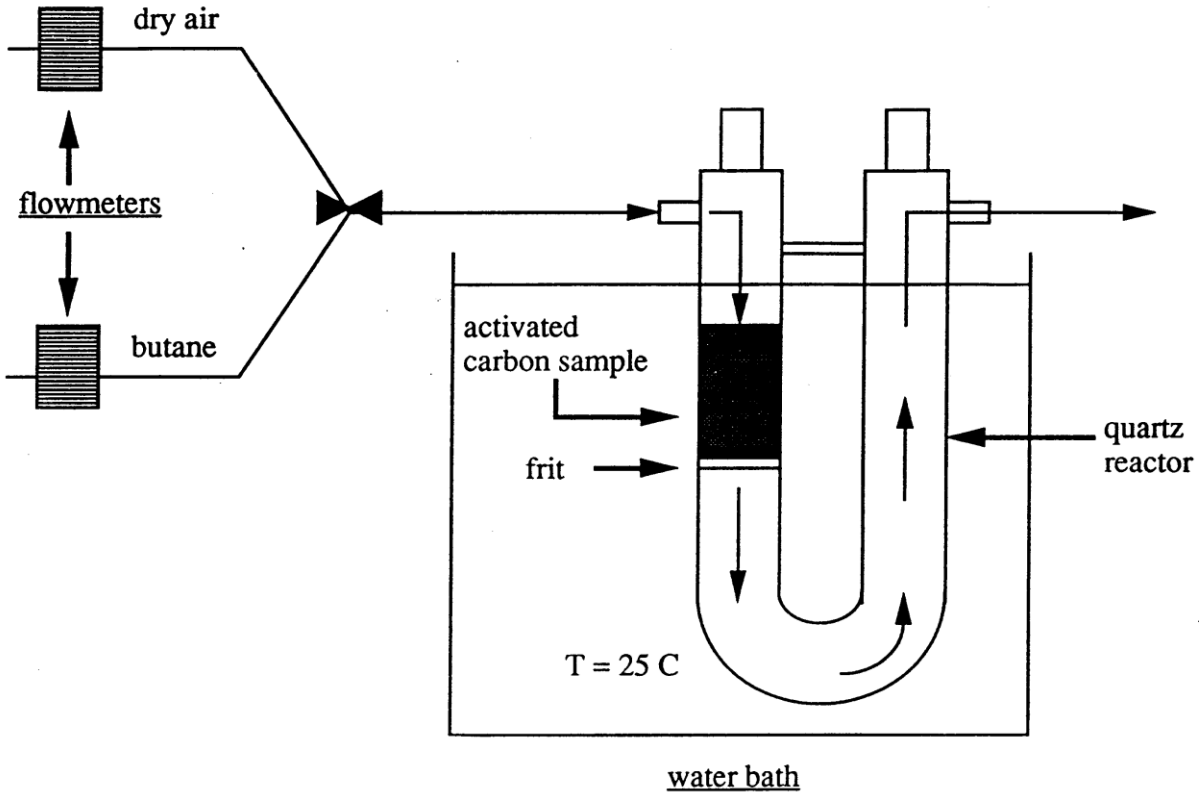


Figure 7-2: Experimental set-up for BWC determination (Allen et al., 1999).

The following equations were used to calculate BWC, butane activity and butane retentivity:

Equation 7-4: $BWC, \frac{w}{w}(\%) = \frac{D-E}{C-B} \times 100$

Equation 7-5: $BWC, w/v\ (g/100ml) = \frac{D-E}{C-B} \times A \times 100$

Equation 7-6: $Butane\ activity\ , \frac{w}{w}(\%) = \frac{D-C}{C-B} \times 100$

Equation 7-7: $Butane\ activity, \frac{w}{v}(g/100ml) = \frac{D-C}{C-B} \times A \times 100$

Equation 7-8: $Butane\ retentivity, w/w\ (\%) = \frac{E-C}{C-B} \times A \times 100$

Equation 7-9: $Butane\ retentivity, \frac{w}{v}(g/100ml) = \frac{E-C}{C-B} \times A \times 100$

Where:

A=apparent density
B=weight of sample tube and stoppers
C=Weight of carbon sample, sample tube and stoppers
D=Weight of saturated carbon, sample tube and stoppers; and
E=Weight of purged carbon, sample tube and stoppers.

7.1.11 Iodine number determination

ASTM Method D4607-94(99) was used to determine the iodine number of the activated carbon samples produced (ASTM, 1994b). The iodine number of an activated carbon is used as an indicator of its relative porosity especially for pore sizes larger than 1nm (Jankowska *et al.*, 1991, Aygün *et al.*, 2003).

The iodine solution is made up to 0.100±0.001N and must be standardised and maintained for all measurements. The standardised iodine solution is treated with three different weights of a sample of activated carbon under specific conditions. The samples are ground until 95% w/w or more will pass through a 100-mesh screen (152µm) and dried at 150°C overnight. The iodine solution is pipetted into a conical flask containing the carbon samples and shaken for 30 seconds.

The carbon is then filtered out and the remaining unadsorbed iodine is determined by titration, using starch solution as an indicator. The results are used to plot an iodine adsorption isotherm and the amount of iodine adsorbed per gram of carbon is reported as the iodine number.

During the adsorption of iodine, it is assumed that iodine at the equilibrium concentration of 0.02N is adsorbed onto the carbon in the form of a monolayer by a pore-filling mechanism similar to that of N_2 at -196°C (Hill and Marsh, 1968) (which was previously discussed in Section 7.1.9) and as such, the iodine number is related to the BET surface area (Jankowska *et al.*, 1991, Marsh and Rodríguez-Reinoso, 2006).

The amount of iodine adsorbed also indicates the extent of the micropore structure in JKWS AC and is also a measure of the adsorptive capacity of the AC (Snoeyink *et al.*, 1969) for low molar mass solutes (Wu *et al.*, 1999, Hall *et al.*, 1966) and is important in the evaluation of AC for their effectiveness in aqueous phase applications (Juhola, 1975). A larger iodine number indicates a higher adsorptive capacity.

7.1.12 Phenol adsorption

Phenol is an organic compound with the chemical formula C_6H_5OH. It consists of a phenyl group with an attached hydroxide group. It is an important precursor to a large collection of drugs, most notably aspirin as well as herbicides and pharmaceutical drugs. Phenol and its derivatives are also used in the synthesis of plastics, colours, pesticides, insecticides, etc. and as such, degradation of these substances leads to the appearance of phenols (and its derivatives) in the environment (Dabrowski *et al.*, 2005).

The presence of phenols can cause unpleasant tastes and odours (from reacting with chlorine during disinfection, producing chlorophenols) as well as causing health problems to humans (Dabrowski *et al.*, 2005, Hameed and Rahman, 2008) such as protein degenerations; tissue erosion; paralysis of the central nervous system; kidney, liver and pancreatic damage (Knop *et al.*, 1985). For these reasons, the removal of phenol and its associated compounds from drinking water is of the utmost importance.

The most widely-used method of phenol removal from water is by adsorption on the surface of activated carbons. The molecular diameter of phenol is 0.62nm, meaning that it is adsorbed within ultramicropores (d<0.7nm) and micropores (d<2nm) (Daifullah and Girgis, 1998).

The pKa of phenol is 9.89 so the adsorbed species above this pH is mainly anionic whereas phenol is mainly in its molecular form below this pH (Snoeyink *et al.*, 1969). It is desirable to keep the pH of

the solution below the pKa of phenol to avoid repulsion between the surface layer of the AC and the anionic phenolate, which would result in reduced adsorption in addition to changing its UV adsorption wavelength, affecting its accurate measurement.

Due to both its hazardous nature and common occurrence in water, phenol is often used as a primary reference solute in aqueous phase adsorption studies (Aygün *et al.*, 2003, Dabrowski *et al.*, 2005).

7.1.12.1 Adsorption kinetic studies

An adsorption kinetics experiment was conducted to determine the time needed for saturation of phenol adsorption in the pores of AC. The AC samples tested were ground to 150µm particle size.

Approximately 20mg aliquots of AC sample were placed in several conical flasks, each containing 100ml of 200ppm phenol solution. The phenol used was of 99.0% purity from Fisher Scientific UK. These were shaken at 150rpm on a rotary shaker and an aliquot was taken at different time intervals (10mins to 48h) from different flasks. The aliquots were then filtered using Whatman 0.45µm syringe filters.

A Shimadzu UV-2401PC UV-Visible spectrum spectrophotometer (Shimadzu Corp., Kyoto, Japan) was calibrated with phenol solutions of 0, 10, 20, 50 and 100ppm concentrations at a wavelength of 270nm and used to determine the concentration of phenol remaining in the filtered solution. The amount of phenol adsorbed at equilibrium q_e was calculated using Equation 7-10:

$$\text{Equation 7-10:}\quad q_e = \frac{(C_0 - C_e)V}{W}$$

Where C_0 =initial concentration of phenol in mg/l; C_e =equilibrium concentration of phenol in mg/l; V= volume pipetted into conical flask in litres and W= mass of AC used in grams.

Values of q_e were plotted against time to produce a plot indicating the minimum time needed for phenol saturation of the activated carbon sample tested.

7.1.12.2 Adsorption isotherm studies

The batch equilibrium studies for phenol adsorption were conducted in a similar manner to the kinetic studies. Instead of having different flasks with the same phenol concentration, there were 5 flasks; each with 100ml of 10, 20, 50, 100 and 200ppm phenol concentrations. 20mg of AC sample were placed in each flask and shaken for 24 h at 150 rpm. The contact time was determined from the adsorption kinetics test.

After 24h, aliquots were taken from each flask, filtered and the equilibrium concentration determined using the UV-Vis spectrophotometer. The Freundlich and Langmuir isotherm models were then used to describe the relationship between the amount of phenol adsorbed and its equilibrium concentrations in the solutions as previously discussed in Sections 3.4.1 and 3.4.2, respectively.

In calculating the maximum monolayer capacity Q_0 for each carbon, the five points required are achieved by varying the initial concentration C_0 of the phenol solution while keeping the amount of carbon constant. This takes into account the effect of different phenol concentrations have on phenol uptake by the carbons. This in turn, leads to an accurate value of Q_0 when compared to obtaining the value from the height of the plateau of the phenol adsorption isotherms (Teng and Hsieh, 1998).

The pH of the phenol solution after adsorption using JKWS AC was measured to ensure that $pH<pK_a=9.89$ to prevent dissociation of phenol into phenolates. This is to minimise the effects of repulsion between the anions and the negative surface structures of the activated carbon. It was discovered that none of the pH values were above the pK_a of phenol after adsorption and thus, buffering of the solution was not required.

7.2 Results and Discussion I: Effect of Activation Temperature

The produced activated carbons are given a prefix based on the precursor (JKWS or JKWR), followed by AC to denote that is has already been steam activated. Three sets of number then denote the activation temperature, activation time and water flow rate, respectively.

7.2.1 Elemental analysis using ICP

Table 7.2 shows the results of the ICP analysis of OTL (oriental tobacco leaves), which was used as a standard to gauge the efficiency of the microwave acid digestion method. Ca, K and Mg values were all within 10% of the OTL certified value. However, for Na the % difference was 58.6%. This was due to the fact that Na was a trace element in OTL and that even minute traces of contamination could affect the Na concentration.

Table 7.2: Alkaline earth metals content of OTL standard.

OTL	Ca/μg g^{-1}	K/μg g^{-1}	Mg/μg g^{-1}	Na/μg g^{-1}
Certified Value	31700 ± 1200	15600 ± 500	4470 ± 210	345*
Digested Value	32836	14238	4376	547
% difference	+3.6	-8.7	-2.1	+58.6

*The standard error was unavailable for the Na content of OTL as it was a trace element in OTL. SD values obtained from 3 different measurements.

In spite of the high percentage difference between the certified and digested Na value of OTL, the microwave acid digestion method described in Section 7.1.2 was adopted for the digestion of JKWS and JKWR biomass and the produced chars as the other three metals were analysed with acceptable results.

The alkaline earth metals content as obtained from the ICP analysis of JKWS, JKWS char, JKWR and JKWR char as well as the respective acid washed chars is shown in Figure 7-3. All ICP analyses were carried out in triplicate and RSD for all analyses were less than 8%, which was deemed acceptable (dos Santos *et al.*, 2007).

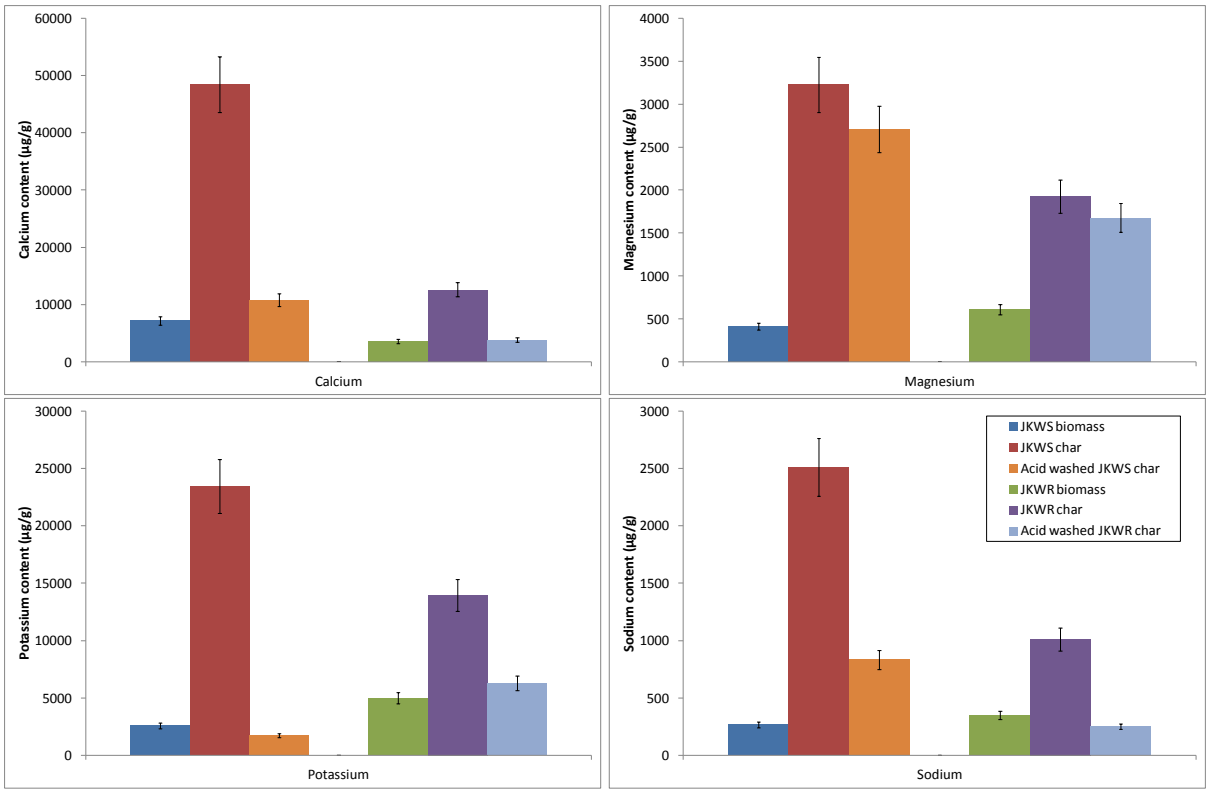


Figure 7-3: Comparison of the alkaline earth metals in JKW biomass, char and acid washed char.

It is observed that both JKWR and JKWS chars had higher amounts of alkaline earth metals than their respective biomasses. This is explained by the carbonisation and devolatilisation reactions which concentrate these inorganic minerals into the char as they are not removed by the aforementioned reactions.

In order to remove as much ash as possible, the 0.2M HCl solution of the ReACT process was used to wash both JKWS and JKWR chars as detailed in Section 7.1.2. After the final wash with hot distilled water, both chars were then analysed for the metals content, with a comparison of the results between unwashed and washed chars shown in Figure 7-3.

The ReACT acid washing method was effective in removing the alkaline earth metals content of both types of chars, as can be seen in Figure 7-3. Calcium content was reduced by 78% and 70%; potassium content by 93% and 55% and sodium content was reduced by 67% and 75% for JKWS and JKWR chars, respectively. The acid wash was not as effective in removing magnesium content where reductions of 16% and 13% were achieved for JKWS and JKWR chars, respectively.

7.2.2 Sample Yields/Burn-off reactions of JKWR and JKWS char with water

Water is volatilised into steam the moment it is pumped into the quartz reactor at the activation temperature. The burn-off gives an indication of the porosity and surface area of the char and is positively correlated to both (Molina-Sabio *et al.*, 1996, González *et al.*, 1994).

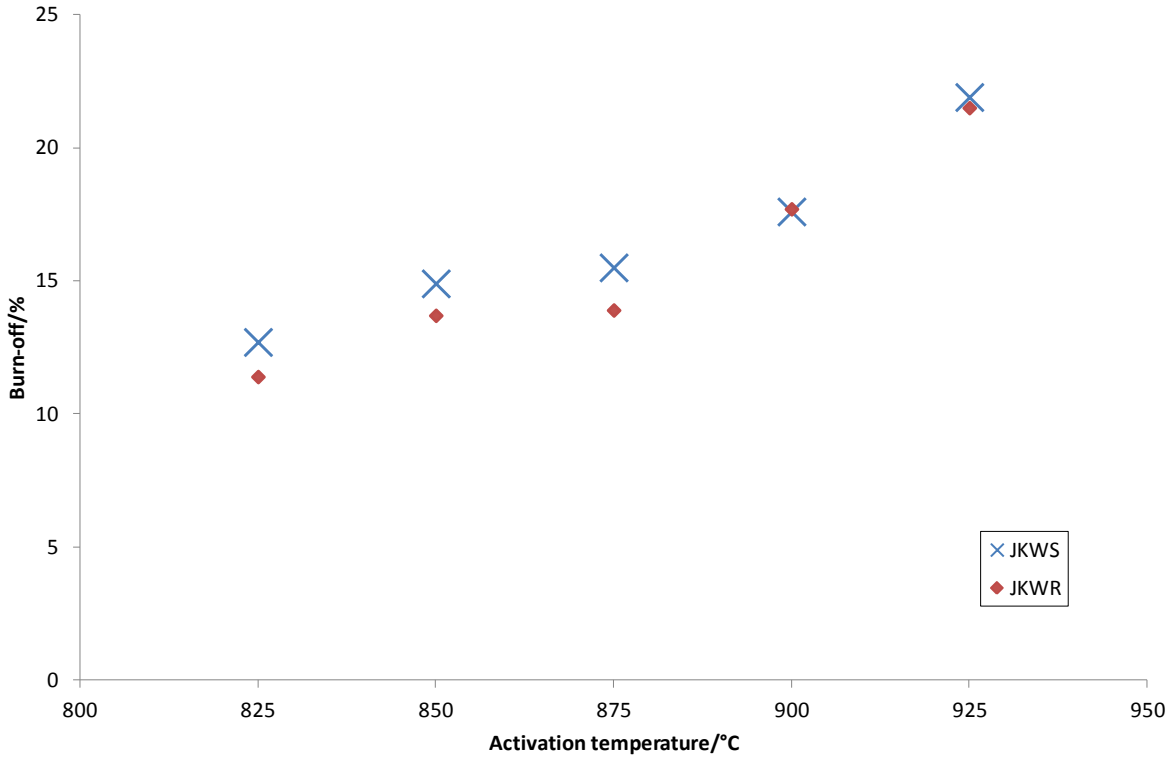


Figure 7-4: Effect of activation temperature on the burn-off of JKWS and JKWR char at 0.5h activation time and 0.1ml/min water flow rate.

The reaction of steam is termed gasification and is the main mechanism that results in the development of pores in the carbon structure. It is responsible for the loss of weight from the char, i.e. burn-off as a result of removal of carbon atoms during C-H_2O reactions (Chang *et al.*, 2000, Rodriguez-Reinoso and Molina-Sabio, 1992). This effect is seen in Figure 7-4, where the increase in activation temperature is accompanied by an increase in the burn-off of JKWS from 12.7% at 825°C to 17.8% at 925°C and the burn-off of JKWR increases from 11.4% at 825°C to 21.5% at 925°C. This has been observed and is in line with steam activation of other forms of biomass (Tancredi *et al.*, 1996, Gergova and Eser, 1996, Hu and Srinivasan, 1999, Balci *et al.*, 1994).

JKWS has marginally higher reactivity than JKWR as can be seen by the higher burn-offs at comparable activation temperatures. This could be due to the different lignocellulosic contents of

JKWS and JKWR, as reported in Section 5.4.3 It has been suggested by Gergova *et al.* (1994) that the difference in lignin and cellulose contents of biomass precursors may influence the burn-off and hence, porous structure of the produced activated carbons. Daud and Ali (2004) observed that was easier to activate chars which have more cellulosic content than having high lignin content and this is reflected in this study for both JKWR and JKWS.

As is known from Section 5.4.3, JKWS possesses higher hemicellulose content (46.7% to JKWR's 24.9%) and lower cellulose content (31.8% to JKWR's 52.4%) and as such, can be partly attributed to the higher reactivity and hence, higher burn-off values of JKWS under comparable steam activating conditions.

It can also be seen in Figure 7-4 that the burn-off levels off at 850°C and 875°C before rising again at 900°C and 925°C. This could be an indication of the limiting effect of the water flow rate, where the existence of a concentration gradient between the inner cavities of the char molecule and the external water environment surrounding the char carbon structure.

According to González *et al.* (1994), the concentration gradient decreases with higher water flow rate and as the concentration of water increase external to the char, allowing for greater diffusion into the char. Wigmans (1989) mentioned in his study that as a result of the burning of carbon during steam activation which results in the formation of CO and H_2 (Equation 3-13), H_2O is not effectively used during the activation process due to the increasing partial pressure of CO that occurs; which causes the water gas shift reaction (Equation 3-14) to favour the forward reaction, increasing the inhibitory effects of H_2 (Marsh and Rodríguez-Reinoso, 2006) and thereby, decreasing the burn-off values achieved during steam activation.

7.2.2.1 *Carbon content*

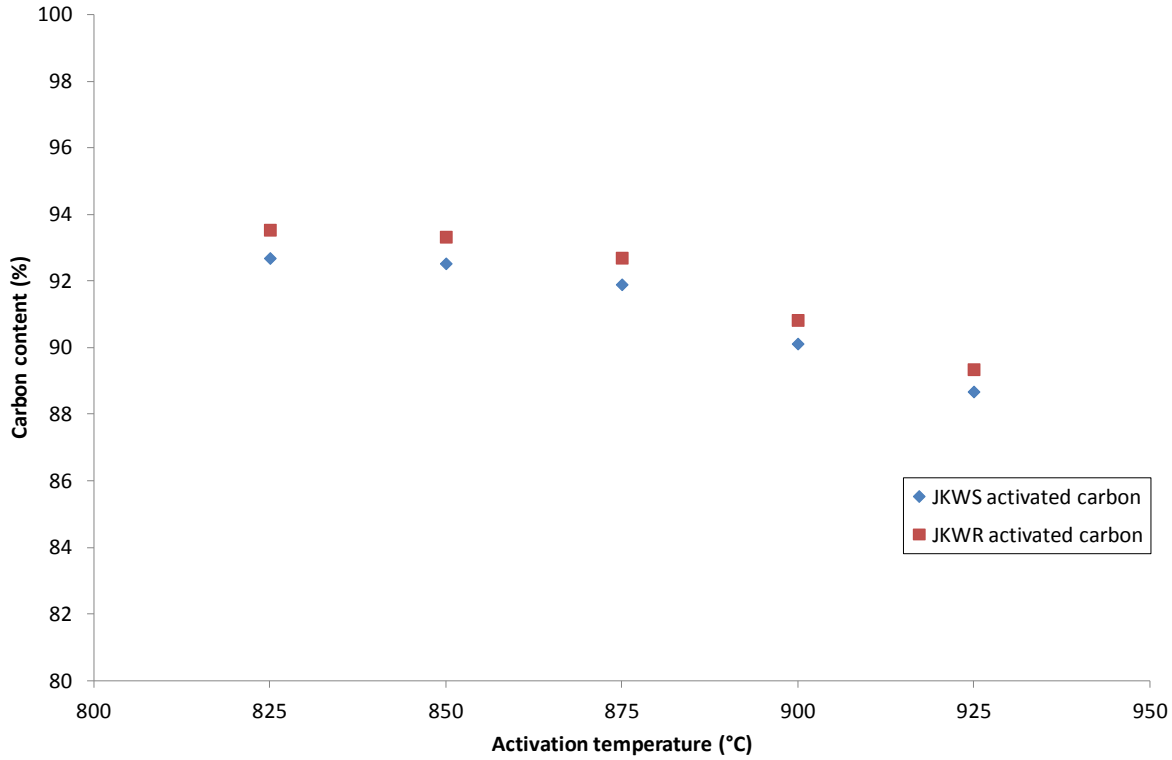


Figure 7-5: The decrease of carbon content of produced JKWS and JKWR activated carbons (0.5h activation time and 0.1ml/min water flow rate) as a function of activation temperature.

Figure 7-5 demonstrates that the increasing activation temperatures results in activated carbons with decreasing carbon contents. The decrease in carbon content is due to the carbon burn-off as a result of C-H_2O reaction experienced by the carbon particles during steam activation, as previously discussed in Section 3.5.4.2.

JKWR activated carbons have relatively higher carbon content than JKWS carbon at all activation temperatures. This observation is in agreement with the relatively higher carbon content of JKWR biomass, as seen in Table 5.2 in Section 5.4.2. The difference in carbon contents between JKWS and JKWR carbons could also be due to the fact that the produced JKWR char at 600°C has a higher bulk density than the equivalent JKWS char as seen in Section 7.1.4. The denser structure of JKWR char would then result slower diffusion of water molecules into the char structure, lowering its steam gasification rate and thus, preserving its relatively higher carbon content due to lower burn-off experienced in comparison to JKWS char.

Table 7.3: Carbon content of JKWS and JKWR biomass, char and activated carbons produced at different activation temperatures (0.5h activation time and 0.1ml/min water flow rate).

	Yield (%)	C content (%)	Sample weight (g)	C content (g of C/ 10g sample)	C content* (%)
JKWS biomass	100.00	45.70	10.00[+]	4.57	45.70
JKWS Char	24.09	91.30	2.41	2.20	21.99
AC at 825°C	87.30	92.69	2.10	1.86	19.49
AC at 850°C	85.10	92.53	2.05	1.85	18.97
AC at 875°C	84.50	91.90	2.04	1.87	18.71
AC at 900°C	82.40	90.12	1.99	1.84	17.89
AC at 925°C	78.10	88.68	1.88	1.74	16.68
	Yield (%)	**C content (%)**	**Sample weight (g)**	**C content (g of C/ 10g sample)**	**C content* (%)**
JKWR biomass	100.00	46.30	10.00[+]	4.63	46.30
JKWR Char	31.09	93.50	3.11	2.91	29.07
AC at 825°C	88.60	93.54	2.75	2.46	25.77
AC at 850°C	86.30	93.33	2.68	2.44	25.04
AC at 875°C	86.10	92.70	2.68	2.48	24.81
AC at 900°C	82.30	90.83	2.56	2.39	23.24
AC at 925°C	78.50	89.35	2.44	2.28	21.81

* corrected for weight losses due to carbonisation and steam activation. [+] Arbitrary biomass sample weight for comparison's sake.

Table 7.3 shows that the corrected carbon content of JKWS and JKWR as a percentage of the original biomass decreases with carbonisation and steam activation. This is a result of correcting the carbon contents in order to make valid comparisons for reasons of carbon sequestration. Although the corrected carbon contents are observed to decrease from biomass to final activated carbon product, this is expected as a result of the carbonisation process (where carbon is 'lost' in bio-oil and syngas) and the steam activation process (where carbon is 'lost' during burn-off as CO and CO_2). The results indicate that a portion of carbon can be sequestered in the form of produced activated carbon, depending on the activation temperature used to manufacture the required activated carbon.

7.2.2.2 SEM analysis

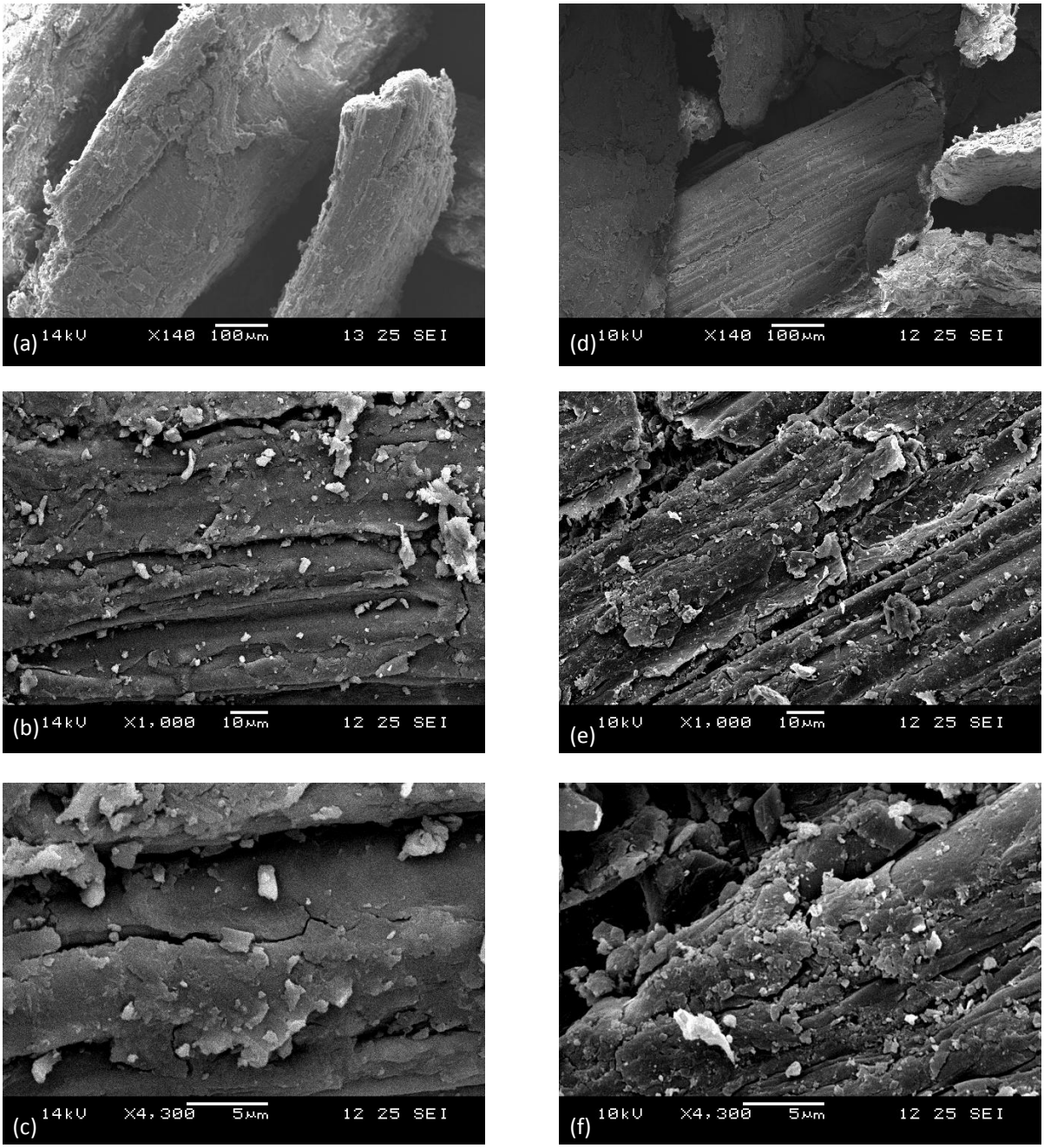


Figure 7-6: SEM photos of JKWR biomass at (a) 140x (b) 1000x (c) 4300x magnification with JKWS biomass at (d) 140x (e) 1000x and (f) 4300x magnification.

It can be seen in Figure 7-6 that both JKWS and JKWR biomass look similar to each other at the lower magnifications. However, at higher magnifications, it is clear that JKWR seems more solid with little evidence of cracks and fissures whereas JKWS biomass is seen to be fragmented, especially in Figure 7-6 (f). Furthermore, there is no evidence of any form of porosity observable in any of these micrographs.

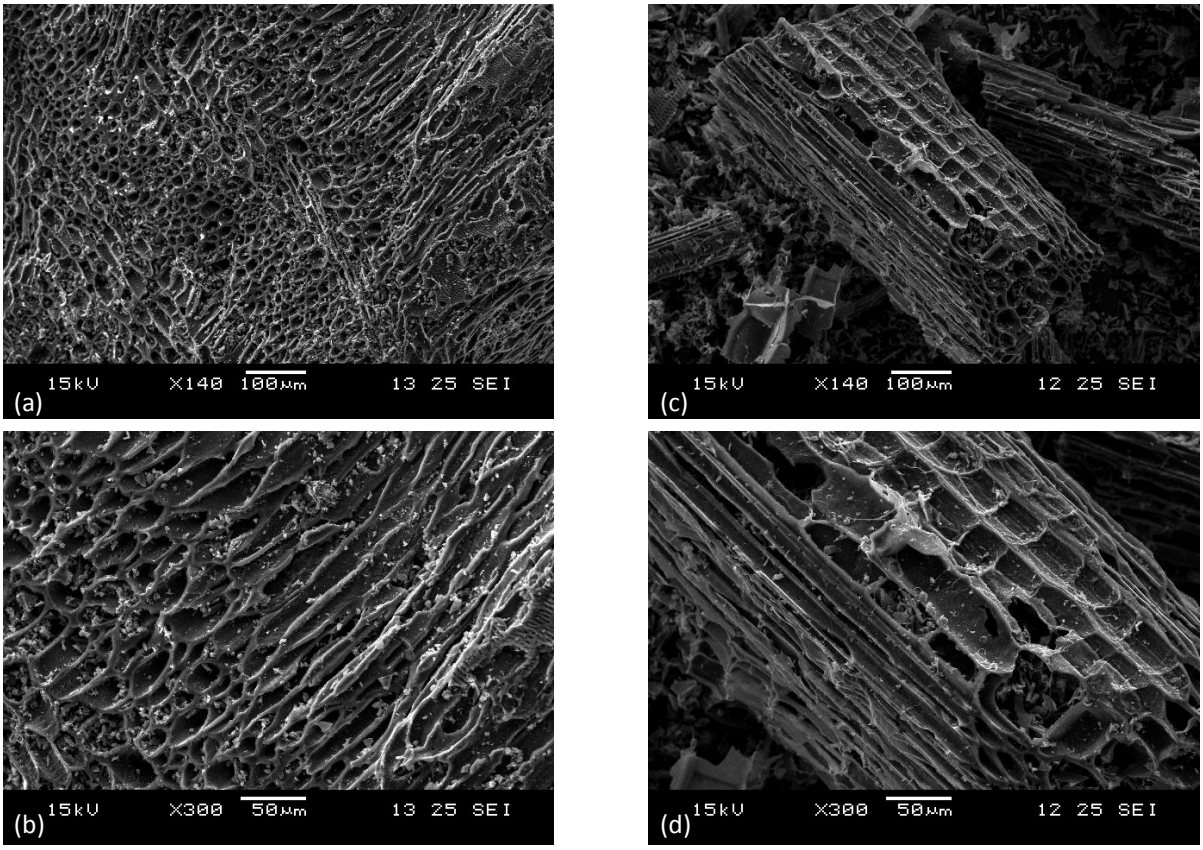


Figure 7-7: SEM photos of JKWR char at (a) 140x (b) 300x magnification with JKWS char at (c) 140x and (d) 300x magnification.

In Figure 7-7, it is can be clearly seen that the carbonisation process has already begun to perforate the structure of JKWR and JKWS. Disorganised fragments of amorphous carbon and residues can also be observed as individual white specks on the SEM photos, blocking the pores. JKWR char already exhibits relatively porous structures at 140X in Figure 7-7 (a) whereas it can be seen that some external burning has occurred with JKWS char in Figure 7-7 (d), which indicates the formation of external porosity whereas the inner structural walls still remain intact. It can also be observed that the basic cellular structure of both JKWS and JKWR biomass is retained after carbonisation, which had also been observed by several other authors for other biomass precursors (Zabaniotou *et al.*, 2008, Martínez *et al.*, 2006).

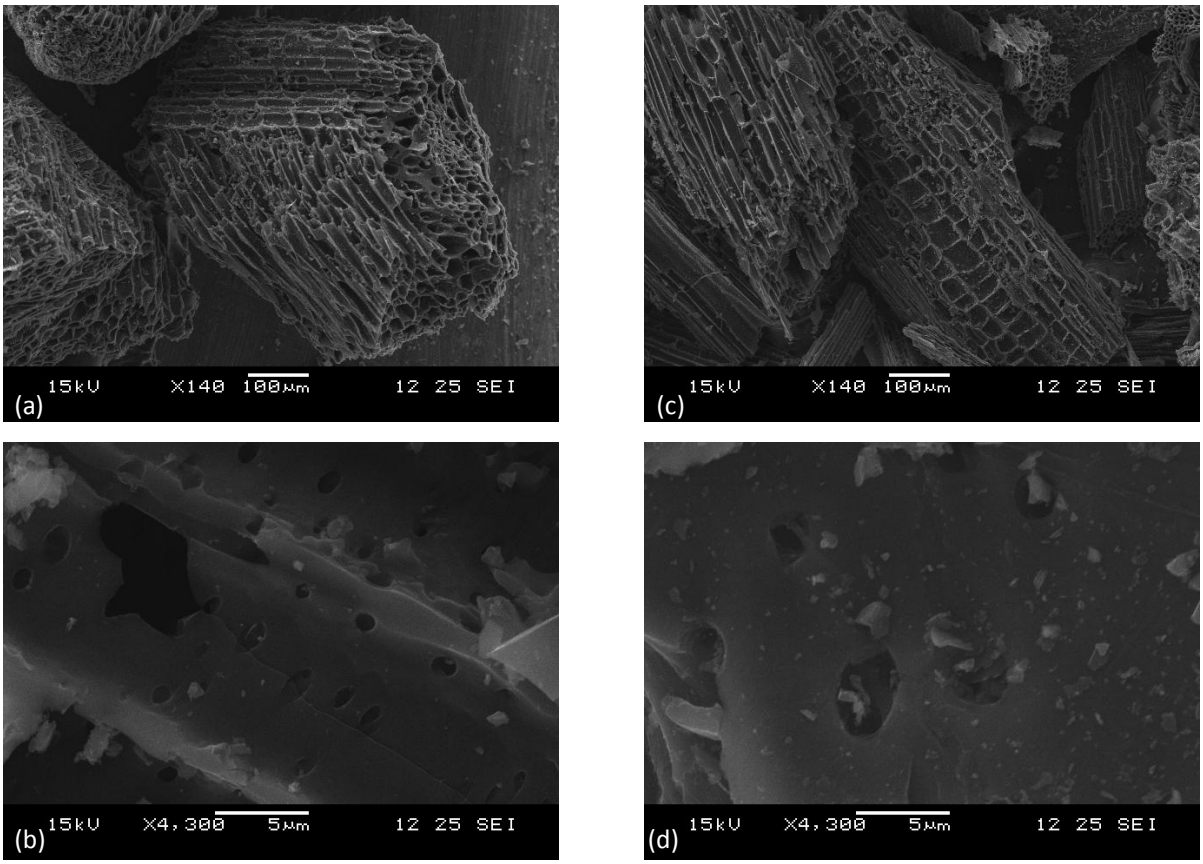


Figure 7-8: SEM photos of JKWR AC 825-0.5-0.1ml at (a) 140x (b) 4300x magnification with JKWS AC 825-0.5-0.1ml at (c) 140x and (d) 4300x magnification.

Comparing Figure 7-7 with Figure 7-8, it is apparent to see the effects of steam activation on the carbon structure of the chars. The development of macropores are observable in Figure 7-8 (b) and Figure 7-8 (d), with the produced JKWS carbon possessing larger macropores than the produced JKWR carbon. The presences of macropores (and mesopores) are beneficial for any adsorption process because these pores serve as feeder pores to smaller micropores (Zabaniotou *et al.*, 2008).

Comparing Figure 7-7 with Figure 7-8 gives the clearest indication of burn-off, where new pores are formed during steam activation as the carbon structure of the chars are being burnt. It can also be observed that there are less amorphous carbon particles after steam activation, which indicates that the aforementioned particles were burnt off during steam activation, giving the produced JKWS and JKWR carbons an organised and regular structure (Nabais *et al.*, 2010).

Figure 7-8 shows that the surface characteristics of the original JKWS and JKWR biomass are not significantly altered by the process of steam activation; this was also observed by Williams and Reed (2006) during their steam activation work using flax biomass fibre waste.

7.2.3 N_2 adsorption at -196°C

The BET surface area was determined by adsorption of N_2 at -196°C using the Coulter Omnisorp as described in Section 7.1.9.

7.2.3.1 Effects of acid-washing on measured BET surface area of JKWS activated carbon

JKWS char was washed according to the ReACT process to minimise the risks of quartz vessel devitrification and potential failure, as caused by the alkaline earth metals content during steam activation. The effects of acid washing on the burn-off and BET surface area of a batch of produced JKWS activated carbons was examined only. This was because further test comparisons required continued steam activation of unwashed char, causing further devitrification and failure of quartz reactors and this was uneconomical for the research. The amounts of JKWS AC sample produced were also insufficient for conducting all the characterisation tests and as such, only N_2 adsorption tests at -196°C using the Coulter Omnisorp were conducted and contrasted.

Table 7.4: Textural properties of JKWS AC produced from acid washed and unwashed chars.

	Unwashed		Acid-washed	
JKWS AC	**Burn-off (%)**	**BET surface area (m^2/g)**	**Burn-off (%)**	**BET surface area (m^2/ g)**
825-1-0.1ml	23.3	552	21.2	523
850-1-0.1ml	24.2	575	23.0	549
875-1-0.1ml	29.7	636	25.3	562
900-1-0.1ml	34.7	720	27.5	575
925-1-0.1ml	36.7	753	30.0	606

Table 7.4 shows a selection of JKWS ACs that were produced from chars that were unwashed and acid washed. At 825-1-0.1ml activating conditions, unwashed JKWS AC had a burn-off of 23.3% vs. 21.2% for washed chars whereas for 925-1-0.1ml conditions, burn-off was 36.7% for unwashed chars and 30.0% for washed chars. The higher burn-offs recorded for unwashed char indicates higher reactivity between carbon and H_2O and as such, unwashed JKWS char resulted in ACs with higher BET surface areas than ACs produced from washed chars as the same activation conditions.

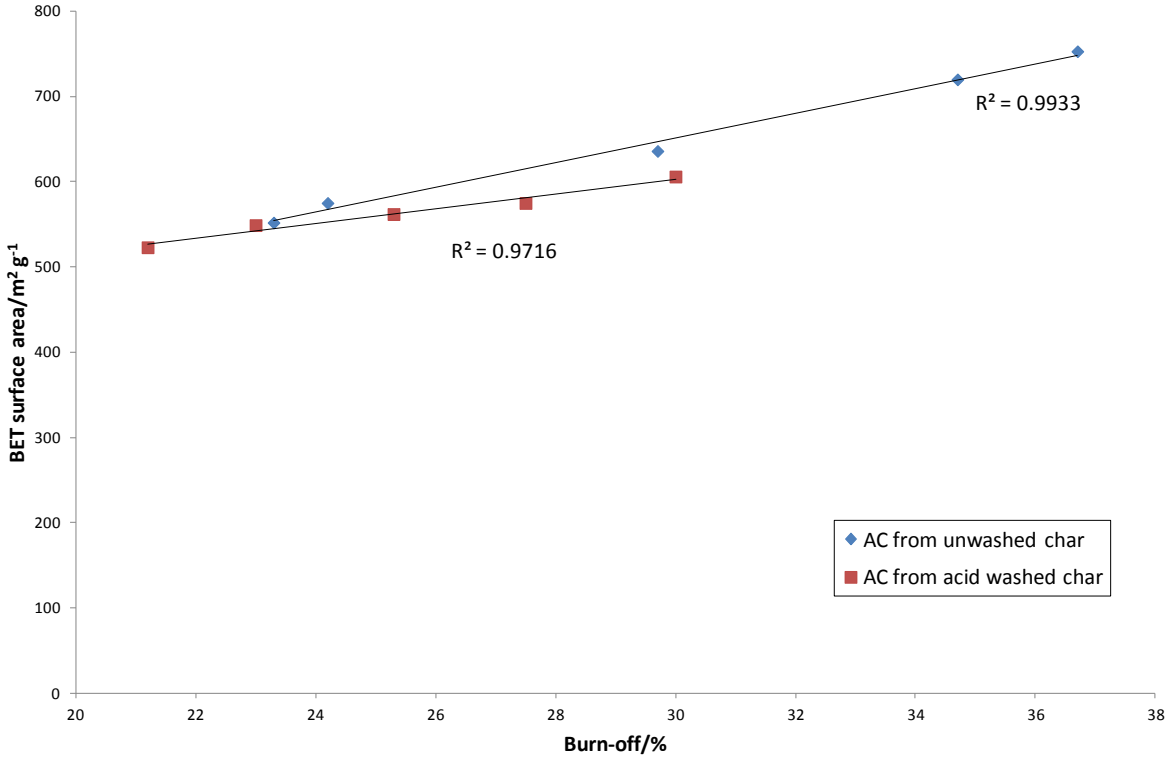


Figure 7-9: Development of BET surface area with burn-off for acid washed and unwashed JKWS AC.

It can also be observed that as the activation conditions increase, BET surface area increases at a higher rate for unwashed char (see Figure 7-9). This is evidenced by the steeper gradient of the plot for unwashed char (14.5m^2/g/% burn-off) vs. washed char (8.7m^2/g/% burn-off). The gradient shows the increase of BET surface area per % burn-off.

The effects of ash removal on burn-off and BET surface area can be explained by the fact that the presence of inorganic minerals in the ash exerts catalytic influence on the rate of steam activation (gasification) as well as the formation of pores as a result of the activation process due to the presence of oxides on the surface of the char carbon structure (Mui *et al.*, 2004). Thus, the ReACT process, discussed in Section 7.1.2.2 was developed to reduce this problem and ensure that the carbons were not "over-activated", especially during regeneration of spent activated carbons. By applying this washing process to the JKW char samples; there is a similar reduction in the extent of activation, as is clearly shown in Table 7.4.

Coincidentally, the alkaline earth metals; which are removed during acid washing are the elements responsible for the catalytic effect, especially calcium (Cunliffe and Williams, 1998, Cazorla-Amorós *et al.*, 1996, Cannon *et al.*, 1994, San Miguel *et al.*, 2001).

Further experiments with JKWS chars or comparisons between unwashed and acid washed JKWR chars were not conducted to investigate the extent of the catalytic effect due to the detrimental consequences on the quartz reactors. As a result, all subsequent results reported have been from experiments conducted using acid washed JKWS and JKWR chars.

7.2.3.2 BET surface area

All JKWS and JKWR activated carbons which were prepared exhibited a mixed Type I/Type IV isotherm with the H4 characteristic hysteresis loop as can be seen in Figure 7-10 and Figure 7-11. The shape of the loop differs from adsorption system to system but the desorption branch is always greater at any given relative pressure than the adsorption branch (Gregg and Sing, 1982). The Type IV isotherm indicates that the carbon measured contains both micropores and mesopores. The BET surface area and t-plot meso- and macroporous surface areas are presented in Table 7.5. All BET plots had R^2 values greater than 0.95 with BET P/P_0 ranges between 0.001 and 0.1.

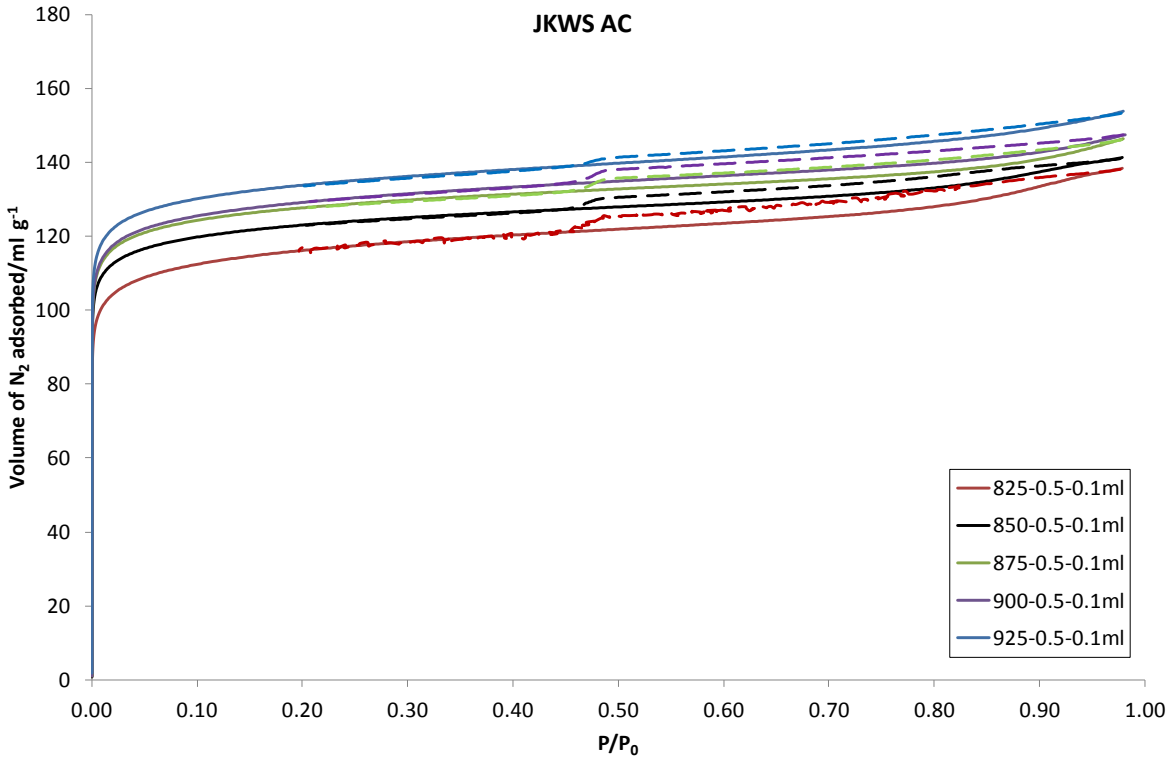


Figure 7-10: N_2 adsorption isotherms of JKWS AC at increasing activation temperatures. The desorption branches are shown in dotted lines.

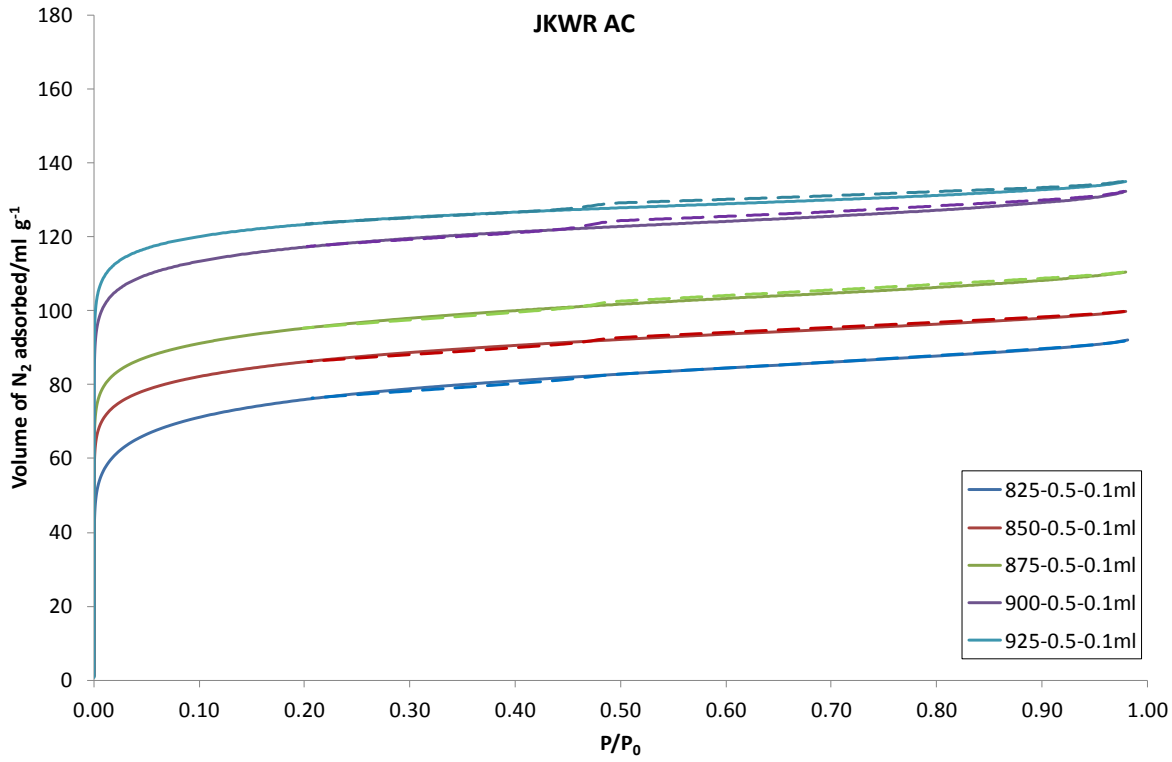


Figure 7-11: N_2 adsorption isotherms of JKWR AC at increasing activation temperatures. The desorption branches are shown in dotted lines.

In Figure 7-11 showing the adsorption isotherms of JKWR carbons, it can be seen that at lower activation temperatures, there is no significant hysteresis loop, which indicates that the mesoporosity of those carbons are very low (Fierro *et al.*, 2008). However, the isotherms start to show increasing/larger hysteresis loops once activation temperatures increase, indicating increasing mesoporosity of the produced carbons.

It can be seen in Figure 7-10 and Figure 7-11 that as the activation temperatures increases at constant activation time and water flow rate that the volume of N_2 adsorbed per gram of carbon increases; which is in agreement with results obtained by other researchers (Román *et al.*, 2008, Marsh and Rodríguez-Reinoso, 2006, González *et al.*, 1994). There is also concurrent development of the BET surface area, as depicted in Table 7.5 as the activation temperature increases.

The adsorption isotherms are indicative of high degrees of microporosity with a lesser degree of mesoporosity, with mixed Type I and Type IV isotherm characteristics. The H4 character indicates that the pores are slit-like and this is confirmed by examining the SEM images in Figure 7-8 in Section 7.2.2. Nevertheless, the effects of steam activation on the N_2 adsorption isotherms of the produced JKWS and JKWR carbons are evident.

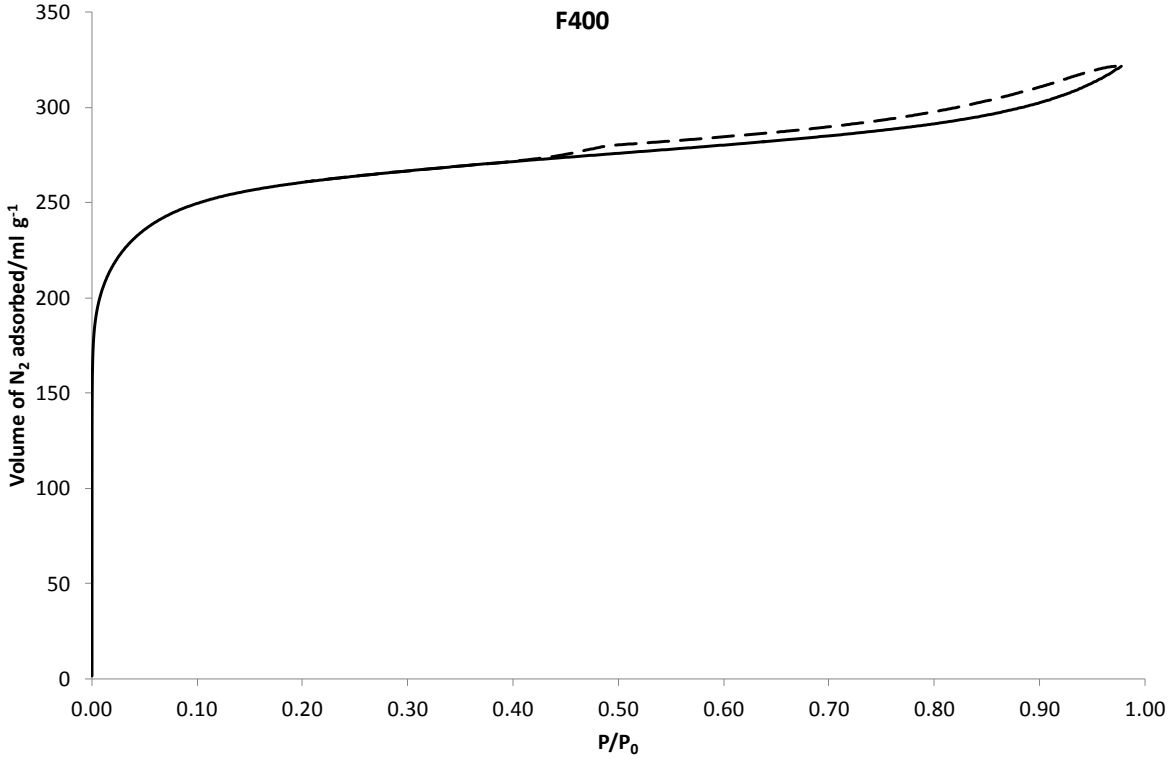


Figure 7-12: N_2 adsorption isotherms of F400, the commercial AC used for comparison purposes.

The significant effect of steam activation on both JKW-derived carbons' micropore characteristics are expressed by all the samples. This is particularly important as it is well-known that micropores make a major contribution to the total surface area and enhance the adsorption capability of activated carbons (Yang *et al.*, 1993, El-Sheikh *et al.*, 2004). However, JKWS and JKWR carbons activated under current parameters are still unable to compete with the commercial comparison F400 as evidenced by the much higher volume of N_2 adsorbed as shown in the isotherm plot of F400 in Figure 7-12. Nevertheless, it can be seen from the hysteresis loop of the adsorption isotherm in Figure 7-12 that F400 exhibits a more mesoporous nature than JKWR or JKWS activated carbons at this point. Furthermore, the slight increase at the tail-end of the isotherm is also indicative of its mesoporous character.

Table 7.5: Parameters obtained from N_2 adsorption data of produced JKWS and JKWR AC at increasing activation temperatures.

		Surface Area (m^2/g)			Micropore:BET (%)	BET C-value	Ash content
JKWR AC	**Burn-off/%**	**BET**	**Micropore**	**Meso- & macropores**			**(%)**
825-0.5-0.1ml	11.4	278.4	253.28	25.12	91.0	802	1.42
850-0.5-0.1ml	13.7	322.1	290.76	31.34	90.3	2722	1.50
875-0.5-0.1ml	13.9	357.6	323.42	34.18	90.4	3671	1.87
900-0.5-0.1ml	17.7	445.8	408.99	36.81	91.7	19372	1.69
925-0.5-0.1ml	21.5	476.0	437.73	38.27	92.0	33740	1.43
JKWS AC							
825-0.5-0.1ml	12.7	441.9	409.75	32.15	92.7	8971	2.89
850-0.5-0.1ml	14.9	474.1	445.96	28.14	94.1	11841	2.75
875-0.5-0.1ml	15.5	491.8	463.08	28.72	94.2	15449	2.65
900-0.5-0.1ml	17.6	496.7	463.38	33.32	93.3	15989	2.57
925-0.5-0.1ml	21.9	516.9	482.81	34.09	93.4	35311	2.99
F400	N/A	977.4	885.84	91.56	90.6	1023	9.00

In Table 7.5, it can be observed that along with the increase in activation temperatures, the burn-off also increases; this indicates an expected correlation between burn-off and BET surface area. It can also be noticed that the micropore surface area makes up the majority of the total BET surface area of all types of carbons tested, including F400 demonstrating the microporous nature of the produced JKWS and JKWR carbons.

The continued increase in BET surface area with activation temperature demonstrates the continual creation of micropores. There is a concurrent development of meso- and macropores, which are formed by the widening of existing micropores in conjunction with external burn-off of the char carbon structure (Pastor-Villegas and Duran-Valle, 2002). The increase in activation temperature allows the endothermic C-H_2O reaction to be thermodynamically favourable (Bouchelta *et al.*, 2008), allowing for greater development of porosity. This event occurs due to the fact that as burn-off increases, the H_2O molecule begins to attack the micropore walls and causes widening to form mesopores, whilst existing mesopores are widened to form macropores (Molina-Sabio *et al.*, 1996, González *et al.*, 1994, Rodriguez-Reinoso and Molina-Sabio, 1992, Rodríguez-Reinoso *et al.*, 1995).

The micropore:BET surface area ratio gives an indication of the degree of relative microporosity of the produced carbons and it is observed that there is no defined trend as the activation temperature increases. This could be due to uneven external burn-off as a result of different reactivity experienced by both JKWS and JKWR chars. It is reasonable to assume that since JKWR experiences lower burn-off than JKWS at the same activating conditions that it is less reactive and this could be due to the different lignocellulosic content of its precursor biomass (Gergova *et al.*, 1994, Suhas *et al.*, 2007, Reed and Williams, 2004), as previously discussed in Section 5.4.3, especially due to its larger cellulose content, which is more stable under high thermal conditions (Yang *et al.*, 2007). It should be noted that the steam activation process is heterogeneous and not only controlled by the chemical reactions between the water molecules and the carbon molecules but is also limited by diffusional mass transfer through the carbon structure (Arriagada *et al.*, 1997). The diffusion of water through the char structure is thus limited by the porosity of the char precursor; where the measured BET surface areas for JKWS char and JKWR char were 110 m^2/g and 17m^2/g, respectively and as such, water molecules are able to penetrate JKWS char much easier than JKWR char.

The BET C-values are a good indicator of the reliability of the BET results where C-values between 2 and 150 are considered to be acceptable (Gregg and Sing, 1982, Sing, 1985). It can be seen in Table 7.5 that the C-values were all outside of the accepted values, which indicate that there are

micropores within the sample and so, the limits of the BET theory are being reached. Nevertheless, the C-values exhibited by JKWS and JKWR carbons are still useful for comparing the textural characteristics of the produced JKWS and JKWR carbons.

The ash contents of produced JKWS carbons were approximately half that of the JKWR carbons. The original JKWS biomass had an ash content of 1.56% whereas JKWR biomass had an ash content of 4.43%. It is recognised that the inorganic metals content manifests itself as ash content and is concentrated in the char during carbonisation and subsequently in the activated carbon during activation but due to the acid-wash process; a significant part of this ash is removed. Thus, the actual ash contents of the JKW carbons were less than the theoretical yield. The acid washing step removes between 75%-82% of the actual JKWS carbon ash content and between 82%-85% of JKWR carbon ash content vs. the theoretical ash contents.

In Table 7.5, it can be observed that as C-values increase as the BET surface area increases for both JKWS and JKWR carbons and that the maximum activation temperature of 925°C produced JKWR carbon with the highest BET surface area of 476m^2/g and the highest BET surface area for JKWS carbons was measured at 517m^2/g.

The activation temperature experiments clearly demonstrated that in order to maximise the BET surface area produced in both JKWS and JKWR carbons, the highest activation temperature tested (925°C) must be used at the same activation time and water flow rate.

7.2.3.3 Pore size distribution

The mesopore size distributions was determined according to the Kelvin Equation, in which the desorption branch of the isotherm was used by Barrett *et al.* (1951) in Section 3.2.2. Examination of the micropore size distribution was possible though the application of the Horvath and Kawazoe (HK) equation in Section 3.2.3. The pore-size distribution of the JKWS AC produced ranged from 0.533nm to 0.550nm and 0.514nm to 0.561nm for JKWR AC i.e., in the micropore range of sizes. In comparison, Calgon F400 has a measured HK pore size distribution of 0.512nm. The HK effective pore diameters for the series of JKWS and JKWR carbons prepared are listed in Table 7.6 along with the total pore volume.

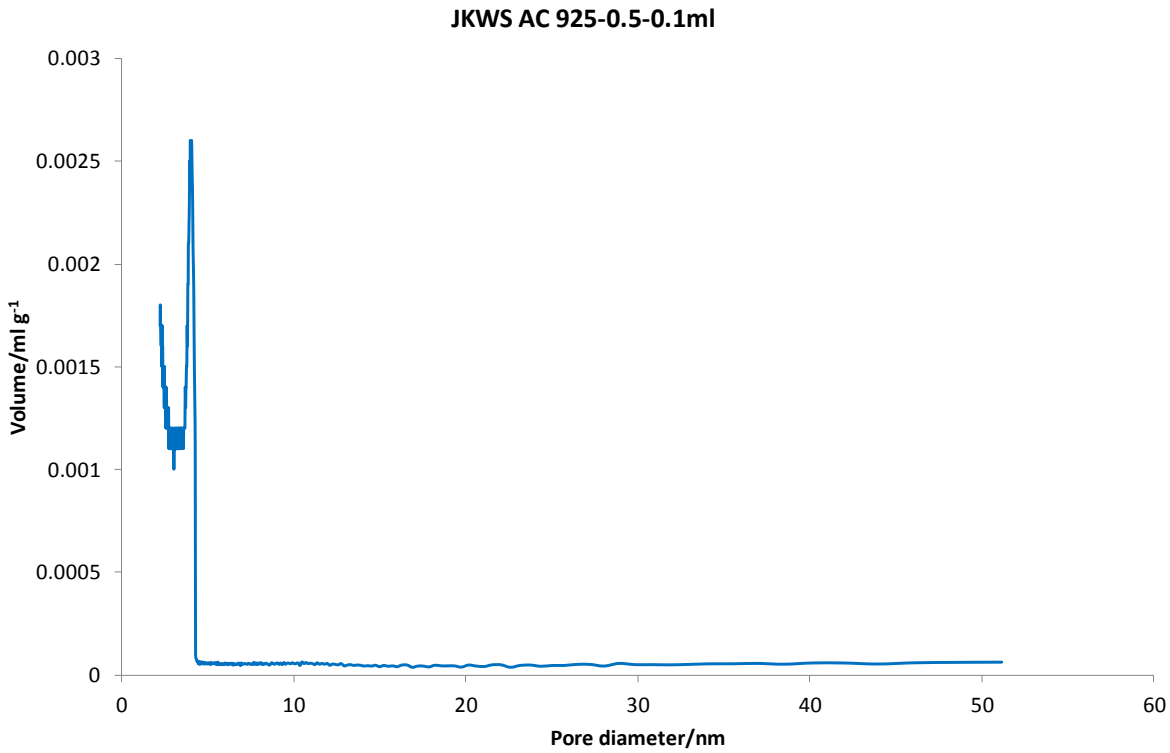


Figure 7-13: Mesopore size distribution for JKWS AC 925-0.5-0.1ml, activated at 925°C for 0.5 hour with 0.1ml/min water flow rate.

The mesopore size distribution of produced JKWS AC was similar enough that a representative plot could be used. The mesopore size distribution analyses for all JKWS carbons are listed in Table 7.6. The same is observed with JKWR carbon in Figure 7-14.

Table 7.6: Pore volume parameters for produced JKWS and JKWR AC at increasing temperatures at 0.5h activation time and 0.1ml/min water flow rate.

JKWR AC	Burn-off (%)	Total pore vol. (ml/g)	Micropore vol. (ml/g)	Meso- & macropore vol. (ml/g)	HK micropore diameter (nm)	Mesopore diameter (nm)
825-0.5-0.1ml	11.4	64.48	0.104	64.376	0.514	3.959
850-0.5-0.1ml	13.7	74.59	0.122	74.468	0.518	4.035
875-0.5-0.1ml	13.9	82.81	0.135	82.675	0.529	4.054
900-0.5-0.1ml	17.7	103.2	0.171	103.029	0.534	4.019
925-0.5-0.1ml	21.5	110.2	0.183	110.017	0.561	4.002
JKWS AC	**Burn-off (%)**	**Total pore vol. (ml/g)**	**Micropore vol. (ml/g)**	**Meso- & macropore vol. (ml/g)**	**HK micropore diameter (nm)**	**Mesopore diameter (nm)**
825-0.5-0.1ml	12.7	102.3	0.169	102.131	0.533	3.863
850-0.5-0.1ml	14.9	109.8	0.181	109.619	0.536	3.975
875-0.5-0.1ml	15.5	113.9	0.188	113.712	0.537	4.069
900-0.5-0.1ml	17.6	115.0	0.189	114.811	0.538	4.033
925-0.5-0.1ml	21.9	119.7	0.196	119.504	0.550	4.024
F400	N/A	226.4	0.371	226.029	0.512	3.966

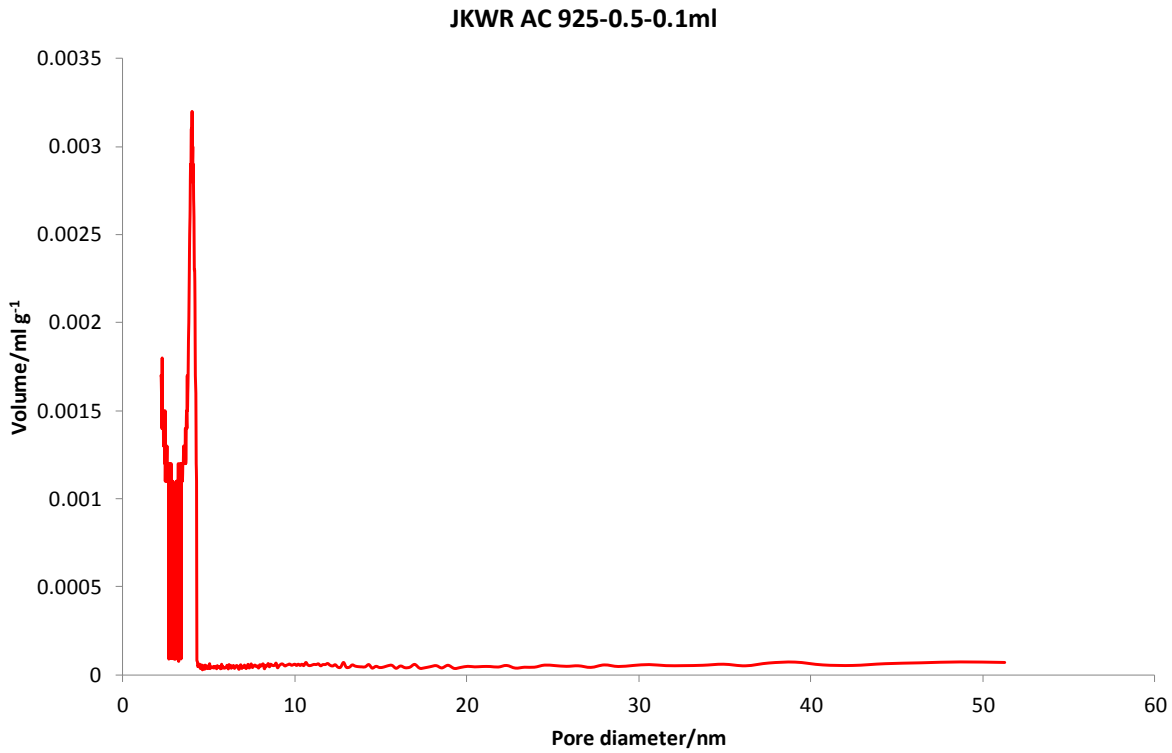


Figure 7-14: Mesopore size distribution for JKWR AC 925-0.5-0.1ml activated at 925°C for 0.5h with 0.1ml/min water flow rate.

The size distributions are only used in a comparative manner and are by no means, absolute. The mesopore size distribution of JKWS and JKWR carbons tend towards the micropore region i.e., they are closer to 2nm (micropore) than 50nm (macropore). Further, both micro- and mesopore size distributions for each JKW-derived activated carbons are essentially similar with minor changes in diameter as a result of increasing activation temperatures. This could be a result of the similar lignin contents of JKWR and JKWS as well as the cellular structures of the JKW biomass as observed in the SEM images in Section 7.2.2.2.

Table 7.6 shows that there was an observed trend of increasing micropore diameter widening for both JKWS and JKWR activated carbons as the activation temperature and hence, carbon burn-off increased. Mesopore diameter is not observed to follow a similar trend.

The total pore volume of F400 exhibited superior micropore volume, indicative of its higher adsorption capacity and surface area. It can also be observed that both micro- and mesopore size diameters of both JKWR and JKWS carbon are similar to that of F400. This demonstrates that although the BET surface area and total pore volume is much lower, both JKWR and JKWS

experiences the same pore distribution development during steam activation as F400. This suggests that with high enough burn-off, JKWR and JKWS carbon could effectively be used as an alternative feedstock for activated carbon production with similar pore characteristics determined by N_2 adsorption as F400.

7.2.4 Butane working capacity

Butane working capacity (BWC) of JKWS and JKWR AC was determined as outlined in Section 7.1.10. It is a particularly suitable test for the effectiveness of the carbons for processes such as evaporative control devices where the adsorbate is trapped and recovered in a cyclic fashion (Allen *et al.*, 1999).

Allen *et al.* (1999) suggested in their work that the optimal pore width for cyclic butane adsorption-desorption is possessed by large micropores and small mesopores.

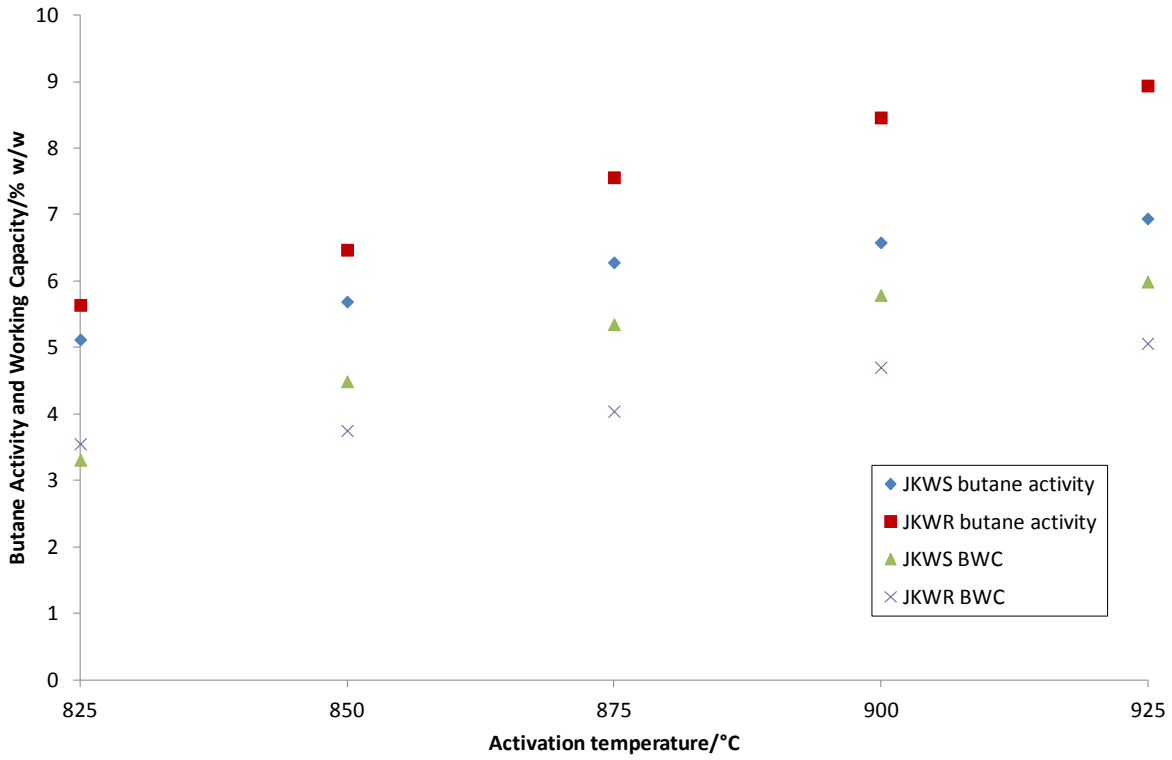


Figure 7-15: The effect of increasing activation temperature on butane activity and BWC of JKWS and JKWR carbons activated at 0.5h and 0.1ml/min water flow rate.

The increase in activation temperature brings about increases in butane activity of the produced JKWS and JKWR carbons. This is a direct result of the development of porosity, in particular the microporosity of the carbons as previously discussed in Section 7.2.3.2. Accordingly, the

enhancement of the microporosity will enable butane molecules to be easily and strongly adsorbed; hence the improved butane activity of the produced activated carbons as the activation temperature increases as can be seen in Figure 7-15. Butane has a molecular diameter of approximately 0.5nm and therefore, will most strongly adsorb in pores of slightly larger width (Allen *et al.*, 1999).

It can be observed that the produced JKWR carbon demonstrated greater butane activity when compared to the produced JKWS carbons. According to the data presented in Table 7.5, the produced JKWS carbons had higher BET surface areas as well as higher micropore surface area which should indicate higher butane activity exhibited by JKWS carbons than by JKWR carbons. However, under this particular test, the reverse was observed and it can be postulated that this could be due to the structural and lignocellulosic differences of the original biomass feedstock. This has also been reported by Allen *et al.* (1999) in their work with activated carbon made from tyres, where activated carbons with similar burn-offs had different butane adsorption capabilities. The differences were attributed to the origin of the tyres and thus, the feedstock physical-chemical composition.

It can also be seen in Figure 7-15 that the BWC of produced JKWS and JKWR carbons exhibits a positive trend with activation temperature. The presence of mesopores are vital in allowing for desorption of butane (Allen *et al.*, 1999) and as such, JKWS carbons have higher BWC owing to the larger coverage of mesopores over JKWR carbons.

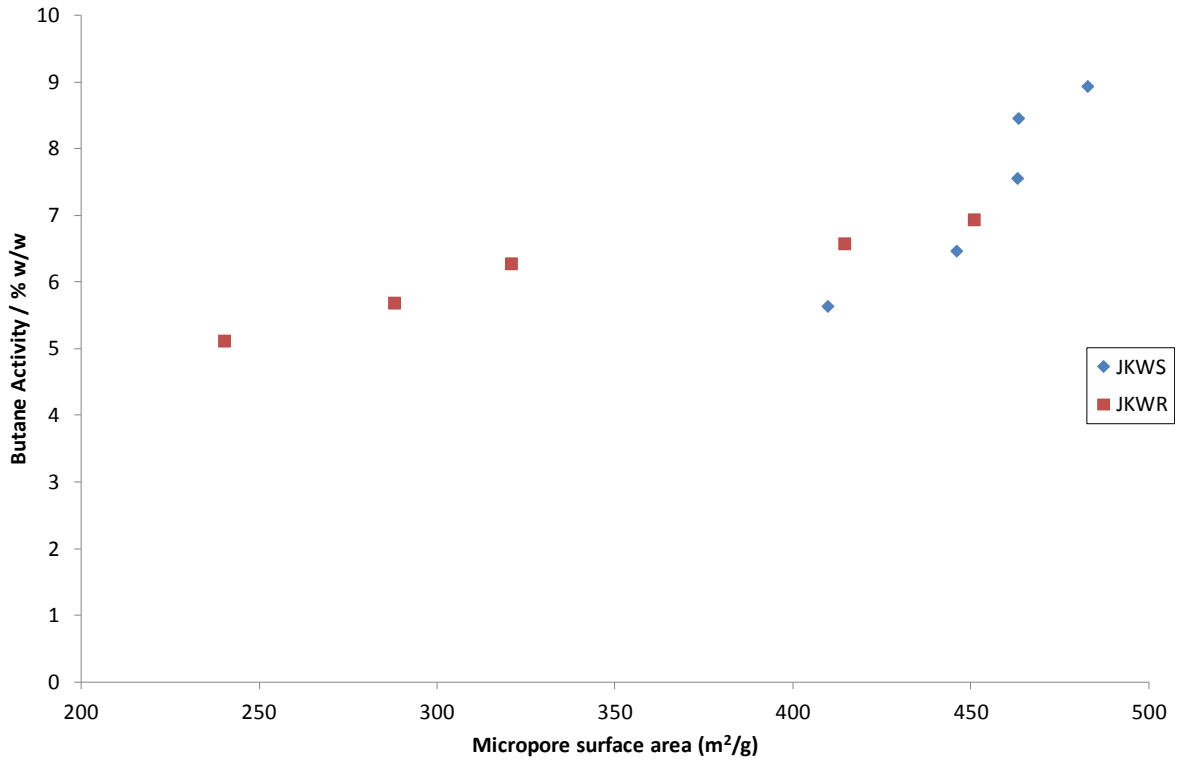


Figure 7-16: Correlation between the increase in butane activity of produced JKWS and JKWR carbons and the micropore surface area.

It is observed that the increasing micropore surface area correlates to the increased butane activity as can be seen in Figure 7-16, confirming what has been reported by Allen *et al.* (1999). There is a rapid increase of butane activity in relation to micropore surface area and this is probably due to the higher reactivity of the JKWS char precursor whereas JKWR is observed to have a gentler development of butane activity with respect to micropore surface area.

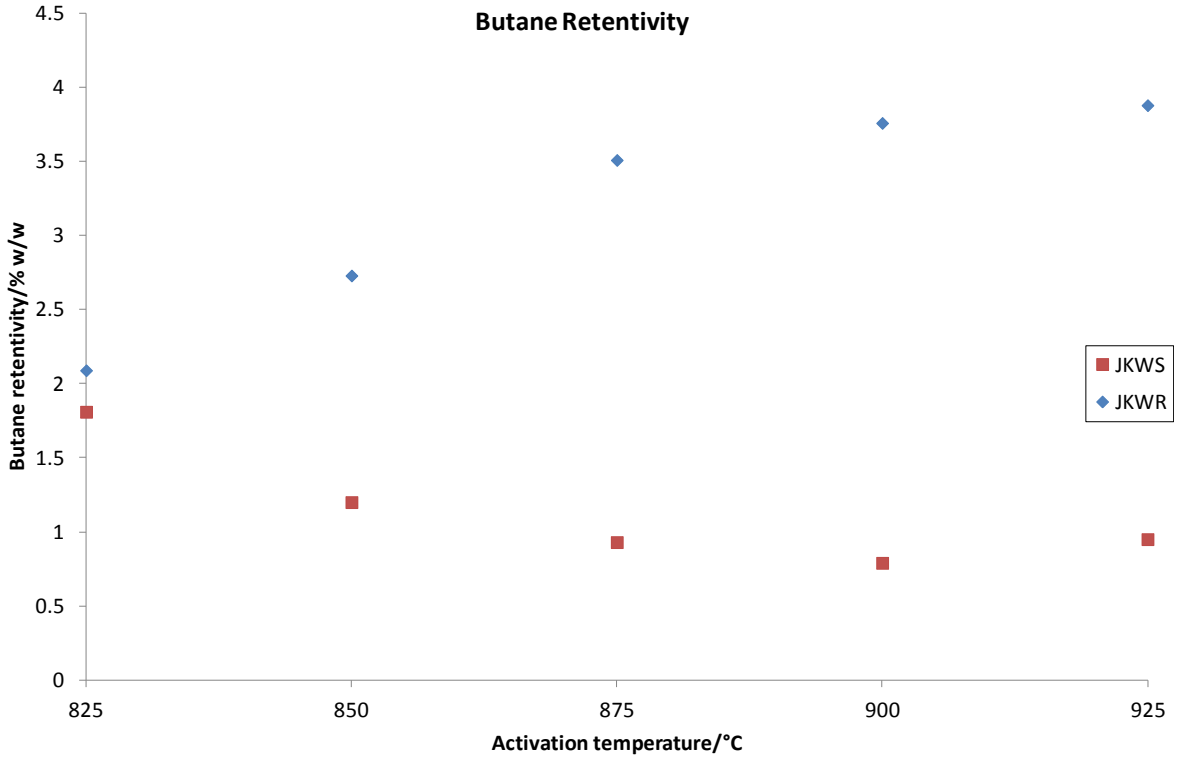


Figure 7-17: The effect of activation temperature on butane retentivity of JKWS and JKWR carbons activated at 0.5h and 0.1ml/min water flow rate.

As can be seen in Figure 7-17, the trend in butane retentivity of JKWS carbon is opposite to that of JKWR carbon. The increasing activation temperature decreases the butane retentivity of JKWS carbon. This can be explained by the increasing mesopore and macropore contribution, relative to the total porosity. As the relative mesoporosity increases (as a percentage of the total porosity), this enables butane to be easily desorbed from the pores, as was observed by Allen *et al.* (1999) for tyres.

The produced JKWR carbon exhibits a trend whereby the retentivity of butane increases with activation temperature, which is a result of the increase in microporosity, which adsorbs the butane molecules very strongly. This enhanced uptake is due to the overlapping potential fields of adjacent micropore walls, working in tandem with each and exerting attractive forces on the butane molecules, as explained by Allen *et al.* (1999).

Table 7.7: Data obtained from determination of BWC of produced JKWS and JKWR carbons.

JKWS AC	BWC (%)	Butane Activity (%)	Butane Retentivity (%)	Apparent Density (kg/m^3)
825-0.5-0.1ml	3.31	5.12	1.81	0.29
850-0.5-0.1ml	4.49	5.69	1.20	0.29
875-0.5-0.1ml	5.35	6.28	0.93	0.29
900-0.5-0.1ml	5.79	6.58	0.79	0.28
925-0.5-0.1ml	5.99	6.94	0.95	0.23
JKWR AC	**BWC (%)**	**Butane Activity (%)**	**Butane Retentivity (%)**	**Apparent Density (kg/m^3)**
825-0.5-0.1ml	3.55	5.64	2.09	0.37
850-0.5-0.1ml	3.75	6.47	2.73	0.39
875-0.5-0.1ml	4.04	7.56	3.51	0.39
900-0.5-0.1ml	4.70	8.46	3.76	0.39
925-0.5-0.1ml	5.06	8.94	3.88	0.37
F400	15.56	24.36	8.82	0.54

F400 outperforms all the produced activated carbons from both types of feedstock, as seen in Table 7.7. This is expected given the much larger BET surface area possessed by F400. Comparing Table 7.6 and Table 7.7, it can be seen that F400 has nearly twice the micropore volume of produced JKWS and JKWR carbons, thus having a much higher butane activity. The high butane retentivity is explained by F400's highly micropore surface area.

The apparent densities of both types of carbon do not deviate significantly and it is observed that JKWR carbons have higher apparent densities than their JKWS counterparts. High apparent density values for the activated carbons suggest that they can be tightly packed into columns, allowing for higher adsorptive capacities per unit volume.

7.2.5 Iodine number determination

The iodine numbers of the produced JKWS and JKWR activated carbons were determined according to ASTM Method D4607-94(99) as mentioned in Section 7.1.11.

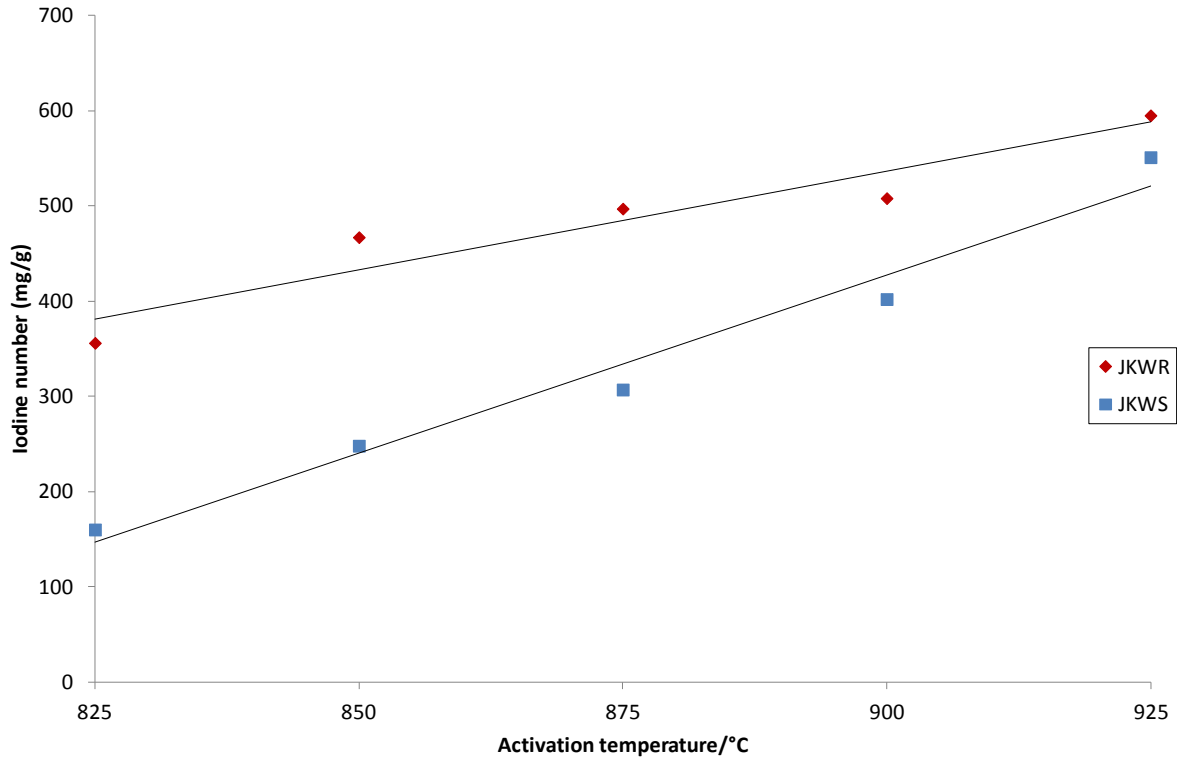


Figure 7-18: Effect of activation temperature on iodine number. Activation time: 0.5h and water flow rate: 0.1ml/min.

The rise in activation temperature from 825°C to 925°C in Figure 7-18 resulted in the iodine numbers increasing from 356mg/g to 595mg/g for JKWR carbons and from 160 to 551mg/g for JKWS carbons. This is an indication that the number of pores larger than 1-1.5nm i.e., large micropores into which iodine molecules can penetrate also increases, as observed by Gergova *et al.* (1994) during their study of agricultural by-products such as grape seeds and cherry stones. As a reference, the iodine molecule is 0.56nm in diameter (Hsieh and Teng, 2000). The maximum iodine number was obtained when JKWR and JKWS chars were activated at 925°C.

It is known that most of the adsorptive capabilities of activated carbons come from the micropores (Yang *et al.*, 1993) and therefore, increases in micropores are accompanied by increases in iodine number. Logically, since the produced JKWS carbons have the higher BET surface area and micropore surface area, the iodine numbers achieved should be higher. However, JKWR carbons are seen to be able to adsorb more iodine than JKWS carbons.

Teng and Hsieh (1998) reasoned that for increased adsorbate uptake, the molecules needs to be accessible to newly-created or existing micropores. An ideal situation would be one in which the

carbon created were constant in character and all micropores were available for adsorption, which would mean that the adsorption of iodine would increase proportionally with surface area increase.

ASTM Method D 4607 (ASTM, 1994b) states that the iodine number may be used as an approximation of the surface area of some types of carbon. If one were to accept the assumption, then the iodine number should mirror the BET surface area of the carbon. In order to calculate the surface area occupied by iodine, one also needs to assume that the iodine molecules is spherical and has a close-packed hexagonal arrangement on the carbon surface. This has been reported as 24.6×10^{-20} m^2 (Hsieh and Teng, 2000). Thus, the fraction of BET surface area occupied by iodine can be estimated according to the iodine number. This is shown as X_{BET}, the fraction of coverage. The total surface area occupied by the iodine molecules can be calculated by multiplying the surface area with Avogardo's number and the iodine number, converted into moles. This data is shown in Table 7.8 and plotted in Figure 7-19 as a function of activation temperature.

Table 7.8: Surface area characteristics of produced JKWR and JKWS carbons with F400.

JKWS AC	Iodine Number/mg g^{-1}	Surface area/m^2 g^{-1}					X_{BET}	X_m
		BET	Micropore	Meso- and macropore	I_2 occupied	Meso:BET		
825-0.5-0.1ml	160	441.9	409.75	32.15	93.29	0.073	0.21	0.23
850-0.5-0.1ml	248	474.1	445.96	28.14	144.59	0.059	0.30	0.32
875-0.5-0.1ml	307	491.8	463.08	28.72	178.99	0.058	0.36	0.39
900-0.5-0.1ml	402	496.7	463.38	33.32	234.38	0.067	0.47	0.51
925-0.5-0.1ml	551	516.9	482.81	34.09	321.25	0.066	0.62	0.67
JKWR AC	**Iodine Number/mg g^{-1}**	**BET**	**Micropore**	**Meso- and macropore**	**I_2 occupied**	**Meso:BET**	**X_{BET}**	**X_m**
825-0.5-0.1ml	356	278.4	253.28	25.12	207.56	0.090	0.75	0.86
850-0.5-0.1ml	467	322.1	290.76	31.34	272.28	0.097	0.85	0.95
875-0.5-0.1ml	497	357.6	323.42	34.18	289.77	0.096	0.81	0.90
900-0.5-0.1ml	508	445.8	408.99	36.81	296.18	0.083	0.66	0.71
925-0.5-0.1ml	595	476.0	437.73	38.27	346.91	0.080	0.73	0.77
F400	1000	977.4	885.84	91.56	583.04	0.094	0.60	0.66

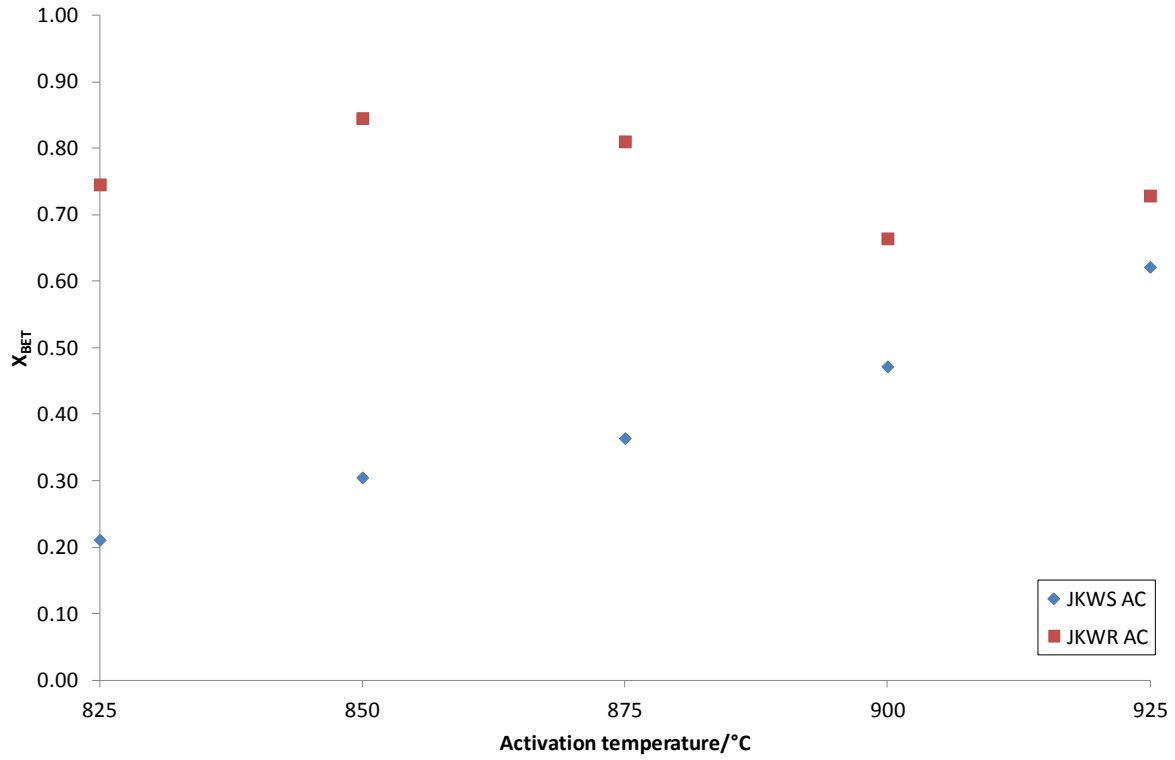


Figure 7-19: Effect of activation temperature of X_{BET} of iodine in produced JKWR and JKWS carbons.

Figure 7-19 shows that only some of the BET surface area is accessible to iodine for JKWS AC due to the fact that $X_{BET} < 1$, i.e. the available BET surface area is not saturated with iodine molecules. However, this fractional coverage increases with increasing activation temperature, as evidenced by the increasing X_{BET} values. A majority of surface area of JKWR carbons activated at the lower temperatures is already exposed to iodine molecules but this decreases throughout the activation temperature range.

There does not appear to be a direct relationship between the iodine number and BET surface area. Even though it was observed that in Table 7.8, JKWS AC had higher BET and micropore surface area than JKWR AC, it does not necessarily mean that there will be a higher uptake of iodine, as evidenced by the lower iodine numbers. As the activation temperatures used to activate both carbons increased, the fraction of iodine adsorbed by BET surface area X_{BET} also increased, indicating that the improved BET surface area plays a role in iodine adsorption, providing more adsorption sites, although other factors could have an influence including pore shape, surface chemistry and internal pore connectivity.

The X_{BET} values <1.0 indicate that not all of the BET surface area is available for adsorption, which is logical when one considers the contribution from the meso- and macropores as they tend to have

lower adsorptive capabilities (Yang *et al.*, 1993). The X_m ratio is the surface coverage of micropores by the iodine molecules and it is observed to be slightly higher than the X_{BET} ratio. This is as expected since it takes into account the meso- and macropore surface area. From Table 7.8, the X_m results indicate that the micropores are not fully utilised during adsorption and this may depend on the diffusion path from the external aqueous environment into the internal microporous cavities of the carbon as well as the size and shape of the pores. If the diffusion path is too long or the pore diameter is too narrow, the chances of pore blockage occurring increases, especially when aggregation of adsorbate molecules occur (Hsieh and Teng, 2000).

Mesopores are essential in enhancing the adsorption capacity of activated carbons in aqueous solutions, especially if the adsorbed molecules involved are large (Hsieh and Teng, 2000) or in the case of this study, the effective micropore diameter is small (approx. 0.5nm). Thus, it can be seen in Table 7.8 that the meso- and macropore surface area and its ratio to BET surface area of JKWR carbons is larger than that of JKWS carbons. Hence, it is reasonable to infer that the higher uptake of iodine by JKWR carbons is due to its better developed mesoporosity, relative to its total BET surface area. It is also for this reason that F400 has high iodine number: the large mesoporosity allows easier access to the adsorbing sites provided by the internal micropores.

The explanation for the role of meso- and macropores in the adsorption of molecules from aqueous solution is that the adsorption path from the external environment to the micropores is shortened and under this circumstance, the mesopores assist in accelerating adsorption and increasing equilibrium coverage of the micropore surface (Hall *et al.*, 1966, Hsieh and Teng, 2000, Teng and Hsieh, 1998).

7.2.6 Phenol adsorption

The factors that affect the adsorption capabilities of activated carbons are as follows (Snoeyink *et al.*, 1969, Dabrowski *et al.*, 2005):

1) Effects of adsorbate such as molecular weight, solubility and polarity
2) Effects of the carbon such as surface chemistry, surface area and porosity
3) Effects of the solution such as pH and competing ions.

The accepted theory of adsorption of phenol onto activated carbons was proposed by Coughlin and Ezra (1968) in which they explained that the π electrons of the phenol ring interacts with the active carbon surface. Coughlin and Ezra (1968) also suggested that the removal of electrons from the π ring could interfere with the bonds. Phenol adsorption onto activated carbons is strongly influenced by oxygen-containing functional groups (Dabrowski *et al.*, 2005).

The mechanisms for the transport of phenol molecules into the AC pores are as follows (Faust and Aly, 1998, Hameed and Rahman, 2008):

a) Phenol molecules migrate through the solution and are concentrated on the carbon surface via film diffusion;
b) This is followed by solute movement from the carbon surface into the interior pore sites by pore diffusion;
c) The phenol molecules are adsorbed onto the active sites in the interior of the carbon particles.

As the adsorption process proceeds, the phenol molecules tends to desorb into the solution and once the rates of adsorption and desorption attain equilibrium, the phenol adsorption capacity is known (Faust and Aly, 1998).

It was previously discussed in Section 3.5.6, the surface structures of activated carbons influences the pH of the solution into which it is placed. Consequently, this will affect the adsorption of the molecule of interest present in the aforementioned solutions. If the solution pH exceeds the pKa value of phenol, the molecule will dissociate into phenolate anions and H^+ ions. The adsorption of its ionic form will then depend on the surface charge of the activated carbon (Dabrowski *et al.*, 2005) which will be reduced when compared to adsorption of the phenol molecule. The pKa value for phenol is 9.89 (Dabrowski *et al.*, 2005). Thus, it is important to keep the solution pH below this point in order to maximise adsorption as there will be less repulsion between the phenol molecule and the activated carbon.

The pH of the phenol solutions after adsorption by JKWR and JKWS carbons were determined and this is shown in Figure 7-20, along with the change in pH due to the addition of the JKW-derived carbons.

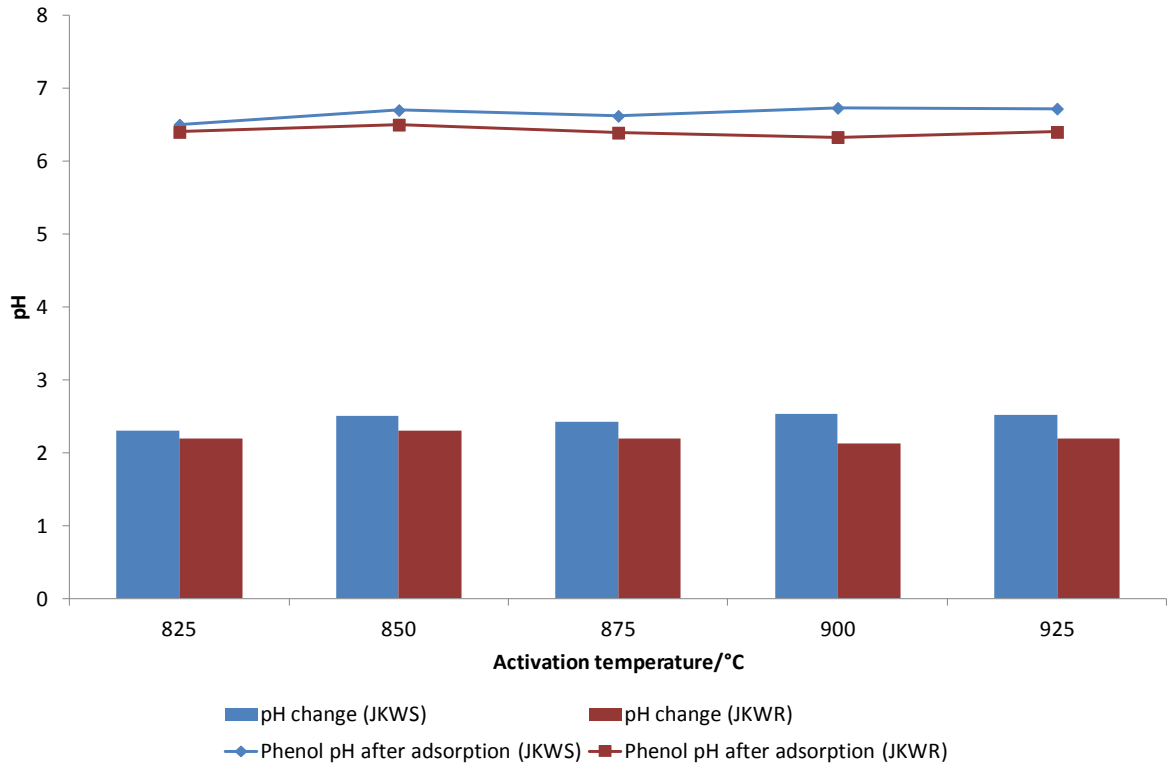


Figure 7-20: Variation of phenol solution pH after adsorption by JKWS and JKWR carbons.

The pH measurements indicated that the both types of carbons were of the 'H' variety which was proposed by Steenberg (1944) as mentioned in Section 3.5.6. This is because of the gain in pH units from the measured average pH 4.2 of phenol (shown by the columns in Figure 7-20) after the addition of JKWR and JKWS carbons, indicating the presence of basic surface groups on the carbons. These results indicate that the main form of phenol present during adsorption was the molecular form and this should result in adsorption by the produced activated carbons without being affected by surface charges and ions.

Phenol is most adsorbed at neutral pH but this decreases as the pH becomes more acidic due to competition from H^+ ions present (Snoeyink *et al.*, 1969). In this case, JKWR and JKWS are well-suited to phenol adsorption due to being able to raise acidic pH values to near neutral levels.

7.2.6.1 Adsorption kinetics

F400 was used as the commercial standard comparison to JKW-derived carbons and as such, the contact time needed for equilibrium to be reached during phenol adsorption for all the tested JKW carbons were based on F400. The adsorption kinetics plot of phenol is presented in Figure 7-21.

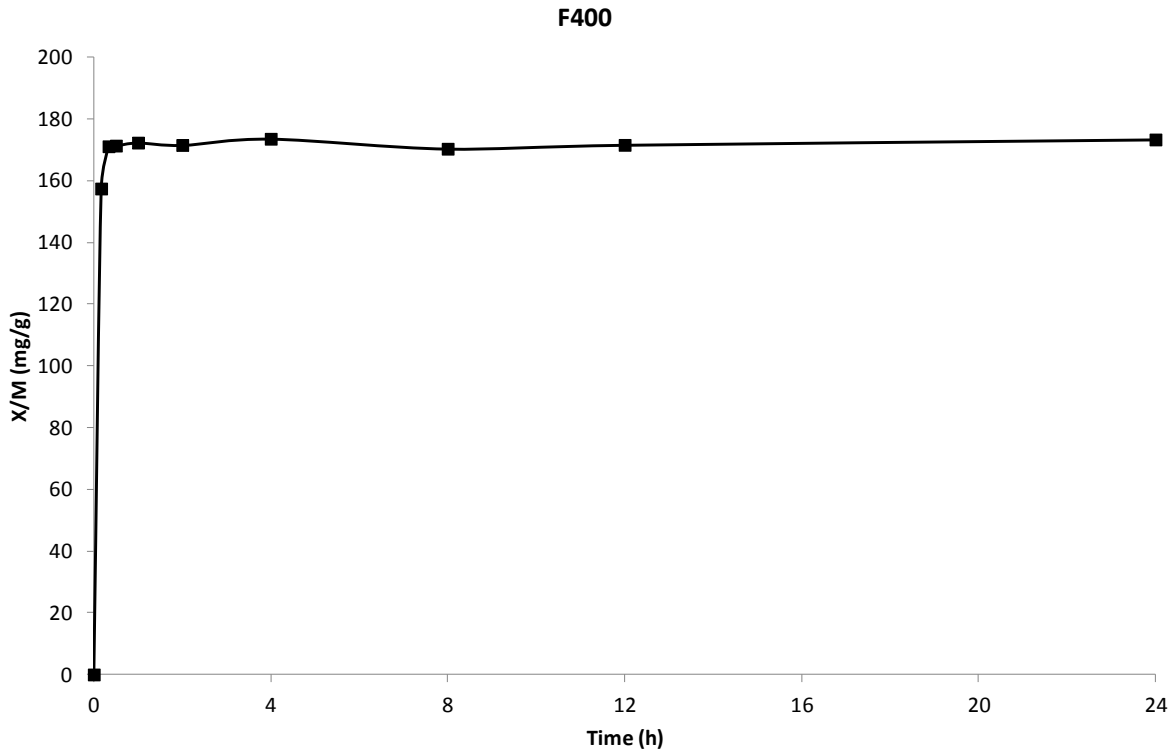


Figure 7-21: Phenol adsorption kinetics of F400. Initial phenol concentration: 200ppm.

From Figure 7-21, it can be seen that F400 was nearly fully-saturated with phenol at t=10mins. This demonstrated that F400 provided plenty of accessible adsorptive sites to the phenol molecules. The minimum contact time needed F400 to reach saturation is 12h. Hence, to ensure full equilibrium was reached as well as valid comparisons between the JKW activated carbon samples, 24h was used as the contact time for equilibration. This doubled contact time also provided a margin of safety to ensure that less activated JKW carbons were allowed sufficient time to reach phenol adsorption equilibrium.

7.2.6.2 Adsorption isotherms

The adsorption isotherms, which result from plotting q_e (concentration adsorbed) against C_e (equilibrium concentration), are shown in Figure 7-22 for JKWS activated carbons and in Figure 7-23 for JKWR activated carbons activated for 0.5h with a water flow rate of 0.1ml/min. A phenol adsorption isotherm of F400 is also presented in Figure 7-24 for comparison purposes. The isotherms are important for understanding how adsorbates interact with the carbon and are vital in optimising the use of the carbon as an adsorbent.

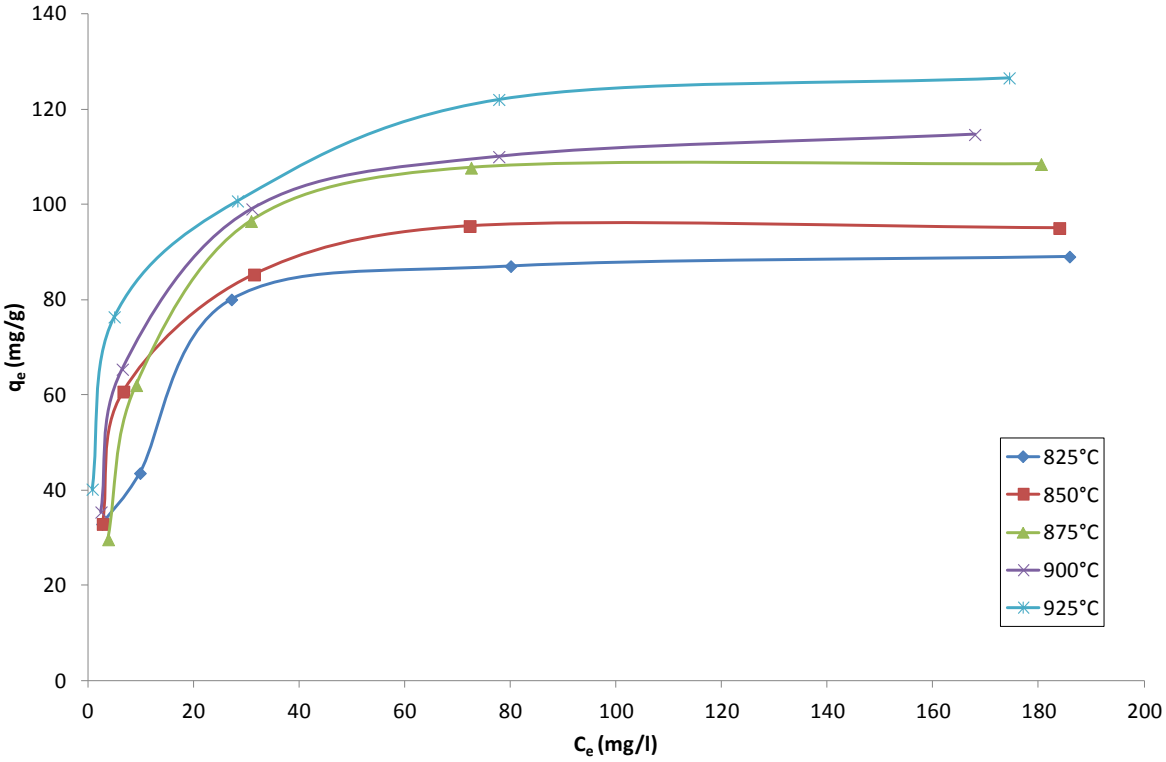


Figure 7-22: Adsorption isotherms for JKWS activated carbons produced at increasing activation temperatures. Activation time: 0.5h and water flow rate: 0.1ml/min.

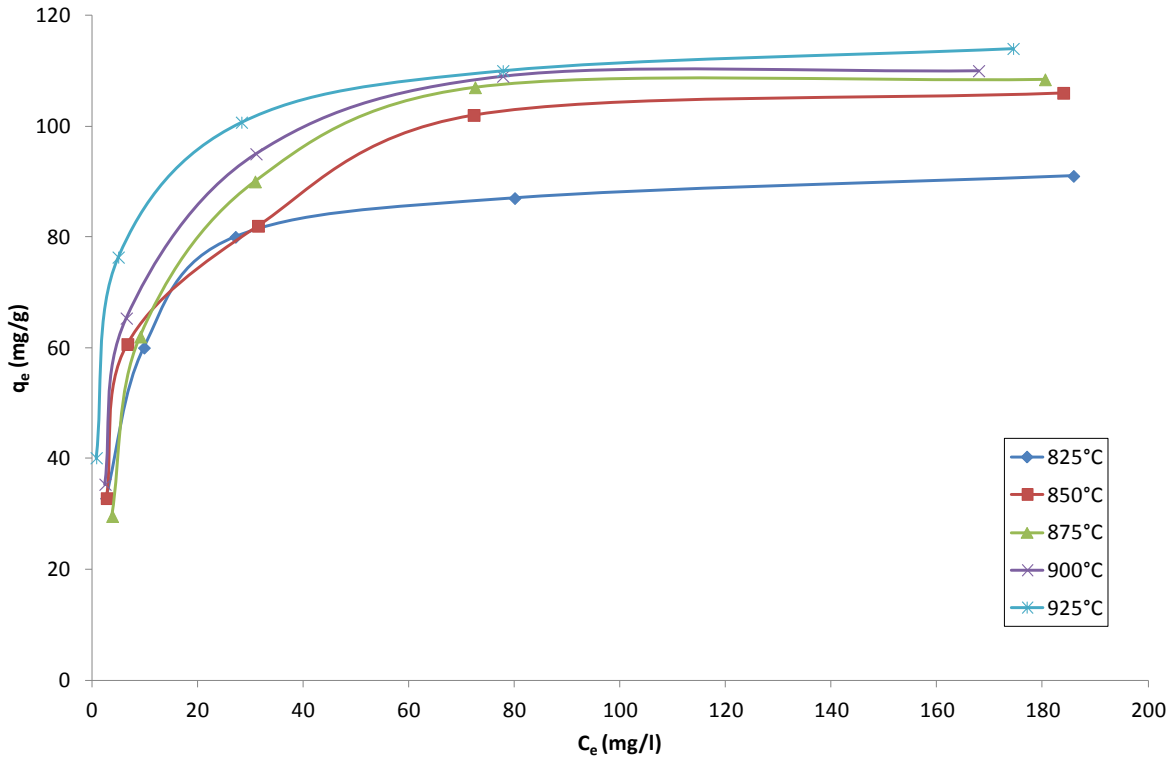


Figure 7-23: Adsorption isotherms for JKWR activated carbons produced at increasing activation temperatures. Activation time: 0.5h and water flow rate: 0.1ml/min.

From Figure 7-22 and Figure 7-23, it is clear that as the activation temperature increases, the amount of phenol adsorbed by the produced JKWS activated carbon increases; from 83mg/g to 128mg/g. The amount of phenol adsorbed increased from 72mg/g to 114mg/g for JKWR carbons as a result of increased activation temperatures. Both results are an indication of the continued development of porosity which is suitable for phenol adsorption. The textural characteristics of both types of carbons are presented in Table 7.9, along with the characteristics of F400.

Table 7.9: Textural characteristics with Langmuir and Freundlich constants for phenol adsorption for JKWR and JKWS ACs.

				Langmuir parameters			Freundlich parameters		
JKWS AC	**Burn-off/%**	**BET surface area/m^2 g^{-1}**	**BET pore volume/ml g^{-1}**	**Q_0 (mg/g)**	**R_L**	**R^2**	**K_F (mg/g)(mg/L)*n***	**n**	**R^2**
825-0.5-0.1ml	12.7	441.9	102.3	83	0.011	0.9922	28	4.06	0.7843
850-0.5-0.1ml	14.9	474.1	109.8	96	0.018	0.9993	32	4.19	0.8243
875-0.5-0.1ml	15.5	491.8	113.9	115	0.039	0.9984	23	2.95	0.8612
900-0.5-0.1ml	17.6	496.7	115	118	0.037	0.9966	34	3.90	0.9015
925-0.5-0.1ml	21.9	516.9	119.7	128	0.026	0.9963	47	4.89	0.9413
JKWR AC									
825-0.5-0.1ml	11.4	278.4	64.48	91	0.061	0.9806	35	5.88	0.9171
850-0.5-0.1ml	13.7	322.1	74.59	106	0.071	0.9754	40	5.49	0.9208
875-0.5-0.1ml	13.9	357.6	82.81	110	0.018	0.9967	34	4.26	0.9588
900-0.5-0.1ml	17.7	445.8	103.2	110	0.018	0.9958	42	5.15	0.9662
925-0.5-0.1ml	21.5	476.0	110.2	114	0.075	0.9905	44	5.51	0.9615
F400	N/A	977.4	226.4	175	0.059	0.9894	34	3.13	0.9869

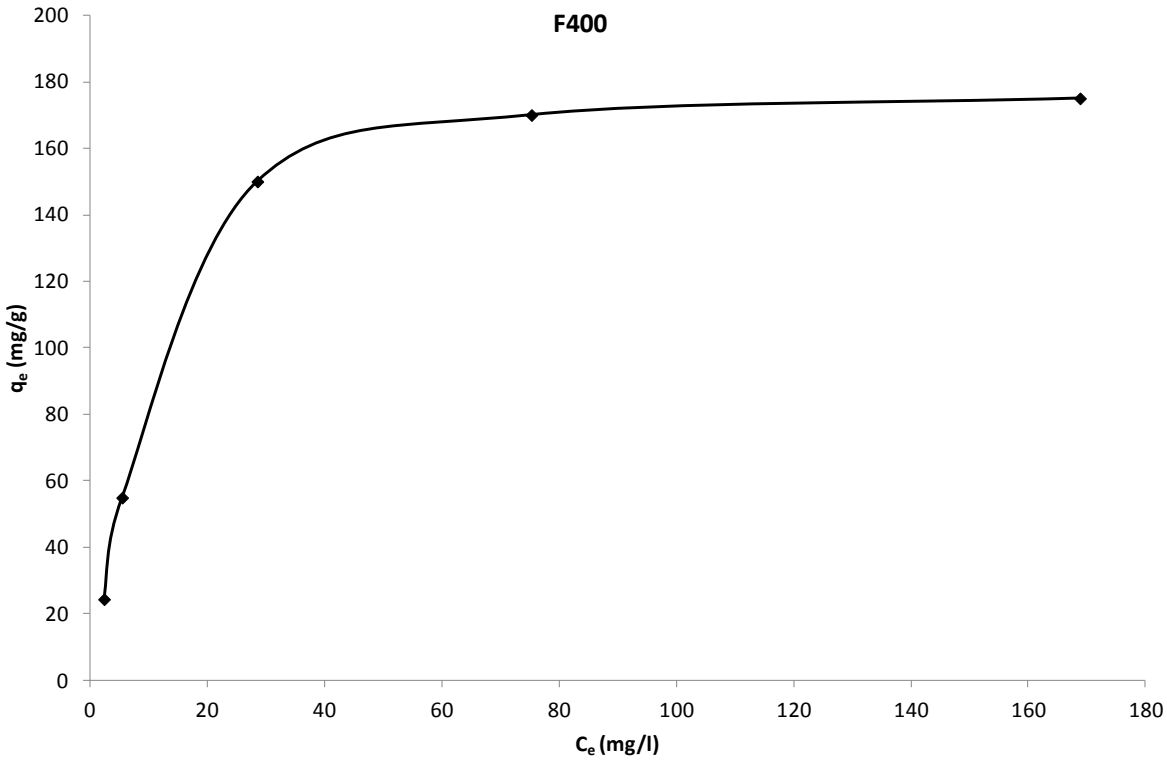


Figure 7-24: Phenol adsorption isotherm of F400 at different C_e values.

It is apparent that none of the current JKW-derived carbons were able to compete with the phenol adsorption capability of F400, which had a maximum capacity of 175mg/g. At these levels of activation, the JKW carbons did not have sufficient porosity to adsorb phenol to the same extent as F400.

All the adsorption isotherms exhibited a L-2 type curve, according to the classification by Giles *et al.* (1974b). This type of isotherm suggests that the adsorption of phenol by the activated carbons follows the premises of the Langmuir theory and that the monolayer has been formed, indicating that the capacity can be determined from the height of the plateau. However, it has been reported that this does not provide a fair comparison of adsorptive capacity (Teng and Hsieh, 1998) and thus, phenol capacity obtained from the simple adsorption isotherms are not used in this study.

It can be seen in Table 7.9 that the increased amount of phenol adsorbed can be directly correlated to the BET surface area (Teng and Hsieh, 1998) as observed in Figure 7-22 and Figure 7-23. Table 7.9 also shows that the increase in activation temperatures, which is linked with increases in burn-off leads to increased meso- and macroporosity. This is in agreement with what has been previously reported in this study as well as in others (Arriagada *et al.*, 1997, González *et al.*, 1994, Molina-Sabio *et al.*, 1996, Rodriguez-Reinoso and Molina-Sabio, 1992). The increasing meso- and macroporosity of

the carbon also highlights their importance in providing a shortened diffusion pathway for phenol molecules to access the interior micropores.

Again, the BET surface area or pore volume of the carbons determine the limiting number of sites available for phenol adsorption since both the surface area and the pore volume increases with activation temperature. JKWS carbons had greater phenol uptake than their JKWR counterparts, possibly due to the higher reactivity to steam and thus, higher surface areas achieved during activation.

The Langmuir and Freundlich isotherm models were used to facilitate the estimation of phenol adsorption capacity of the JKW carbons, as discussed in Section 3.4. An example of the straight line Langmuir adsorption plot from which Q_0, the monolayer capacity of the carbon is obtained from the gradient of the plot is shown in Figure 7-25. The plot shown in Figure 7-25 is of JKWS AC 925-0.5-0.1ml. The Langmuir plot of the equivalent JKWR-derived carbon was not shown as it was similar to the plot shown in Figure 7-25.

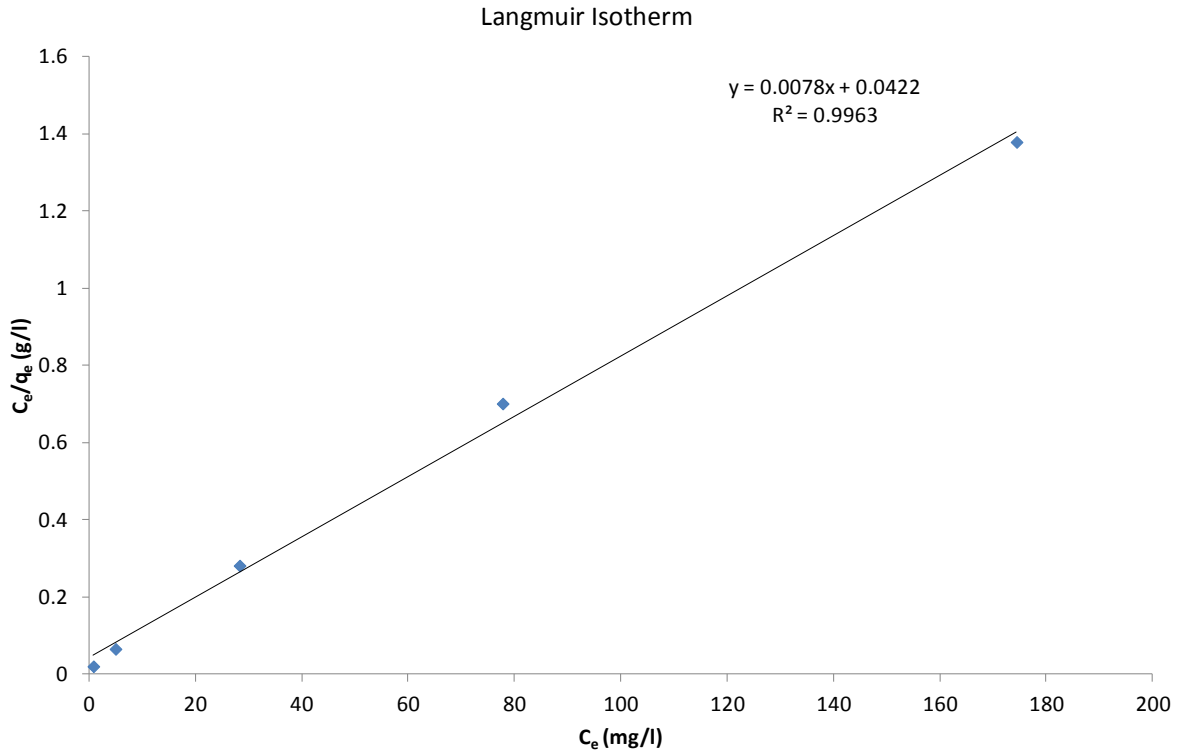


Figure 7-25: Langmuir plot of JKWS AC 925-0.5-0.1ml, produced at 925°C for 0.5h at 0.1ml/min water flow rate.

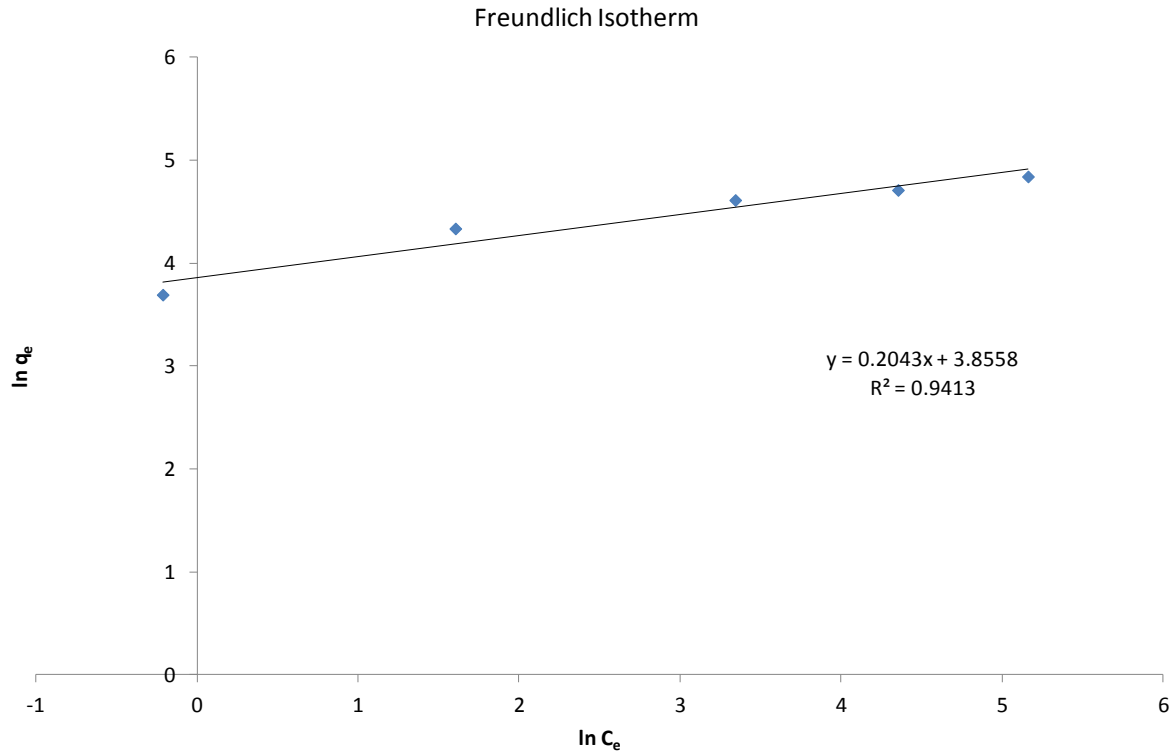


Figure 7-26: Freundlich isotherm plot of JKWS AC 925-0.5-0.1ml, produced at 925°C for 0.5h at 0.1ml/min water flow rate.

The Freundlich isotherm plot of JKWS AC 925-0.5-0.1ml is shown in Figure 7-26, where the Freundlich parameter, K_F is the y-intercept of the graph. K_F provides an indication of the adsorption capacity of the carbon and 1/n, the slope of the plot is indicative of adsorption intensity, as discussed in Section 3.4.1. As with the Langmuir plot, the equivalent JKWR-derived carbon exhibited a similar Freundlich isotherm plot and hence, is not shown.

Each of the adsorption equations shows different levels of applicability to phenol adsorption by the JKWS and JKWR carbons. The R^2 value of the plots can be used as an indicator to determine if either or both of the equations show a reasonable fit to the data obtained.

The Langmuir and Freundlich parameters for phenol adsorption are summarised in Table 7.9. The adsorption data presented for phenol could be interpreted very well by the Langmuir model, as evidenced by R^2 values >0.97. However for some of the carbons, interpretation by the Freundlich model was less amenable as shown by the relatively lower R^2 values. Although the *n* values of the Freundlich model in Table 7.9 indicate that adsorption of phenol was favourable, there does not seem to be an obvious trend in the values of K_F. Indeed, the seemingly random behaviour of K_F values infers that the Freundlich model is not the best-fitting model for the adsorption of phenol by JKWS

and JKWR activated carbons. Thus, the emphasis has been placed on using the Langmuir model as the main theory for phenol adsorption by the produced JKWS and JKWR activated carbons.

The values of the constant, *n* of the Freundlich model given in Table 7.9 indicated that the adsorptions which occurred was favourable (Hameed and Rahman, 2008). The R_L value (as discussed in Section 3.4.2) is a dimensionless factor which can be used to determine whether the Langmuir isotherm model is favourable (Fierro *et al.*, 2008) and the values presented in Table 7.9 indicate that the model was suitable for the adsorption of phenol under the conditions used in the study.

The optimum Langmuir Q_0 values obtained was from adsorption by JKWS and JKWR carbons produced at 925°C, indicating that it is the optimum temperature for JKWS and JKWR steam activation to produce activated carbons for phenol adsorption.

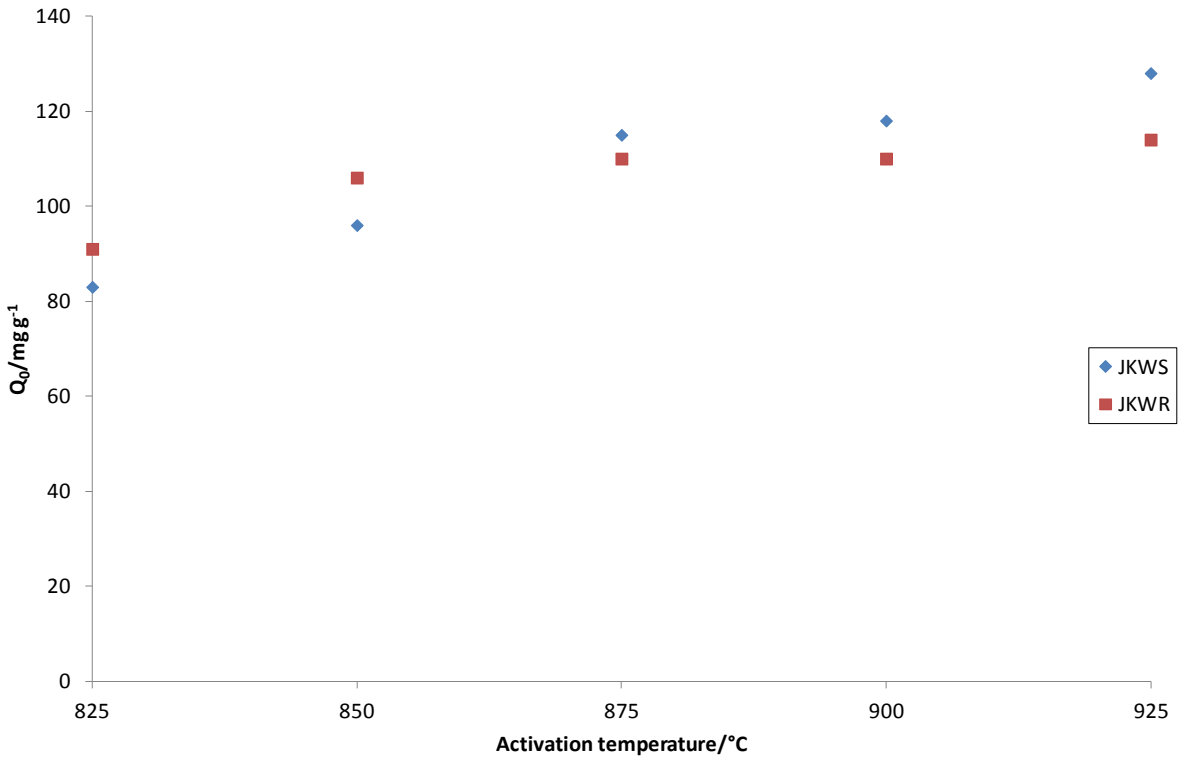


Figure 7-27: Effect of activation temperature on Q_0 of produced JKWS and JKWR carbons.

From Figure 7-27, the monolayer capacity continuously increases with activation for temperature for JKWS carbons but stays relatively constant for JKWR carbons. It is known that the increase in Q_0 is a function of BET surface area (Juang *et al.*, 2002, Teng and Hsieh, 1998) as shown in Figure 7-28, which is in turn a function of activation temperature. The relatively constancy of Q_0 for JKWR

carbons is due to the minor increase of BET surface area in relation to activation temperature, as observed in Figure 7-28.

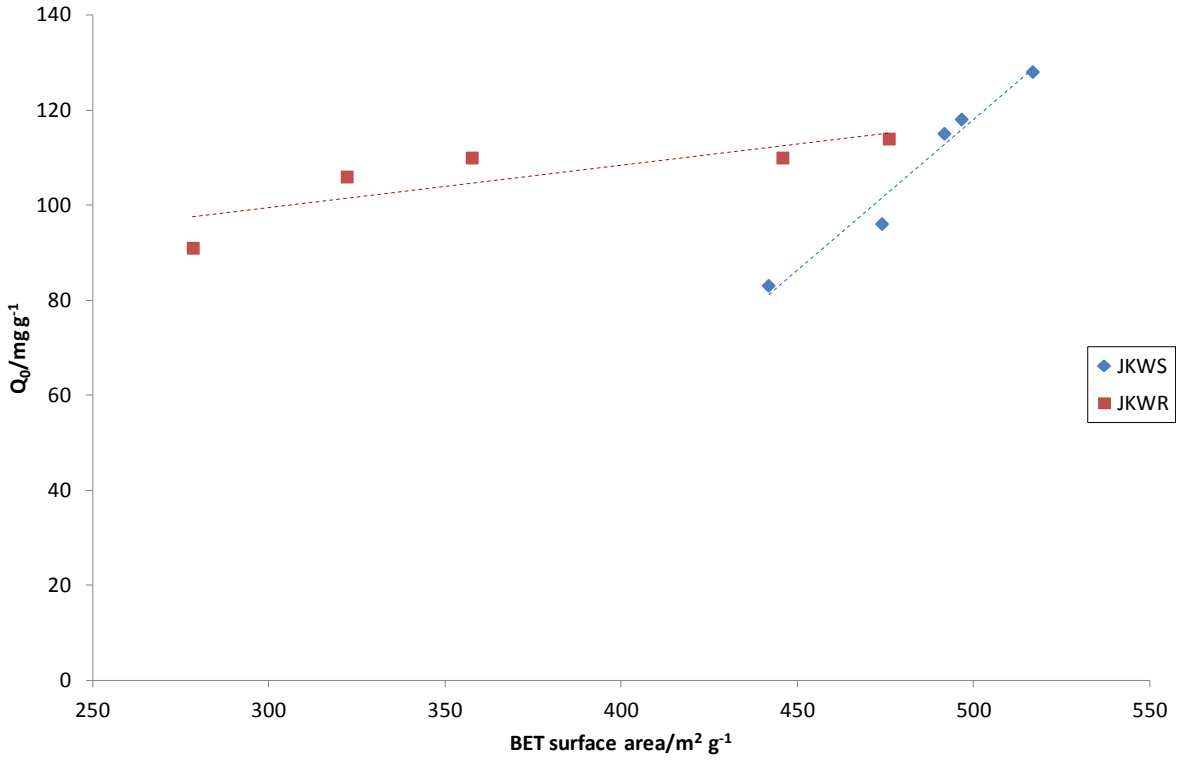


Figure 7-28: Change in Q_0 against BET surface area of produced JKWS and JKWR carbons.

In Figure 7-28, the rate of change of Q_0 against BET surface area is greater for JKWS than it is for JKWR as can be seen from the gradients of the trendlines. This trend was also observed in Figure 7-16 of Section 7.2.4. Although JKWR had a greater mesopore:BET surface area ratio as previously discussed in Section 7.2.5, it is unable to compete with the higher absolute BET surface area of JKWS, which undoubtedly allows for higher phenol uptake. The difference in reactivity and development of BET surface area can be attributed to the different physical and lignocellulosic contents of JKWS and JKWR as previously discussed in Section 5.4.3 and Section 7.2.3.2.

In order to examine whether the meso- and macropores of the activated carbon affect the adsorption of phenol, X_{BET} and X_m values were calculated for the carbons, as previously discussed in Section 7.2.5 and is shown in Table 7.10 and plotted in Figure 7-29. The area occupied by a phenol molecule is 30.2 x 10^{-20} m^2 and its molecular diameter is 0.62nm (Hsieh and Teng, 2000).

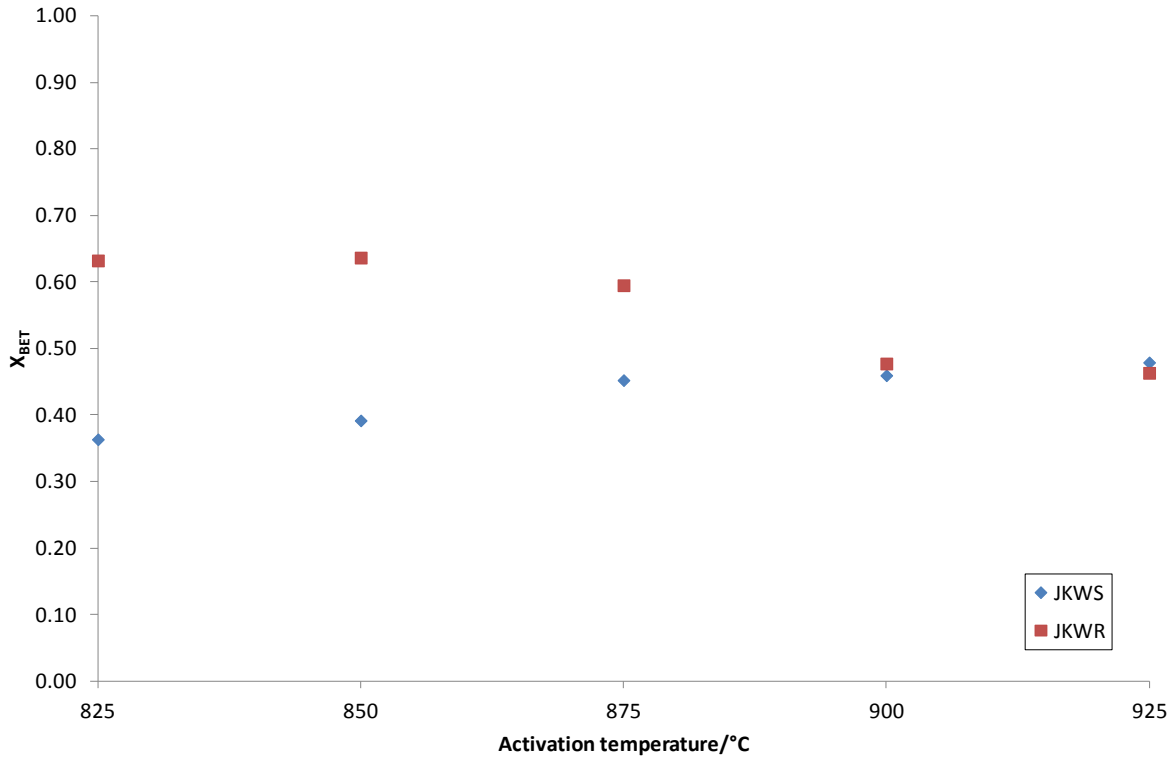


Figure 7-29: Values of X_{BET} as a function of activation temperature for produced JKWS and JKWR carbons.

It can be seen in Figure 7-29 that at low activation temperatures, JKWR AC had a relatively high coverage of phenol molecules. This is a result of a high mesopore:BET surface area ratio as previously discussed in Section 7.2.5. X_{BET} values <1.0 indicate that only partial coverage of the BET surface area was achieved during phenol adsorption. However, JKWR X_{BET} values were seen to decrease whereas the X_{BET} values for JKWS were seen to increase with activation temperature. This is most probably due to the fact that the increase in Q_0 does not follow the same rate of increase of BET surface area, as seen in Figure 7-28. It is possible that the accessibility of the pores of the produced JKWR AC to phenol changes with increasing activation temperature. This is explained by the opening of new micropores and deepening of existing micropores and under these conditions, the increased mean diffusion path restricts the accessibility of the carbon porosity to phenol. This was observed by Teng and Hsieh (1998) in their work of phenol adsorption with activated carbon from coal.

Table 7.10: Surface area analysis and Langmuir model data for JKWS and JKWR carbons produced at different activation temperatures.

JKWS AC	Burn-off/%	BET surface area/ $m^2 g^{-1}$	Meso:BET	Langmuir Q_0 (mg/g)	Phenol SA (m^2)	X_{BET}	X_m
825-0.5-0.1ml	12.7	441.9	0.073	83	160.53	0.36	0.39
850-0.5-0.1ml	14.9	474.1	0.059	96	185.67	0.39	0.42
875-0.5-0.1ml	15.5	491.8	0.058	115	222.42	0.45	0.48
900-0.5-0.1ml	17.6	496.7	0.067	118	228.22	0.46	0.49
925-0.5-0.1ml	21.9	516.9	0.066	128	247.56	0.48	0.51
JKWR AC	**Burn-off/%**	**BET surface area/ $m^2 g^{-1}$**	**Meso:BET**	**Langmuir Q_0 (mg/g)**	**Phenol SA (m^2)**	**X_{BET}**	**X_m**
825-0.5-0.1ml	11.4	278.4	0.090	91	176.00	0.63	0.69
850-0.5-0.1ml	13.7	322.1	0.097	106	205.01	0.64	0.71
875-0.5-0.1ml	13.9	357.6	0.096	110	212.75	0.59	0.66
900-0.5-0.1ml	17.7	445.8	0.083	110	212.75	0.48	0.52
925-0.5-0.1ml	21.5	476.0	0.080	114	220.49	0.46	0.50
F400	N/A	977.4	0.094	175	338.46	0.35	0.38

7.2.7 Summary of effect of activation temperature

The results at this stage of the research have indicated that increasing the temperature of steam activation has a positive effect on the activated carbon burn-off, which indicates that the water molecules react more readily with the char carbon structure, resulting in weight losses of the char and simultaneously increasing the porosity of the char. The porosity development of the carbon, as measured using the BET theory resulted in increased BET surface area and total pore volume of the activation carbon. The increased activation temperatures are also observed to decrease the carbon contents of the produced activated carbons.

The effects of increased steam activation temperature are:

- Increased burn-off
- Increased BET surface area and total pore volume
- Increased BWC and butane activity
- Increased phenol and iodine adsorption

The activated carbons made from JKWS experienced higher burn-offs at equivalent activation temperatures and thus, had higher BET surface areas than similar JKWR carbons. At the observed burn-off levels, JKWR carbons exhibited less microporosity than JKWS carbons both at equivalent burn-off level and activation conditions. However, by virtue of having higher BET surface areas, the produced JKWS carbons outperformed the JKWR carbons in most of the characterisation tests, except for iodine adsorption; where larger degrees of meso- and macroporosity allowed for quicker access to the strongly adsorptive micropores in the inner cavities of the activated carbon.

The steam activation of JKWS and JKWR char at 925°C has been identified as the optimum temperature for the maximum development of activated carbon porosity from both feedstocks. The next stage of the optimisation aspect of the research was to determine the effects of activation time and water flow rate on the above measured characteristics of the produced JKWR and JKWS carbons.

7.3 Results and Discussion II: Effect of activation time and water flow rate

The optimum steam activation temperature of 925°C was used for both JKWR and JKWS char activation under the following parameters:

Table 7.11: Steam activation parameters for JKWR and JKWS char.

JKWS and JKWR AC	Activation temperature/°C	Activation time/h	Water flow rate/ml min^{-1}
925-0.5-0.1ml	925	0.5	0.1
925-1-0.1ml	925	1.0	0.1
925-0.5-0.3ml	925	0.5	0.3
925-1-0.3ml	925	1.0	0.3
925-0.5-0.5ml	925	0.5	0.5
925-1-0.5ml	925	1.0	0.5

7.3.1 Sample Yields/Burn-off reactions of JKWR and JKWS char with water

In Section 7.2.2, it was determined that the burn-off increased with increasing activation temperature and that the burn-off values of JKWS carbons were greater than that of JWR carbons. The effect of varying the water flow rate and activation time of both types of carbons activated at 925°C is shown in Figure 7-30.

It is apparent that with the proportional increases in water flow rate, that the increases in burn-off for both types of carbons at both activation times are proportional as well. The highest rate of burn-off was exhibited by JKWS carbons at 1h activation time whereas the least reactive was observed from JKWR carbon at 0.5h. As observed previously in Section 7.2.2, JKWS carbons were more reactive than JKWR at all three water flow rates and at the increased activation time.

The above observations infer that at constant activation temperature, the burn-off of both types of carbons increases with water flow rate. It can also be observed that the burn-off increases with activation time.

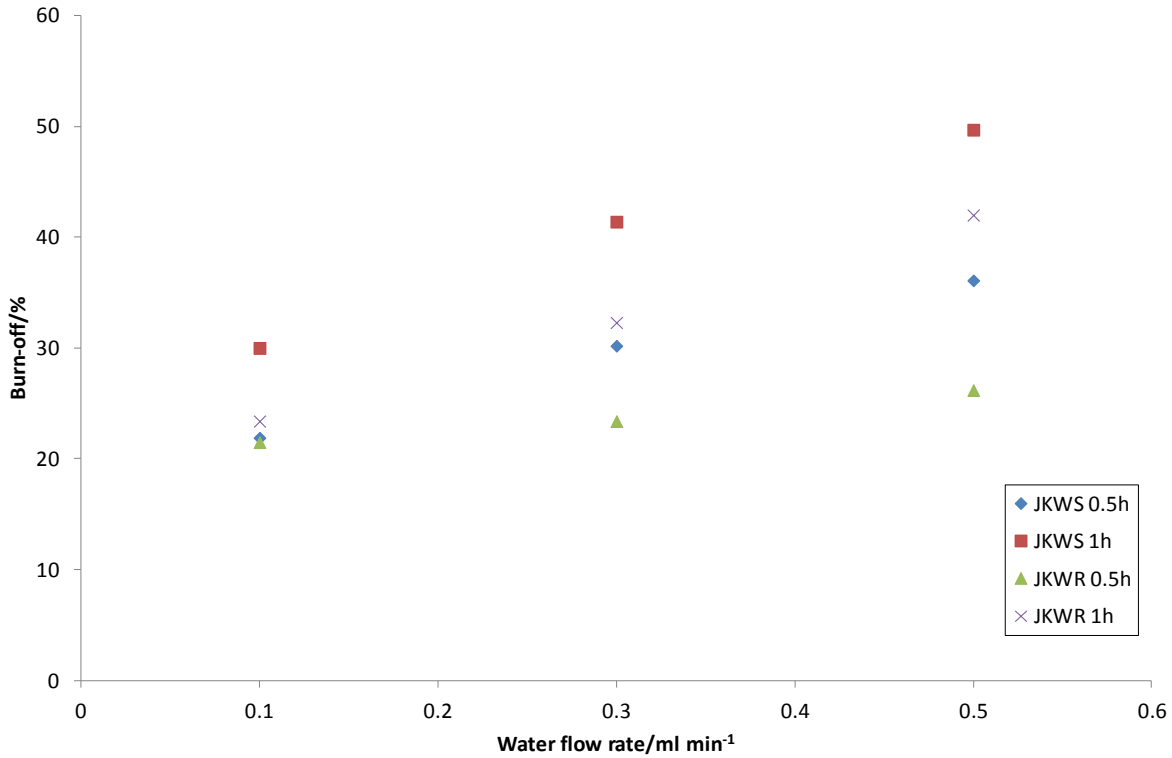


Figure 7-30: The effect of water flow rate and activation time on JKWS and JKWR carbons activated at 925°C.

It is apparent that burn-off is a function of all three steam activation parameters: temperature, time and water flow-rate (González *et al.*, 1994, Fan *et al.*, 2004, Arriagada *et al.*, 1994). The only noticeable difference is the rate of burn-off experienced by the carbons and this is affected by its reactivity to water, which in turn is affected by its lignocellulosic content. As such, it is possible to use burn-off values to determine the extent of steam activation and use it as a common denominator in order to compare all the produced activated carbons.

7.3.1.1 Carbon content

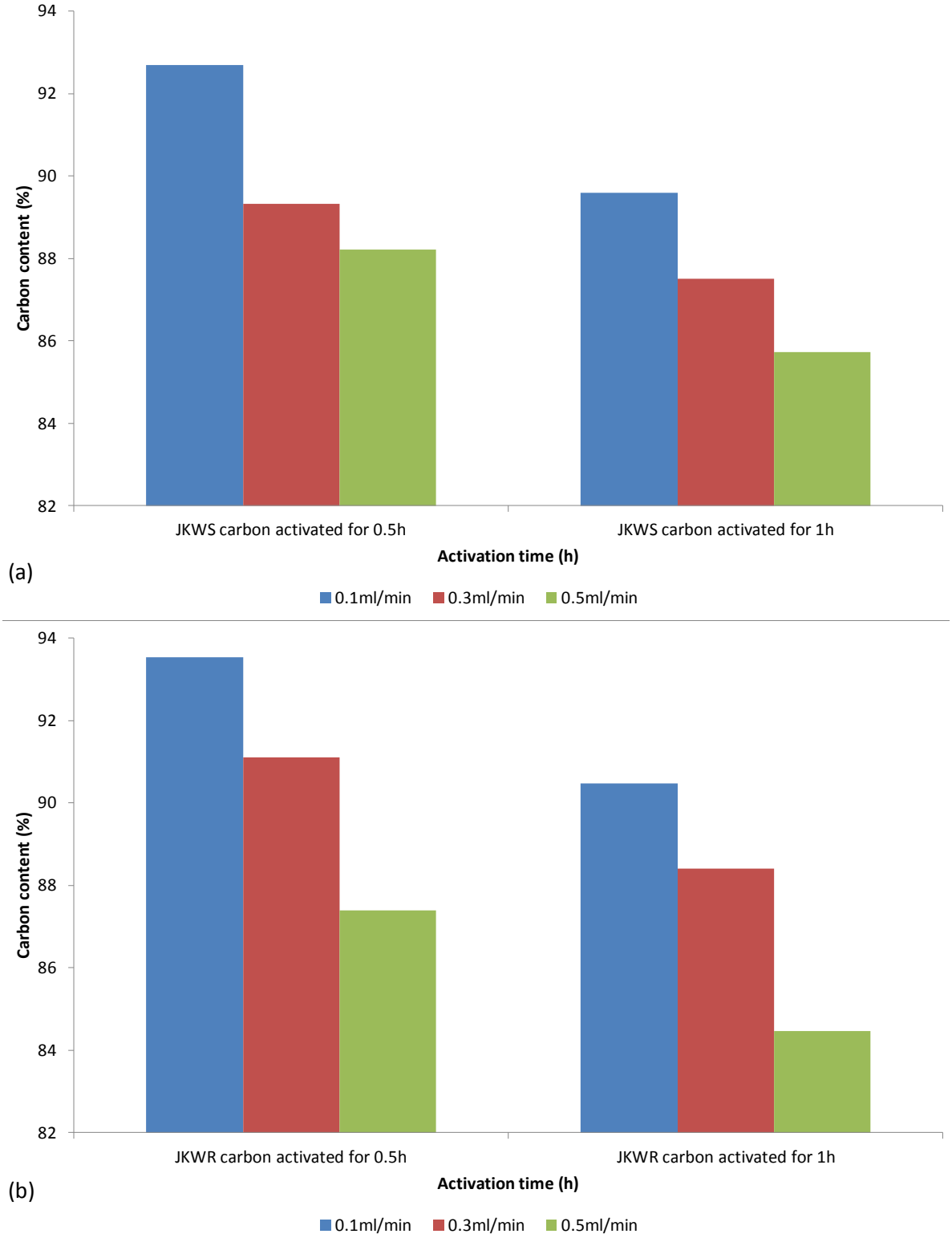


Figure 7-31: Carbon contents of (a) JKWS and (b) JKWR carbons produced at 925°C activation temperature.

It can be observed from Figure 7-31 that increasing both the activation time and water flow rate at an activation temperature of 925°C results in decreased carbon contents of JKWS and JKWR activated carbons. This is expected as the increased activation times and water flow rates results in increased burn-off; which was previously discussed in Section 7.3.1, is responsible for the development of porosity in the activated carbon as can be seen in Section 7.2.3.2.

It can be observed that JKWR activated carbons contained marginally more carbon than JKWS activated carbons, as previously documented in Section 0.

7.3.2 N_2 adsorption at -196°C

Figure 7-32 and Figure 7-33 show the effects of increased activation time and water flow rate on the measured BET surface areas of the JKWS and JKWR carbons produced at 925°C. The gas adsorption isotherms indicate that the Type IV behaviour with its H4 characteristics observed in Section 7.2.3.2 remains.

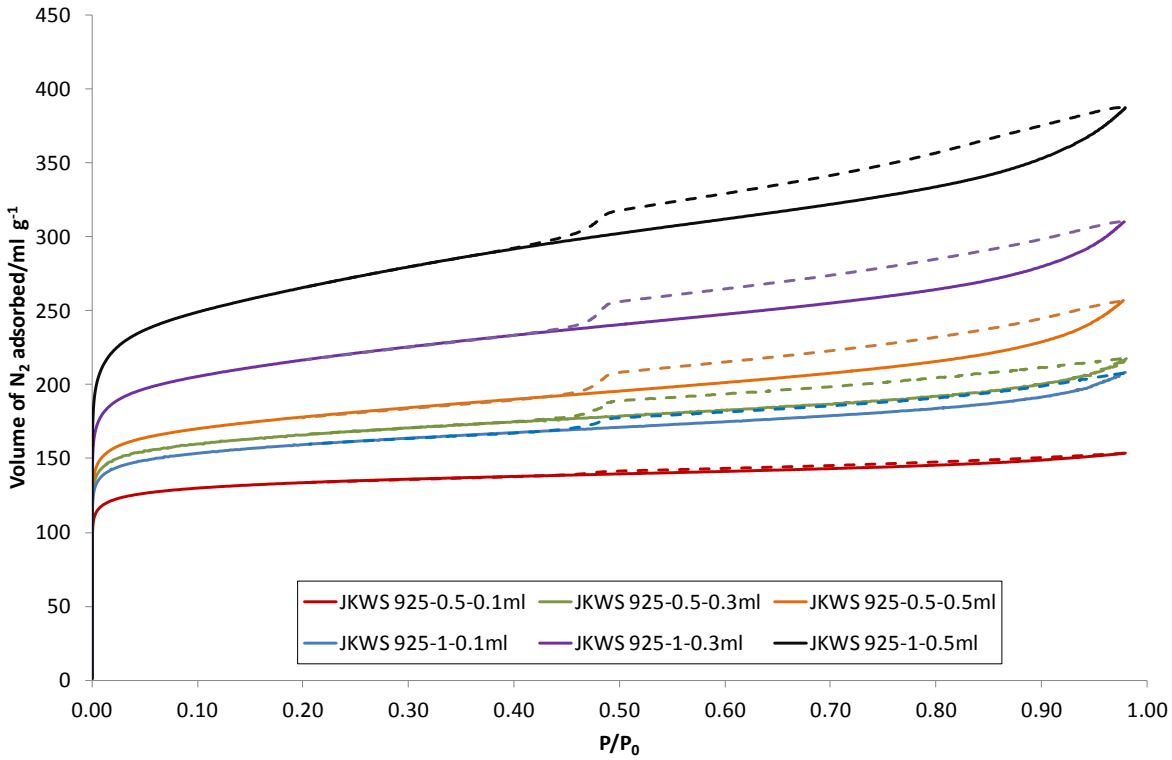


Figure 7-32: N_2 adsorption isotherms for JKWS carbon.

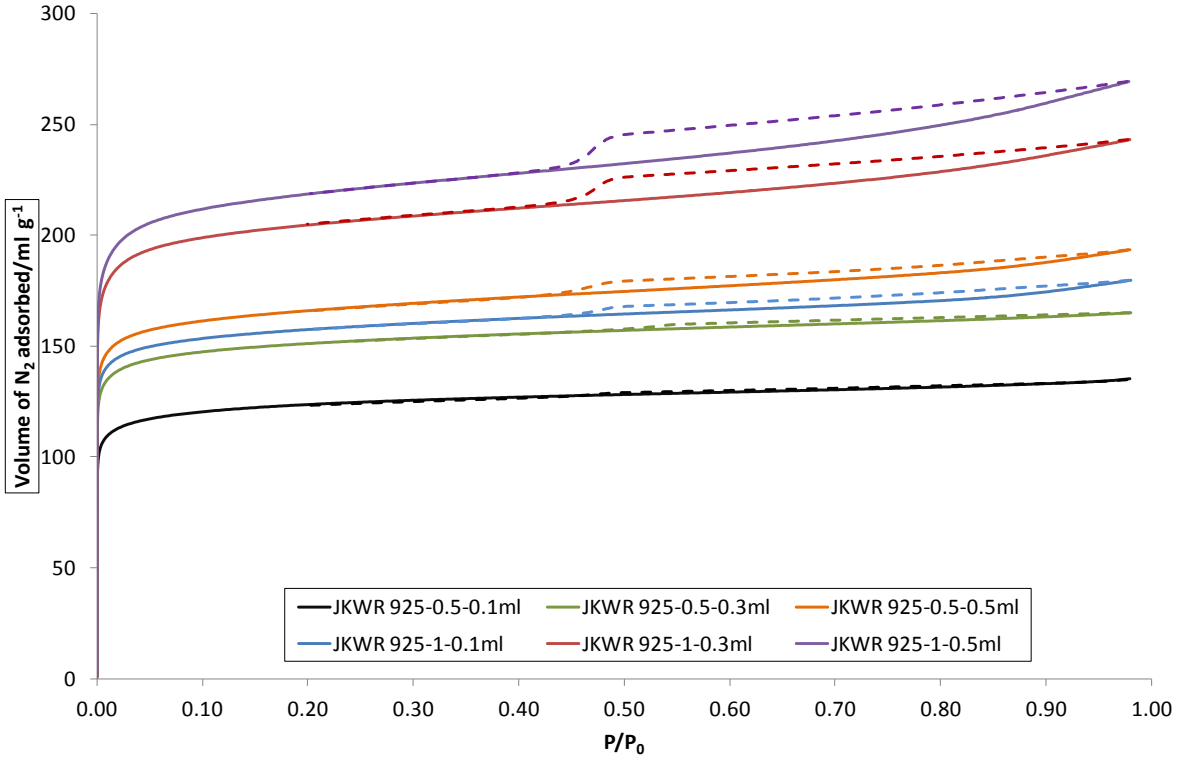


Figure 7-33: N_2 adsorption isotherm for JKWR carbon.

The adsorption isotherms show increasing mesoporosity with both activation time and water flow rate. This trend can also be correlated with the burn-off experienced by the produced activated carbons, as seen in Table 7.12. The lowest burn-off values (JKWS and JKWR AC 925-0.5-0.1ml) resulted in an isotherm almost parallel to the x-axis, indicating a highly microporous nature with low degrees of meso- and macroporosity. The increased burn-offs then creates new micropores and widens existing micropores into meso- and macropores, as previously discussed. It can be observed in Table 7.12 that doubling the activation time from 0.5h to 1h using the same water flow rate does not double the burn-off, indicating that any increase in reaction rate will not be linear. This could possibly be due to the limited diffusion of water molecules into the char particles.

The results showed that JKWS and JKWR carbons produced at 925°C using 0.5ml/min water flow rate for 1h exhibited the highest BET surface area and total pore volume.

It can be observed in both Figure 7-32 and Figure 7-33, that there is a large increase in N_2 adsorbed by JKWS and JKWR carbons when the activating water flow rate increases from 0.1ml/min to 0.3ml/min whereas the increase between 0.3ml/min and 0.5ml/min is less striking. This can be explained by the fact that the initial increase was a threefold increase of water flow rate whereas

the increase from 0.3ml/min to 0.5ml/min was less and that water diffusion saturation was being reached.

The micropores were seen to decrease in their contribution to overall BET surface area as the burn-off increases as shown in Table 7.12. This parallels the observations in Figure 7-32 and Figure 7-33 of increasing mesoporosity of the carbons. JKWS carbons exhibit a lesser microporous nature than JKWR carbons although the carbons were measured to possess higher overall BET surface area. This was previously discussed in Section 7.2.2.

However, it was observed that the activated carbons made from JKWR contained a larger degree of microporosity than those carbons made from JKWS. In Section 5.4.3, the lignin content of JKWR was determined to be marginally higher than JKWS and this could account for the increased degree of microporosity generated during steam activation. This has been observed by Reed and Williams (2004) using biomass natural fibre wastes. Another potential reason for this difference was observed by Gergova *et al.* (1994) where they reported that higher microporosity in activated carbon made from apricot stones was attributed to a higher cellulose content. Thus, similar conclusions can be drawn for both types of JKWS and JKWR produced carbons, where JKWR had the higher cellulose content.

A point of interest in the investigation of various water flow rates and increased activation times is the fact that JKWS and JKWR feedstock are able to produce activated carbons which are very similar to F400 in terms of BET surface area but possessing less ash content, as shown in Table 7.12. The most similar activated carbons are JKWS and JKWR AC 925-1-0.5ml i.e., the two carbons with the highest burn-off values. Activated carbons produced from JKWS in particular, are observed to nearly match F400 with BET surface area measured. However, both of the mentioned carbons had higher meso- and macroporosity than F400, which contributed about 25% of their BET surface area results. In terms of microporous surface area, F400 has the higher surface area. It is however, not unreasonable to expect that at higher burn-off values, the activated carbons made from JKWS and JKWR will match and exceed the adsorptive properties of F400.

Table 7.12: Parameters of JKWS and JKWR determined from gas adsorption data.

JKWS AC	Burn-off (%)	Surface area (m^2/g)			Micropore:BET surface area (%)	BET Volume (ml/g)	C-value	Ash content (%)
		BET	Micropore	Meso- and macropore				
925-0.5-0.1ml	21.9	516.9	482.81	94.09	93.4	119.7	15747	1.43
925-0.5-0.3ml	30.2	628.1	547.20	80.90	87.1	145.5	29617	1.15
925-0.5-0.5ml	36.1	667.5	553.40	114.10	82.9	154.6	9180	0.90
925-1-0.1ml	30.0	605.5	530.99	74.51	87.7	140.2	12569	1.16
925-1-0.3ml	41.4	805.9	655.90	150.00	81.4	186.6	5185	1.29
925-1-0.5ml	49.7	974.6	752.00	222.60	77.2	225.7	3048	2.05
JKWR AC								
925-0.5-0.1ml	21.5	476.0	437.73	38.27	92.0	110.2	7213	2.99
925-0.5-0.3ml	23.0	583.9	544.40	39.50	93.2	135.2	5624	3.23
925-0.5-0.5ml	26.2	616.0	571.42	44.58	92.8	142.7	16684	3.48
925-1-0.1ml	23.4	606.4	560.11	46.29	92.4	140.4	7893	3.56
925-1-0.3ml	32.3	784.6	713.72	70.88	91.0	181.7	8029	3.40
925-1-0.5ml	42.0	915.6	797.90	117.70	87.1	212.0	4888	3.58
F400	N/A	977.4	885.84	91.56	90.6	226.4	1023	9.00

7.3.3 Pore size distribution

The results of the pore size analysis were not wholly conclusive with respect to trends and optimal activation time and water flow rates, which are summarised in Table 7.13. The HK micropore size decreases with increasing burn-off and the micropores are larger in JKWS carbons than in the equivalent JKWR carbon.

Mesopore size distributions of both types of carbon do not exhibit any trend and are all similar in size to each other. The produced JKWS carbons also possess the larger mesopore size distribution. It can be inferred that the larger micropore and mesopore size distribution can be attributed to the higher reactivity of JKWS char towards steam as a result of its lower cellulose content of its organic feedstock in comparison to JKWR.

Table 7.13: Effective Horvath-Kawazoe micropore size diameter and mesopore size diameter of produced JKWS and JKWR carbons.

JKWS AC	Burn-off/%	HK micropore size/nm	Mesopore size/nm
925-0.5-0.1ml	21.9	0.551	4.048
925-0.5-0.3ml	30.2	0.548	4.214
925-0.5-0.5ml	36.1	0.539	4.161
925-1-0.1ml	30.0	0.540	5.083
925-1-0.3ml	41.4	0.538	4.112
925-1-0.5ml	49.7	0.540	4.123
JKWR AC	**Burn-off/%**	**HK micropore size/nm**	**Mesopore size/nm**
925-0.5-0.1ml	21.5	0.537	3.956
925-0.5-0.3ml	23.0	0.529	4.402
925-0.5-0.5ml	26.2	0.527	3.968
925-1-0.1ml	23.4	0.546	4.030
925-1-0.3ml	32.3	0.536	4.039
925-1-0.5ml	42.0	0.525	4.018
F400	N/A	0.512	3.966

7.3.4 Butane working capacity

The BWC is seen to increase depending on water flow rate, activation time and type of activated carbon. Activated carbons produced from JKWS are the most susceptible to BWC improvement due to increased water flow rates, as observed in Figure 7-34. It can be seen that doubling the activation time for JKWS had a greater influence on JKWS than JKWR derived carbons. Activated carbons from JKWR are less easily activated, for reasons previously discussed in Section 7.2.2.

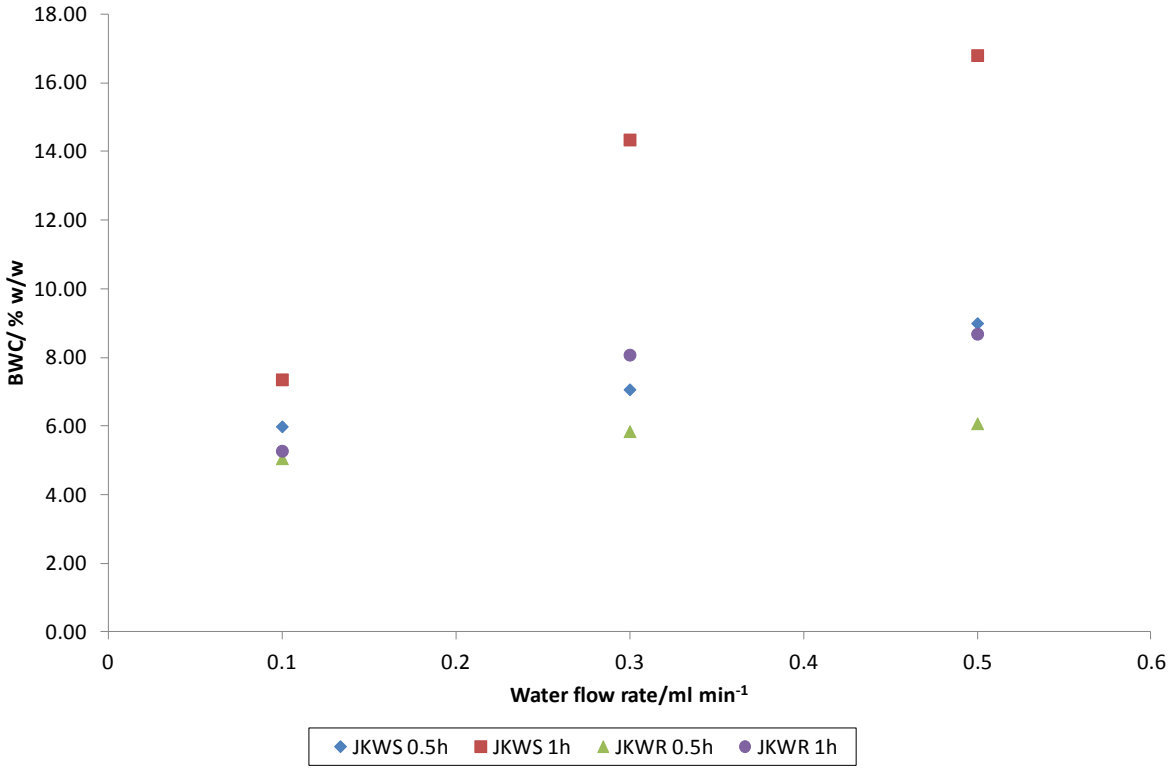


Figure 7-34: The effect of water flow rate and activation time on the BWC of produced JKWS and JKWR carbons at 925°C.

The JKWS carbons produced at 1h and 0.5ml/min water flow rate shows the highest BWC of all the produced JKWS and JKWR carbons, exceeding even the BWC of F400, as seen in Table 7.14. This demonstrates that it is possible to tailor the steam activation of JKWS in order to attain similar BWC as F400.

Table 7.14: Butane adsorption and desorption characteristics of produced JKWS and JKWR carbon at 925°C activation temperature.

JKWS AC	BWC (%)	Butane Activity (%)	Butane Retentivity (%)	Apparent Density (kg/m^3)
925-0.5-0.1ml	5.99	6.94	0.95	0.23
925-0.5-0.3ml	7.07	9.16	2.09	0.27
925-0.5-0.5ml	9.00	13.15	4.15	0.24
925-1-0.1ml	7.36	10.37	3.01	0.26
925-1-0.3ml	14.35	17.83	3.48	0.20
925-1-0.5ml	16.81	22.12	5.31	0.24
JKWR AC	**BWC (%)**	**Butane Activity (%)**	**Butane Retentivity (%)**	**Apparent Density (kg/m^3)**
925-0.5-0.1ml	5.06	8.94	3.88	0.37
925-0.5-0.3ml	5.85	11.37	5.53	0.42
925-0.5-0.5ml	6.08	10.73	4.65	0.39
925-1-0.1ml	5.28	8.91	3.63	0.44
925-1-0.3ml	8.08	16.16	8.08	0.38
925-1-0.5ml	8.69	16.73	8.02	0.34
F400	15.56	24.36	8.82	0.54

The butane retentivity of JKWR derived carbons is much higher than that of JKWS carbons. This is because JKWR carbons contained higher micropore surface area and micropore:BET ratios, seen in Table 7.12. As previously discussed in Section 7.2.4, the increasing microporosity is responsible for the retention of butane gas within the carbon structure. Similarly, the butane activity is increased as a result of the augmentation of the micropore volumes of the produced carbons (see Table 7.12).
There is no observable trend for the apparent densities of the produced carbon except for JKWR carbons activated for 1h. They can be observed to decrease in apparent density with increasing water flow rate, which could be explained by the increased burn-off experienced.

7.3.5 Iodine number

The JKWS and JKWR carbons produced at 900°C and 925°C at 1h activation time and 0.5ml.min water flow rate performed remarkably well in the iodine number determination against F400 as

seen in Table 7.15. Both JKWS and JKWR carbons activated at 0.3ml/min and 0.5ml/min water flow rates exhibited iodine numbers which exceeded those of F400.

Table 7.15: Iodine numbers of produced JKWS and JKWR carbons at 925°C with different activation times and water flow rates.

			Surface area (m^2/g)		
JKWS AC	**Burn-off (%)**	**Iodine number (mg/g)**	**BET**	**Meso- and macropore**	**Meso- and macropore:BET**
925-0.5-0.1ml	21.9	551	516.9	35.44	0.069
925-0.5-0.3ml	30.2	870	628.1	80.90	0.129
925-0.5-0.5ml	36.1	956	667.5	114.1	0.171
925-1-0.1ml	30.0	795	605.5	74.51	0.123
925-1-0.3ml	41.4	1104	805.9	150.00	0.186
925-1-0.5ml	49.7	1307	974.6	222.60	0.228
JKWR AC	**Burn-off (%)**	**Iodine number (mg/g)**	**BET**	**Meso- and macropore**	**Meso- and macropore:BET**
925-0.5-0.1ml	21.5	595	476.0	38.27	0.080
925-0.5-0.3ml	23.0	813	583.9	39.50	0.068
925-0.5-0.5ml	26.2	821	616.0	44.58	0.072
925-1-0.1ml	23.4	708	606.4	46.29	0.076
925-1-0.3ml	32.3	1139	784.6	70.88	0.090
925-1-0.5ml	42.0	1190	915.6	117.70	0.129
F400	N/A	1100	977.4	91.56	0.094

The meso- and macropore:BET ratio increases with burn-off and this has an effect on the increasing iodine number of the activated carbons shown in Table 7.15 for reasons discussed in Section 7.2.5. As such, the increasing mesoporosity of produced JKWS activated carbons along with their higher BET surface area has the advantage in the adsorption of iodine in comparison to JKWR derived carbons.

7.3.6 Phenol adsorption

The phenol adsorption capacities of these carbons, given in Table 7.16, are higher than those observed for the carbons activated in Section 7.2.6. This is expected, given the higher burn-off values achieved and the resulting increases in porosity of the produced activated carbons.

Both the R_L constant of the Langmuir model and the n value of the Freundlich model indicate that phenol adsorption was favourable under laboratory conditions. However, as with the results presented in Section 7.2.6, the R^2 values of the Freundlich model are generally lower than those of the Langmuir model.

The greatest phenol adsorption capacity according to the Langmuir model was exhibited by JKWS carbons generated at 925°C for 1h at 0.5ml/min water flow rate. The adsorption capacity Q_0 of phenol, as determined from the Langmuir model is observed to be a strong property of the JKW carbons. All of the JKW carbons activated at 925°C for 1h with 0.3ml/min water flow rate possessed Q_0 values that exceeded those of F400. This is a positive result as it has good implications on the exploitation of JKWS and JKWR as an alternative commercial feedstock for activated carbons.

Table 7.16: Langmuir and Freundlich parameters for phenol adsorption by JKWS and JKWR carbons produced at 925°C with different activation times and water flow rates.

	Langmuir parameters			Freundlich parameters		
JKWS AC	**Q_0 (mg/g)**	**R_L**	**R^2**	**K_F (mg/g)(mg/L)*n***	**n**	**R^2**
925-0.5-0.1ml	128	0.0259	0.9963	47	4.89	0.9413
925-0.5-0.3ml	152	0.0195	0.9978	64	5.73	0.9922
925-0.5-0.5ml	172	0.0398	0.9978	37	3.33	0.9204
925-1-0.1ml	143	0.0229	0.9999	41	3.68	0.8619
925-1-0.3ml	185	0.0309	0.9988	45	3.31	0.8868
925-1-0.5ml	256	0.0684	0.9798	40	2.74	0.9596
JKWR AC						
925-0.5-0.1ml	114	0.0751	0.9905	44	5.51	0.9615
925-0.5-0.3ml	145	0.0241	0.9993	52	4.61	0.8949
925-0.5-0.5ml	167	0.0420	0.9822	61	5.36	0.9689
925-1-0.1ml	149	0.0304	0.9966	47	5.17	0.9533
925-1-0.3ml	196	0.0188	0.9994	58	3.77	0.9272
925-1-0.5ml	222	0.0266	0.9980	55	3.63	0.9417
F400	175	0.059	0.9894	34	3.13	0.9869

7.4 Summary

JKWS and JKWR char were prepared in batches from carbonisation of their respective biomass at 600°C for 1h. A combination of 5 activation temperatures, 2 activation times and 3 water flow rates were used to vary the carbon burn-off during steam activation.

The products were then evaluated for their adsorptive properties in gaseous and aqueous environments and the results were compared to a commercial carbon. These were assessed using nitrogen gas and butane gas for gaseous adsorption abilities and phenol and iodine were used to assess the aqueous adsorptive properties. Additionally, the adsorption of nitrogen gas was used to determine the surface area and pore-size distributions.

JKWS and JKWR biomass contained relatively high amounts of alkaline earth metals (sodium, potassium, calcium and magnesium) and these are concentrated in their respective chars. Upon

steam activation, the metals cause the devitrification of the quartz reactor and cause its failure. As a remedy, the chars were acid-washed and dried prior to steam activation.

After determining the effect of activation temperature resulting in adsorbents with the highest BET surface area, the activation time and water flow rates were varied to study their effects upon the final product. The effects of these changes upon the adsorptive properties were quantified using the same parameters as above.

Increasing the activation temperature at constant activation time and water flow rate (0.5h and 0.1ml/min, respectively) resulted in carbon burn-off, indicating the creation of new pores and the widening of existing pores. This also resulted in a decrease in activated carbon yield. The activation temperature which resulted in the highest BET surface area for both feedstocks was 925°C.

All the carbons produced were of the "H" variety. Nitrogen gas adsorption analysis of the carbons resulted in Type I/Type IV adsorption isotherms with hysteresis loops, indicating they were mainly microporous with lesser degrees of mesoporosity. The isotherms also showed that as the activation temperature increased, the mesopore gradually contributed more to the overall porosity of the produced carbons. At this stage, JKWS carbons were determined to have higher degrees of microporosity than the equivalent JKWR carbons as a result of the difference in lignocellulosic content of their organic precursors. Additionally, none of the produced carbons possessed surface areas which could compete with F400. In spite of this, the produced carbons showed promising results when tested with the above mentioned adsorbates.

The doubling of activation time from 0.5h to 1h increased the overall burn-off values of both JKWS and JKWR carbons. The same effect was observed for increases in water flow rates from 0.1ml/min to 0.5ml/min. As previously discussed, burn-off increases are accompanied by higher BET surface areas and total pore volumes. This in turn, is responsible for increased uptake of butane, iodine and phenol molecules. At this stage of higher burn-off values (>25%), the JKWR carbons exhibited a relatively more microporous nature to JKWS at the same activating conditions, as a result of the higher cellulose content of the JKWR biomass.

The degree/ease of activation was also determined by the intrinsic reactivity of the two carbons. JKWS carbons were determined to have higher reactivity towards water as evidenced by higher burn-offs and greater development of porosity in comparison to JKWR.

The maximum BET surface area and total pore volumes were achieved when both JKWS and JKWR char were activated at 925°C for 1h at a water flow rate of 0.5ml/min. These represent the optimum activating conditions for the purpose of this research. Additionally, these two produced carbons were able to match and in some cases, exceed the adsorptive properties of F400. This implies the possibility of using either JKWS or JKWR char as an alternative feedstock to F400's coal precursor.

The subsequent chapter considers the application of optimised JKWS and JKWR carbon. The focus of applications testing was to examine their effectiveness in adsorbing Bisphenol-A (BPA), which is an emerging water pollutant under laboratory conditions.

Chapter 8. Application testing (Bisphenol-A adsorption)

8.1 Introduction

The JKW-derived ACs manufactured, tested and discussed in this work clearly demonstrated that both JKWS and JKWR proved amenable to activation using steam; as such JKWS and JKWR carbons were produced with adsorption properties (BET surface areas) comparable to those of F400. The performance of the optimised JKWR AC and JKWS AC (ACs with the highest BET surface areas) were competitive, especially in aqueous adsorption tests using phenol and iodine.

It is common to use biomass-sourced feedstock to manufacture activated carbons for use in medicinal and drinking water purposes. The JKW carbons should fit into this classification, given that they are derived from a renewable, biomass material which can be considered benign (not containing any harmful components). Thus, these activated carbons should be viable for safe application to drinking water streams to remove any trace organic impurities that might be present after drinking water treatment processes such as flocculation, sedimentation, sand filtration, chlorination and/or ozonation, as shown in Figure 8-1. Further, if there were any possible contaminants such as herbicides present on the JKW stems or rhizomes, these would be rendered inert during the carbonisation and steam activation processes.

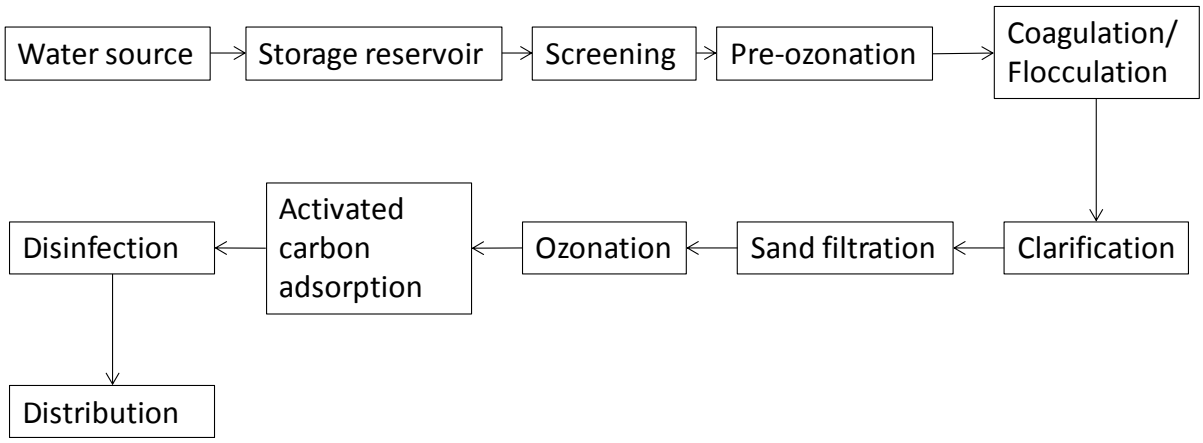


Figure 8-1: Typical flow sheet for drinking water treatment for lowland river.

There are many different and increasing types of organic contaminants which are of interest and concern due to the increased discharge of man-made agents into water courses and the environment in general. There have been significant improvements over recent years in the variety

and sensitivity of analytical techniques used for water analysis (e.g. Liquid chromatography-mass spectrometers). This has resulted in hitherto unknown groups of compounds being detected in the aqueous environment. Amongst the organic impurities found in drinking water is a group known as endocrine-disrupting compounds (EDCs).

Endocrine Disrupting Chemicals mimic hormones in the human body and has the potential to influence reproductive functions. Thus, they are a high priority group of organic compound for the assessment of human health risk because they are considered to present the greatest potential for human exposure and has been classified as a reproductive toxin (Diamanti-Kandarakis *et al.*, 2009). An EDC is defined by the U.S. EPA as "an exogenous agent that interferes with synthesis, secretion, transport, metabolism, binding action or elimination of natural blood-borne hormones that are present in the body and are responsible for homeostasis, reproduction and developmental process" (Diamanti-Kandarakis *et al.*, 2009).

The disruption of the endocrine system can be caused by (USEPA, 2011):

- the mimicking of natural hormones which can lead to an over-response to the stimuli or responding at inappropriate times;
- the blocking of hormonal binding sites from certain receptors, preventing natural hormones from triggering a response;
- direct stimulation or inhibition of the endocrine system causing over- or underproduction of hormones.

Bisphenol-A (BPA) is the common name for 2,2-(4,4-dihydroxydiphenyl) propane, an organic compound with the chemical formula $(CH_3)_2C(C_6H_4OH)_2$. The molecular formula of BPA is obtained from a combination of 2 moles of phenol with one more of acetone and is shown in Figure 8-2.

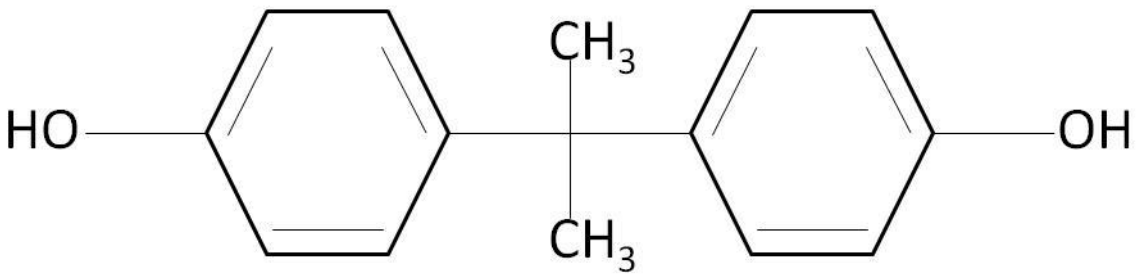


Figure 8-2: Molecular formula of BPA.

BPA was characterised by Bautista-Toledo *et al.* (2005) and they reported the following characteristics: largest distance between the hydroxyl groups of the aromatic rings=0.94nm; height=0.53nm; benzoic ring width=0.43nm; volume=0.70nm^3; surface area=4.32nm^2 and electrostatic potential from -4.56 to 34eV. BPA begins to dissociate at solution pH 9.6 and pH 10.2 (Staples *et al.*, 1998, Lee *et al.*, 2003).

BPA is one of the top 50 chemicals in world-wide production (Gilbert and Epel, 2009). It has been reported that about 347,000 tonnes per annum was produced in 1993 (Fürhacker *et al.*, 2000). BPA is manufactured by condensing phenol with acetone under low pH and high temperature conditions in the presence of catalysts. The crude product is then refined by distillation; filtered and dried. BPA usually forms flakes or crystals. During manufacture, BPA may be inadvertently released as dust emissions during processing, handling and transportation. Further routes of exposure include washing residues and wastewaters generated during manufacture (Staples *et al.*, 1998).

It is used as a plasticiser during the manufacture of polycarbonate polymers and epoxy resins (Staples *et al.*, 1998). Polycarbonates, which have become the most widely-used material in engineered plastic account for 60% of the total demand for BPA. Epoxy resins are used in many application including product finishing, decorative floor manufacture, breaking petroleum emulsions, structural steel coating, lacquer coatings in cans and other vessels used for foodstuffs, tank coatings, can and drum linings and floor varnishes (Perez *et al.*, 1998). Staples *et al.* (1998) have identified some routes of human exposure to BPA: from chemical leaching from the inner plastic coating of canned foodstuffs and from commercial composites and sealants used in dentistry. In both pathways, BPA was found to be the agent responsible for oestrogenic activity.

Oestrogen is a hormone that interacts with other steroids to regulate the normal development of the reproductive system and other tissues (Rigol *et al.*, 2002). BPA exhibits a weak oestrogen-like effect when ingested into the human body (Bautista-Toledo *et al.*, 2005) and the effects which have become apparent in humans over the past half century are consistent with those seen in animals after exposure to high doses of EDCs. These effects include: an increase in genital abnormality in boys; earlier sexual maturation in girls (Howdeshell *et al.*, 1999) and predisposes tissues to earlier onset of disease, reduced fertility and mammary and prostate cancer (Staples *et al.*, 1998). Low doses of BPA were reported to have caused significant effects in experimental animals including adverse effects in blood levels within and below the average safety margin in humans (Diamanti-

Kandarakis *et al.*, 2009) as well as proliferation of human prostate cancer cells, cardiovascular diseases, Type II diabetes and liver enzyme abnormalities (Stackelberg *et al.*, 2007).

Krishnan *et al.* (1993) reported that BPA leached from the autoclaving of polycarbonate flasks, which increases the rate of proliferation of human breast cancer cells, MCF-7. Consequently, the leaching of BPA from plastic food containers (as well as from plastic-lined cans into foodstuff), particularly during repeated use can pose a potential threat to human health (Nakada *et al.*, 2007). More reviews on the effects of BPA can be found in literature (Kimura *et al.*, 2004, Choi *et al.*, 2005, Liu *et al.*, 2009) but it is evident that the widespread use and release into the environment of EDCs could have significant long-term implications for human and animal health.

Although most of the studies published relate to animal testing, these effects suggest that humans may also be affected by BPA. Some of these effects have been demonstrated by epidemiological studies which link BPA to ovarian diseases and miscarriages (Takeuchi *et al.*, 2004, Sugiura-Ogasawara *et al.*, 2005). The concerns over EDCs have been picked up by the press. For example, a recent BBC news article reported that BPA was readily ingested from eating canned soup and detected in significant amounts in the urine of test subjects (Roberts, 2011).

As a safety precaution, BPA was banned from use in the manufacture of infant feeding bottles (implemented on 22/04/2011) and all BPA-containing bottles on the EU market should be replaced by the middle of 2011 (European Commission, 2011). Recently, France has banned all use of BPA in baby food packaging and all food containers by 2015 (AFP, 2012). The European Food Safety Authority (EFSA) concluded that the permanent Tolerable Daily Intake (TDI) of 0.05mg/kg body weight could remain as it provided a safe enough limit (Erickson, 2008). Similar precautions have been taken by worldwide governments including the US, Australia, New Zealand and Canada in order to provide a sufficient margin of safety for consumers (Diamanti-Kandarakis *et al.*, 2009).

8.1.1 BPA removal

BPA is detected in municipal and industrial wastewater treatment streams as a result of either direct discharge into sewers or via storm-water run-off. Other point sources of BPA in the environment come from sewage treatment effluent, landfill leachate (via hydrolysis of plastics (Krishnan *et al.*, 1993) and natural degradation of polycarbonate plastics due to moderate water solubility and low

vapour pressure. Paper mill effluents also contribute significant amounts of BPA in wastewater and wastewater sludge (Howdeshell *et al.*, 1999).

Due to their health effects as outlined in Section 8.1, the removal of EDCs and particularly, BPA from drinking water is an issue of major concern. A number of methods have been used to remove BPA from water and these are shown in Table 8.1.

Table 8.1: Efficiencies of BPA removal techniques found in literature.

Treatment technique	Removal efficiency	References
Ozonation and sand filtration	>80%	Nakada *et al.* (2007)
Chlorination	76%	Stackelberg *et al.* (2007)
Reverse osmosis membrane filtration	18-83%	Kimura *et al.* (2004)
Activated carbon	>99% (at initial BPA concentrations of 500ng/l)	(Yoon *et al.*, 2003)

Presently, adsorption by activated carbons is considered to be one of the most efficient methods for the removal of organic material in water (Liu *et al.*, 2009). This is due to its relatively low capital cost when compared to the methods listed in Table 8.1 and low toxicity when placed in contact with water. Activated carbons possessing high surface area, pore volumes and low surface polarity were considered beneficial to the increased adsorption of BPA (Tsai *et al.*, 2006, Choi *et al.*, 2005, Bautista-Toledo *et al.*, 2005).

8.2 Experimental protocols

The investigation of the adsorption of BPA by optimised JKWS and JKWR carbons along with F400 commercial carbon was conducted in stages. The first stage focused on observing the effects of pH on the adsorption process. The next stage was to determine the adsorption kinetics of BPA adsorption to identify a suitable and reasonable equilibrium time for adsorption. Adsorption isotherm experiments were then performed to investigate the adsorption capacity of the carbons. Additional activated carbon characterisation tests such as surface chemistry, hardness and bulk density where also performed.

8.2.1 pH and point of zero charge determination

The solution pH is a parameter of great interest in the process of adsorption from aqueous phases as it determines the charge of both the carbon and adsorbate molecules and as such, governs the adsorbent-adsorbate interactions (Radovic *et al.*, 2001).

The pH of the BPA solutions was determined as described in Section 7.1.7 for phenol solutions. During spectrophotometric measurement of the solutions at pH 11, the solution pH must be adjusted to below the dissociation pH of BPA (pH 9.6). Otherwise, the measured results are not representative due to the significant extent of the dissociated bisphenolate anion. This was done by the addition of 1M HCl to the sample before analysis.

The point of zero charge, pH_{PZC} is the pH at which the carbon exhibits any total surface charges (Moreno-Castilla, 2004). The carbon samples exhibit a positive total surface charge at solution pH<pH_{PZC} and a negative total surface charge at solution pH>pH_{PZC} (Ferro-Garcia *et al.*, 1998). Hence, in knowing the pH_{PZC} of the activated carbon, the pH of the solution can be adjusted for maximum BPA adsorption.

The pH_{PZC} of the carbons were determined using the pH drift test (Ferro-Garcia *et al.*, 1998). 50ml of 0.01M NaCl solution was placed in a jacketed titration vessel at 25°C with N_2 gas bubbling through the solution to minimise the effects of dissolved CO_2. The pH of the solution was adjusted between pH 3 and pH 11 using either HCl or NaOH. Once adjusted, ca. 0.15g of activated carbon was mixed into the solution and a magnetic stirrer was used to ensure constant mixing. The mixture was allowed to equilibrate for 3h and the final pH thereafter was measured and plotted against the starting pH of the solution. The pH at which the curve crosses the $pH_{initial}$=pH_{final} line is the PZC of the activated carbon.

8.2.2 Surface chemistry using Boehm titration

The general titration procedure to determine the surface chemistry of the activated carbons were carried out according to Boehm (1966) but using a modified approach to the procedure, as suggested by Goertzen *et al.* (2010) and Oickle *et al.* (2010).

Approximately 1.5g of activated carbon was added to 50ml of one of three reaction bases of 0.05M concentration: $NaHCO_3$, Na_2CO_3 and NaOH as well as to 50ml of 0.05M HCl. The samples were agitated at 150rpm for 24h and then filtered to remove the carbon. 10ml aliquots were removed using a pipette and then acidified by adding 20ml of 0.05M HCl to the reaction base aliquots. The aliquots of Na_2CO_3 were acidified by adding 30ml of the acid to ensure complete neutralisation of the diprotic base. The acidified solutions were then back-titrated using 0.05M NaOH and a calibrated Fisher brand Hydrus 500 pH meter with a VWR electrode was used to determine the end-point.

To ensure correct concentrations for NaOH and HCl, NaOH was standardised using dried potassium hydrogen phthalate (KHP). A mass of ca. 10g was accurately weighed to 0.01mg and dissolved to make 1L of solution. A 25ml aliquot of KHP was pipetted into a conical flask and titrated using 0.05M NaOH. The standardised 0.05M NaOH solution was then used as a titrant in the standardisation of HCl. A calibrated pH meter was used to determine the end-point of approximately pH 7 for HCl-NaOH titration and approximately pH 8.7 for NaOH-KHP titration.

The dissolved CO_2 in the acidified aliquots was removed by bubbling N_2 gas through the solutions for 2h and titrated immediately with constant N_2 degassing during the titration to ensure sufficient removal of CO_2. This was done to prevent the introduction of environmental CO_2 into the sample (Goertzen *et al.*, 2010) which will interfere with the results.

The equation used to determine the quantity of surface groups by back-titration is given by:

Equation 8-1: $$[HCl]V_{HCl} = [NaOH]V_{NaOH} + \left(\frac{n_{HCl}}{n_B}[B]V_B - n_{CSF}\right)\frac{V_a}{V_B}$$

Equation 8-2: $$n_{CSF} = \frac{n_{HCl}}{n_B}[B]V_B - ([HCl]V_{HCl} - [NaOH]V_{NaOH})\frac{V_B}{V_a}$$

[B] = Concentration of reaction base mixed with carbon

V_B = Volume of reaction base mixed with carbon

n_{CSF} = Moles of carbon surface functionalities on carbon surface reacting with base

V_a = Volume of aliquot taken from V_B

[HCl] = Concentration of acid added to aliquot taken from original sample

V_{HCl} = Volume of acid added to aliquot taken from original sample

[NaOH] = Concentration of the titrant in the back-titration

V_{NaOH} = volume of the titrant in the back-titration

$\frac{n_{HCl}}{n_B}$ = molar ratio of acid to base (reaction of monoprotic vs. diprotic bases).

The amount of surface groups present on the carbon surface is calculated through the difference in the amount of surface functionalities that reacted with the bases or the acid. NaOH is a strong base and thus, reacts with all surface groups present (carboxylic acids/carboxyls, lactones/lactols and phenols) and will have an n_{CSF} value that includes all of these groups. Na_2CO_3 reacts with carboxyl and lactonic groups whereas $NaHCO_3$ reacts only with carboxylic groups. In this way, subtracting known amounts from the unknown will allow the determination of the quantities of surface group functionalities present on the activated carbon. The amount of carbon surface functionalities presented in this section is given with RSD within 10% based on three experimental points.

8.2.3 Ball-pan hardness

The ball-pan hardness test was used to determine the resistance of activated carbons to particle size degradation under service conditions (ASTM, 1979). The test method used in this research was taken from Smith *et al.* (2012), who adapted it from ASTM method D3802-79 (ASTM, 1979).

Hardness is important in applications such as solvent recovery or catalyst supports but is less vital in water treatment where the hydraulic pressures are not high enough. However, possessing a high hardness number is useful in minimising fines generation during usage (Roskill Information Services Ltd., 2003).

The method used the 0.5-2mm particle fraction of the carbon samples, which was obtained using ASTM method D2862-97 (ASTM, 1997). 50cm^3 of the aforementioned size fraction was placed into a 200mm receiver pan, which was obtained using ASTM method D2854-96 (ASTM, 1996b). 15 large and 15 small steel balls, each 13mm and 9.5mm in diameter, respectively were placed into the receiver pan. Five sieves of arbitrary mesh sizes were stacked on top of the receiver pan and the stack was placed onto an Endecotts Octagon Digital sieve shaker (Endecotts, London, UK). The shaker was switched on for 0.5min and the recovered sample from the receiver pan was placed onto a 0.5mm sieve and shaken for a further 10mins. The ball pan hardness was calculated from the percentage by mass of the recovered sample that passed through the 0.5mm sieve.

8.2.4 BPA adsorption

Similar to the procedure detailed in Section 7.1.12 pertaining to phenol adsorption tests, the adsorption kinetics of BPA by the activated carbons was first determined. Approximately 20mg of samples were placed in 100ml of 200mg/l BPA solutions in different conical flasks and aliquots were removed and filtered to be measured spectrophotometrically at specific time intervals to determine the amount of BPA adsorbed. Prior to taking measurements, a wavelength scan was initiated to indentify the optimum wavelength for detecting BPA as mentioned in literature. The wavelength confirmed was 275.5nm as used in work by Bautista-Toledo *et al.* (2005).

The BPA stock solution was made by weighing 1g of BPA (≥99% purity, Sigma Aldrich) into 5 litres of deionised water. A magnetic stirrer was used to dissolve the solid crystals for 24h as BPA has moderate water solubility of 120-300mg/l at pH 7 (Staples *et al.*, 1998).

Five different BPA concentrations (10, 20, 50, 100 and 200mg/l) were used as calibration data points and a Shimadzu UV-2401PC UV-Vis spectrophotometer (Shimadzu Corp., Kyoto, Japan) was used to measure the BPA solution adsorption. The test concentrations were prepared by serial dilution from the 200ppm stock solution in order to minimise any errors in weighing out small masses of the solid BPA crystals.

Absorption kinetics tests were used to determine the equilibration time need for BPA to reach saturation adsorption by the optimised JKW carbons. This was performed in the same manner as described in Section 7.1.12.1 for phenol adsorption kinetics tests.

Adsorption isotherm tests were conducted to determine the BPA adsorption capacity of the samples. The procedure closely mimics the procedure of the earlier adsorption tests described in Section 7.1.12.2. Aliquots were removed and filtered through 0.45µm Whatman syringe filter papers (Whatman Ltd., London, UK) before residual BPA concentration measurement by the spectrophotometer. pH values were determined before and after adsorption experiments using a calibrated pH electrode as described earlier.

Adsorption experiments related to determining the influence of pH was conducted by adjusting the pH of the BPA solutions using 1M NaOH or 1M HCl. Once the pH was adjusted, the procedure is the same as previously described. All experiments were performed in triplicate.

8.3 Results and Discussion

In order to obtain sufficient sample amounts of optimised JWS-derived activated carbons, JKWS and JKWR char were each activated at the optimised conditions three times. The results obtained are shown in Table 8.2.

Table 8.2: Repeatability of the AC yields of JKWS and JKWR activated at optimised conditions (925°C for 1h with 0.5ml/min water flow rate). SD values obtained from 3 different measurements.

Test	JKWS yield (%)	JKWR yield (%)
1	49.7	42.0
2	49.8	42.3
3	49.6	41.8
Average	49.7	42.0
SD	0.1	0.3
RSD	0.2	0.6

As previously hypothesised in Section 5.5, the produced yields of JKW-derived carbons are highly repeatable, as evidenced by the low SD and RSD values.

8.3.1 pH, pH_{PZC} and surface chemistry

Table 8.3: Surface chemistry of optimised JKWS and JKWR carbons and F400.

Carbon	Phenol groups (mmol/g)	Lactone groups (mmol/g)	Carboxylic groups (mmol/g)	Basic groups (mmol/g)	Acidic groups (mmol/g)	pH_{PZC}
JKWS	0.050	0.207	0.000	1.088	0.257	8.3
JKWR	0.013	0.023	0.000	0.842	0.035	8.5
F400	0.009	0.177	0.089	0.438	0.275	7.0

It can be seen in Table 8.3 that optimised JKWS and F400 contain similar amounts of acidic groups whereas optimised JKWR had fewer acidic groups. These acidic groups comprise the phenol, lactone and carboxylic groups whereas the constituents of the basic groups are less well-known. The acidic

groups lend the activated carbons their hydrophilic and polar character and are known to affect the adsorption properties of the activated (Bansal, 2005, Burg and Cagniant, 2007, Liu *et al.*, 2009).

The results in Table 8.3 confirm that both optimised JKWS and JKWR carbons exhibit basic tendencies, as shown by H-type activated carbons. This was a result of the delocalised π electrons in the basal plane, acting as a Lewis base (Nabais *et al.*, 2010). This was also further evidenced by the high amounts of basic groups determined via Boehm titration in Table 8.3. On the other hand, F400 has been demonstrated as a neutral carbon, as shown by Al-Degs *et al.* (2000).

8.3.2 BPA adsorption kinetics

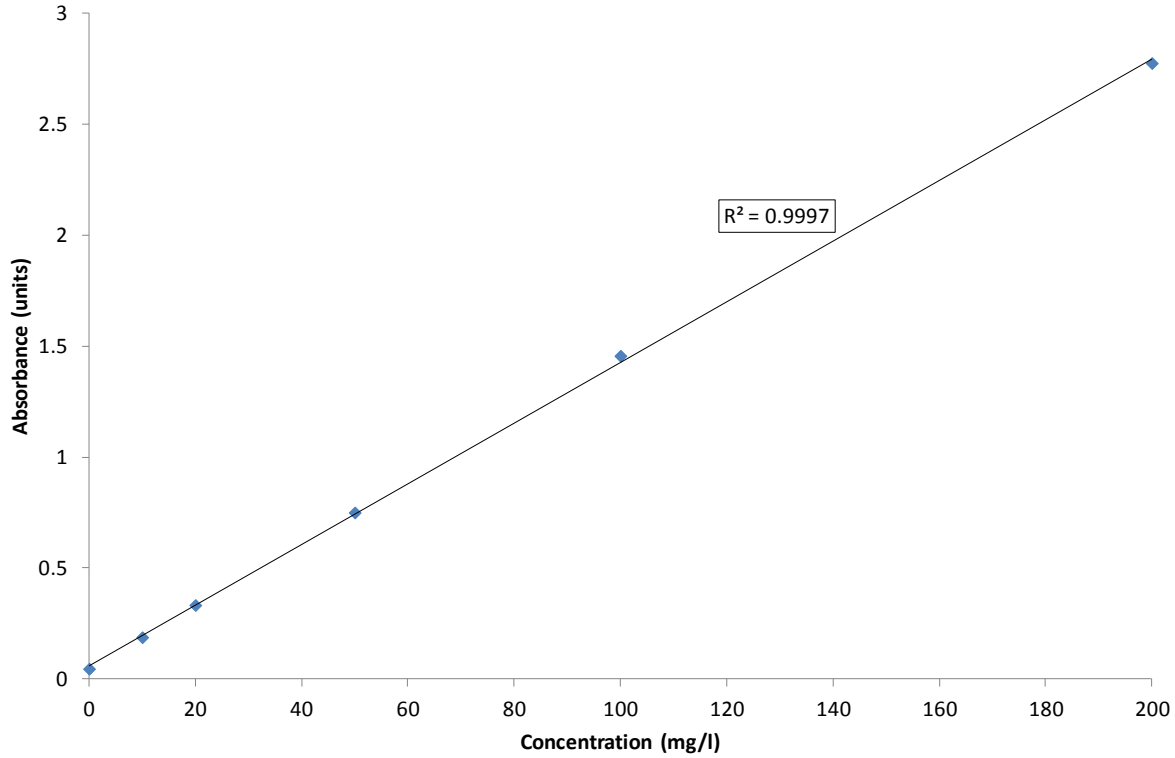


Figure 8-3: Calibration plot of BPA at 275.5nm wavelength.

The calibration plot of BPA using five different data points is shown in Figure 8-3. The high R^2 value indicates good methodology as well as demonstrating that the UV/Vis response of BPA concentrations is linear up to at least 200mg/l.

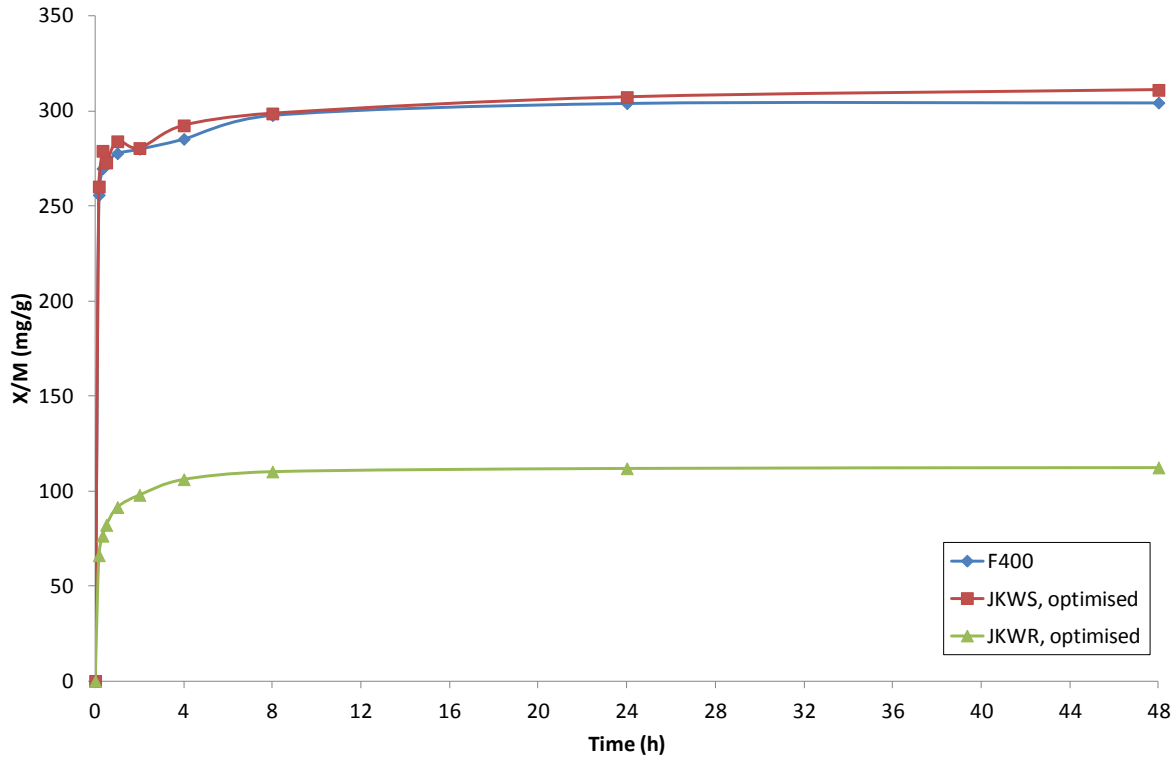


Figure 8-4: BPA adsorption kinetics isotherms of F400 and optimised JKWS and JKWR carbons. Initial BPA concentration: 200ppm.

The adsorption kinetics measured for BPA adsorption by the optimised carbons and F400 are shown in Figure 8-4. They indicate that BPA uptake already occurs at t=10mins and saturation begins at t=8h for all three carbon samples.

It is evident that the optimised JKWS carbon performed as well as F400 during BPA adsorption whereas optimised JKWR carbon had two-third less capacity than either F400 or optimised JKWS carbon. Optimised JKWS carbon and F400 show a maximum Q_0 of 311mg/g and 304mg/g respectively, whereas optimised JKWR carbon had a maximum Q_0 of 110mg/g.

The relatively low adsorption of BPA by optimised JKWR carbon could be due to the fact that BPA exhibits a polar character (Nakamura and Daishima, 2004, Hu *et al.*, 2007, Cai *et al.*, 2003, Basheer and Lee, 2004) and would be best adsorbed by carbons which exhibit the same polar character. Consequently, the low amount of acidic surface groups possessed by optimised JKWR carbon as demonstrated in Table 8.3 of Section 8.3.1 indicates that its low polar nature would not perform well in the adsorption of BPA.

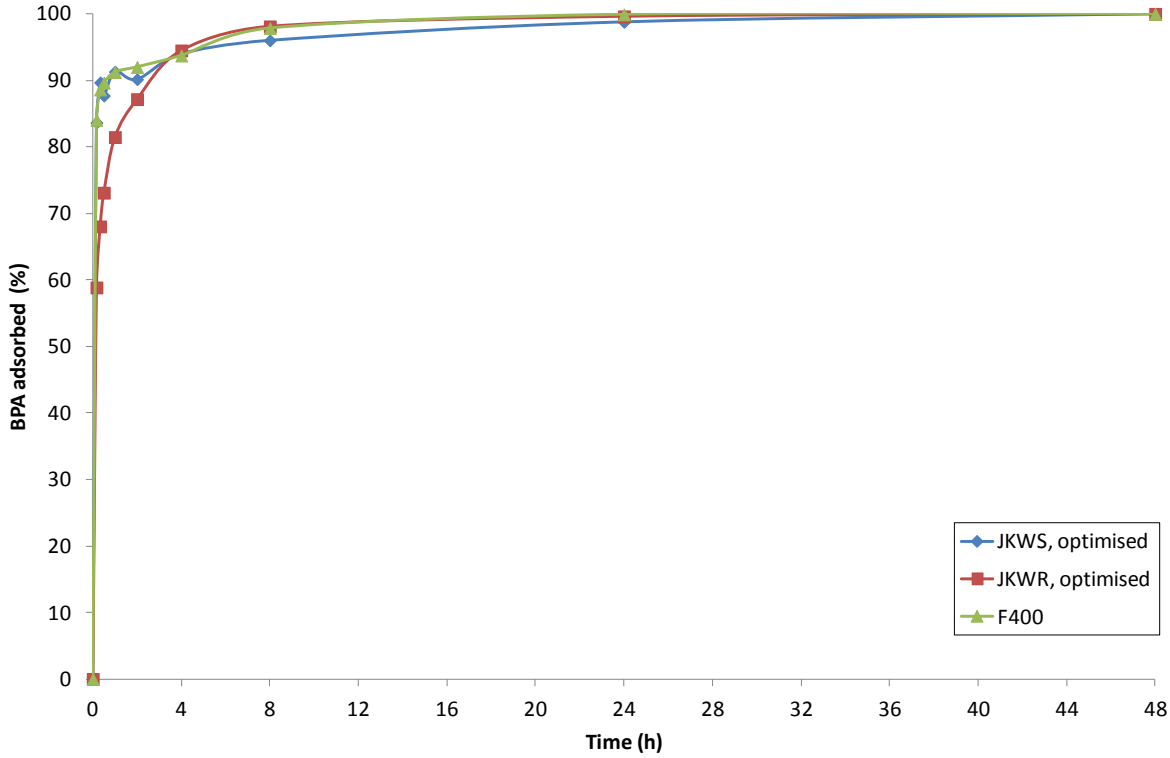


Figure 8-5: Percentage BPA adsorption by produced carbons and F400.

It can be seen in Figure 8-5 that optimised JKWS and F400 had ca. 85% BPA adsorption in 10 min whereas JKWR carbon took 90mins to reach 85% saturation. Full saturation was achieved in 8h for optimised JKWR carbon and F400 and in 24h for optimised JKWS carbon. Hence, it can be agreed that the equilibration time needed for total saturation is 24h and as such, the adsorption isotherm experiments will be conducted for 24h.

8.3.3 BPA adsorption isotherms

The adsorption kinetics tests reported in the previous Section 8.3.2 indicated that after 24h, the BPA adsorption had reached equilibrium on the carbon samples. It had been demonstrated in Section 0 that the aqueous adsorption data obtained did not fit the Freundlich model and as a result, only results fitted to the Langmuir theory are presented. During the experiments, it was noted that at the 2 lowest BPA concentrations (10 and 20 mg/l), all detectable traces of BPA were completely adsorbed by all three carbon samples in 24h and consequently, did not yield any data points. Subsequently, additional data points were obtained by omitting 10 and 20mg/l BPA and using 80 and 150mg/l concentrations instead.

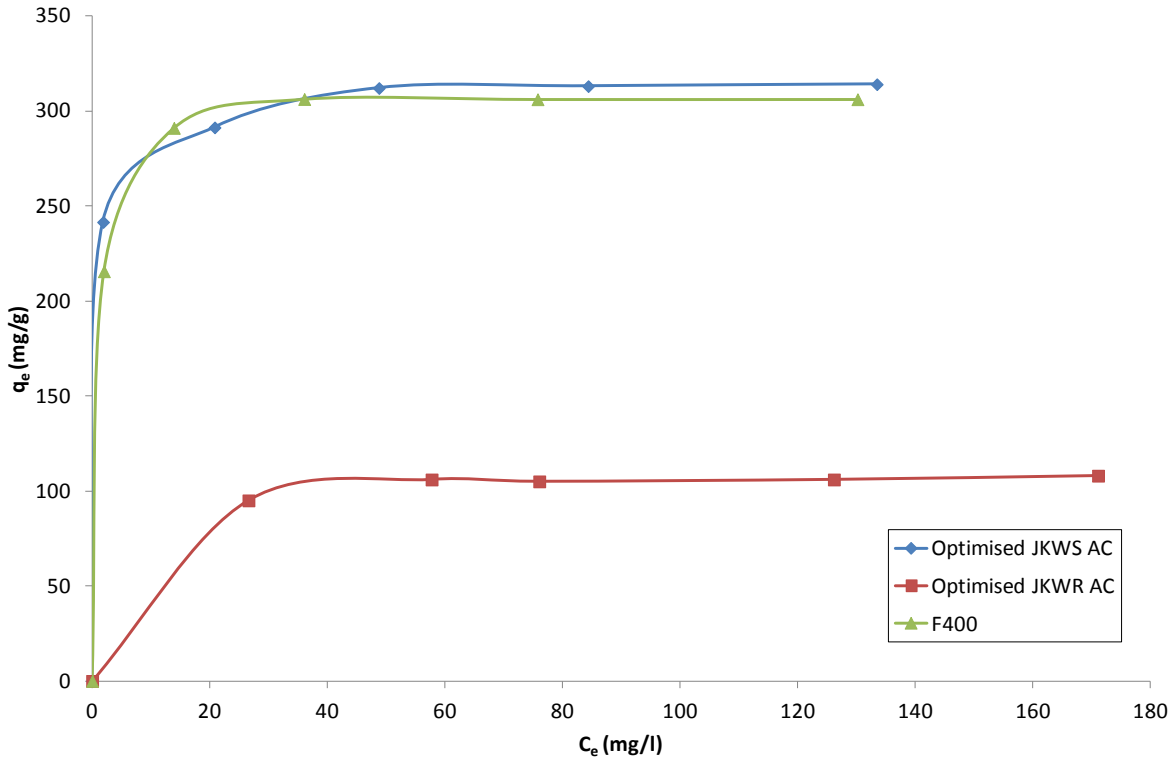


Figure 8-6: Langmuir adsorption isotherms of BPA adsorption using optimised JKW carbons and F400.

It can be seen in Figure 8-6 that optimised JKWS carbon performs similarly to F400 whereas optimised JKWR did not perform as well. The C_e of optimise JKWR carbon is also observed to be much higher compared to the other two test samples and this indicates that a high equilibrium concentration is needed in order for optimised JKWR carbon to adsorb BPA.

The BPA adsorption isotherm of optimised JKWS carbon and F400 followed a 'H2'-type isotherm, according to the Giles classification (Giles *et al.*, 1974b). This indicates very strong adsorptive bonds between adsorbent and adsorbate (Giles *et al.*, 1974a). The strong polar bonds between the acidic surface groups of optimised JKWS carbon & F400 (shown in Table 8.3) and the BPA molecules are responsible for the shape of the BPA adsorption isotherm shown in Figure 8-6.

On the other hand, the isotherm shape of optimised JKWR carbon exhibited a type "L2" isotherm, which indicates that as more adsorption sites are filled, it becomes increasingly difficult for adsorbate molecules to find empty sites (Ferro-Garcia *et al.*, 1998) and thus, higher C_e values are needed for adsorption to reach equilibrium.

Table 8.4: Langmuir parameters for optimised JKWS and JKWR carbons and F400.

Carbon	Q_0 (mg/g)	R_L	R^2	X_{BET} (mg/m^2)
JKWS	312	0.009	0.9980	0.29
JKWR	105	0.041	0.9833	0.11
F400	303	0.002	0.9996	0.31

The data presented in Table 8.4 was carried out in unbuffered solutions and was determined from five experimental points, as previously described in Section 7.1.12.2 for phenol adsorption. The pH of BPA is approximately between pH 5.6 and pH 5.9. Upon the addition of the optimised JKW carbons, the pH of the solution was raised to between pH 8.8 and pH 9.4. The R_L values indicate that the adsorption of BPA is favourable and R^2 values indicate very good fit of trendlines through all the data points. Furthermore, at the aforementioned BPA solution pH values, there is no dissociation of BPA molecules and all 3 carbon samples exhibit positive total surface charges, indicating that there are no repulsions between adsorbent and adsorbate.

X_{BET} values indicate the fraction of BET surface area of the samples being occupied by BPA molecules. It also serves to normalise the Q_0 results in order to aid comparisons between the samples. As observable in Table 8.4, optimised JKWR carbon performed poorly in relation to the other two samples for reasons explained in the previous Section 8.3.2.

8.3.3.1 Influence of pH

Figure 8-7 shows the results of BPA adsorption on the three carbon samples at different solution pH.

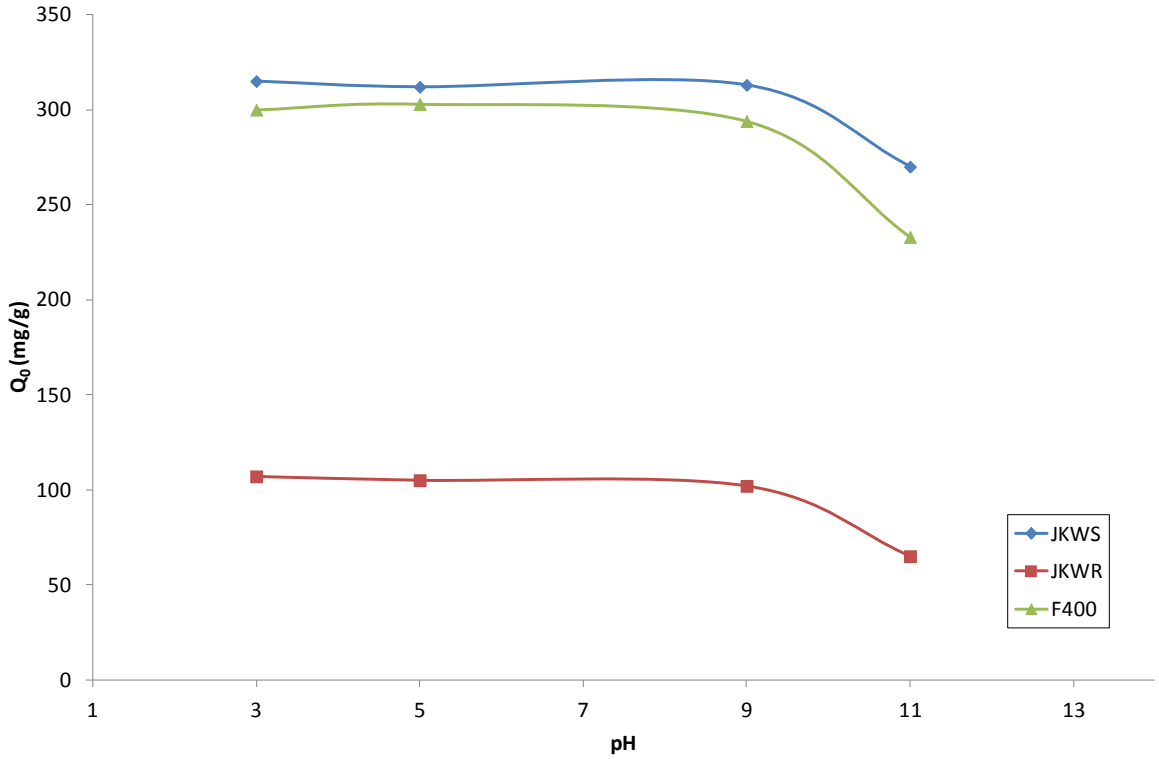


Figure 8-7: Influence of solution pH on BPA adsorption by optimised JKWS and JKWR carbons and F400.

Q_0 represents the Langmuir adsorption capacity of BPA onto the carbon samples. In all three carbons, the adsorption capacity was highest at acidic and mildly basic pH levels. However, it is observed that above a certain pH, the Q_0 value decreases. This behaviour can be explained by the opposing charges of the carbons and BPA at basic pH levels.

At pH 11, the solution pH is much greater than the pH_{PZC} of all three carbon samples and thus, the carbons exhibit a negative total surface charge. The BPA molecule dissociates into its bisphenolate anion and H^+ ions at solution pH > 9.6 or 10.2. Consequently, the increased electrostatic repulsion between the negatively-charged carbon and the bisphenolate anion results in reduced adsorption capacity of the carbons, as observed by Bautista-Toledo *et al.* (2005), Tsai *et al.* (2006) and Liu *et al.* (2009).

8.3.4 Ball-pan hardness

The attrition resistance of the optimised JKWS and JKWR carbons were assessed using their ball-pan hardness in comparison to F400, as shown in Table 8.5.

Table 8.5: Ball-pan hardness numbers of optimised carbons and F400.

Carbon	Ball-pan hardness number
JKWS, optimised	18.2
JKWR, optimised	73.6
F400	93.1

Both optimised carbons exhibited lower hardness numbers than F400, especially optimised JKWS carbon. However, it is not unexpected that F400 had a much higher hardness number as activated carbons made from coal are harder than those made from biomass (Roskill Information Services Ltd., 2003). Heschel and Klose (1995) concluded in their work with agricultural by-products that the morphology of the biomass is the main factor influencing the hardness, density and porosity of the carbon. This is due to the cross-linking of cellulose, hemicellulose and lignin molecules in the original plant biomass. As a result, the higher hardness number of optimised JKWR carbon could be attributed to its higher cellulose content.

Table 8.6: Particles size distributions and bulk densities of optimised JKWS and JKWR carbons with precursor char bulk densities.

Mesh size (mm)	JKWS	JKWR
4.00	9.65	6.43
2.80	6.14	30.41
2.00	27.19	18.13
1.00	35.96	20.18
0.50	9.65	14.62
0.25	7.89	3.51
0.15	3.51	2.92
Char bulk density (g/cm^3)	0.11	0.29
Optimised carbon bulk density (g/cm^3)	0.06	0.24

The structure of the initial biomass feedstock could also affect the hardness of the produced carbons (Reed and Williams, 2004). From Figure 7-6 in Section 7.2.2, the JKWS biomass is observed to be more fibrous than JKWR biomass, with more cracks in its structure. As a result of the steam activation process where the process of burn-off removes some of the carbon, this weakens the cracked and fibrous structure of JKWS carbon. This is also exhibited as a decrease in the bulk density of the optimised JKWS carbon compared to its char in

Table 8.6. In contrast, optimised JKWR carbon showed less of a decrease in bulk density. The large decrease in bulk density after steam activation for JKWS carbon is also an indication of its reactivity towards the activation process.

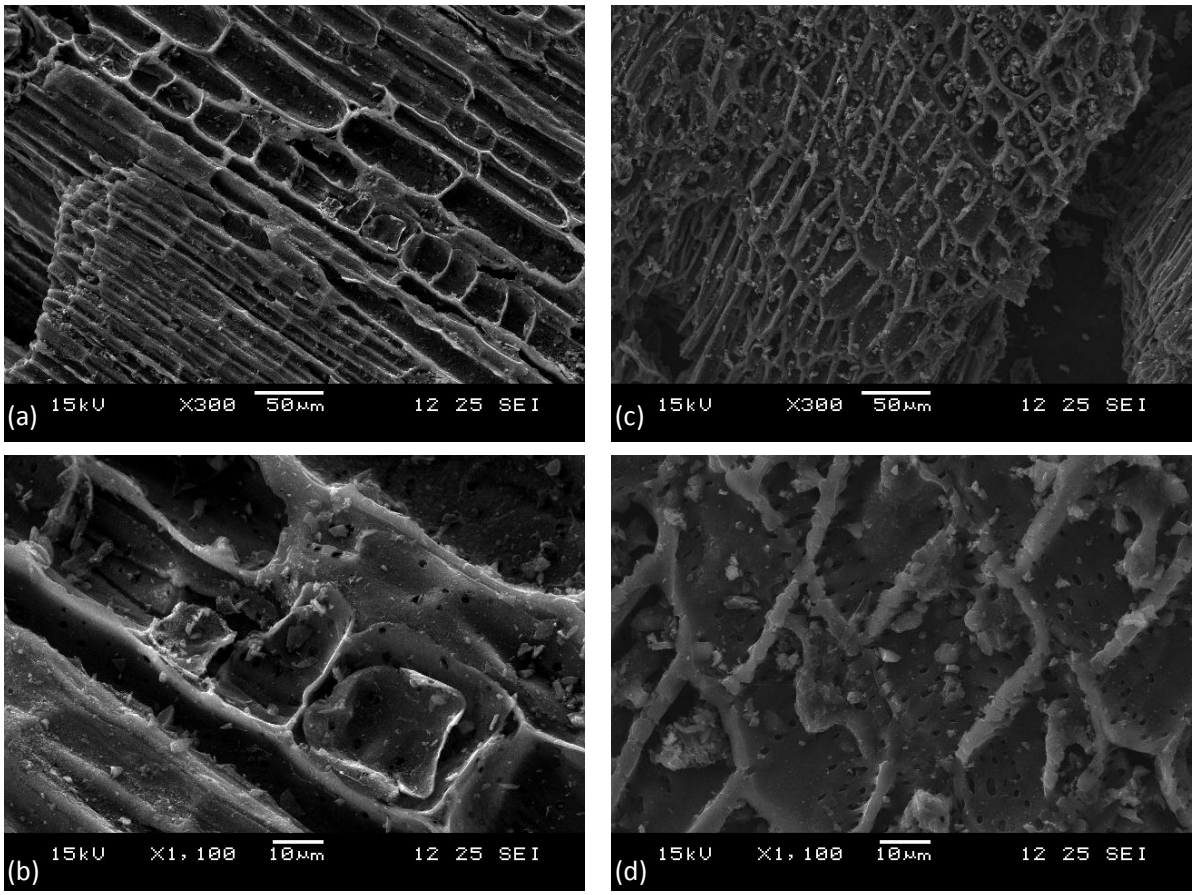


Figure 8-8: SEM photographs of optimised JKWS carbon at (a) 300X, (b) 1100X and optimised JKWR carbon at (c) 300X and (d) 1100x.

Observations from the SEM images in Figure 8-8 also indicate that the pore walls of JKWS carbon appear much thinner than those of optimised JKWR carbons, lending to the lower hardness value of JKWS carbon. Furthermore, the structure of optimised JKWR carbon is seen to be more regular and latticed, giving it structural strength.

Figure 8-8 (b) and (d) show the fine details of the porosity of the optimised JKW-derived carbons as a result of steam activation. The pores on the structural walls are observable at high magnification. It can also be seen that the cellular structure of JKW is preserved at high burn-off values.

8.4 Summary

The ability of the JKW derived activated carbons to remove BPA has been demonstrated in this work. This is important due to the detrimental effects of BPA on the human health along with its increasing presence and persistence in the environment (Lee and Peart, 2000, Kawahata *et al.*, 2004) and the relative ease of exposure to humans via plastics. Furthermore, BPA is not readily biodegradable (Fürhacker *et al.*, 2000) and must be removed from water. This can be easily rectified using the produced JKWS and JKWR activated carbons. Although optimised JKWR carbon did not perform as well as optimised JKWS and F400, the Q_0 value of 105mg/g is significantly greater than the amounts found to occur in the exposure pathways and environment (Gehring *et al.*, 2004, Fürhacker *et al.*, 2000) and as such, will be more than capable of adsorbing the BPA found in actual scenarios.

The adsorption kinetics experiments demonstrated that the BPA adsorption process took at least 8h to reach equilibrium. This was observed for all three carbon samples. However, 85% adsorption was attained in 10mins for optimised JKWS carbon but 90mins was required for optimised JKWR carbon as a result of the low polar character of the carbon.

The solution pH is a significant factor when examining the uptake of BPA by the carbon samples. The produced JKWS and JKWR carbons were H-type carbons (according to pH_{PZC}) due to the large amounts of basic surface groups present whereas F400 was a neutral carbon. Very alkaline solutions (pH>9) had a detrimental effect on the adsorption of BPA by all of the tested carbons due to the repulsive electrostatic effects experienced by both the negatively-charged carbon surface and the negatively-charged, dissociated bisphenolate anion. As a result, in order to maximise BPA adsorption by the optimised carbons, the solution pH should be kept below pH 9.

The optimised carbons did not demonstrate very high hardness numbers as a result of the structure and lignocellulosic content of their biomass predecessors. However, this could be counteracted by mixing the carbons with binder and pelletising them to increase hardness, especially carbons made from JKWS. Optimised JKWR carbons are harder and should stand up better to attrition. Furthermore, hardness is less vital in potable water treatment where the activated carbon is not subject to high enough hydraulic pressure to be crushed during service (Roskill Information Services Ltd., 2003).

All three carbon samples demonstrated good adsorption capabilities for BPA. Considering the fact that most BPA levels found in water courses were 8 ng/ml according to Kang *et al.* (2006) and studies conducted in the US and in several European countries. Even when BPA was concentrated in landfill leachate, the average concentration found was 269ng/l (Kang *et al.*, 2006), indicating that the optimised carbons would be able to easily and quickly adsorb the BPA contamination.

Chapter 9. Overall discussions and suggestions for future work

Economic development leads to higher consumption rate of goods and service. Thus, there is an increase in the generation of waste materials. As the rate of waste generation increases, the effects on the environment become apparent. As such, sustainable management methods must be applied to stem the health and environmental impacts of waste. In the widely-accepted waste management hierarchy pyramid, re-use and reduction is promoted above all other forms of waste management methods, with disposal the least desired option. This also ties in the with the concept of a circular economy, which is a mode of economic development based on ecological circulation of natural materials, requiring compliance with ecological laws and sound utilisation of natural resources to achieve economic development (Feng and Yan, 2007).

Japanese knotweed does not constitute municipal waste but it is biodegradable and thus, disposal to landfill is the least desirable option. In trying to control or eradicate Japanese knotweed, the three main routes of disposal (burning, burial and landfilling) begin with the excavation of plant biomass. This is important as the rhizome allows for efficient re-establishment of the plant, if not entirely removed. All aforementioned disposal methods result in the eventual release of carbon into the atmosphere in the form of CO_2. The use of herbicides is tightly-controlled, costly, long-term and potentially harmful to the environment. In summary, there is no sustainable method of controlling Japanese knotweed in the UK. In fact, there is nothing much that can be done to eradicate this invasive species without enormous financial and time expenditure.

If one were to extrapolate burning as a method of disposal, one could infer that the Japanese knotweed biomass could be incinerated for energy. However, some factors that need consideration are (Williams, 2006):

- Flue gas treatment as dictated by the EU Waste Incineration Directive;
- Treatment and disposal process for ash residues, which could end up in landfill at further cost; especially when co-incinerated with hazardous wastes.

Furthermore, the biogenic carbon contained within the plant biomass would be entirely released as CO_2 or CO gas depending on the incineration behaviour and carbon capture methods, further exacerbating climate change.

The conversion of Japanese knotweed into activated carbons would be an alternative way to tackle the problem of disposal. During carbonisation, the production of bio-oil and syngas can be captured and used as an alternative source of bio-fuel. Calorific values of bio-oil fuel have been shown to reach 16-19 MJ/kg (Mohan *et al.*, 2006) which is higher than the typical calorific value for MSW of 8.4MJ/kg (Williams, 2006). Syngas also has high calorific value of 48-63MJ/m^3 (Mohan *et al.*, 2006). The use of these by-products of the carbonisation of Japanese knotweed could offset the energy requirements of the reaction as well as compensate for the energy required during steam activation. In fact, depending on the amount of JKW biomass carbonised for activation, any surplus bio-oil and syngas could be sold for electricity generation purposes. This could help the UK in achieving a low carbon economy by 2050 in accordance with the Climate Change Act 2008; which calls for 80% reduction of GHG emissions below 1990 levels and a medium-term goal of 34% reduction by 2020. One of the contributing emitters of GHGs is the energy sector and to decrease emissions, it is predicted that the share of renewable energy sources need to increase from its current 6% to 31% by 2020 (Department of Energy and Climate Change, 2009). The use of JKW bio-oil and syngas in electricity generation could help meet this goal due to its biomass origin. Furthermore, the Renewable Obligation (RO) provides financial incentives for renewable electricity generators as part of the UK Low Carbon Transition Plan (Department of Energy and Climate Change, 2009). This is especially useful for the JKW bio-oil and syngas scenario as the RO Certificates can be sold without the electricity they represent, which means that they provide generators with financial support above what is received from selling their electricity in the wholesale market. Additionally, RO certificates depend on the different technologies to account for differences in technology costs. Furthermore, energy from waste biomass is listed as one of the new developments in the first UK Renewable Energy Roadmap (Department of Energy and Climate Change, 2011), where the UK attempts to produce electricity and heat from renewable sources.

The conversion to activated carbons can also be regarded as a form of carbon capture and sequestration (CCS). CCS also forms part of the UK Low Carbon Transition Plan. CCS has already been proposed by using bio-chars (Laird, 2008, Novak *et al.*, 2009, Lehmann, 2007, Lehmann *et al.*, 2006, Steinbeiss *et al.*, 2009, Fowles, 2007). It is therefore, not unreasonable to postulate that activated carbon can fulfil this role, especially those produced by steam activation as it is non-toxic and physically and chemically stable. Data has shown that global CO_2 emissions in 2012 reached 35.6 billion tonnes, which was a 2.6% increase from 2011 and 58% increase from 1990 levels (Kinver, 2012) and drastic action needs to be taken. During the plant's growth, anthropogenic carbon is extracted from the atmosphere and incorporated into its biomass and during carbonisation and

activation; some of the carbon is stabilised in the char and subsequent activated carbon. The 'sequestration' and stabilisation of carbon during the conversion of Japanese knotweed biomass into char and activated carbon is evidenced in preceding sections of this research. In order to minimise the transportation (and spread) of JKW biomass, it can be carbonised locally at the source with all the by-products collected and utilised on-site. Once carbonisation is completed, the char can then be transported to activation plants. In fact, this could be a valuable stream of income in the form of carbon credits/allowances where the UK is incentivised to sequester carbon made from JKW in the form of activated carbon, as part of the EU Emissions Trading System (EU ETS). The EU ETS is a system where member states 'cap and trade' the carbon emissions generated. Companies receive emission allowances and are allowed to sell or buy allowances from one another as required. The number of allowances is reduced over time so that total emissions will be reduced. Emissions generated in 2020 will be 21% less than in 2005 (European Commission, 2012b). CCS is given fuller recognition within the system under the revised EU ETS Directive (2009/29/EC) which takes effect in Phase III of the EU ETS in 2013, incentivising CCS (Wartmann *et al.*, 2009)

The conversion of JKW biomass into activated carbons is particularly useful as it would mean controlling the spread of JKW by constant excavation, vacating land for local use and amenities and sequestering anthropogenic carbon in the form of stable activated carbon; which is by itself, a valuable commodity. This has the added benefit of reducing the impacts of JKW on the biodiversity of local flora and fauna. However, it is more likely that JKW will only be removed from areas of construction and not from natural environments unless necessary.

The UK has activated carbon production capabilities of more than 23,000 tonnes per year and at an average UK export price of USD$3800/tonne, the financial benefits of producing approximately USD$88 million worth of activated carbon are not insignificant (Roskill Information Services Ltd., 2003).

The most widely-used raw material for the production of activated carbons is coal and the forecast is that demand will increase due to growing demand in water treatment and flue gas desulphurisation (Roskill Information Services Ltd., 2003). Based on available data, world consumption of activated carbon was 750,000 tonnes in 2003 and predicted world consumption is to approach 1.9 million tonnes in 2016 (Freedonia, 2012) and as such, the continued usage of coal as the main feedstock is likely to be unsustainable. Subsequently, other sources need to be utilised and JKW could be a good sustainable alternative for several reasons: Availability in large quantities; fast-growing; non-toxic;

status as unwanted waste biomass; easy to activate; low ash content and excellent adsorptive capabilities when activated.

Additionally, the utilisation of JKW as a carbon precursor would fulfil the principles of a circular economy, where 'waste does not exist' and 'the energy required to fuel the cycle of re-use should be renewable' (Ellen MacArthur Foundation, 2012). This is because:

- JKW would not be seen as a waste for disposal but as a resource,
- The energy used to activate the carbons could be derived from the bio-oil and syngas by-products,
- There will be less reliance on activated carbon imports (resource independence), mitigating price volatility and supply risks,
- JKW-derived carbons can be regenerated after being spent (Roskill Information Services Ltd., 2003) for improved service life.

To this end, the steam activation technology has been investigated and shown to be suitable for converting JKW biomass into activated carbons. This has the two-pronged approach of sustainably managing a waste biomass and producing a product that has inherent value, with no polluting potential and sequesters carbon permanently. In addition, the steam activation renders the plant biomass incapable of regenerating itself.

9.1 Chemical characterisation, thermal analysis and carbonisation of waste biomass

Waste biomass is gaining traction in activated carbon usage as the world realises that using non-renewable sources as feedstock is unsustainable. In doing so, workers need to analyse the chemical constituents of the biomass feedstock to determine their suitability as activated carbon feedstock. These included CHN, ash and lignocellulosic contents as seen in Table 5.2 and Table 5.3.

Green waste was characterised and was found to be unsuitable as an activated carbon feedstock due to its high ash content and low carbon content. During the GW carbonisation experiments, the ash-free-basis carbon contents of the produced char were insufficient for steam activation. Hence, the research has focussed on determining the suitability of JKW as a feedstock.

Prior to this research, there has been no work on the chemical analysis of Japanese knotweed. This was useful in explaining the differences in the effects of steam activation on the two distinct components that make up Japanese knotweed biomass: the stems and the rhizomes. Another property of interest was the lignocellulosic content. It was discovered that although both components belong to the same plant, there are large differences in the make-up of the plant. Chemical analysis also determined the unsuitability of green waste as a feedstock due to its low carbon and extremely high ash content.

Thermal analysis of milligram amounts of the 3 feedstocks in a thermal analyser contributed to a better understanding of how the samples degraded in an inert atmosphere. This aided the research in estimating char yields at different temperature and determining a suitable carbonisation temperature for bulk production of char. All three samples (GW, JKWS and JKWR) followed similar thermal degradation patterns with a maximum weight loss occurring at ca. 300°C. It is known that the degradation behaviour is a product of the different combinations and amounts of lignocellulosic material present in the respective biomasses, which was demonstrated in this research by the 3 samples. These results were presented in Section 5.4.4.

Small-scale batches of samples were carbonised using a quartz reactor in a rotary furnace to verify TGA results. Subsequently, GW was excluded from further testing due to having erratic carbonisation product yields as well as the previously mentioned incompatible chemical characteristics. The JKWS and JKWR biomass showed different results during carbonisation at the same temperature; JKWR char yields were higher than JKWS char yields by virtue of the different lignocellulosic contents. The optimum carbonisation temperature was selected based on the conditions which produced chars that had the lowest volatile matter emissions from the chars as determined by thermal analysis using a TGA. This was determined to be at 600°C for 1h. Thereafter, bulk carbonisation of JKWS and JKWR was carried out to produce sufficient char samples under the identical conditions to aid comparison in the subsequent steam activated chars.

9.2 Steam activation optimisation

Steam activation was chosen due to its popularity in the activated carbon industry (Roskill Information Services Ltd., 2003) and it is also a more reactive activating agent when compared to other physical activating agents such as CO_2. It also has a smaller environmental footprint in

comparison to chemical activation methods and there is the added benefit of being able to regenerate spent steam activated carbons (Roskill Information Services Ltd., 2003).

JKWS and JKWR biomass were discovered to contain high amount of alkaline earth metals which was concentrated in their respective chars after carbonisation. These high amounts of Ca, Mg, Na and K proved detrimental to the service life of the quartz reactor used in the steam activation process and consequently, an acid-washing step of the carbonised chars was incorporated into the pre-activation process, with positive results in the removal of the inorganic minerals. The effect of acid-washing also decreased the catalytic effect provided by the inorganic minerals, resulting in lower carbon burn-off and the consequent smaller BET surface area. Hence, this prevented the JKW-derived carbons from being over-activated.

9.2.1 Influence of activation temperature

Three different groups of activation parameters were tested: the first was variations in increasing the activation temperature followed by doubling the activation time and finally, by increasing the water flow rate. Steam activation is known to activate chars by initially creating micropores and at higher burn-off; widen the existing micropores into meso- and macropores. This was confirmed by the results shown in the research.

The effect of varying the steam activation temperature upon the activated carbon yield and carbon is shown in Section 7.2.2. It is observed that the carbon burn-off increases with activation temperature and the adsorptive capabilities of the produced carbons also increases. JKWS carbon is observed to exhibit higher degrees of microporosity than JKWR carbon at burn-off levels below 25%. However, due to the higher reactivity of JKWS carbons towards steam activation; it is able to generate higher BET surface areas and thus, have better (more) adsorptive capabilities than the equivalent JKWR carbon. The tested activated carbons exhibited mixed Type I/Type IV isotherms with H4 hysteresis loops, which indicated that the carbons were microporous with varying degrees of mesoporosity as seen in Figure 7-10 and Figure 7-11. It is noticed that increasing activation temperatures increases the degree of mesoporosity generated in the carbons, with JKWR carbons exhibiting lesser degrees of mesoporosity development than JKWS carbons. This was attributed to the different lignocellulosic contents of the original biomass, with JKWS containing higher amounts of hemicellulose and less cellulose than JKWR.

The produced carbons did not perform well in BWC experiments, especially when compared to the commercial-grade comparison F400. In adsorption experiments with butane gas, the butane activity of the produced JKWS and JKWR carbons both increased with activation temperature as a result of the increased porosity development. JKWS carbons have higher butane activity and working capacity but lower butane retentivity than JKWR carbons. This was due to the different degrees of micro- and mesoporosity of the carbons and pore shapes. At the low carbon burn-off levels generated by mild steam activation, the produced carbons were not able to compete with F400.

As expected, iodine numbers for both types of carbons increased with activation temperature. The type of porosity also plays a role in adsorption as JKWR carbons with their higher mesoporosity adsorbed more iodine molecules as a result of the shortened diffusion pathway from aqueous solution to micropores of the carbon although the produced JKWS carbons had higher BET surface areas. This was shown in Section 7.2.5.

The carbons were all of the H-variety according to the classification of Steenberg (1944), where the carbons contained higher proportions of basic surface groups and thus, exhibited alkaline properties in aqueous solution as seen in Figure 7-20. The plotted adsorption kinetics isotherms showed that 24h is required for phenol adsorption to reach equilibrium during carbon adsorption and as such, all phenol adsorption experiments were carried out for 24h.

The plotted adsorption isotherms were interpretable using the Langmuir model and all results exhibited R^2 values larger than 0.97. However, the data did not fit the Freundlich model as well due to lower R^2 values. All the steam activated JKW carbons exhibited Langmuir Q_0 values that were much lower than F400, due to the lower surface area and pore volumes, as seen in Table 7.9.

9.2.2 Influence of activation time and water flow rate

In order to further optimise the steam activation conditions of manufacturing JKW activated carbons, the activation time was doubled from 0.5h and two additional water flow rates were tested to include 0.1, 0.3 and 0.5ml/min.

It was observed that the increased water (steam) flow rate had the effect of enhancing burn-off. The same result was reported for doubling the activation time. As previously mentioned, JKWS carbons

experienced higher burn-offs (and thus, had lower yields) than the JKWR carbons, as seen in Figure 7-30.

N_2 adsorption experiments indicated that the extra burn-off achieved by increased water flow rates and doubled activation times had the effect of increasing the micro- and mesoporosity of the carbons. Additionally, the contributions of meso- and macroporosity to the total BET surface area increased with higher burn-off. In contrast to what was reported earlier, JKWR carbons now comprised higher degrees of microporosity than JKWS carbons. Moreover, both types of JKW-derived carbons have developed BET surface areas similar to that exhibited by F400. As a result, the JKW carbons were now able to compete with F400 in terms of adsorptive abilities. This was observed as increases in iodine numbers, BWC and phenol adsorption capacity. The most activated carbons (JKWS and JKWR) were shown to perform better than F400 in most of the aforementioned characterisation tests.

9.3 Application of optimised JKWS and JKWR carbons for BPA adsorption

The optimised JKWS and JKWR carbon were then tested to evaluate their adsorptive capabilities for BPA in aqueous solution. BPA was chosen as it is an emerging water pollutant of concern with oestrogen-like effects on the human body. BPA enters waterways as a result of washing residues and wastewaters generated during plastics manufactured (Suzuki *et al.*, 2004) as well as from its application.

The initial stages of this part of the research involved examining the adsorption kinetics to determine the equilibration time for BPA uptake by optimised JKWS and JKWR carbon along with F400. It was recognised that equilibrium was attained in 8h for optimised JKWS and F400 but 24h for optimised JKWR carbon. Consequently, all adsorption experiments involving BPA adsorption was conducted with a contact time of 24h.

Observations indicated that there were other factors besides surface area and porosity affecting the relatively slower and lower adsorption of BPA by optimised JKWR carbon and the Boehm titration determined that the low amounts of acidic surface groups was a contributing cause.

Adsorption isotherms were plotted for all three carbon samples and they were able to be interpreted using the Langmuir theory with all results having R^2 values >0.98. However, the data did

not fit the Freundlich model well. The Langmuir Q_0 values showed that optimised JKWS carbon performed as well as F400.

The adsorption of BPA was very dependent upon the solution pH. The acid/base character of the carbon samples also played a vital role in determining their adsorption capabilities. It was established that the adsorption capacity of all three carbon samples remained constant at acidic and mildly basic pH levels but decreased greatly at pH > 9. This was explained by the dissociated BPA anion being repelled by the negative total surface charges present on the carbons at high solution pH levels.

The ball-pan hardness numbers of optimised JKWS and JKWR carbons were lower than that of F400, especially that of optimised JKWS carbon. This might be a potential barrier for use in water treatment due to fines generation. However, mixing powdered carbons with binder and subsequent pelletisation could rectify the low hardness. F400 is an agglomerated carbon which was made by crushing coal char and pelletising the crushed particles and this is a common, commercial practise. Thus, the relative low hardness of optimised JKWS carbons is not a major obstruction to its commercial viability.

9.4 Conclusions

This research has, for the first time, undertaken the analysis and study of Japanese knotweed as a potential precursor for activated carbon manufacture. These analyses included chemical and physical properties such as CHNS, lignocellulosic content, ash content and moisture contents. It should be noted that prior to this research, there had been no record of CHNS and lignocellulosic data of JKW. It has conclusively demonstrated that the conversion of Japanese knotweed biomass into activated carbons is a viable, attractive and novel means of reusing this otherwise problematic plant biomass.

In converting the original JKW biomass into activated carbons via carbonisation and steam activation, the following is achieved:

- The biomass is rendered inactive and hence, unable to propagate;
- Excavated plant biomass is sustainably managed without burning or disposal to landfill, thus meeting the EU Landfill Directive of reducing BMW;

- The carbonisation process produces calorific by-products such as bio-oil and syngas which can be utilised for energy production, on- or off-site.

The steam activation technology is proven, well-established and widely-accepted without leaving a large environmental footprint. Hence, it is ideal for producing usable activated carbon from JKW biomass. By varying the steam activation conditions such as temperature, time and water flow rate, the activated carbons can be tailored to possess superior adsorptive properties that are able to rival and outperform a commercial-grade carbon. In doing so, it has the advantage of being derived from waste biomass that is sustainable and renewable, unlike coal.

There is a singular lack of work pertaining to JKW in terms of its recycling. Thus, these are some of the contributions to scientific knowledge from this research in different areas:

- Chemical (CHNS and lignocellulosic content) and physical (moisture content, ash content and thermal degradation behaviour) analyses of JKWS and JKWR;
- JKW biomass was shown to contain high amount of Ca, Mg, K and Na;
- JKW was for the first time proven as an easy-to-activate alternative activated carbon feedstock to coal with the highly activated JKW-derived carbons outperforming the commercial comparison carbon;
- JKW-derived activated carbons were demonstrated to adsorb BPA, an emerging water pollutant.

The increase in activation temperature, activation time and water flow rate all increases the porosity of the produced JKWS and JKWR activated carbons. The effects of increased activation parameters are:

- Increased burn-off
- Increased BET surface area and total pore volume
- Increased BWC and butane activity
- Increased phenol and iodine adsorption

The key processes for the production of JKW-derived activated carbons optimised for BET surface area and hence, maximum BPA adsorption is as follows:

- The harvested JKWS or JKWR biomass is dried, crushed and sieved between 10mm and 1mm particle sizes;
- The crushed samples are carbonised at 600°C for 1 hour with a nitrogen flow rate of 10ml/min in a quartz rotary reactor;
- The char samples are washed using 0.2M HCl acid for 24 hours, three times and oven-dried in order to reduce the alkaline earth metal content of the char samples;
- The washed and dried char is then activated using steam at 925°C for 1 hour with a water flow rate of 0.5ml/min. The aforementioned activation parameters allow for the maximum development of porosity of both JKWS and JKWR char.

9.5 Suggestions for future work

During the course of this research, it was not possible to follow all potential research opportunities that arose as the work progressed. Potential research programmes are briefly outlined below:

- During preparation of JKW biomass samples, a lot of soil was removed during cleaning and as such, the recovery and reuse (or disposal) must be taken into account if large-scale work were to be considered.

- Further work is required to determine the actual amount of JKW found in the UK. The data obtained for this research was published in 1994 and this plant is spreading quickly.

- Furthermore, there is the issue of pre-drying the biomass before carbonisation. Possibilities exist where the energy used for the drying stage could be derived from the syngas and bio-oil produced during carbonisation and this option could be further explored.

- Carbonisation of the biomass produced bio-oils and syngas that were not considered but analysis by gas chromatography-mass spectrometry (GC-MS) would provide an insight into the types of degradation reactions that occurred during carbonisation, thus enabling an in-depth analysis of the influence of feedstock composition upon the char and volatile products.

- The bio-oils and syngas may have possible reuse opportunities beyond simple energy recovery, so a complete analysis of the composition of these by-products could be of significant interest and may provide a new source of chemical precursors.

- Higher carbon burn-off (>50%) could also be investigated to determine the prolonged effect of steam activation on Japanese knotweed chars.

- Regeneration tests could be carried out to determine the maximum number of regeneration cycles before disposal.

- A life-cycle analysis (LCA) of the steam activation process from excavation or harvesting of JKW biomass to final disposal of activated carbon.

- If disposal of the activated carbons were required, there could be tests done to determine their carbon sequestration potential.

- Adsorption tests from a mixed solution with more than 1 adsorbate could be conducted to determine competitive effects for adsorption

- A final need for further research is to study the economics of the steam activation process of JKW and compare it to other forms of activation processes. Without a full assessment of the costs involved, the potential of this method in using JKW cannot be fully utilised.

Chapter 10. References

ABDULLAH, H. & WU, H. (2009). Biochar as a Fuel: 1. Properties and Grindability of Biochars Produced from the Pyrolysis of Mallee Wood under Slow-Heating Conditions. *Energy & Fuels,* 23**,** 4174-4181.

ADACHI, N., TERASHIMA, I. & TAKAHASHI, M. (1996). Mechanisms of Central Die-back of Reynoutria japonica in the Volcanic Desert on Mt. Fuji. A Stochastic Model Analysis of Rhizome Growth. *Annals of Botany,* 78**,** 169-179.

AFP. 2012. France bans contested chemical BPA in food packaging. Available: http://uk.news.yahoo.com/france-bans-contested-chemical-bpa-food-packaging-190638980.html.

AL-DEGS, Y., KHRAISHEH, M. A. M., ALLEN, S. J. & AHMAD, M. N. (2000). Effect of carbon surface chemistry on the removal of reactive dyes from textile effluent. *Water Research,* 34**,** 927-935.

ALLEN, J. L., GATZ, J. L. & EKLUND, P. C. (1999). Applications for activated carbons from used tires: butane working capacity. *Carbon,* 37**,** 1485-1489.

AMAYA, A., MEDERO, N., TANCREDI, N., SILVA, H. & DEIANA, C. (2007). Activated carbon briquettes from biomass materials. *Bioresource Technology,* 98**,** 1635-1641.

ANDERSEN, J. K., BOLDRIN, A., CHRISTENSEN, T. H. & SCHEUTZ, C. (2010). Mass balances and life-cycle inventory for a garden waste windrow composting plant (Aarhus, Denmark). *Waste management & research,* 28**,** 1010-1020.

ANDRE, S. & MARK, D. (2004). *Fischer-Tropsch Technology*, Elsevier.

ARRIAGADA, R., GARCIA, R., MOLINA-SABIO, M. & RODRIGUEZ-REINOSO, F. (1997). Effect of steam activation on the porosity and chemical nature of activated carbons from Eucalyptus globulus and peach stones. *Microporous materials,* 8**,** 123-130.

ARRIAGADA, R., GARCIA, R. & REYES, P. (1994). Steam and carbon dioxide activation of Eucalyptus globulus charcoal. *Journal of chemical technology and biotechnology,* 60**,** 427-433.

ASTM (1979) *Method D3802-79 (1999) Standard Test Method for Ball-Pan Hardness of Activated Carbon*.

ASTM (1984) *Method D1109-84 (2007) Standard test method for 1% sodium hydroxide solubility of wood* Washington, D.C., USA ASTM International.

ASTM (1992) *Method D5228-92 (96) Standard test method for the butane working capacity of activated carbon* Washington, D.C., USA ASTM International.

ASTM (1994a) *Method D2866-94 (99) Standard test method for total ash content of activated carbon* Washington,D.C, USA ASTM International.

ASTM (1994b) *Method D4607-94(99) Standard test method for determination of iodine number of activated carbon* Washington, D.C., USA ASTM International.

ASTM (1996a) *Method D1106-96 (2007) Standard test method for acid-insoluble lignin in wood* Washington, D.C., USA ASTM International.

ASTM (1996b) *Method D2854-96 Standard test method for apparent density of activated carbon* Washington, D.C., USA ASTM International.

ASTM (1997) *Method D2862-97 Standard test method for particle size distribution of granular activated carbon* Washington, D.C. USA ASTM International.

ASTM (2007a) *D1102 - 84(2007) Standard Test Method for Ash in Wood* ASTM International.

ASTM (2007b) *D4442-07 Standard Test Methods for Direct Moisture Content Measurement of Wood and Wood-Base Materials* ASTM International.

AUDIT COMMISSION (2008) *Well disposed: Responding to the waste challenge*.

AYGÜN, A., YENISOY-KARAKAŞ, S. & DUMAN, I. (2003). Production of granular activated carbon from fruit stones and nutshells and evaluation of their physical, chemical and adsorption properties. *Microporous and Mesoporous Materials,* 66**,** 189-195.

AZARGOHAR, R., DALAI, A. & DALAI, A. K. (2006). Biochar as a precursor of activated carbon. *Applied biochemistry and biotechnology,* 129-132**,** 762-73.

BABU, B. V. (2008). Biomass pyrolysis: A state-of-the-art review. *Biofuels, bioproducts & biorefining,* 2**,** 393-414.

BACAOUI, A., YAACOUBI, A., DAHBI, A., BENNOUNA, C., LUU, R. & MALDONADO-HODAR, F. (2001). Optimization of conditions for the preparation of activated carbons from olive-waste cakes. *Carbon,* 39**,** 425-432.

BAGREEV, A., ADIB, F. & BANDOSZ, T. J. (2001). pH of activated carbon surface as an indication of its suitability for H2S removal from moist air streams. *Carbon,* 39**,** 1897-1905.

BAILEY, J. (2003). Japanese Knotweed s.l. at home and abroad. *Plant Invasions: Ecological threats and management solutions***,** 183-196.

BAILEY, J. (2012). The Japanese knotweed invasion viewed as a vast unintentional hybridisation experiment. *Heredity*.

BAILEY, J. & CONOLLY, A. (2000). Prize-winners to pariahs - a history of Japanese knotweed (*Polygonaceae*) in the British Isles. *Watsonia,* 23**,** 93-110.

BALCI, S., DOĞU, T. & YÜCEL, H. (1994). Characterization of activated carbon produced from almond shell and hazelnut shell. *Journal of Chemical Technology & Biotechnology,* 60**,** 419-426.

BANSAL, R. C. (2005). *Activated carbon adsorption*, CRC.

BANSAL, R. C., DONNET, J. P. & STOECKLI, F. (1988). *Active Carbon,* New York, USA, M. Dekker.

BARRETT, E. P., JOYNER, L. G. & HALENDA, P. P. (1951). The determination of pore volume and area distributions in porous substances. I. Computations from nitrogen isotherms. *Journal of the American Chemical society,* 73**,** 373-380.

BASHEER, C. & LEE, H. K. (2004). Analysis of endocrine disrupting alkylphenols, chlorophenols and bisphenol-A using hollow fiber-protected liquid-phase microextraction coupled with injection port-derivatization gas chromatography–mass spectrometry. *Journal of Chromatography A,* 1057**,** 163-169.

BASHTANOVA, U. B., BECKETT, K. P. & FLOWERS, T. J. (2009). Review: Physiological Approaches to the Improvement of Chemical Control of Japanese Knotweed (Fallopia japonica). *Weed Science,* 57**,** 584-592.

BASSO, M. C., CERRELLA, E. G. & CUKIERMAN, A. L. (2002). Lignocellulosic Materials as Potential Biosorbents of Trace Toxic Metals from Wastewater. *Industrial & Engineering Chemistry Research,* 41**,** 3580-3585.

BAUTISTA-TOLEDO, I., FERRO-GARCÍA, M. A., RIVERA-UTRILLA, J., MORENO-CASTILLA, C. & VEGAS FERNÁNDEZ, F. J. (2005). Bisphenol A Removal from Water by Activated Carbon. Effects of Carbon Characteristics and Solution Chemistry. *Environmental science & technology,* 39**,** 6246-6250.

BBC. (2010). *Non-native species cost 'British economy £1.7bn'* [Online]. Available: http://www.bbc.co.uk/news/uk-11996801 [Accessed 22/11/2012.

BBC. (2011a). *Call for joint action on Japanese knotweed* [Online]. Available: http://www.bbc.co.uk/news/world-europe-guernsey-12999059 [Accessed 22/11/2012.

BBC. (2011b). *Japanese knotweed invasion causes Hertfordshire home price drop* [Online]. Available: http://www.bbc.co.uk/news/uk-england-beds-bucks-herts-15461880 [Accessed 22/11/2012.

BBC. (2011c). *'Killer' shrimps worst alien invader of waterways* [Online]. Available: http://www.bbc.co.uk/news/uk-14428585 [Accessed 6/8/2011 2011].

BBC. (2012). *Japanese Knotweed delays Guernsey social housing build* [Online]. Available: http://www.bbc.co.uk/news/world-europe-guernsey-20249865 [Accessed 22/11/2012.

BECK-FRIIS, B., PELL, M., SONESSON, U., JÖNSSON, H. & KIRCHMANN, H. (2000). Formation and Emission of N2O and CH4 from Compost Heaps of Organic Household Waster. *Environmental Monitoring and Assessment,* 62**,** 317-331.

BEERLING, D. J., BAILEY, J. P. & CONOLLY, A. P. (1994). Fallopia Japonica (Houtt.) Ronse Decraene. *Journal of Ecology,* 82**,** 959-979.

BEIS, S. H., ONAY, Ö. & KOÇKAR, Ö. M. (2002). Fixed-bed pyrolysis of safflower seed: influence of pyrolysis parameters on product yields and compositions. *Renewable Energy,* 26**,** 21-32.

BESHARA, A. 2010. *Novel processes for improved waste management for spent bleaching earth in Egypt.* PhD, Imperial College.

BISCO, J. & WARRENS, B. E. (1942). An X-ray study of carbon black. *Journal of Applied Physics,* 13**,** 364-371.

BOEHM, H. P. (1966). Chemical identification of surface groups. *Advances in catalysis,* 16**,** 179-274.

BOKROS, J. (1969). Deposition, structure and properties of pyrolytic carbon. *Chemistry and Physics of Carbon,* 5**,** 1-118.

BOLDRIN, A. & CHRISTENSEN, T. H. (2010). Seasonal generation and composition of garden waste in Aarhus (Denmark). *Waste Management,* 30**,** 551-557.

BOND, W. & TURNER, R. (2006). *The biology and non-chemical control of Japanese knotweed (Fallopia japonica (Houtt))* [Online]. Available: http://www.gardenorganic.org.uk/organicweeds/downloads/fallopia%20japonica.pdf [Accessed 06/08/2010.

BOOTH, R. 2007. Knotweed sets Olympics £70m challenge. *The Sunday Times*.

BOUCHELTA, C., MEDJRAM, M. S., BERTRAND, O. & BELLAT, J.-P. (2008). Preparation and characterization of activated carbon from date stones by physical activation with steam. *Journal of analytical and applied pyrolysis,* 82**,** 70-77.

BRIDGWATER, A., MEIER, D. & RADLEIN, D. (1999). An overview of fast pyrolysis of biomass. *Organic Geochemistry,* 30**,** 1479-1493.

BROCK, J. & WADE, M. 1992. Regeneration of Japanese knotweed (*Fallopia japonica*) from rhizomes and stems: observation from greenhouse trials. IXe Colloque international sur la biologie des mauvaises herbes, 16-18 September 1992, Dijon, France., 1992. Paris France: Anpp, 85-94.

BROCK, J. H. (1994). Technical note: Standing crop of Reynoutria japonica in the autumn of 1991 in the United Kingdom. *Preslia (Prague),* 66**,** 337-343.

BRUNAUER, S., DEMING, L. S., DEMING, W. E. & TELLER, E. (1940). On a Theory of the van der Waals Adsorption of Gases. *Journal of the American Chemical Society,* 62**,** 1723-1732.

BSBI. (2011). *Botanical Society of the British Isles Hectad map of Fallopia japonica (Japanese Knotweed) in GB and Ireland* [Online]. Available: http://www.bsbimaps.org.uk/atlas [Accessed July 2012.

BÜNGER, J., ANTLAUF-LAMMERS, M., SCHULZ, T. G., WESTPHAL, G. A., MÜLLER, M. M., RUHNAU, P. & HALLIER, E. (2000). Health complaints and immunological markers of exposure to bioaerosols among biowaste collectors and compost workers. *Occupational and Environmental Medicine,* 57**,** 458-464.

BURG, P. & CAGNIANT, D. 2007. Characterization of Carbon Surface Chemistry. *Chemistry & Physics of Carbon.* CRC Press.

BURNLEY, S. J. (2007). A review of municipal solid waste composition in the United Kingdom. *Waste Management,* 27**,** 1274-1285.

BUTTERMAN, H. C. & CASTALDI, M. J. (2010). Biomass to Fuels: Impact of Reaction Medium and Heating Rate. *Environmental Engineering Science,* 27**,** 539-555.

CAI, Y., JIANG, G., LIU, J. & ZHOU, Q. (2003). Multiwalled Carbon Nanotubes as a Solid-Phase Extraction Adsorbent for the Determination of Bisphenol A, 4-n-Nonylphenol, and 4-tert-Octylphenol. *Analytical Chemistry,* 75**,** 2517-2521.

CANNON, F. S., SNOEYINK, V. L., LEE, R. G. & DAGOIS, G. (1994). Reaction mechanism of calcium-catalyzed thermal regeneration of spent granular activated carbon. *Carbon,* 32**,** 1285-1301.

CAZORLA-AMORÓS, D., RIBES-PÉREZ, D., ROMÁN-MARTÍNEZ, M. C. & LINARES-SOLANO, A. (1996). Selective porosity development by calcium-catalyzed carbon gasification. *Carbon,* 34**,** 869-878.

CHANG, C.-F., CHANG, C.-Y. & TSAI, W.-T. (2000). Effects of Burn-off and Activation Temperature on Preparation of Activated Carbon from Corn Cob Agrowaste by CO2 and Steam. *Journal of Colloid and Interface Science,* 232**,** 45-49.

CHANG, C., CHEN, I. & YANG, S. (2009). Methane and carbon dioxide emissions from different composting periods. *TAO,* 20**,** 511-520.

CHILD, L. E. & WADE, M. (2000). *The Japanese Knotweed Manual: The Management and Control of an Invasive Alien Weed,* Chicester, UK, Packard Publishing Ltd.

CHOI, K. J., KIM, S. G., KIM, C. W. & KIM, S. H. (2005). Effects of activated carbon types and service life on removal of endocrine disrupting chemicals: amitrol, nonylphenol, and bisphenol-A. *Chemosphere,* 58**,** 1535-1545.

CONFESOR, R. B., HAMLETT, J. M., SHANNON, R. D. & GRAVES, R. E. (2008). Potential pollutants from farm, food and yard waste composts at differing ages: Part I. Physical and chemical properties. *Compost Science & Utilization,* 4**,** 228-238.

CORBITT, R. A. (1999). *Standard Handbook of Environmental Engineering.,* New York, McGraw-Hill Publishers.

COUGHLIN, R. W. & EZRA, F. S. (1968). Role of surface acidity in the adsorption of organic pollutants on the surface of carbon. *Environmental Science & Technology,* 2**,** 291-297.

COULTER (1991). *Reference Manual - Coulter Omnisorp 100/360 Series,* Luton, England., Coulter Corp.

CUNLIFFE, A. M. & WILLIAMS, P. T. (1998). Influence of Process Conditions on the Rate of Activation of Chars Derived from Pyrolysis of Used Tires. *Energy & Fuels,* 13**,** 166-175.

CZERNIK, S. & BRIDGWATER, A. (2004). Overview of applications of biomass fast pyrolysis oil. *Energy & Fuels,* 18**,** 590-598.

DABROWSKI, A., PODKOSCIELNY, P., HUBICKI, Z. & BARCZAK, M. (2005). Adsorption of phenolic compounds by activated carbon - a critical review. *Chemosphere,* 58**,** 1049-1070.

DAIFULLAH, A. A. M. & GIRGIS, B. S. (1998). Removal of some substituted phenols by activated carbon obtained from agricultural waste. *Water Research,* 32**,** 1169-1177.

DAUD, W. M. A. W. & ALI, W. S. W. (2004). Comparison on pore development of activated carbon produced from palm shell and coconut shell. *Bioresource Technology,* 93**,** 63-69.

DEFRA (2003) *Review of Non-native Species Policy*.

DEFRA (2007) *Waste Strategy for England*

DEFRA 2008. Waste Wood as a Biomass Fuel. *In:* PROGRAMME, W. I. D. (ed.). Crown Copyright.

DEFRA (2010a) *Environmental benefits of recycling - 2010 update*.

DEFRA. (2010b). *UK meets 2010 Landfill Directive target and responds to landfill consultations* [Online]. Available: http://www.defra.gov.uk/news/2010/09/08/landfill-directive-target/ [Accessed 28/11/2012.

DEFRA 2011. Environmental Statistics. UK.

DEMIRBAS, A. (2004). Effects of temperature and particle size on bio-char yield from pyrolysis of agricultural residues. *Journal of analytical and applied pyrolysis,* 72**,** 243-248.

DEMIRBAŞ, A. (2003). Relationships between lignin contents and fixed carbon contents of biomass samples. *Energy conversion and management,* 44**,** 1481-1486.

DEMIRBAS, A. & ARIN, G. (2002). An overview of Biomass pyrolysis. *Energy Sources,* 24**,** 471-482.

DEPARTMENT OF ENERGY AND CLIMATE CHANGE (2009) *The UK Low Carbon Transition Plan: National strategy for climate and energy.*

DEPARTMENT OF ENERGY AND CLIMATE CHANGE (2011) *UK Renewable Energy Roadmap*.

DEVON COUNTY COUNCIL. (2010). *Japanese Knotweed - What's the problem?* [Online]. Available: http://www.devon.gov.uk/index/environmentplanning/natural_environment/biodiversity/japanese_knotweed/whats_the_problem.htm [Accessed 06/08/2010.

DIAMANTI-KANDARAKIS, E., BOURGUIGNON, J.-P., GIUDICE, L. C., HAUSER, R., PRINS, G. S., SOTO, A. M., ZOELLER, R. T. & GORE, A. C. (2009). Endocrine-Disrupting Chemicals: An Endocrine Society Scientific Statement. *Endocrine Reviews,* 30**,** 293-342.

DIAS, J. M., ALVIM-FERRAZ, M. C. M., ALMEIDA, M. F., RIVERA-UTRILLA, J. & SÁNCHEZ-POLO, M. (2007). Waste materials for activated carbon preparation and its use in aqueous-phase treatment: A review. *Journal of Environmental Management,* 85**,** 833-846.

DOS SANTOS, E. J., HERRMANN, A. B., CHAVES, E. S., VECHIATTO, W. W. D., SCHOEMBERGER, A. C., FRESCURA, V. L. A. & CURTIUS, A. J. (2007). Simultaneous determination of Ca, P, Mg, K and Na in biodiesel by axial view inductively coupled plasma optical emission spectrometry with internal standardization after multivariate optimization. *J. Anal. At. Spectrom.,* 22**,** 1300-1303.

DRISCOLL-WOODFORD, H. 2010. Can Surrey gardeners be blamed for knotweed invasion? *BBC*.

DUBININ, M. M. (1960). The potential theory of adsorption of gases and vapors for adsorbents with energetically nonuniform surfaces. *Chemical Reviews,* 60**,** 235.

EL-GEUNDI, M. S. (1997). Adsorbents for industrial pollution control. *Adsorption science & technology,* 15**,** 777-787.

EL-HENDAWY, A.-N. A., SAMRA, S. & GIRGIS, B. (2001). Adsorption characteristics of activated carbons obtained from corncobs. *Colloids and Surfaces A: Physicochemical and Engineering Aspects,* 180**,** 209-221.

EL-SHEIKH, A. H., NEWMAN, A. P., AL-DAFFAEE, H. K., PHULL, S. & CRESSWELL, N. (2004). Characterization of activated carbon prepared from a single cultivar of Jordanian Olive stones by chemical and physicochemical techniques. *Journal of Analytical and Applied Pyrolysis,* 71**,** 151-164.

ELLEN MACARTHUR FOUNDATION (2012) *Towards the circular economy: Economics and business rationale for an accelerated transition*.

ENVIRONMENT AGENCY. (2012a). *European Waste Catalogue* [Online]. Available: http://www.environment-agency.gov.uk/business/topics/waste/31873.aspx [Accessed 02/01/2013.

ENVIRONMENT AGENCY (2012b) *The Knotweed Code of Practice: Managing Japanese Knotweed on development sites*.

ENVIRONMENT AGENCY. (2012c). *What is hazardous waste?* [Online]. Available: http://www.environment-agency.gov.uk/business/topics/waste/32200.aspx.

ENVIRONMENTAL PROTECTION AGENCY 2000. Biosolids Technology Fact Sheet: In-Vessel Composting of Biosolids. *In:* ENVIRONMENTAL PROTECTION AGENCY, U. (ed.). Washington, D.C.

ERICKSON, B. E. (2008). Bisphenol A under scrutiny. *Chemical and Engineering News,* 86**,** 36-39.

EUROPEAN COMMISSION 2011. Commission Directive 2011/8/EU on the restriction of use of Bisphenol A in plastic infant feeding bottles. Brussels, Belgium.

EUROPEAN COMMISSION. (2012a). *Directive 2008/98/EC on waste (Waste Framework Directive)* [Online]. Available: http://ec.europa.eu/environment/waste/framework/index.htm.

EUROPEAN COMMISSION. (2012b). *European Union Emissions Trading System (EU ETS)* [Online]. Available: http://ec.europa.eu/clima/policies/ets/index_en.htm.

EUROSTAT (2005) *Waste generated and treated in Europe: Data 1995-2003*.

FAGBEMI, L., KHEZAMI, L. & CAPART, R. (2001). Pyrolysis products from different biomasses: application to the thermal cracking of tar. *Applied energy,* 69**,** 293-306.

FAN, M., MARSHALL, W., DAUGAARD, D. & BROWN, R. C. (2004). Steam activation of chars produced from oat hulls and corn stover. *Bioresource Technology,* 93**,** 103-107.

FAUST, S. D. & ALY, O. M. (1998). *Chemistry of Water Treatment, Second Edition*, Taylor & Francis.

FENG, Z. & YAN, N. (2007). Putting a circular economy into practice in China. *Sustainability Science,* 2**,** 95-101.

FERRO-GARCIA, M., RIVERA-UTRILLA, J., BAUTISTA-TOLEDO, I. & MORENO-CASTILLA, C. (1998). Adsorption of humic substances on activated carbon from aqueous solutions and their effect on the removal of Cr (III) ions. *Langmuir,* 14**,** 1880-1886.

FIERRO, V., TORNÉ-FERNÁNDEZ, V., MONTANÉ, D. & CELZARD, A. (2008). Adsorption of phenol onto activated carbons having different textural and surface properties. *Microporous and Mesoporous Materials,* 111**,** 276-284.

FITZER, E., MUELLER, K. & SCHAEFER, W. (1971). The chemistry of the pyrolytic conversion of organic compounds to carbon. *Chemistry and Physics of Carbon,* 7**,** 237-383.

FLETCHER, A. J. (2008). *Porosity and Sorption Behaviour* [Online]. Available: http://personal.strath.ac.uk/ashleigh.fletcher/adsorption.htm#top [Accessed July 2012.

FOWLER, G. D. 1995. *The thermal conversion of contaminated soil into carbonaceous adsorbents.* PhD, Imperial College, University of London.

FOWLER, G. D. (Personal communication.

FOWLES, M. (2007). Black carbon sequestration as an alternative to bioenergy. *Biomass & bioenergy,* 31**,** 426-432.

FREEDONIA (2012) *World Activated Carbon Market*.

FREUNDLICH, H. M. F. (1906). Over the adsorption in solution. *The journal of physical chemistry. A,* 57**,** 385.

FUKUMOTO, Y., OSADA, T., HANAJIMA, D. & HAGA, K. (2003). Patterns and quantities of NH3, N2O and CH4 emissions during swine manure composting without forced aeration--effect of compost pile scale. *Bioresource Technology,* 89**,** 109-114.

FÜRHACKER, M., SCHARF, S. & WEBER, H. (2000). Bisphenol A: emissions from point sources. *Chemosphere,* 41**,** 751-756.

GARTEN, V., WEISS, D. & WILLIS, J. (1957). A new interpretation of the acidic and basic structures in carbons. I. Lactone groups of the ordinary and fluorescein types in carbons. *Australian journal of chemistry,* 10**,** 295-308.

GEHRING, M., TENNHARDT, L., VOGEL, D., WELTIN, D. & BILITEWSKI, B. (2004). Bisphenol A contamination of wastepaper, cellulose and recycled paper products. *Waste Management and the Environment II. WIT Transactions on Ecology and the Environment,* 78**,** 294-300.

GERBER, E., KREBS, C., MURRELL, C., MORETTI, M., ROCKLIN, R. & SCHAFFNER, U. (2008). Exotic invasive knotweeds (Fallopia spp.) negatively affect native plant and invertebrate assemblages in European riparian habitats. *Biological Conservation,* 141**,** 646-654.

GERGOVA, K. & ESER, S. (1996). Effects of activation method on the pore structure of activated carbons from apricot stones. *Carbon,* 34**,** 879-888.

GERGOVA, K., PETROV, N. & ESER, S. (1994). Adsorption properties and microstructure of activated carbons produced from agricultural by-products by steam pyrolysis. *Carbon,* 32**,** 693-702.

GILBERT, S. F. & EPEL, D. (2009). *Ecological developmental biology: integrating epigenetics, medicine, and evolution*, Sinauer Associates Sunderland, MA.

GILES, C. H., D'SILVA, A. P. & EASTON, I. A. (1974a). A general treatment and classification of the solute adsorption isotherm part. II. Experimental interpretation. *Journal of Colloid and Interface Science,* 47**,** 766-778.

GILES, C. H., SMITH, D. & HUITSON, A. (1974b). A general treatment and classification of the solute adsorption isotherm. I. Theoretical. *Journal of Colloid and Interface Science,* 47**,** 755-765.

GOERTZEN, S., THERIAULT, K., OICKLE, A., TARASUK, A. & ANDREAS, H. (2010). Standardization of the Boehm titration. Part I. CO(2) expulsion and endpoint determination. *Carbon,* 48**,** 1252-1261.

GOLDSTEIN, J. (2003). *Scanning Electron Microscopy and X-Ray Microanalysis*, Kluwer Academic/Plenum Publishers.

GONZALEZ, J., ROMAN, S., ENCINAR, J. & MARTINEZ, G. (2009). Pyrolysis of various biomass residues and char utilization for the production of activated carbons. *Journal of analytical and applied pyrolysis,* 85**,** 134-141.

GONZÁLEZ, J. F., ENCINAR, J. M., CANITO, J. L., SABIO, E. & CHACÓN, M. (2003). Pyrolysis of cherry stones: energy uses of the different fractions and kinetic study. *Journal of analytical and applied pyrolysis,* 67**,** 165-190.

GONZÁLEZ, M. T., MOLINA-SABIO, M. & RODRÍGUEZ-REINOSO, F. (1994). Steam activation of olive stone chars, development of porosity. *Carbon,* 32**,** 1407-1413.
GREGG, S. J. & SING, K. S. W. (1982). *Adsorption, Surface Area and Porosity,* London, Academic Press Inc.
GREGORY, A. P. (2007). *Green Energy* [Online]. Available: http://www.research.uky.edu/odyssey/winter07/green_energy.html.
GROUNDGROCER.COM. (2012). *Compost Windrow Turner* [Online]. Available: http://www.groundgrocer.com/products/-Compost-Windrow-Turner.html.
GUO, J. & CHONG LUA, A. (1998). Characterization of chars pyrolyzed from oil palm stones for the preparation of activated carbons. *Journal of analytical and applied pyrolysis,* 46**,** 113-125.
HALL, K., EAGLETON, L., ACRIVOS, A. & VERMEULEN, T. (1966). Pore-and solid-diffusion kinetics in fixed-bed adsorption under constant-pattern conditions. *Industrial & Engineering Chemistry Fundamentals,* 5**,** 212-223.
HAMEED, B. H. & RAHMAN, A. A. (2008). Removal of phenol from aqueous solutions by adsorption onto activated carbon prepared from biomass material. *Journal of Hazardous Materials,* 160**,** 576-581.
HAYKIRI-ACMA, H., YAMAN, S. & KUCUKBAYRAK, S. (2006). Gasification of biomass chars in steam–nitrogen mixture. *Energy Conversion and Management,* 47**,** 1004-1013.
HELLEBRAND, H. J. (1998). Emission of Nitrous Oxide and other Trace Gases during Composting of Grass and Green Waste. *Journal of Agricultural Engineering Research,* 69**,** 365-375.
HESCHEL, W. & KLOSE, E. (1995). On the suitability of agricultural by-products for the manufacture of granular activated carbon. *Fuel,* 74**,** 1786-1791.
HILL, A. & MARSH, H. (1968). A study of the adsorption of iodine and acetic acid from aqueous solutions on characterized porous carbons. *Carbon,* 6**,** 31-39.
HOLLINGSWORTH, M. L. & BAILEY, J. P. (2000). Evidence for massive clonal growth in the invasive weed Fallopia japonica (Japanese Knotweed). *Botanical Journal of the Linnean Society,* 133**,** 463-472.
HORVATH, G. & KAWAZOE, K. (1983). Method for the calculation of effective pore size distribution in molecular sieve carbon. *Journal of Chemical Engineering of Japan,* 16**,** 470-475.
HOWDESHELL, K. L., HOTCHKISS, A. K., THAYER, K. A., VANDENBERGH, J. G. & VOM SAAL, F. S. (1999). Environmental toxins: exposure to bisphenol A advances puberty. *Nature,* 401**,** 763-764.
HSIEH, C.-T. & TENG, H. (2000). Influence of mesopore volume and adsorbate size on adsorption capacities of activated carbons in aqueous solutions. *Carbon,* 38**,** 863-869.
HU, Y., ZHENG, Y., ZHU, F. & LI, G. (2007). Sol–gel coated polydimethylsiloxane/β-cyclodextrin as novel stationary phase for stir bar sorptive extraction and its application to analysis of estrogens and bisphenol A. *Journal of Chromatography A,* 1148**,** 16-22.
HU, Z. & SRINIVASAN, M. P. (1999). Preparation of high-surface-area activated carbons from coconut shell. *Microporous and Mesoporous Materials,* 27**,** 11-18.
HUMPHREY, J. & KELLER, I. (1997). *Separation Process Technology*, McGraw-Hill, New York.
IOANNIDOU, O. & ZABANIOTOU, A. (2007). Agricultural residues as precursors for activated carbon production—A review. *Renewable and Sustainable Energy Reviews,* 11**,** 1966-2005.
IPCC, I. P. O. C. C. (2001) *Climate Change 2001, Radiative Forcing of Climate Change, The Scientific Basis*.
JÄCKEL, U., THUMMES, K. & KÄMPFER, P. (2005). Thermophilic methane production and oxidation in compost. *FEMS Microbiology Ecology,* 52**,** 175-184.
JANKOWSKA, H., ŚWIĄTKOWSKI, A. & CHOMA, J. (1991). *Active carbon*, E. Horwood.
JONES, A., NESARATNAM, S. & PORTEOUS, A. (2008) *The Open University Household Waste Study: Waste Composting* The Open University.
JUANG, R.-S., WU, F.-C. & TSENG, R.-L. (2002). Characterization and use of activated carbons prepared from bagasses for liquid-phase adsorption. *Colloids and Surfaces A: Physicochemical and Engineering Aspects,* 201**,** 191-199.

JUHOLA, A. J. (1975). Iodine adsorption and structure of activated carbons. *Carbon,* 13**,** 437-442.

JULCOUR LEBIGUE, C., ANDRIANTSIFERANA, C., N'GUESSAN, K., AYRAL, C., MOHAMED, E., WILHELM, A.-M., DELMAS, H., LE COQ, L., GERENTE, C., SMITH, K. M., PULLKET, S., FOWLER, G. D. & GRAHAM, N. J. D. (2010). Application of sludge-based carbonaceous materials in a hybrid water treatment process based on adsorption and catalytic wet air oxidation. *Journal of Environmental Management,* 91**,** 2432-2439.

KADIRVELU, K., KAVIPRIYA, M., KARTHIKA, C., RADHIKA, M., VENNILAMANI, N. & PATTABHI, S. (2003). Utilization of various agricultural wastes for activated carbon preparation and application for the removal of dyes and metal ions from aqueous solutions. *Bioresource Technology,* 87**,** 129-132.

KANG, J.-H., KONDO, F. & KATAYAMA, Y. (2006). Human exposure to bisphenol A. *Toxicology,* 226**,** 79-89.

KARAGÖZ, S., TAY, T., UCAR, S. & ERDEM, M. (2008). Activated carbons from waste biomass by sulfuric acid activation and their use on methylene blue adsorption. *Bioresource Technology,* 99**,** 6214-6222.

KATYAL, S., THAMBIMUTHU, K. & VALIX, M. (2003). Carbonisation of bagasse in a fixed bed reactor: influence of process variables on char yield and characteristics. *Renewable Energy,* 28**,** 713-725.

KAWAHATA, H., OHTA, H., INOUE, M. & SUZUKI, A. (2004). Endocrine disrupter nonylphenol and bisphenol A contamination in Okinawa and Ishigaki Islands, Japan—within coral reefs and adjacent river mouths. *Chemosphere,* 55**,** 1519-1527.

KIMURA, K., TOSHIMA, S., AMY, G. & WATANABE, Y. (2004). Rejection of neutral endocrine disrupting compounds (EDCs) and pharmaceutical active compounds (PhACs) by RO membranes. *Journal of Membrane Science,* 245**,** 71-78.

KINVER, M. 2012. Carbon emissions are 'too high' to curb climate change. *BBC* [Online]. Available: http://www.bbc.co.uk/news/science-environment-20556703.

KJELDSEN, P., BARLAZ, M. A., ROOKER, A. P., BAUN, A., LEDIN, A. & CHRISTENSEN, T. H. (2002). Present and Long-Term Composition of MSW Landfill Leachate: A Review. *Critical Reviews in Environmental Science and Technology,* 32**,** 297-336.

KNOP, A., PILATO, L. A. & BVHMER, V. (1985). *Phenolic resins: chemistry, applications, and performance: future directions*, Springer-Verlag Berlin.

KOMILIS, D. P. & HAM, R. K. (2003). The effect of lignin and sugars to the aerobic decomposition of solid wastes. *Waste Management,* 23**,** 419-423.

KOMILIS, D. P., HAM, R. K. & PARK, J. K. (2004). Emission of volatile organic compounds during composting of municipal solid wastes. *Water Research,* 38**,** 1707-1714.

KRISHNAN, A. V., STATHIS, P., PERMUTH, S. F., TOKES, L. & FELDMAN, D. (1993). Bisphenol-A: an estrogenic substance is released from polycarbonate flasks during autoclaving. *ENDOCRINOLOGY-PHILADELPHIA-,* 132**,** 2279-2279.

KUCUK, M. & DEMIRBAS, A. (1993). Delignification of Ailanthus-Altissima and Spruce-Orientalis with Glycerol or Alkaline glycerol at Atmospheric Pressure. *Cellulose chemistry and technology,* 27**,** 679-686.

LAIRD, D. (2008). The charcoal vision: A win-win-win scenario for simultaneously producing bioenergy, permanently sequestering carbon, while improving soil and water quality. *Agronomy Journal,* 100**,** 178-181.

LAIRD, D., BROWN, R., AMONETTE, J. & LEHMANN, J. (2009). Review of the pyrolysis platform for coproducing bio-oil and biochar. *Biofuels, bioproducts & biorefining,* 3**,** 547-562.

LAL, R. (2004). Soil Carbon Sequestration Impacts on Global Climate Change and Food Security. *Science,* 304**,** 1623-1627.

LANGE, J. P. (2007). Lignocellulose conversion: an introduction to chemistry, process and economics. *Biofuels, Bioproducts and Biorefining,* 1**,** 39-48.

LANGMUIR (1918). The adsorption of gases on plane surfaces of glass, mica and platinum. *Journal of the American Chemical Society,* 40**,** 1361-1403.
LEE, H. B. & PEART, T. E. (2000). Bisphenol A contamination in Canadian municipal and industrial wastewater and sludge samples. *Water Quality Res J Canada,* 35**,** 283-298.
LEE, J., PARK, H. & YOON, J. (2003). Ozonation characteristics of bisphenol A in water. *Environmental technology,* 24**,** 241-248.
LEHMANN, J. (2007). Bio-energy in the black. *Frontiers in Ecology and the Environment,* 5**,** 381-387.
LEHMANN, J., GAUNT, J. & RONDON, M. (2006). Bio-char sequestration in terrestrial ecosystems - a review. *Mitigation and adaptation strategies for global change,* 11**,** 403-427.
LESTER, J. N., MACLEOD, C. & BIRKETT, J. (1999). *Microbiology and Chemistry for Environmental Scientists and Engineers*, Taylor & Francis.
LEVIN, D. A. (2000). *The Origin, Expansion, And Demise Of Plant Species*, Oxford University Press.
LIMA, I., BOATENG, A. & KLASSON, K. (2009). Pyrolysis of Broiler Manure: Char and Product Gas Characterization. *Industrial & Engineering Chemistry Research,* 48**,** 1292-1297.
LIPPENS, B. C. & DE BOER, J. H. (1965). Studies on pore systems in catalysts: V. The t method. *Journal of Catalysis,* 4**,** 319-323.
LIU, G., MA, J., LI, X. & QIN, Q. (2009). Adsorption of bisphenol A from aqueous solution onto activated carbons with different modification treatments. *Journal of Hazardous Materials,* 164**,** 1275-1280.
LÓPEZ, G., OLAZAR, M., ARTETXE, M., AMUTIO, M., ELORDI, G. & BILBAO, J. (2009). Steam activation of pyrolytic tyre char at different temperatures. *Journal of analytical and applied pyrolysis,* 85**,** 539-543.
LUA, A. C., YANG, T. & GUO, J. (2004). Effects of pyrolysis conditions on the properties of activated carbons prepared from pistachio-nut shells. *Journal of analytical and applied pyrolysis,* 72**,** 279-287.
LUNDIE, S. & PETERS, G. M. (2005). Life cycle assessment of food waste management options. *Journal of Cleaner Production,* 13**,** 275-286.
LUSSIER, M. G., SHULL, J. C. & MILLER, D. J. (1994). Activated carbon from cherry stones. *Carbon,* 32**,** 1493-1498.
MAERZ, J., BLOSSEY, B. & NUZZO, V. (2005). Green frogs show reduced foraging success in habitats invaded by Japanese knotweed. *Biodiversity and conservation,* 14**,** 2901-2911.
MALIK, P. K. (2003). Use of activated carbons prepared from sawdust and rice-husk for adsorption of acid dyes: a case study of Acid Yellow 36. *Dyes and Pigments,* 56**,** 239-249.
MARCHAND, G., LAVOIE, J. & LAZURE, L. (1995). Evaluation of Bioaerosols in a Municipal Solid Waste Recycling and Composting Plant. *Journal of the Air & Waste Management Association,* 45**,** 778-781.
MARSH, H. & RODRÍGUEZ-REINOSO, F. (2006). *Activated Carbon*, Elsevier.
MARTIN, A. & SCOTT, I. A. N. (2003). The Effectiveness of the UK Landfill Tax. *Journal of Environmental Planning and Management,* 46**,** 673-689.
MARTÍNEZ, M. L., TORRES, M. M., GUZMÁN, C. A. & MAESTRI, D. M. (2006). Preparation and characteristics of activated carbon from olive stones and walnut shells. *Industrial Crops and Products,* 23**,** 23-28.
MCKENDRY, P. (2002). Energy production from biomass (part 1): overview of biomass. *Bioresource Technology,* 83**,** 37-46.
MEDAC LTD. 2007. Method for the analysis of CHNS & O using the Thermo FlashEA 1112.
MERCHANT, A. & PETRICH, M. (1993). Pyrolysis of scrap tires and conversion of chars to activated carbon. *AIChE journal,* 39**,** 1370-1376.
MOHAN, D., PITTMAN, C. U. & STEELE, P. H. (2006). Pyrolysis of Wood/Biomass for Bio-oil: A Critical Review. *Energy & Fuels,* 20**,** 848-889.

MOLINA-SABIO, M., GONZALEZ, M. T., RODRIGUEZ-REINOSO, F. & SEPÚLVEDA-ESCRIBANO, A. (1996). Effect of steam and carbon dioxide activation in the micropore size distribution of activated carbon. *Carbon,* 34**,** 505-509.

MOLINA-SABIO, M. & RODRíGUEZ-REINOSO, F. (2004). Role of chemical activation in the development of carbon porosity. *Colloids and Surfaces A: Physicochemical and Engineering Aspects,* 241**,** 15-25.

MOMENTIVE. 2012. Reactivity of Fused Quartz. Available: http://www.momentive.com/Products/ProductLiterature.aspx?id=20400.

MOORE, A. (2008). Biofuels are dead: long live biofuels(?) - Part one. *New Biotechnology,* 25**,** 6-12.

MORENO-CASTILLA, C. (2004). Adsorption of organic molecules from aqueous solutions on carbon materials. *Carbon,* 42**,** 83-94.

MUI, E. L. K., KO, D. C. K. & MCKAY, G. (2004). Production of active carbons from waste tyres—a review. *Carbon,* 42**,** 2789-2805.

NABAIS, J. M. V., LAGINHAS, C., CARROTT, P. J. M. & CARROTT, M. M. L. R. (2010). Thermal conversion of a novel biomass agricultural residue (vine shoots) into activated carbon using activation with CO2. *Journal of Analytical and Applied Pyrolysis,* 87**,** 8-13.

NAKADA, N., SHINOHARA, H., MURATA, A., KIRI, K., MANAGAKI, S., SATO, N. & TAKADA, H. (2007). Removal of selected pharmaceuticals and personal care products (PPCPs) and endocrine-disrupting chemicals (EDCs) during sand filtration and ozonation at a municipal sewage treatment plant. *Water Research,* 41**,** 4373-4382.

NAKAMURA, S. & DAISHIMA, S. (2004). Simultaneous determination of alkylphenols and bisphenol A in river water by stir bar sorptive extraction with in situ acetylation and thermal desorption–gas chromatography–mass spectrometry. *Journal of Chromatography A,* 1038**,** 291-294.

NAWDO (1998) *Composting Green Waste: A Guidance to Local Authority* Institute of Wastes Management Business Services Ltd.

NNSS. (2011). *Statistics and Facts* [Online]. Available: https://secure.fera.defra.gov.uk/nonnativespecies/index.cfm?pageid=258.

NOVAK, J., BUSSCHER, W., LAIRD, D., AHMEDNA, M., WATTS, D. & NIANDOU, M. (2009). Impact of biochar amendment on fertility of a southeastern Coastal Plain soil. *Soil science,* 174**,** 105-112.

OICKLE, A., GOERTZEN, S., HOPPER, K., ABDALLA, Y. & ANDREAS, H. (2010). Standardization of the Boehm titration: Part II. Method of agitation, effect of filtering and dilute titrant. *Carbon,* 48**,** 3313-3322.

PANDEY, M. P. & KIM, C. S. (2011). Lignin Depolymerization and Conversion: A Review of Thermochemical Methods. *Chemical Engineering & Technology,* 34**,** 29-41.

PARFITT, J. (2002) *Analysis of household waste composition and factors driving waste increases* WRAP.

PARFITT, J. (2010) *Municipal Waste Composition: A Review of Municipal Waste Component Analyses* Defra.

PARFITT, J. P., LOVETT, A. A. & SÜNNENBERG, G. (2001). A classification of local authority waste collection and recycling strategies in England and Wales. *Resources, Conservation and Recycling,* 32**,** 239-257.

PASTOR-VILLEGAS, J. & DURAN-VALLE, C. (2002). Pore structure of activated carbons prepared by carbon dioxide and steam activation at different temperatures from extracted rockrose. *Carbon,* 40**,** 397-402.

PENDYAL, B., JOHNS, M. M., MARSHALL, W. E., AHMEDNA, M. & RAO, R. M. (1999). The effect of binders and agricultural by-products on physical and chemical properties of granular activated carbons. *Bioresource Technology,* 68**,** 247-254.

PEREZ, P., PULGAR, R., OLEA-SERRANO, F., VILLALOBOS, M., RIVAS, A., METZLER, M., PEDRAZA, V. & OLEA, N. (1998). The estrogenicity of bisphenol A-related diphenylalkanes with various

substituents at the central carbon and the hydroxy groups. *Environmental health perspectives,* 106**,** 167.
POLLARD, S. J. T. 1990. *Low-cost adsorbents from industrial wastes.* PhD, Imperial College, University of London.
RADOVIC, L., MORENO-CASTILLA, C. & RIVERA-UTRILLA, J. (2001). Chemistry and Physics of Carbon, vol. 27. *Marcel Dekker, New York, Basel***,** 227.
REED, A. R. & WILLIAMS, P. T. (2004). Thermal processing of biomass natural fibre wastes by pyrolysis. *International Journal of Energy Research,* 28**,** 131-145.
RENGARAJ, S., MOON, S.-H., SIVABALAN, R., ARABINDOO, B. & MURUGESAN, V. (2002). Agricultural solid waste for the removal of organics: adsorption of phenol from water and wastewater by palm seed coat activated carbon. *Waste Management,* 22**,** 543-548.
RIGOL, A., LATORRE, A., LACORTE, S. & BARCELÓ, D. (2002). Determination of toxic compounds in paper-recycling process waters by gas chromatography–mass spectrometry and liquid chromatography–mass spectrometry. *Journal of Chromatography A,* 963**,** 265-275.
ROBERTS, M. 2011. Eating canned soup 'poses a chemical risk'. *BBC News* [Online]. Available: http://www.bbc.co.uk/news/health-15834072.
ROBINSON, J., KINGMAN, S., BARRANCO, R., SNAPE, C. & AL-SAYEGH, H. (2010). Microwave Pyrolysis of Wood Pellets. *Industrial & Engineering Chemistry Research,* 49**,** 459-463.
RODRÍGUEZ-MIRASOL, J., CORDERO, T. & RODRÍGUEZ, J. J. (1993). Preparation and characterization of activated carbons from eucalyptus kraft lignin. *Carbon,* 31**,** 87-95.
RODRIGUEZ-REINOSO, F. & MOLINA-SABIO, M. (1992). Activated carbons from lignocellulosic materials by chemical and/or physical activation: an overview. *Carbon,* 30**,** 1111-1118.
RODRÍGUEZ-REINOSO, F., MOLINA-SABIO, M. & GONZÁLEZ, M. T. (1995). The use of steam and CO2 as activating agents in the preparation of activated carbons. *Carbon,* 33**,** 15-23.
RODRíGUEZ-REINOSO, F., PASTOR, A. C., MARSH, H. & MARTíNEZ, M. A. (2000). Preparation of activated carbon cloths from viscous rayon. Part II: physical activation processes. *Carbon,* 38**,** 379-395.
ROMÁN, S., GONZÁLEZ, J. F., GONZÁLEZ-GARCÍA, C. M. & ZAMORA, F. (2008). Control of pore development during CO2 and steam activation of olive stones. *Fuel Processing Technology,* 89**,** 715-720.
ROSKILL INFORMATION SERVICES LTD. (2003) *The Economics of Activated Carbon*.
SAN MIGUEL, G., FOWLER, G. D. & SOLLARS, C. J. (2003). A study of the characteristics of activated carbons produced by steam and carbon dioxide activation of waste tyre rubber. *Carbon,* 41**,** 1009-1016.
SAN MIGUEL, G., LAMBERT, S. D. & GRAHAM, N. J. D. (2001). The regeneration of field-spent granular-activated carbons. *Water Research,* 35**,** 2740-2748.
SEIGER, L. (1991). *Elemental Stewardship Abstract for Polygonum cuspidatum - Japanese knotweed, Mexican bamboo* [Online]. Available: http://www.invasive.org/gist/esadocs/documnts/polycus.pdf.
SHAFIZADEH, F. (1982). Introduction to pyrolysis of biomass. *Journal of analytical and applied pyrolysis,* 3**,** 283-305.
SHAW, R. H., BRYNER, S. & TANNER, R. (2009). The life history and host range of the Japanese knotweed psyllid, Aphalara itadori Shinji: Potentially the first classical biological weed control agent for the European Union. *Biological Control,* 49**,** 105-113.
SIMPSON, J. & WEINER, E. (2002). *The Oxford English Dictionary*, Oxford University Press.
SING, K. S. W. (1967). Assessment of microporosity. *Chemistry and Industry*.
SING, K. S. W. (1985). Reporting physisorption data for gas/solid systems. *Pure and applied chemistry,* 57**,** 603.
SMÍŠEK, M. & ČERNÝ, S. (1970). *Active carbon: manufacture, properties and applications*, Elsevier Pub. Co.

SMITH, K. M., FOWLER, G. D., PULLKET, S. & GRAHAM, N. J. D. (2012). The production of attrition resistant, sewage–sludge derived, granular activated carbon. *Separation and Purification Technology,* 98**,** 240-248.

SNOEYINK, V. L., WEBER, W. J. & MARK, H. B. (1969). Sorption of phenol and nitrophenol by active carbon. *Environmental science & technology,* 3**,** 918-926.

SOETAERT, W. & VANDAMME, E. J. (2009). *Biofuels*, Wiley.

SOLL, J. (2004). *Controlling knotweed (Polygonum cuspidatum, P. sachalinense, P. polystachyum and hybrids) in the Pacific Northwest* [Online]. Available: http://www.invasive.org/gist/moredocs/polspp01.pdf.

SOLTES, E. J. & ELDER, T. J. 1981. Pyrolysis. *In:* GOLDSTEIN, I. S. (ed.) *Organic Chemicals From Biomass.* CRC Press.

STACKELBERG, P. E., GIBS, J., FURLONG, E. T., MEYER, M. T., ZAUGG, S. D. & LIPPINCOTT, R. L. (2007). Efficiency of conventional drinking-water-treatment processes in removal of pharmaceuticals and other organic compounds. *Science of the Total Environment,* 377**,** 255-272.

STAPLES, C. A., DOME, P. B., KLECKA, G. M., OBLOCK, S. T. & HARRIS, L. R. (1998). A review of the environmental fate, effects, and exposures of bisphenol A. *Chemosphere,* 36**,** 2149-2173.

STEENBERG, B. 1944. *Adsorption and exchange of ions on activated charcoal.* Stockholms hogskola.

STEINBEISS, S., GLEIXNER, G. & ANTONIETTI, M. (2009). Effect of biochar amendment on soil carbon balance and soil microbial activity. *Soil Biology and Biochemistry,* 41**,** 1301-1310.

STOECKLI, F. & BALLERINI, L. (1991). Evolution of microporosity during activation of carbon. *Fuel,* 70**,** 557-559.

STRATEGY UNIT 2002. Waste Not, Want Not: A strategy for tackling the waste problem in England. UK.

STURGESS, J. (2001) *Redruth Smelting Works, Cornwall: Archaeological Assessment*.

SUGIURA-OGASAWARA, M., OZAKI, Y., SONTA, S., MAKINO, T. & SUZUMORI, K. (2005). Exposure to bisphenol A is associated with recurrent miscarriage. *Human reproduction,* 20**,** 2325-2329.

SUHAS, CARROTT, P. J. M. & RIBEIRO CARROTT, M. M. L. (2007). Lignin – from natural adsorbent to activated carbon: A review. *Bioresource Technology,* 98**,** 2301-2312.

SUZUKI, T., NAKAGAWA, Y., TAKANO, I., YAGUCHI, K. & YASUDA, K. (2004). Environmental Fate of Bisphenol A and Its Biological Metabolites in River Water and Their Xeno-estrogenic Activity. *Environmental Science & Technology,* 38**,** 2389-2396.

SWATLOSKI, R. P., SPEAR, S. K., HOLBREY, J. D. & ROGERS, R. D. (2002). Dissolution of Cellose with Ionic Liquids. *Journal of the American Chemical Society,* 124**,** 4974-4975.

TAHA, M. P. M., DREW, G. H., LONGHURST, P. J., SMITH, R. & POLLARD, S. J. T. (2006). Bioaerosol releases from compost facilities: Evaluating passive and active source terms at a green waste facility for improved risk assessments. *Atmospheric Environment,* 40**,** 1159-1169.

TAKEUCHI, T., TSUTSUMI, O., IKEZUKI, Y., TAKAI, Y. & TAKETANI, Y. (2004). Positive relationship between androgen and the endocrine disruptor, bisphenol A, in normal women and women with ovarian dysfunction. *Endocrine journal,* 51**,** 165.

TANCREDI, N., CORDERO, T., RODRÍGUEZ-MIRASOL, J. & RODRÍGUEZ, J. J. (1996). Activated carbons from Uruguayan eucalyptus wood. *Fuel,* 75**,** 1701-1706.

TAY, T. (2009). Preparation and characterization of activated carbon from waste biomass. *Journal of Hazardous Materials,* 165**,** 481-485.

TENG, H. & HSIEH, C.-T. (1998). Influence of Surface Characteristics on Liquid-Phase Adsorption of Phenol by Activated Carbons Prepared from Bituminous Coal. *Industrial & Engineering Chemistry Research,* 37**,** 3618-3624.

TENNANT, M. & MAZYCK, D. (2003). Steam-pyrolysis activation of wood char for superior odorant removal. *Carbon,* 41**,** 2195-2202.

THEANDER, O. (1985). Cellulose, hemicellulose and extractives. *Fundamentals of Thermochemical Biomass Conversion***,** 35-60.

TSAI, W.-T., LAI, C.-W. & SU, T.-Y. (2006). Adsorption of bisphenol-A from aqueous solution onto minerals and carbon adsorbents. *Journal of Hazardous Materials,* 134**,** 169-175.

USEPA (1996) *Method 3051a Microwave Assisted Acid Dissolution of Sediments, Sludges, Soils and Oils* Washington, D.C. US Environmental Protection Agency.

USEPA. (2011). *What Are Endocrine Disruptors?* [Online]. Available: http://www.epa.gov/endo/pubs/edspoverview/whatare.htm.

VALIX, M., CHEUNG, W. H. & MCKAY, G. (2004). Preparation of activated carbon using low temperature carbonisation and physical activation of high ash raw bagasse for acid dye adsorption. *Chemosphere,* 56**,** 493-501.

VEHLOW, J., BERGFELDT, B., VISSER, R. & WILÉN, C. (2007). European Union waste management strategy and the importance of biogenic waste. *Journal of Material Cycles and Waste Management,* 9**,** 130-139.

VRCHOTOVA, N. & SERA, B. (2008). Allelopathic properties of knotweed rhizome extracts. *Plant, soil and environment,* 54**,** 301-303.

VRIJHEID, M. (2000). Health effects of residence near hazardous waste landfill sites: a review of epidemiologic literature. *Environmental health perspectives,* 108**,** 101.

WARTMANN, S., GROENENBERG, H. & BROCKETT, S. (2009). Monitoring and reporting of GHG emissions from CCS operations under the EU ETS. *Energy Procedia,* 1**,** 4459-4466.

WASTE MANAGEMENT PAPER 26B 1995. Landfill Design, Construction and Operational Practice. *In:* ENVIRONMENT, D. O. T. (ed.). London: HMSO.

WESTON, L., BARNEY, J. & DITOMMASO, A. (2005). A review of the biology and ecology of three invasive perennials in New York State: Japanese knotweed (Polygonum cuspidatum), mugwort (Artemisia vulgaris) and pale swallow-wort (Vincetoxicum rossicum). *Plant and soil,* 277**,** 53-69.

WIGMANS, T. (1989). Industrial aspects of production and use of activated carbons. *Carbon,* 27**,** 13-22.

WILLIAMS, I. D. & KELLY, J. (2003). Green waste collection and the public's recycling behaviour in the Borough of Wyre, England. *Resources, Conservation and Recycling,* 38**,** 139-159.

WILLIAMS, P. T. (2006). *Waste treatment and disposal,* GB, John Wiley & Sons Ltd.

WILLIAMS, P. T. & BESLER, S. (1996). The influence of temperature and heating rate on the slow pyrolysis of biomass. *Renewable Energy,* 7**,** 233-250.

WILLIAMS, P. T. & REED, A. R. (2006). Development of activated carbon pore structure via physical and chemical activation of biomass fibre waste. *Biomass and Bioenergy,* 30**,** 144-152.

WRAP. (2010). *Garden and Food Waste Processing* [Online]. Available: http://www.wrap.org.uk/composting/production/index.html 2010].

WU, F.-C., TSENG, R.-L. & JUANG, R.-S. (1999). Pore structure and adsorption performance of the activated carbons prepared from plum kernels. *Journal of Hazardous Materials,* 69**,** 287-302.

YANG, H., YAN, R., CHEN, H., LEE, D. H. & ZHENG, C. (2007). Characteristics of hemicellulose, cellulose and lignin pyrolysis. *Fuel,* 86**,** 1781-1788.

YANG, O. B., KIM, J. C., LEE, J. S. & KIM, Y. G. (1993). Use of activated carbon fiber for direct removal of iodine from acetic acid solution. *Industrial & Engineering Chemistry Research,* 32**,** 1692-1697.

YOON, Y., WESTERHOFF, P., SNYDER, S. A. & ESPARZA, M. (2003). HPLC-fluorescence detection and adsorption of bisphenol A, 17β-estradiol, and 17α-ethynyl estradiol on powdered activated carbon. *Water Research,* 37**,** 3530-3537.

ZABANIOTOU, A., STAVROPOULOS, G. & SKOULOU, V. (2008). Activated carbon from olive kernels in a two-stage process: Industrial improvement. *Bioresource Technology,* 99**,** 320-326.

ZANZI, R., SJÖSTRÖM, K. & BJÖRNBOM, E. (2002). Rapid pyrolysis of agricultural residues at high temperature. *Biomass and Bioenergy,* 23**,** 357-366.

Appendix I

According to BSBI (2011), there are 2879 hectads contaminated with Japanese knotweed, where 1 hectad is 10,000 hectares. Therefore, there are 2.879×10^7 hectares contaminated with Japanese knotweed. With the data obtained from Brock (1994), where it was estimated there was an average of 9365kg/ha of Japanese knotweed stem and 14677kg/ha of Japanese knotweed rhizome, we are able to calculate that on average, the total mass of Japanese knotweed found in the UK in 1991 was 2.6×10^8 tonnes of stems and 4.3×10^8 tonnes of rhizomes. Unfortunately, this was the most up-to-date data obtained and it is expected to have increased, as a result of the virility of the species.